Dredging Processes

The Loading Process of a Trailing Suction Hopper Dredge

Dr.ir. Sape A. Miedema

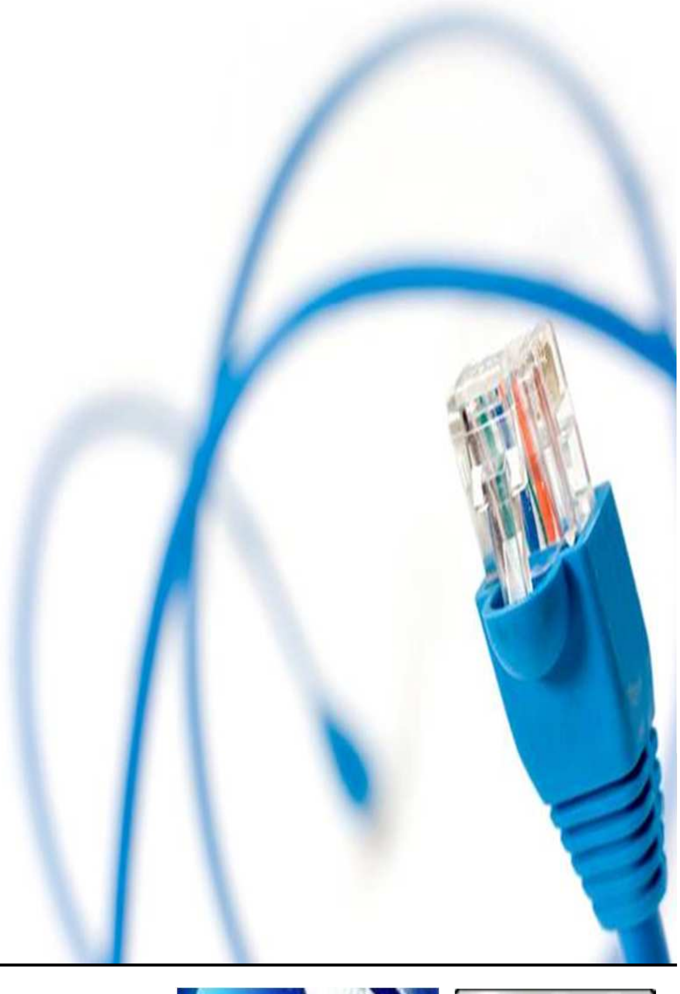

TU Delft

Dredging Processes The Loading Process of a Trailing Suction Hopper Dredge

by

Dr.ir. Sape A. Miedema

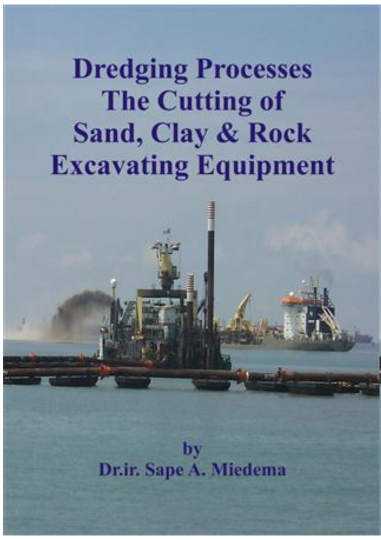
Dredging Processes
The Cutting of
Sand, Clay & Rock
Excavating Equipment
by
Dr.ir. Sape A. Miedema

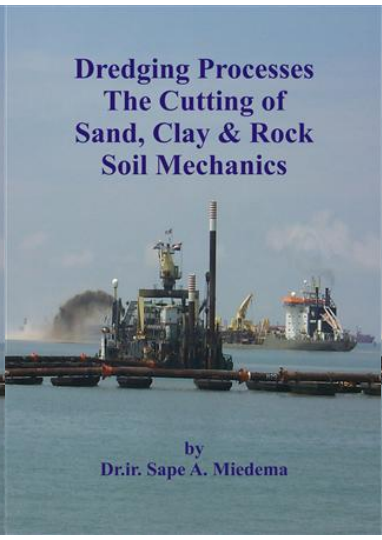
Dredging Processes
The Cutting of
Sand, Clay & Rock
Soil Mechanics
by
Dr.ir. Sape A. Miedema

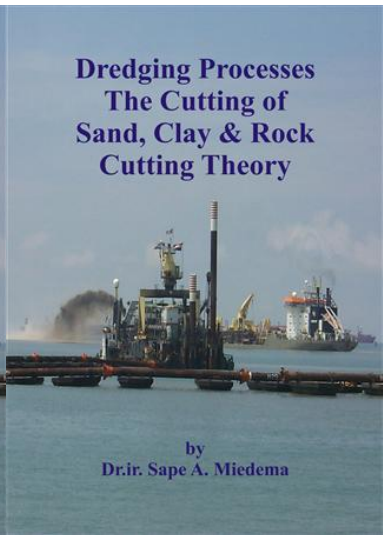
Dredging Processes
The Cutting of
Sand, Clay & Rock
Cutting Theory
by
Dr.ir. Sape A. Miedema

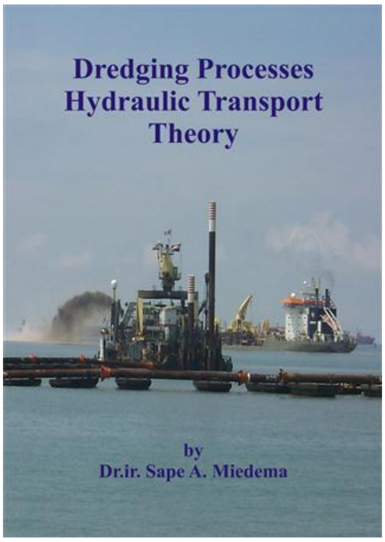
Dredging Processes
Hydraulic Transport
Theory
by
Dr.ir. Sape A. Miedema

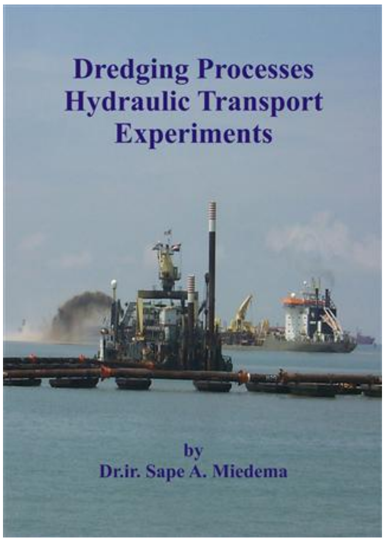
Dredging Processes
Hydraulic Transport
Experiments
by
Dr.ir. Sape A. Miedema

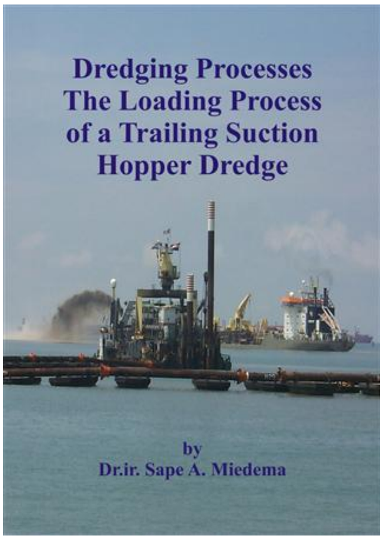
Dredging Processes
The Loading Process
of a Trailing Suction
Hopper Dredge
by
Dr.ir. Sape A. Miedema

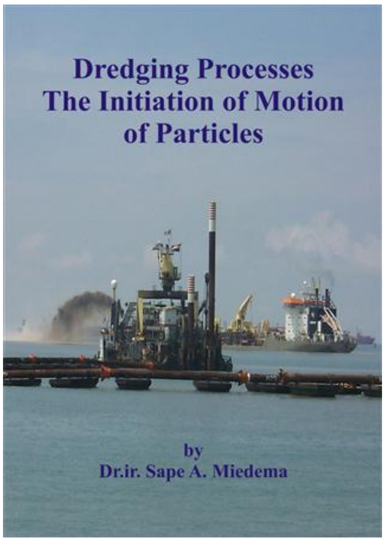
Dredging Processes
The Initiation of Motion
of Particles
by
Dr.ir. Sape A. Miedema

Dredging Processes
The Loading of Trailing Suction Hopper Dredges

By

Dr.ir. Sape A. Miedema

Dredging Processes
The Loading of Trailing Suction Hopper Dredges

Preface

Lecture notes for the course OE4626 Dredging Processes, for the MSc program Offshore & Dredging Engineering, at the Delft University of Technology.

By Dr.ir. Sape A. Miedema, Sunday, January 13, 2013

In dredging, trenching, (deep sea) mining, drilling, tunnel boring and many other applications, sand, clay or rock has to be excavated. The productions (and thus the dimensions) of the excavating equipment range from mm^3/sec - cm^3/sec to m^3/sec. In oil drilling layers with a thickness of a magnitude of 0.2 mm are cut, while in dredging this can be of a magnitude of 0.1 m with cutter suction dredges and meters for clamshells and backhoe's. Some equipment is designed for dry soil, while others operate under water saturated conditions. Installed cutting powers may range up to 10 MW. For both the design, the operation and production estimation of the excavating equipment it is important to be able to predict the cutting forces and powers. After the soil has been excavated it is usually transported hydraulically as a slurry over a short (TSHD's) or a long distance (CSD's). Estimating the pressure losses and determining whether or not a bed will occur in the pipeline is of great importance. Fundamental processes of sedimentation, initiation of motion and ersosion of the soil particles determine the transport process and the flow regimes. In TSHD's the soil has to settle during the loading process, where also sedimentation and erosion will be in equilibrium. In all cases we have to deal with soil and high density soil water mixtures and its fundamental behavior. Publications of the author on hopper sedimentation:

1. Miedema, S. (1981). The flow of dredged slurry in and out hoppers and the settlement process in hoppers. Delft, the Netherlands: Delft University of Technology.
2. Vlasblom, W., & Miedema, S. (1995). A Theory for Determining Sedimentation and Overflow Losses in Hoppers. *WODCON IV.* Amsterdam, Netherlands: WODA.
3. Miedema, S., & Vlasblom, W. (1996). Theory of Hopper Sedimentation. 29th Annual Texas A&M Dredging Seminar. New Orleans: WEDA/TAMU.
4. Miedema, S., & Rhee, C. v. (2007). A sensitivity analysis on the effects of dimensions and geometry of Trailing Suction Hopper Dredges. WODCON. Orlando, Florida, USA: WODA.
5. Miedema, S. (2008). An Analytical Approach to the Sedimentation Process in Trailing Suction Hopper Dredges. Terra et Aqua 112, pp. 15-25.
6. Miedema, S. (2008). An analytical method to determine scour. WEDA XXVIII & Texas A&M 39. St. Louis, USA: Western Dredging Association (WEDA).
7. Miedema, S. (2009A). The effect of the bed rise velocity on the sedimentation process in hopper dredges. Journal of Dredging Engineering, Vol. 10, No. 1, pp. 10-31.
8. Miedema, S. (2009B). A sensitivity analysis of the scaling of TSHD's. WEDA 29 & TAMU 40 Conference. Phoenix, Arizona, USA: WEDA.
9. Miedema, S. (2010). Constructing the Shields Curve, a New Theoretical Approach and its Applications. World Dredging Conference (p. 19 pages). Beijing: WODA.
10. Miedema, S. (2010). Constructing the Shields curve, a new theoretical approach and its applications. WODCON XIX (p. 22 pages). Beijing, September 2010: WODA.

This book will enable engineers to determine the loading process of Trailing Suction Hopper Dredges and is the **4th** of **7** books.

Part 1: The Cutting of Sand, Clay & Rock – Excavating Equipment.
Part 2: The Cutting of Sand, Clay & Rock – Soil Mechanics.
Part 3: The Cutting of Sand, Clay & Rock – Cutting Theory.
Part 4: The Loading Process of a Trailing Suction Hopper Dredge.
Part 5: The Initiation of Motion of Particles.
Part 6: Hydraulic Transport – Theory.
Part 7: Hydraulic Transport – Experiments.

Dr.ir. S.A. Miedema

Dr.ir. Sape A. Miedema
Delft University of Technology
Delft, the Netherlands
Sunday, January 13, 2013

Contents

Chapter 1: The Trailing Suction Hopper Dredge

1.1 Introduction

In the last decennia there has been a strong development in the enlargement of TSHD's (Trailing Suction Hopper Dredges) from roughly 10.000 m^3 in the early 90's up to 50.000 m^3 expected loading capacity nowadays. Because of the economy of the loading process, but also environmental regulations, it is important to predict the overflow losses that are occurring.

For the estimation of the sedimentation process in TSHD's a number of models have been developed. The oldest model used is the Camp (1936), (1946) and (1953) model which was developed for sewage and water treatment tanks. Camp and Dobbins (1944) added the influence of turbulence based on the two-dimensional advection-diffusion equation, resulting in rather complicated equations. Miedema (1981) used the Camp model to develop an analytical model. Groot (1981) added the effects of hindered settling. Vlasblom & Miedema (1995) and Miedema & Vlasblom (1996) simplified the Camp equations by means of regression and included a rising sediment zone, as well as hindered settling and erosion and an adjustable overflow. Van Rhee (2002C) modified the implementation of erosion in the Camp model, but concluded that the influence is small due to the characteristics of the model. Ooijens (1999) added the time effect, since the previous models assume an instantaneous response of the settling efficiency on the inflow of mixture. Yagi (1970) developed a new model based on the concentration distribution in open channel flow.

The models mentioned above are all black box approaches assuming simplified velocity distributions and an ideal basin. Van Rhee (2002C) developed a more sophisticated model, the 2DV model. This model is based on the 2D (horizontal and vertical) Reynolds Averaged Navier Stokes equations with a k-ε turbulence model and includes suspended sediment transport for multiple fractions.

1.2 The Loading Cycle of a Hopper Dredge

The loading cycle of a TSHD is considered to start when the hopper is filled with soil and starts to sail to the dump area. This point in the loading cycle was chosen as the starting point in order to be able to show the optimal load in a graph. The loading cycle then consists of the following phases:

- Phase 1: The water above the overflow level flows away through the overflow. The overflow is lowered to the sediment level, so the water above the sediment can also flow away. In this way minimum draught is achieved. Sailing to the dump area is started.

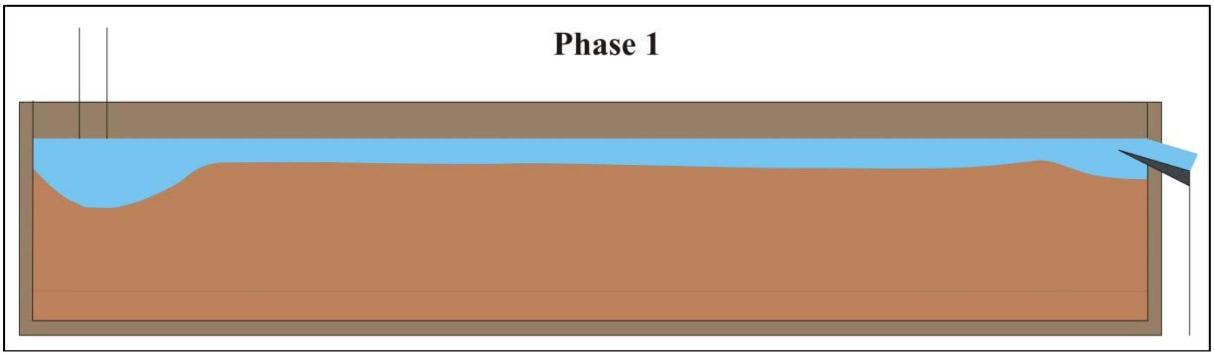

Figure 1-1: Phase 1 of the loading cycle.

- Phase 2: Continue sailing to the dump area.

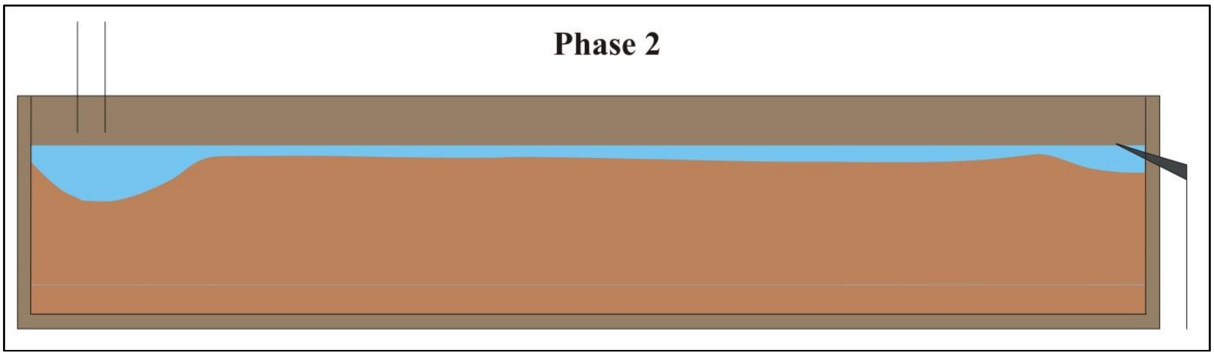

Figure 1-2: Phase 2 of the loading cycle.

- Phase 3: Dump the load in the dump area. Dumping can be carried out in 3 different ways, using the bottom dumping system, pumping ashore or rain bowing.

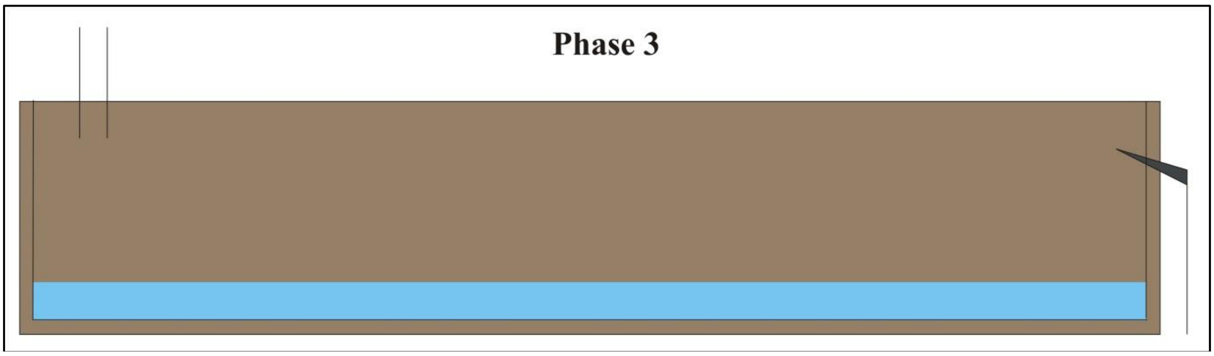

Figure 1-3: Phase 3 of the loading cycle.

- Phase 4: Pump the remaining water out of the hopper and sail to the dredging area. Often the water is not pumped out, but instead water is pumped in, to have the pumps as low as possible, in order to dredge a higher density, which should result in a shorter loading time.

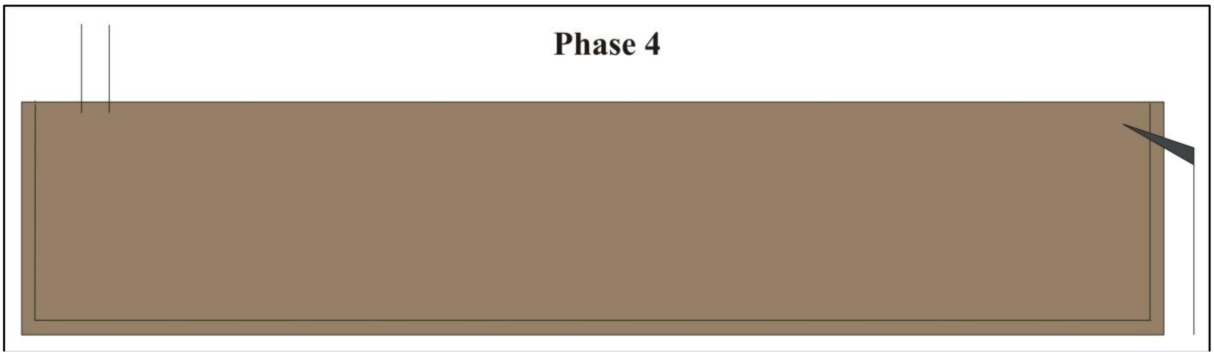

Figure 1-4: Phase 4 of the loading cycle.

- Phase 5: Start dredging and fill the hopper with mixture to the overflow level, during this phase 100% of the soil is assumed to settle in the hopper.

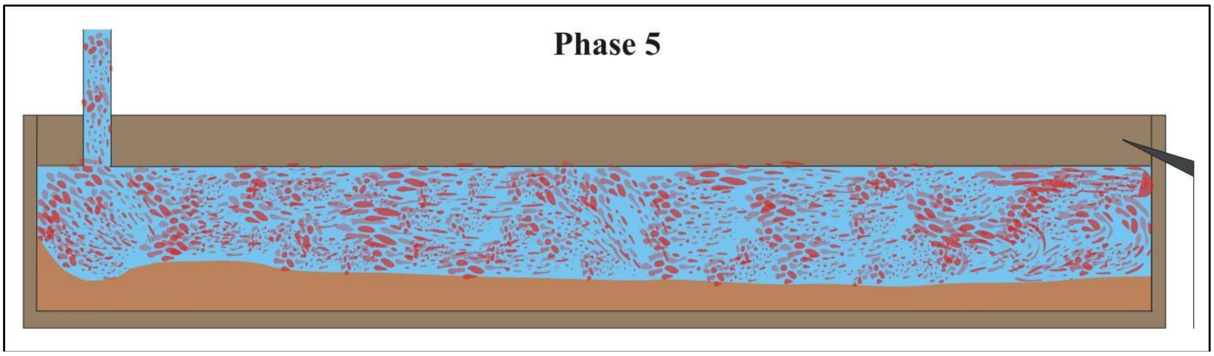

Figure 1-5: Phase 5 of the loading cycle.

- Phase 6: Continue loading with minimum overflow losses, during this phase a percentage of the grains will settle in the hopper. The percentage depends on the grain size distribution of the sand.

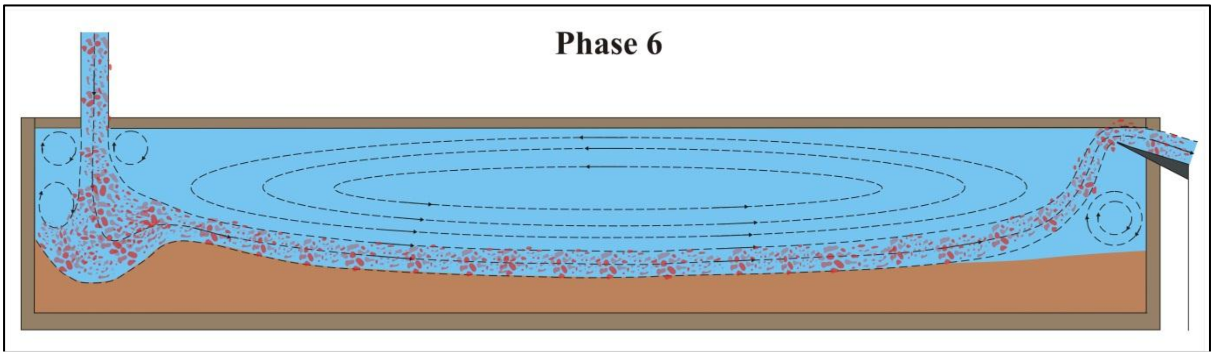

Figure 1-6: Phase 6 of the loading cycle.

- Phase 7: The maximum draught (CTS, Constant Tonnage System) is reached. From this point on the overflow is lowered.

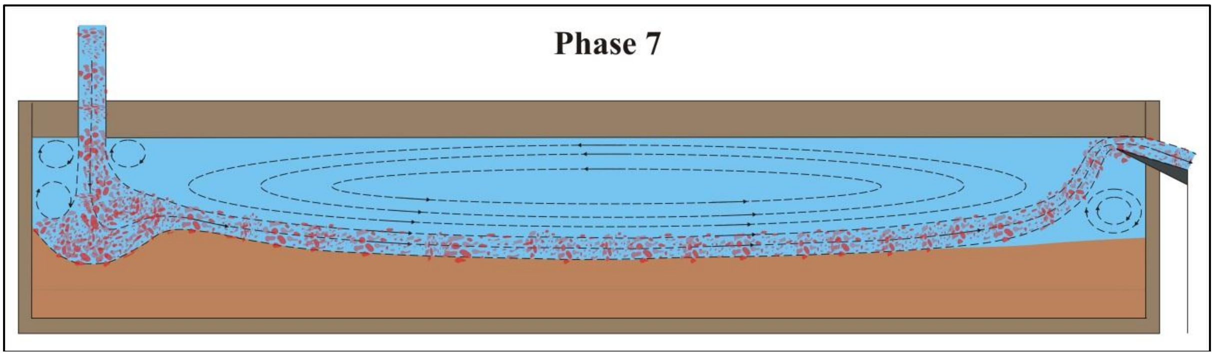

Figure 1-7: Phase 7 of the loading cycle.

- Phase 8: The sediment in the hopper is rising due to sedimentation, the flow velocity above the sediment increases, resulting in scour. This is the cause of rapidly increasing overflow losses.

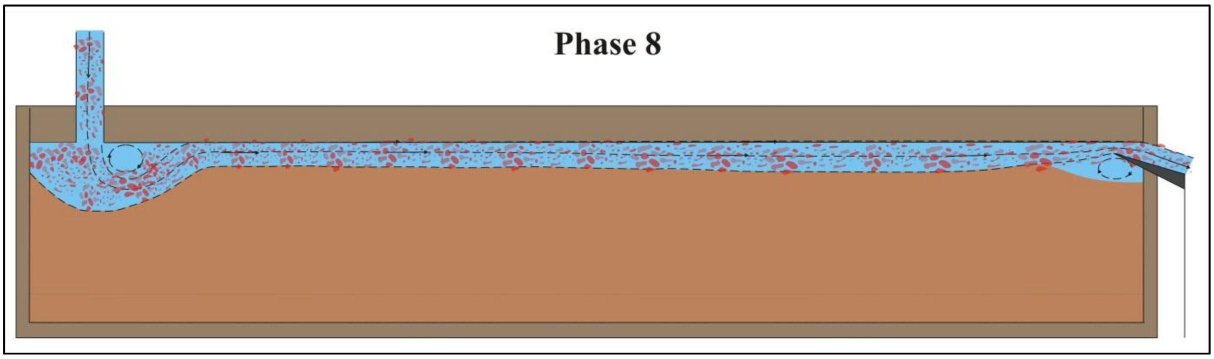

Figure 1-8: Phase 8 of the loading cycle.

Figure 1-9 and Figure 1-10 show the total load, the effective load, the TDS and the overflow losses during these phases. The way each phase occurs in the cycle, depends on the type of hopper dredge, the working method and of course, the type of soil to be dredged.

Basically there are two main methods for loading the hopper. The ‘Constant Volume System’ (CVS). This system has a fixed overflow level so the effective volume of the hopper is constant. The TSHD is designed for filling the hopper with sediment with a density of 1.9-2.0 ton/m^3. The ‘Constant Tonnage System’ (CTS). The system has an adjustable overflow level. The hopper is designed for a density of 1.3-1.7 ton/m^3 in combination with a maximum tonnage. When the content of the hopper reaches the maximum tonnage, the overflow is lowered in order to keep the tonnage of the hopper content constant. This system has certain advantages, like reaching the maximum tonnage sooner than with CVS, resulting in the pumps to be as low as possible, giving a higher mixture density. De Koning (1977) has compared both systems.
The sedimentation in the hopper occurs during the phases 5, 6, 7 and 8. During phase 5 the hopper is filled with mixture until the overflow level is reached. During this phase 100% of the soil is assumed to stay in the hopper and settle. When the overflow level is reached, phase 6, depending on the grain distribution, a specified percentage of the soil will not settle and will leave the hopper via the overflow. During this phase scouring does not have much influence on the sedimentation process. When the maximum weight of the hopper contents is reached, the overflow will be lowered continuously in order to keep the weight of the hopper contents constant at its maximum (only CTS system). When the sediment level rises, phase 8, the flow velocity above the sediment increases and scouring will re suspend settled particles. The overflow losses increase with time. The transition between phase 5 and 6 is very sharp, as is the transition between the phases 6 and 7 for the graph of the total load, but this does not exist in the graph of the effective load (Figure 1-10). However, the transition between the phases 7 and 8 is not necessarily very sharp. When this transition occurs depends on the grain distribution of the soil dredged. With very fine sands this transition will be near the transition between phases 6 and 7, so phase 7 is very short or may not occur at all. With very coarse sands and gravel scouring is minimal, so phase 8 is hardly present. In this case the sediment level may be higher than the overflow level. With silt the phases 7 and 8 will not occur, since after reaching the overflow level the overflow losses will be 100%.

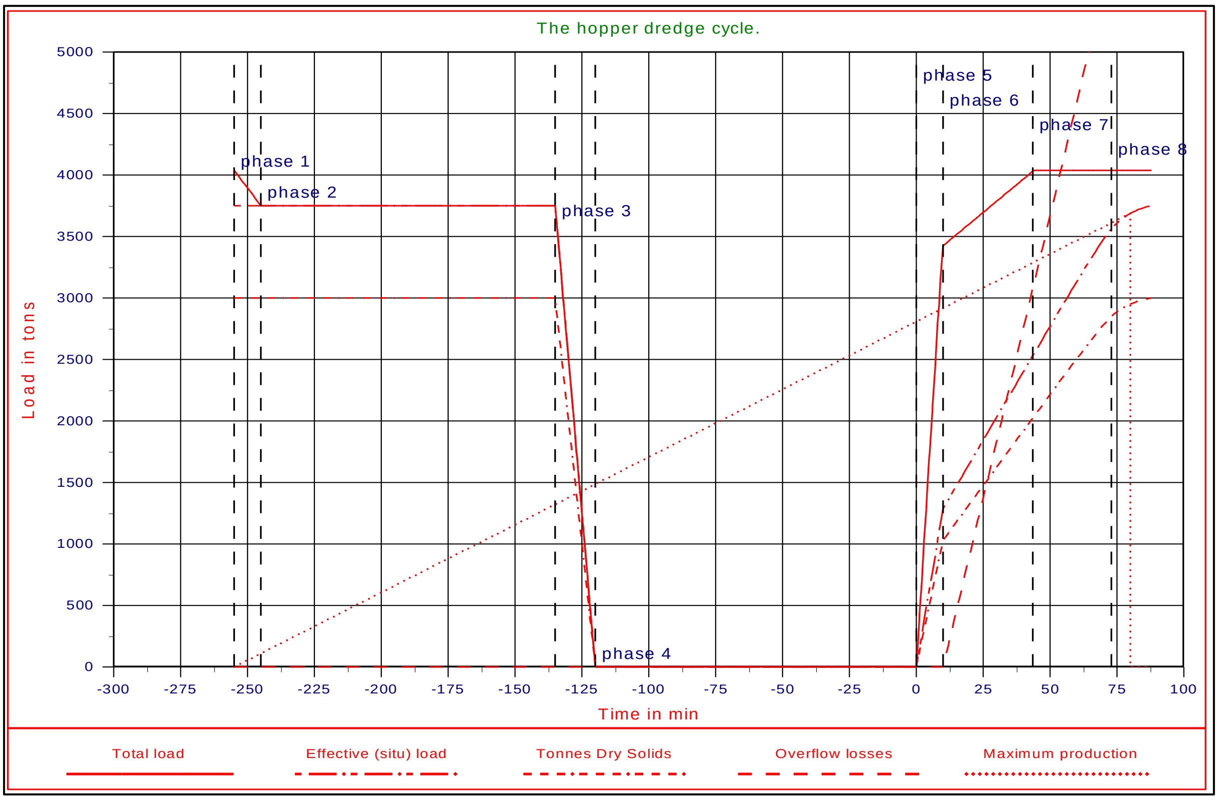

Figure 1-9: The loading cycle of a TSHD.

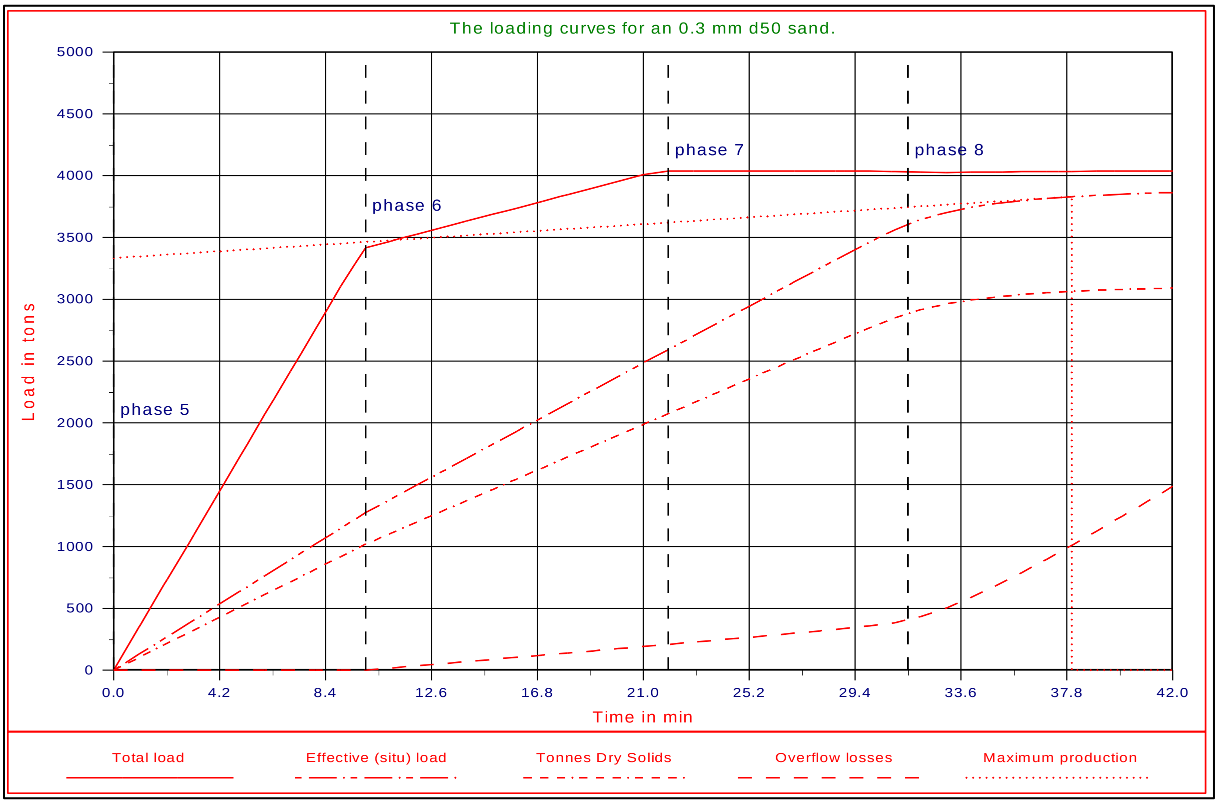

Figure 1-10: The loading part of the cycle of a TSHD.

So far the total load in the hopper has been described. A contractor is, of course, interested in the "Tonnes Dry Solids" (TDS) or situ cubic meters. The total load or gross load consists of the sediment with water in the pores and a layer of water or mixture above the sediment. The TDS consists of the weight of the soil grains only. The net weight in the hopper consists of the weight of the sediment, including the weight of the pore water. If the porosity of the sediment is considered to be equal to the in-situ porosity, then the volume of the sediment in the hopper equals the removed situ-volume. Although, in practice, there will be a difference between the in-situ porosity and the sediment porosity, here they will be considered equal. The net weight (weight of the sediment $\mathbf{W_s}$) is equal to the weight in the hopper $\mathbf{W_h}$ minus the weight of the water above the sediment $\mathbf{W_w}$:

$$\mathbf{W_s = W_h - W_w} \tag{1-1}$$

The net volume (volume of the sediment $\mathbf{V_s}$) is equal to the volume of the hopper $\mathbf{V_h}$ minus the volume of the water above the sediment $\mathbf{V_w}$.

$$\mathbf{V_s = V_h - V_w} \tag{1-2}$$

Multiplying the volumes with the densities gives:

$$\mathbf{V_s \cdot \rho_s = W_h - V_w \cdot \rho_w \quad and \quad V_w = V_h - V_s} \tag{1-3}$$

$$\mathbf{V_s \cdot \rho_s = W_h - (V_h - V_s) \cdot \rho_w} \tag{1-4}$$

$$\mathbf{V_s \cdot (\rho_s - \rho_w) = W_h - V_h \cdot \rho_w} \tag{1-5}$$

Rearranging the terms of equation (1-5) gives an expression for the volume of situ cubic meters.

$$\mathbf{V_s = \frac{(W_h - V_h \cdot \rho_w)}{(\rho_s - \rho_w)}} \tag{1-6}$$

Multiplying the situ volume $\mathbf{V_s}$ with the situ density $\boldsymbol{\rho_s}$ gives for the situ weight $\mathbf{W_s}$:

$$\mathbf{W_s = V_s \cdot \rho_s = \frac{(W_h - V_h \cdot \rho_w) \cdot \rho_s}{(\rho_s - \rho_w)}} \tag{1-7}$$

To find the weight of the sand grains only (without the pore water), the situ density $\boldsymbol{\rho_s}$ has to be replaced by the quarts density (or particle density) $\boldsymbol{\rho_q}$:

$$\mathbf{TDS = W_s \cdot \frac{\rho_s - \rho_w}{\rho_q - \rho_w} \cdot \frac{\rho_q}{\rho_s} = \frac{(W_h - V_h \cdot \rho_w) \cdot \rho_q}{(\rho_q - \rho_w)}} \tag{1-8}$$

The net weight (situ weight) according to equation (1-7) can be approximated by the total weight of the load in the hopper minus the weight of the same volume of water and the result multiplied by 2. For the TDS this factor is about 1.2, according to equation (1-8). This is of course only valid for a specific density of the sediment of 2 tons per cubic meter.

With these equations the hopper cycle for the net weight and the TDS can be derived, this is shown in Figure 1-9 and Figure 1-10. The hopper dredge is optimally loaded, when the effective load (weight) or the TDS divided by the total cycle time $\mathbf{dW_s/dt}$ reaches its maximum. This is shown in Figure 1-9 and Figure 1-10 and is the reason for the starting point of the loading cycle in Figure 1-9.

1.3 The Calculation Model

Consider a rectangular hopper of width **W**, height **H** and length **L**. A mixture with a mixture density ρ_m and with a specified grain distribution is being dredged. Depending on the operational conditions such as dredging depth, the pump system installed, the grain distribution (PSD, Particle Size Distribution) and mixture density ρ_m, a mixture flow **Q** will enter the hopper. If the porosity **n** of the sediment is known, the flow of sediment can be determined according to:

The mass flow of the mixture into the hopper is:

$$Q_{in} \cdot \rho_m = Q_{in} \cdot (\rho_w \cdot (1-C_v) + \rho_q \cdot C_v) \tag{1-9}$$

The mass flow of the solids into the hopper is now:

$$\frac{dTDS}{dt} = Q_{in} \cdot \rho_q \cdot \frac{(\rho_m - \rho_w)}{(\rho_q - \rho_w)} = Q_{in} \cdot C_v \cdot \rho_q \tag{1-10}$$

From this, the mass flow of situ sediment into the hopper is:

$$\frac{dW_s}{dt} = Q_{in} \cdot C_v \cdot (\rho_q + e \cdot \rho_w) \tag{1-11}$$

With:

$$e = \frac{n}{(1-n)} \tag{1-12}$$

Part of this mass flow will settle in the hopper and another part will leave the hopper through the overflow. The ratio between these parts depends on the phase of the loading process. During phase 5 the hopper is loaded to the overflow level, so the mass flow into the hopper will stay in the hopper. This means that the total settling efficiency η_b during this phase equals 1. During phase 6 the loading continues until the maximum load in the hopper is reached (CTS). If scouring does not occur, the mass flow that will settle into the sediment can be calculated with equation (1-13) and (1-14), where the settling efficiency η_b should be determined with equation (2-26) and (2-27), Chapter 2:.

The mass flow of the solids staying in the hopper is now:

$$\frac{dTDS}{dt} = Q_{in} \cdot C_v \cdot \rho_q \cdot \eta_b \tag{1-13}$$

From this, the mass flow of situ sediment into the hopper is:

$$\frac{dW_s}{dt} = Q_{in} \cdot C_v \cdot (\rho_q + e \cdot \rho_w) \cdot \eta_b \tag{1-14}$$

During phase 7 the loading continues, but with a CTS, the overflow is lowered to ensure that the total weight in the hopper remains constant. As scour does not yet occur, the above equation is still valid. During phase 8 scouring occurs. If scouring does occur, the mass flow that will settle into the sediment can also be calculated with equation (1-13) and (1-14), but the settling efficiency should be determined with equation (2-26) and (2-27) taking into account the effect of scouring. Scouring is the cause of increasing overflow losses. Scour depends upon the velocity of the flow above the sediment. Since in a hopper the sediment is not removed, the sediment level rises during the loading of the hopper. This means that the height of the mixture flow above the sediment decreases during the loading process, resulting in an increasing flow velocity. The scour velocity can now be determined by:

$$s_s = \frac{Q_{in}}{B \cdot H_w} \tag{1-15}$$

The height of the water/mixture layer H_w above the sediment, is equal to the overflow height **H** minus the sediment height H_s:

$$H_w = H - H_s = H - \frac{W_s}{\rho_s \cdot W \cdot L} \tag{1-16}$$

The overflow height **H** is a constant for a Constant Volume System (CVS), but this height changes for a CTS, because the overflow is lowered from the moment, the maximum weight in the hopper is reached. If a maximum weight W_m is considered, the height of the layer of water above the sediment H_w for a CTS can be determined by:

$$H_w = \frac{W_m - \rho_S \cdot H_s \cdot B \cdot L}{\rho_W \cdot B \cdot L} \tag{1-17}$$

The hopper loading curve can now be determined by first calculating the time required to fill the hopper (phase 6), given a specified mixture flow Q_{in}. From the mixture density ρ_m the mass and given a specified porosity, the volume of the sediment can be calculated. From this point the calculations are carried out in small time steps (phases 7 and 8). In one time step, first the height of the sediment and the height of the water layer above the sediment are determined. The height of the water layer can be determined with equation (1-16) for a CVS hopper and equation (1-17) for a CTS hopper. With equation (1-15) the scour velocity can now be determined. Using equations (2-25) the fraction of the grains that will be subject to scour can be determined. If this fraction p_s is zero equation (2-20) has to be used to determine the mass flow that will stay in the hopper. If this fraction is not equal to zero equation (2-26) has to be used. Equations (1-13) and (1-14) can now be used to determine the mass flow. This mass flow multiplied by the time step results in an increment of the sediment mass that is added to the already existing mass of the sediment. The total sediment mass is the starting point for the next time step. This is repeated until the overflow losses are 100%. When the entire loading curve is known, the optimum loading time can be determined. This is shown in Figure 1-9, where the dotted line just touches the loading curve of the effective (situ) load or the TDS. The point determined in this way gives the maximum ratio of effective load or TDS in the hopper and total cycle time. In chapter 2 and chapter 3 the determination of the settling efficiency η_b will be discussed in detail.

1.4 The Layer Thickness of the Layer of Water above Overflow Level

Where an obstacle is constructed on the bottom of an open channel, the water surface is raised and passes over it. Structures of this type are called weirs. Aside from special cases, flow over weirs may be regarded as steady, i.e. unchanging with respect to time, and suddenly varied, as in most hydraulic structures. The most important problem arising in connection with weirs is the relationship between the discharge over the weir and the characteristics of the weir. Many authors have suggested various relationships (e.g. Poleni, Weissbach, Boussinesq, Lauck, Pikalow) generally along the same theoretical lines and with similar results. So it seems satisfactory to introduce only the relationship of Weissbach.

$$Q_{out} = \frac{2}{3} \cdot C_e \cdot b \cdot \sqrt{2 \cdot g} \left(\left(h + \frac{v^2}{2 \cdot g} \right)^{3/2} - \left(\frac{v^2}{2 \cdot g} \right)^{3/2} \right) \tag{1-18}$$

If **h/(M+h)** tends towards zero (because **h** is small compared to **M**) then $v^2/2gh$ also tends towards zero; so a simplified relationship can be reached as introduced first by Poleni about 250 years ago:

$$Q_{out} = \frac{2}{3} \cdot C_e \cdot b \cdot h \cdot \sqrt{2 \cdot g \cdot h} \tag{1-19}$$

The above equation (1-19) gives the relation between the layer thickness h and the flow Q_{out} for the stationary process. During the dredging process of a TSHD however, the process is not always stationary. At the start of the loading process when the overflow level is reached the layer of water will build up, while at the end when the pumps stop the layer thickness will decrease to zero. If the TSHD makes turns and the poor mixture is pumped overboard directly, also the layer thickness will decrease and as soon as the mixture is pumped back in the hopper the layer will build up again.

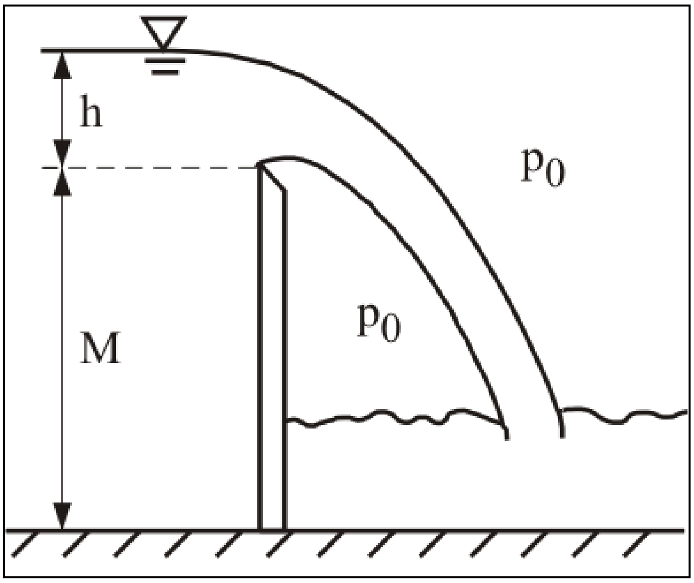

Figure 1-11: A sharp crested weir.

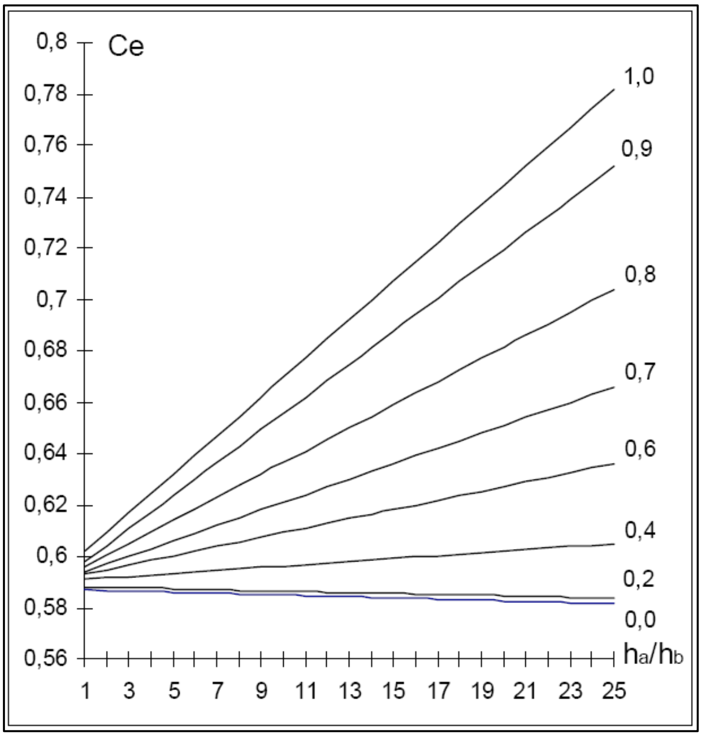

Figure 1-12: Values for the coefficient C_e as a function of h_a/h_b=h/M.

First the increase of the layer thickness will be considered. This increase per unit of time multiplied by the width and the length of the hopper equals the difference between the flow into the hopper and the flow leaving the hopper through the overflow according to:

$$\mathbf{b \cdot L \cdot \frac{dh}{dt} = Q_{in} - Q_{out}} \tag{1-20}$$

Substituting equation (1-19) in this equation gives a non-linear differential equation of the first order for the layer thickness **h**.

$$\mathbf{b \cdot L \cdot \frac{dh}{dt} = Q_{in} - C_e \cdot \frac{2}{3} \cdot \sqrt{2 \cdot g} \cdot b \cdot h^{3/2}} \tag{1-21}$$

This equation can be solved numerically, for example in Excel, using the starting condition **t=0**, **h=0** and the following two equations:

$$\Delta \mathrm{h} = \frac{\mathrm{Q_{in}} - \mathrm{C_e} \cdot \frac{2}{3} \cdot \sqrt{2 \cdot \mathrm{g}} \cdot \mathrm{b} \cdot \mathrm{h}^{3/2}}{\mathrm{b} \cdot \mathrm{L}} \cdot \Delta \mathrm{t} \tag{1-22}$$

$$\mathrm{h_{i+1}} = \mathrm{h_i} + \Delta \mathrm{h} \tag{1-23}$$

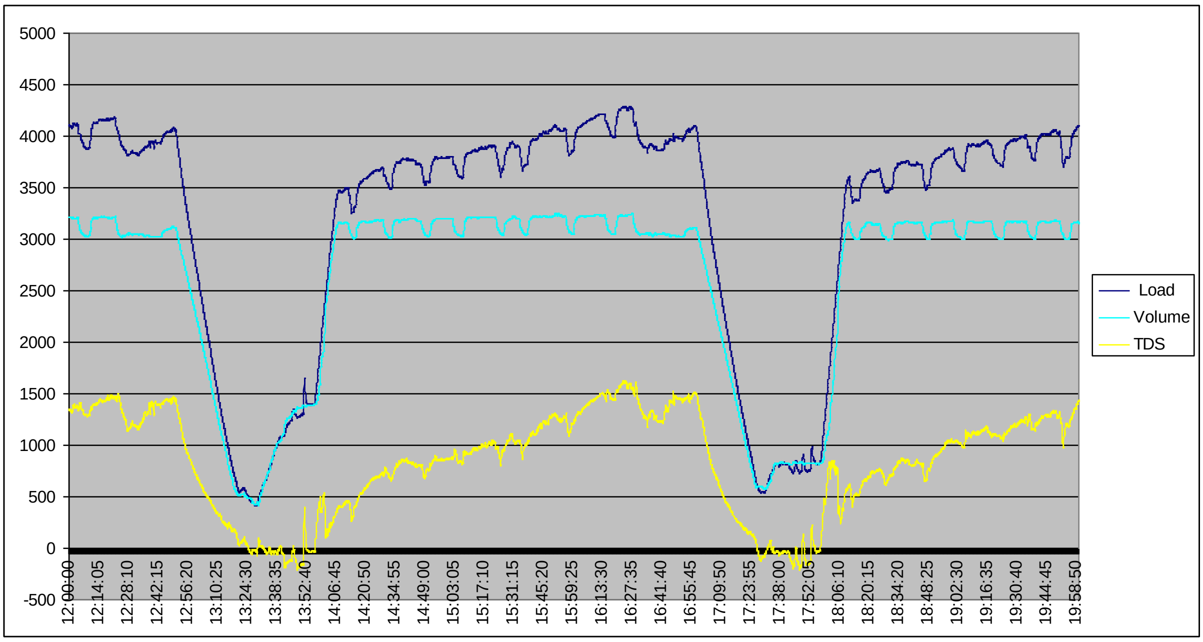

Figure 1-13: An example of a loading cycle of a TSHD with many turns.

In the equilibrium situation where $\mathbf{Q_{in}}$=$\mathbf{Q_{out}}$, the maximum layer thickness $\mathbf{h_{max}}$ is found according to:

$$\mathrm{h_{max}} = \left(\frac{\mathrm{Q_{in}}}{\mathrm{C_e} \cdot \frac{2}{3} \sqrt{2 \cdot \mathrm{g}} \cdot \mathrm{b}} \right)^{2/3} = \left(\frac{\mathrm{Q_{in}}}{2.95 \cdot \mathrm{C_e} \cdot \mathrm{b}} \right)^{2/3} \tag{1-24}$$

From the start, **t=0**, until the maximum layer thickness is reached, $\mathbf{h_{max}}$, the layer thickness **h** is a function of time that can be approximated according to:

$$\mathrm{h(t)} = \left(\frac{\mathrm{Q_{in}}}{2.95 \cdot \mathrm{C_e} \cdot \mathrm{b}} \right)^{2/3} \cdot \left(1 - \mathrm{e}^{\frac{-\mathrm{t}}{0.452 \cdot \mathrm{L} \cdot \left(\frac{2.95 \cdot \mathrm{C_e} \cdot \mathrm{b}}{\mathrm{Q_{in}}} \right)^{1/3}}} \right) = \mathrm{h_{max}} \cdot \left(1 - \mathrm{e}^{-\frac{\mathrm{t}}{\tau}} \right) \tag{1-25}$$

$$\tau = 0.452 \cdot \mathrm{L} \cdot \left(\frac{2.95 \cdot \mathrm{C_e} \cdot \mathrm{b}}{\mathrm{Q_{in}}} \right)^{1/3} = 0.452 \cdot \mathrm{L} \cdot \mathrm{h_{max}^{-1/2}} \tag{1-26}$$

The decrease of the layer thickness h when the pumps are stopped or the poor mixture is pumped overboard follows from equation (1-20) when $\mathbf{Q_{in}}$ is set to zero, this can be approximated by:

$$\Delta \mathrm{h} = \frac{-\mathrm{C_e} \cdot \frac{2}{3} \cdot \sqrt{2 \cdot \mathrm{g}} \cdot \mathrm{b} \cdot \mathrm{h}^{3/2}}{\mathrm{b} \cdot \mathrm{L}} \cdot \Delta \mathrm{t} \tag{1-27}$$

$$\mathrm{h_{i+1}} = \mathrm{h_i} + \Delta \mathrm{h} \tag{1-28}$$

Solving this gives:

$$h(t) = h_{max} - \frac{h_{max}}{\left(1 + C_d \cdot h_{max}^{2/3} \cdot t^{4/3}\right)} \quad \text{with:} \quad C_d = \frac{(3.27 + 0.0486 \cdot b)}{b^{0.22}} \cdot L^{-1.284} \qquad \textbf{(1-29)}$$

Figure 1-15 shows the discharge and the loading of the layer of water above the overflow level for a hopper with a length of 40 m, a width of 9 m and a height of 9 m and a flow of 5.8 m^3/sec. Both the exact solution and the approximation are shown versus an in situ measurement. The effective width of the overflow is assumed to be equal to the width of the hopper.

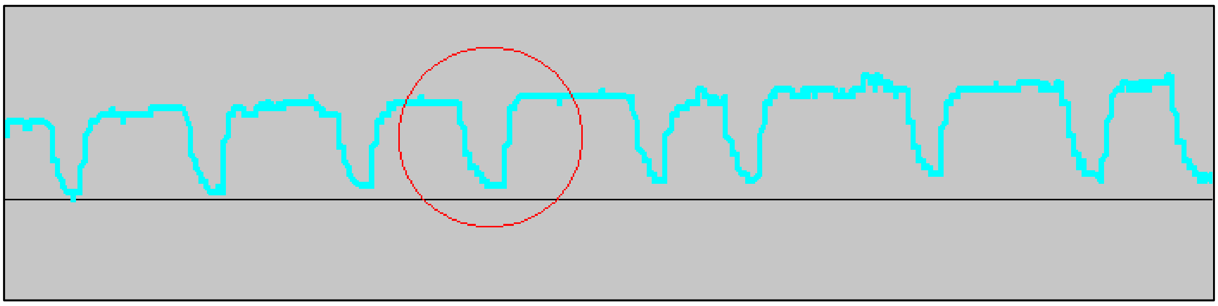

Figure 1-14: A close up of the hopper volume registration.

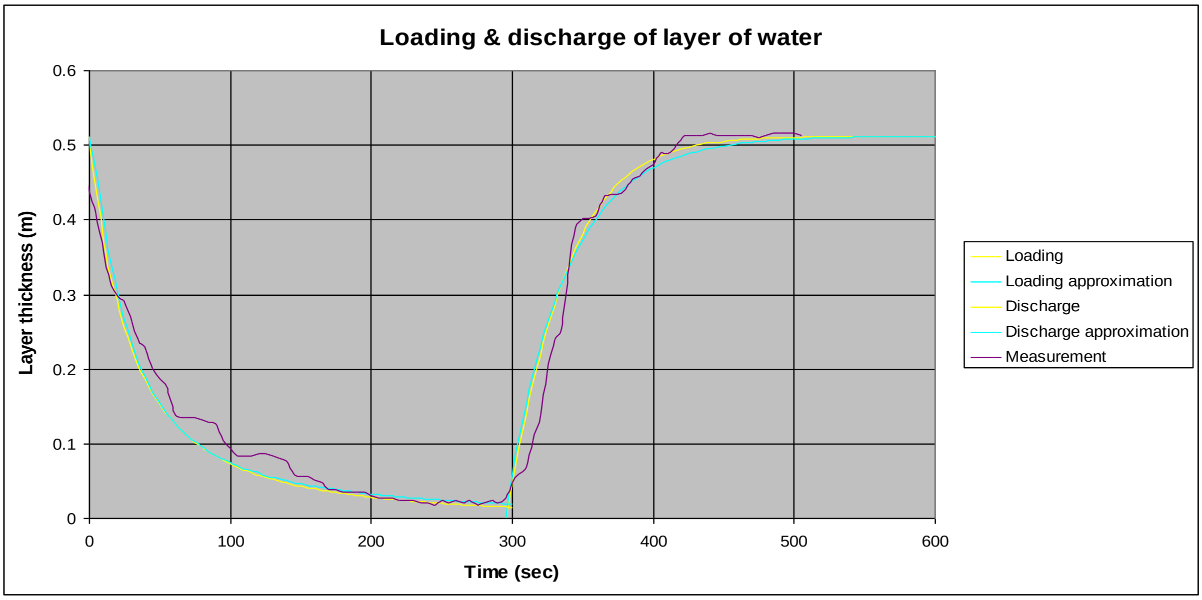

Figure 1-15: The layer thickness during a turn, registration and approximation.

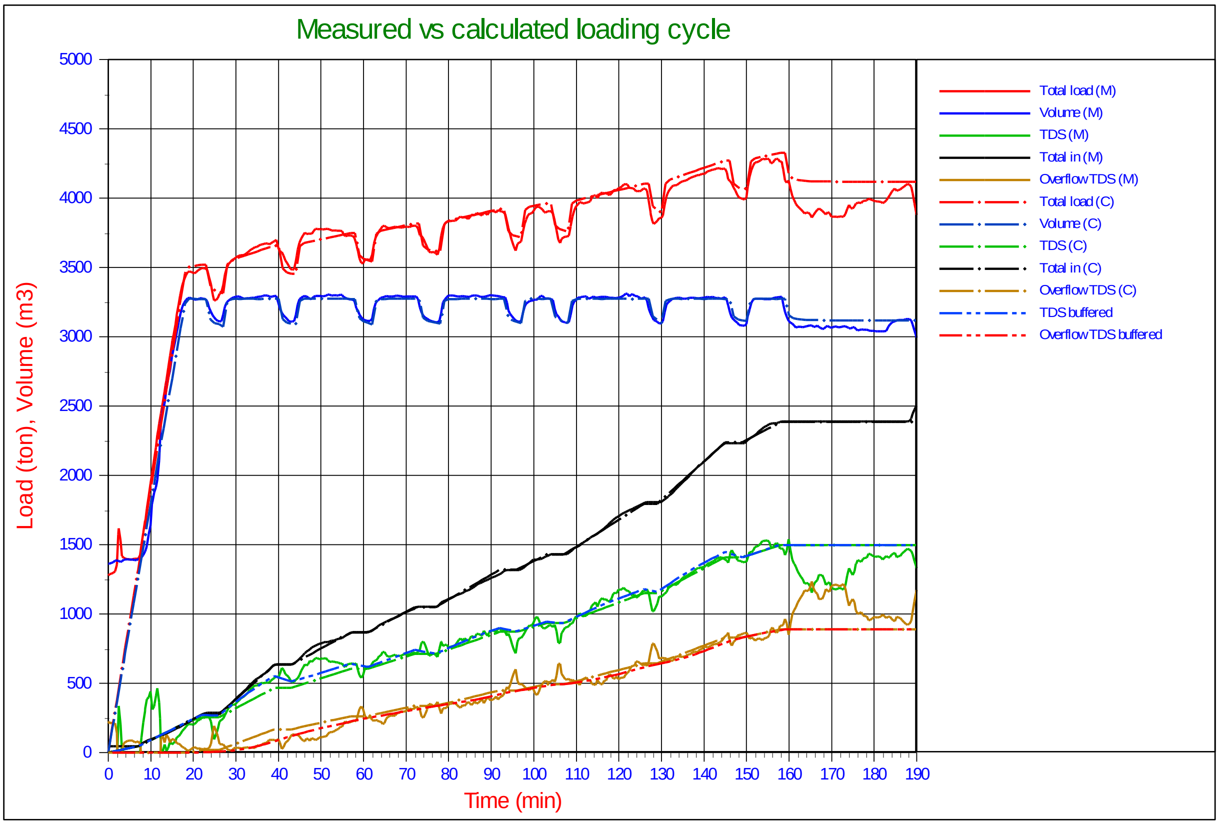

Figure 1-16: The cycle as registered is simulated with the theoretical model.

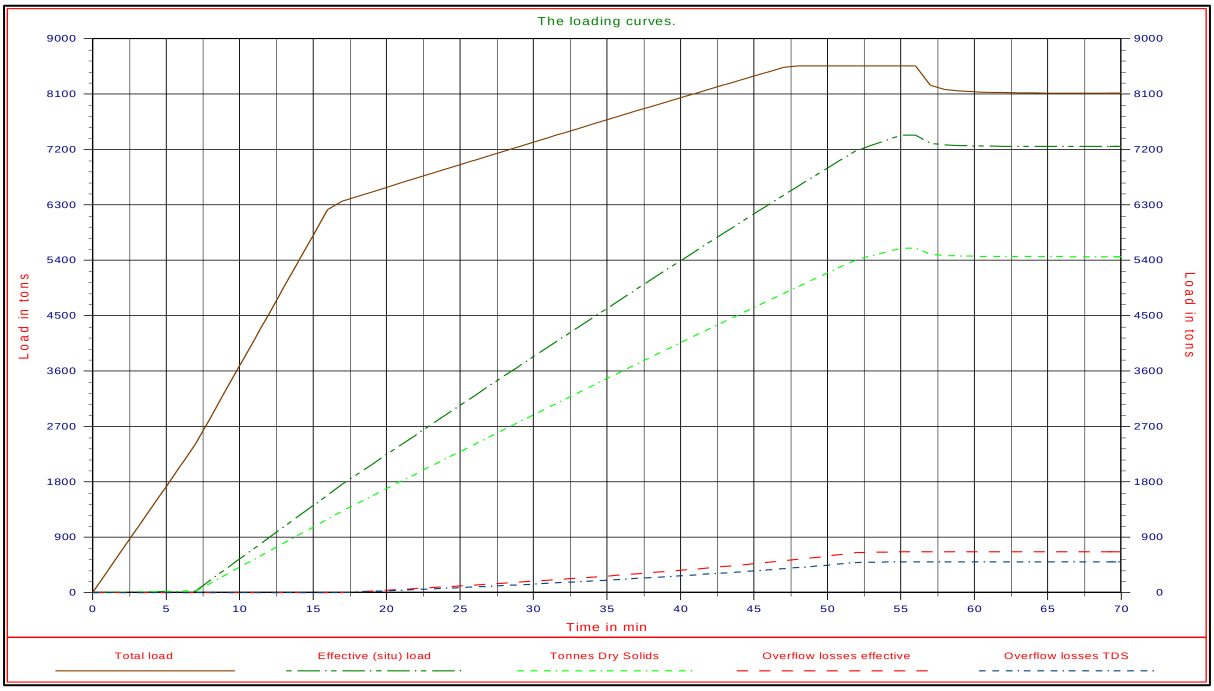

Figure 1-17: The decreasing of the height of the layer of water above the overflow at the end of the cycle.

1.5 The Storage Effect

In the Miedema & Vlasblom model (1996) upon entrance of a particle in the hopper it is decided whether the particle will settle or not. In reality the particles that will not settle first have to move through the hopper before they reach the overflow. This means that these particles are part of the TDS in the hopper during the time they stay in the hopper. Ooijens (1999) discovered that using the time delay to determine the overflow losses improved the outcome of the Miedema & Vlasblom model (1996) considerably. Overflow losses with time delay can be derived from the overflow losses without a time delay according to the following equation:

$$\mathbf{ov_b(t) = \frac{1}{\tau} \cdot \int_{t-\tau}^{t} ov_c(t) \cdot dt + \frac{s}{\tau} \cdot \int_{0}^{t-\tau} (ov_c(t) - ov_b(t)) \cdot dt} \qquad \textbf{(1-30)}$$

The first term in equation (1-30) gives the time delay for the situation with a constant bed height. Since the height of the bed increases during the loading process, the rising bed pushes part of the mixture out of the hopper. This is represented by the second term on the right hand.

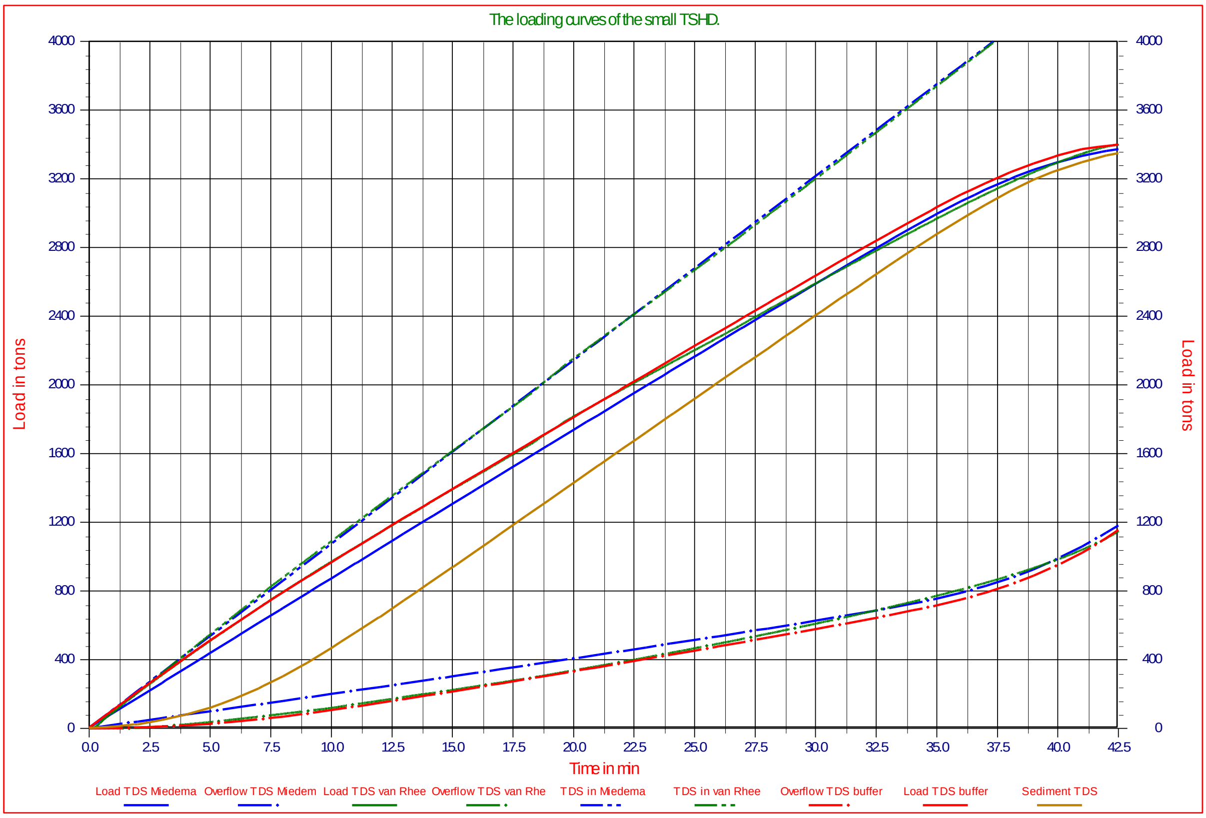

Figure 1-18: Loading curves according to Miedema & van Rhee (2007) with and without time delay.

Figure 1-18 shows the loading and overflow curves with and without the time delay or storage effect for a case considered by Miedema & van Rhee (2007). Table 1-1 gives the main data of the TSHD used in this case.

Table 1-1: The data of the TSHD used.

Hopper	Load	Volume	Length	Width	Empty height	Flow	Hopper load v_0	Mixture density
	ton	m^3	m	m	m	m^3/sec	m/sec	ton/m^3
Small	4400	2316	44.0	11.5	4.577	4	0.0079	1.3

From top to bottom Figure 1-18 contains 9 curves. The first two curves (blue and green) are almost identical and represent the TDS that enters the hopper. Since the flow and the density are constant, these curves are straight. The 3rd curve (red) represents the total TDS in the hopper according to the Miedema & Vlasblom (1996) model, so including the TDS that is still in suspension above the sediment of which part will leave the hopper through the overflow. The 4th curve (green) represents this according to van Miedema & van Rhee (2007). The 5th curve (blue) represents the TDS that will stay in the hopper excluding the time delay effect, according to Miedema &

Vlasblom (1996). The 6th (brown) curve represents the TDS in the sediment in the hopper. The 7th curve (blue) is the overflow losses according to Miedema & Vlasblom (1996), so excluding the time delay or buffering effect. The 8th curve (green) represents the overflow losses according to the 2DV model of van Rhee (2002C), which automatically includes the time delay effect. The 9th curve (red) represents the overflow losses according to the Miedema & Vlasblom (1996) model including the time delay effects according to equation (1-30).

1.6 The Hopper of a TSHD as an Ideal Settlement Basin

As stated before, the ideal settlement basin is a rectangular basin with an entrance zone, a settlement and sedimentation zone and an overflow zone. The hopper geometry and configuration aboard of the TSHD can be quite different from the ideal situation, so a method to schematize the hopper dimensions is required.

1. The height **H** of the hopper can be defined best as the hopper volume divided by the hopper area **L·W**. This means that the base of the ideal hopper, related to the maximum overflow height is at a higher level than the ship's base. This assumption results in a good approximation at the final phases (7 and 8) of the loading process, while in phase 6 of the loading process the hopper is filled with mixture and so the material stays in the hopper anyway.

2. Near the loading chute of the hopper or in cases where a deep loading system is used, the turbulence of the flow results in a good and sufficient distribution of the concentration and particle size distribution over the cross-section of the hopper, so the entrance zone can be kept small. For example between the hopper bulkhead and the end of the loading chute.

3. In the ideal settlement basin there are no vertical flow velocities except those resulting from turbulence. However in reality vertical velocities do occur near the overflow, therefore it is assumed that the overflow zone starts where the vertical velocities exceed the horizontal velocities. An estimate of where this will occur can easily be made with a flow net.

4. Although the presence of beams and cylinder rods for the hopper doors does increase the turbulence, it is the author’s opinion, that an additional allowance is not required, neither for the hopper load parameter, nor for the turbulence parameter.

5. As is shown in Figure 1-6 and Figure 1-7, a density current may occur during the loading phases 6 and 7, resulting in a non-uniform velocity and density distribution. This does not affect the so called hopper load parameter as is proven in Chapter 2:, so for the schematization of the hopper a uniform velocity and density distribution are assumed.

6. The validity of the schematizations and simplifications will be proven by some examples with model and prototype tests.

Chapter 2: The Modified Camp Model

Sedimentation is a treatment process where suspended particles, like sand and clay are re-moved from the water. Sedimentation can take place naturally in reservoirs or in compact settling installations. Sedimentation is applied in groundwater treatment installations for backwash water treatment and in TSHD's. In horizontal flow settling tanks water is uniformly distributed over the cross-sectional area of the tank in the inlet zone. A stable, non-turbulent, flow in the settling zone takes care for the settling of suspended matter in the settling zone. The sludge accumulates on the bottom, or is continuously removed. In the outlet zone the settled sludge must be prevented from being re-suspended and washed out with the effluent. Sedimentation occurs because of the difference in density between suspended particles and water. The following factors influence the sedimentation process: density and size of suspended particles, water temperature, turbulence, stability of flow, bottom scour and flocculation:

- Density, the higher the density of the particles, the faster the particles settle
- Size, the larger the particles are, the faster they settle
- Temperature, the lower the temperature of the water is, the higher the viscosity is, so the slower the particles settle
- Turbulence, the more turbulent the flow is, the slower the particles settle
- Stability, instability can result in short circuit flow, influencing the settling of particles
- Bottom scour, by bottom scour settled particles are re-suspended and washed out with the effluent

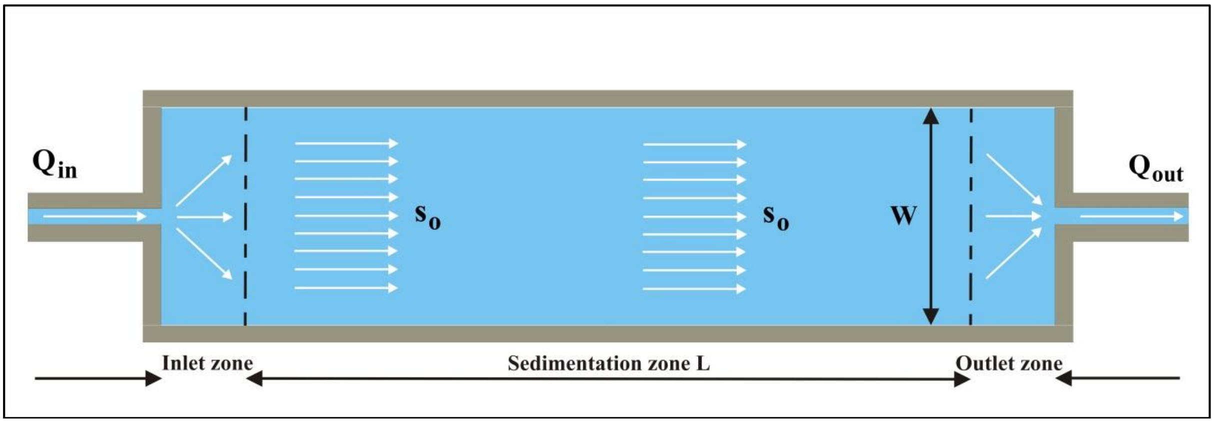

Figure 2-1: The top view of the ideal basin.

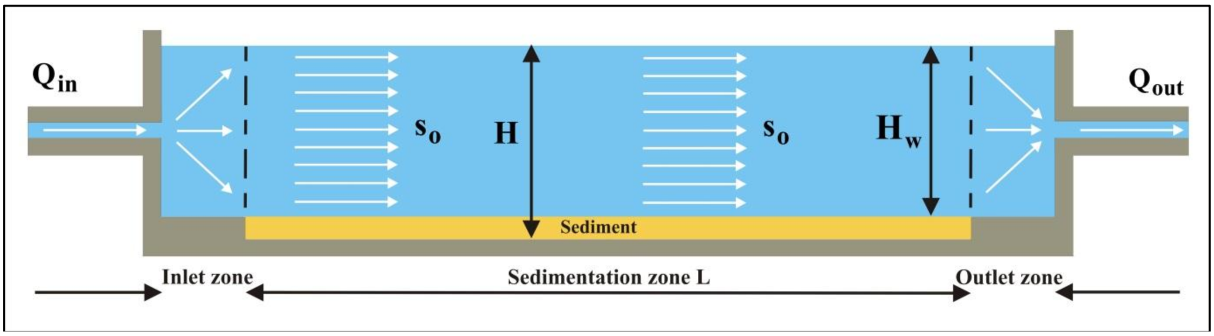

Figure 2-2: The side view of the ideal basin.

The ideal settlement basin consists of an entrance zone where the solid/fluid mixture enters the basin and where the grain distribution is uniform over the cross-section of the basin, a settlement zone where the grains settle into a sediment zone and a zone where the cleared water leaves the basin, the overflow zone. It is assumed that the grains are distributed uniformly and are extracted from the flow when the sediment zone is reached. Each particle stays in the basin for a fixed time and moves from the position at the entrance zone, where it enters the basin towards the sediment zone, following a straight line. The slope of this line depends on the settling velocity v and the flow velocity above the sediment $\mathbf{s_o}$. Figure 2-1 shows a top view of the ideal settlement basin. Figure 2-2 shows the side view and Figure 2-3, Figure 2-4 and Figure 2-5 the path of individual grains. All particles with a diameter $\mathbf{d_o}$ and a settling velocity $\mathbf{v_o}$ will settle, a particle with this diameter, entering the basin at the top, reaches the end of the sediment zone. Particles with a larger diameter will all settle, particles with a smaller diameter will partially settle. Miedema & Vlasblom (1996) adapted the Camp model to be used for hopper sedimentation. The biggest difference between the original Camp (1936), (1946) and (1953) model and the Miedema & Vlasblom model is the height $\mathbf{H_w}$ above the sediment zone. In the Camp model this is a fixed height, in the Miedema & Vlasblom model this height decreases during the loading process.

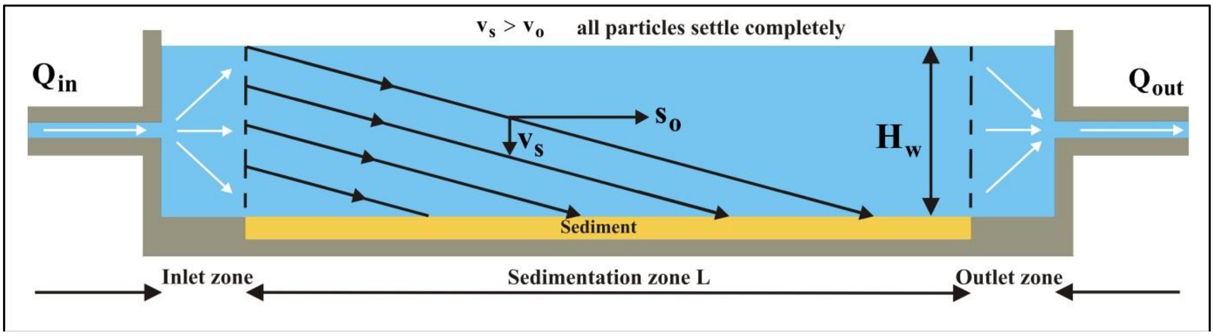

Figure 2-3: The path of a particle with a settling velocity greater than the hopper load parameter.

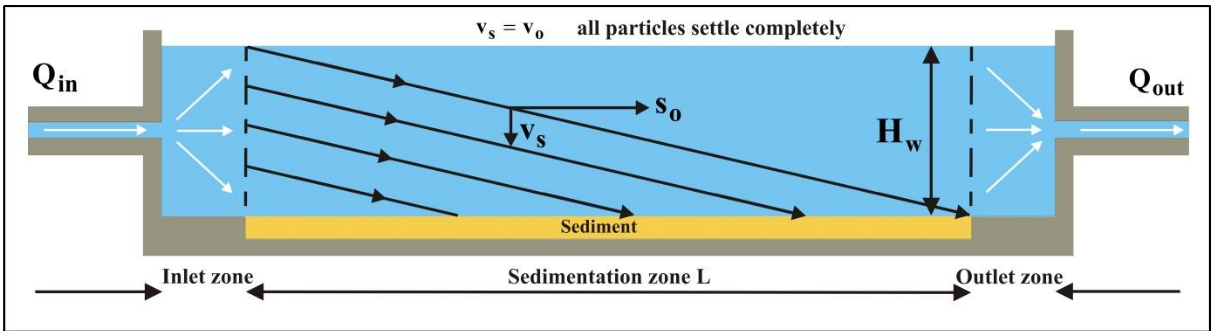

Figure 2-4: The path of a particle with a settling velocity equal to the hopper load parameter.

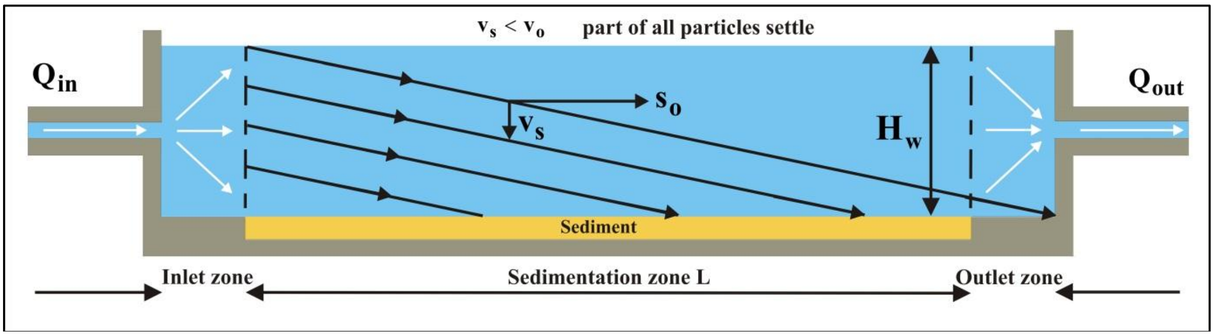

Figure 2-5: The path of a particle with a settling velocity smaller than the hopper load parameter.

The average horizontal velocity $\mathbf{s_o}$ in the basin, when the height $\mathbf{H_w}$ above the sediment is known (see equations (1-16) and (1-17)), equals to:

$$\mathbf{s_o = \frac{Q_{in}}{W \cdot H_w}} \qquad \textbf{(2-1)}$$

The hopper load parameter $\mathbf{v_o}$ is defined as the settling velocity of a particle that enters the basin (hopper) at the top and reaches the sediment at the end of the basin, after traveling a distance **L,** see Figure 2-4. This can be determined according to (with a uniform velocity distribution):

$$\mathbf{\frac{v_o}{s_o} = \frac{H_w}{L}} \quad \text{thus:} \quad \mathbf{v_o = s_o \cdot \frac{H_w}{L} = \frac{Q_{in}}{W \cdot L}} \qquad \textbf{(2-2)}$$

If the velocity distribution is non-uniform, like in Figure 2-6, the hopper load parameter can be derived by integrating the horizontal velocity **s(z)** over the time the particle, entering at the top of the basin, needs to reach the sediment at the end, so traveling a horizontal distance **L**.

$$\int_0^T s(z)\cdot dt = L \tag{2-3}$$

With:

$$T = \frac{H_w}{v'_o} \quad , \quad z = v'_o\cdot t \quad , \quad dz = v'_o\cdot dt \quad , \quad Q_{in} = W\cdot\int_0^{H_w} s(z)\cdot dz \tag{2-4}$$

Equation (2-3) can be written as:

$$\frac{1}{v'_o}\cdot\int_0^{H_w} s(z)\cdot dz = \frac{1}{v'_o}\cdot\frac{Q_{in}}{W} = L \tag{2-5}$$

Thus the hopper load parameter does not change because of a non-uniform velocity distribution.

$$v'_o = \frac{Q_{in}}{W\cdot L} = v_o \tag{2-6}$$

During the transport of a particle from the top of the inlet to the overflow however, the sediment level rises by **$\Delta H = v_{sed}\cdot\Delta t$,** where **$\Delta t$** equals the traveling time of the particle and **v_{sed}** equals the sediment (bed) rise velocity. The thickness of the layer of fluid above the sediment thus decreases from **H_w** when the particle enters the hopper to **H_w-ΔH** when the particle reaches the sediment at the end of the hopper due to the settling velocity of the particle. The average thickness **H_a** of the layer of water above the sediment during the transport of the particle is now:

$$H_a = H_w - 0.5\cdot\Delta H \tag{2-7}$$

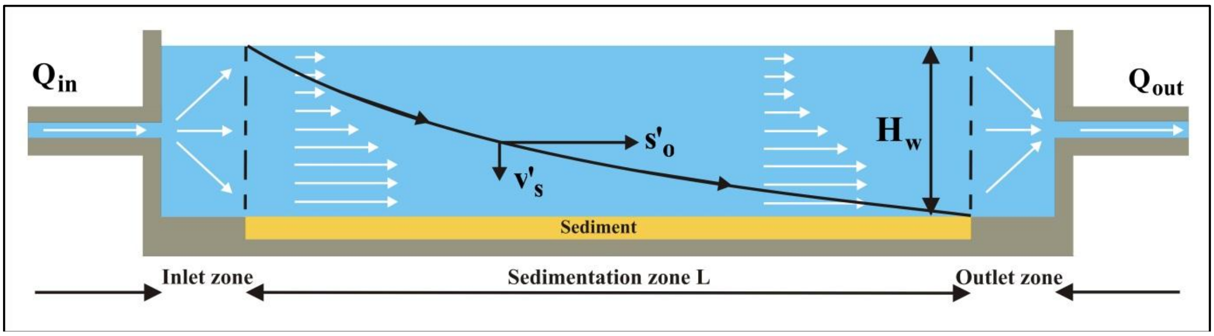

Figure 2-6: The path of a particle with a non-uniform velocity distribution.

The average horizontal velocity **s_o** in the hopper during the stay of the particle in the hopper is thus:

$$s_o = \frac{Q_{in}}{W\cdot(H_w - 0.5\cdot\Delta H)} = \frac{Q_{in}}{W\cdot H_a} \tag{2-8}$$

The time it takes for the particle to be transported over the length of the hopper is thus:

$$\Delta t = \frac{L}{s_o} = \frac{W\cdot L\cdot H_a}{Q_{in}} \tag{2-9}$$

The vertical distance traveled by a particle that enters the hopper at the top and just reaches the sediment at the end of the hopper is (see Figure 2-7):

$$v_{oo}\cdot\Delta t = v_{oo}\cdot\frac{W\cdot L\cdot H_a}{Q_{in}} = H_w - \Delta H = H_a - 0.5\cdot\Delta H \tag{2-10}$$

This gives for the settling velocity of such a particle:

$$\mathbf{v_{oo} = \frac{Q_{in}}{W \cdot L \cdot H_a} \cdot (H_a - 0.5 \cdot \Delta H) = \frac{Q_{in}}{W \cdot L} \cdot \left(1 - \frac{0.5 \cdot \Delta H}{H_a}\right)} \quad \text{(2-11)}$$

With:

$$\mathbf{\Delta H = v_{sed} \cdot \Delta t = v_{sed} \cdot \frac{W \cdot L \cdot H_a}{Q_{in}}} \quad \text{(2-12)}$$

This gives for the modified hopper load parameter:

$$\mathbf{v_{oo} = \frac{Q_{in}}{W \cdot L} - \frac{v_{sed}}{2}} \quad \text{(2-13)}$$

A smaller hopper load parameter means that smaller grains will settle easier. From Figure 2-3 the conclusion can be drawn that grains with a settling velocity greater than $\mathbf{v_o}$ will all reach the sediment layer and thus have a settling efficiency $\mathbf{\eta_g}$ of 1. Grains with a settling velocity smaller then $\mathbf{v_o}$, Figure 2-5, will only settle in the sedimentation zone, if they enter the basin below a specified level. This gives for the modified settling efficiency of the individual grain:

$$\mathbf{\eta_{gg} = \left(\frac{v_s}{v_{oo}}\right)} \quad \text{(2-14)}$$

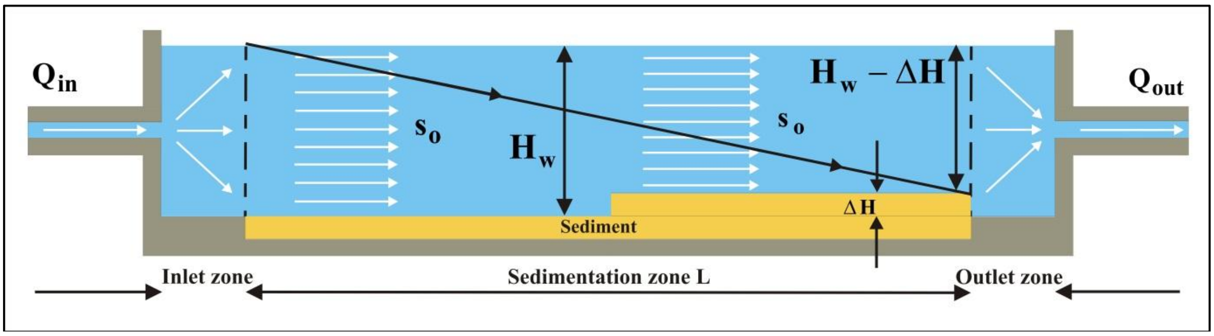

Figure 2-7: The effect of a rising sediment level.

In the case of a non-uniform velocity distribution, Figure 2-6, the settling efficiency can also be defined as the ratio of the horizontal distances traveled in the time a particle needs to reach the sediment, although this is not 100% true because the ratio of the vertical distance traveled gives the exact settling efficiency, it's a good approximation:

$$\mathbf{\eta_g = \left(\frac{L_{v_o}}{L_v}\right)} \quad \text{(2-15)}$$

The horizontal distance traveled by a particle in the time to reach the sediment level is:

$$\mathbf{L_v = \int_0^T s(z) \cdot dt} \quad \text{(2-16)}$$

With:

$$\mathbf{T = \frac{H_w}{v_s} \quad , \quad z = v_s \cdot t \quad , \quad dz = v_s \cdot dt \quad , \quad Q_{in} = W \cdot \int_0^{H_w} s(z) \cdot dz} \quad \text{(2-17)}$$

Equation (2-17) can be written as:

$$\frac{1}{v_s}\cdot\int_0^{H_w} s(z)\cdot dz = \frac{1}{v_s}\cdot\frac{Q_{in}}{W} = L_v \tag{2-18}$$

This also gives a settling efficiency according to:

$$\eta_g = \left(\frac{v_s}{v_o}\right) \tag{2-19}$$

The settling efficiency of a particle with a settling velocity smaller than the hopper load parameter $\mathbf{v_o}$, does not change due to a non-uniform velocity distribution. If the fraction of grains with a settling velocity greater than $\mathbf{v_o}$ equals $\mathbf{p_o}$, then the settling efficiency for a grain distribution $\boldsymbol{\eta_b}$ can be determined by integrating the grain settling efficiency for the whole grain distribution curve, according to Figure 2-8. The blue surface equals the basin settling efficiency according to equation (2-20).

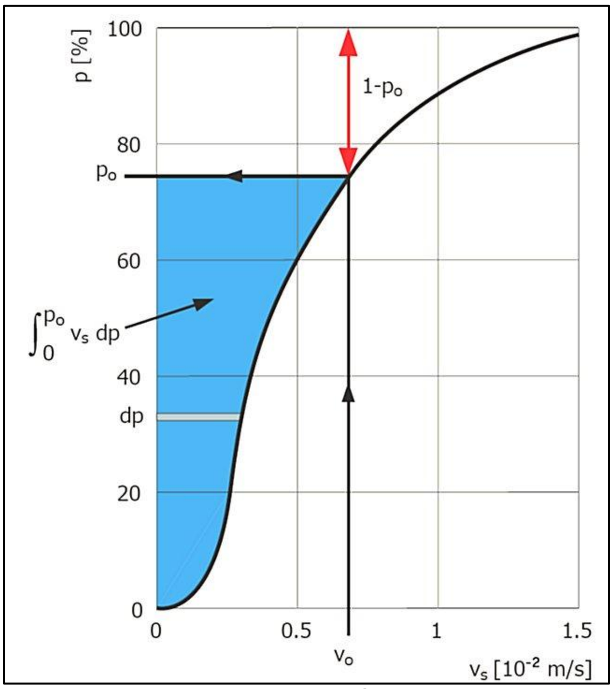

Figure 2-8: Determination of the basin settling efficiency.

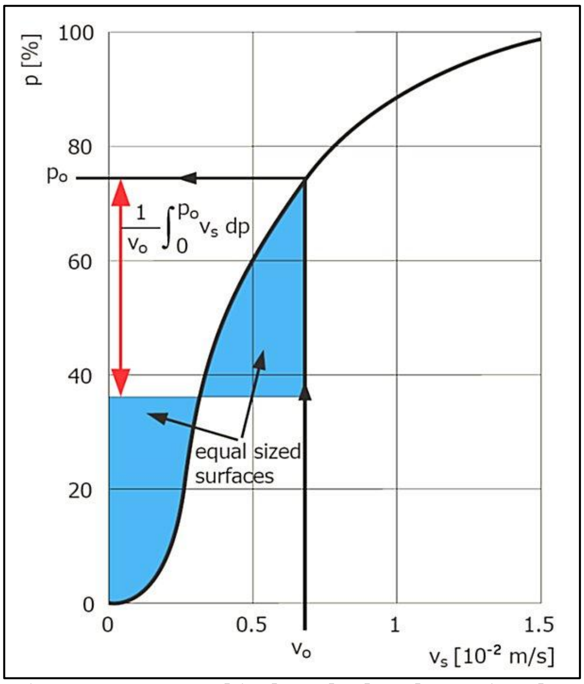

Figure 2-9: A graphical method to determine the settling efficiency.

$$\eta_b = \left(1 - p_o\right) + \int_0^{p_o} \eta_g \cdot dp \tag{2-20}$$

In theory a particle is removed from the water when it reaches the bottom of the settling tank. In practice, however, it is possible that re-suspension of already settled particles occurs.
When the sediment level in the hopper is rising, the horizontal velocity increases and there will be a point where grains of a certain diameter will not settle anymore due to scour. First the small grains will not settle or erode and when the level increases more, also the bigger grains will stop settling, resulting in a smaller settling efficiency. The effect of scour is taken into account by integrating with the lower boundary $\mathbf{p_s}$. The fraction $\mathbf{p_s}$ is the fraction of the grains smaller then $\mathbf{d_s}$, matching a horizontal velocity in the hopper of $\mathbf{s_s}$.

The shear force of water on a spherical particle is:

$$\tau = \frac{1}{4}\cdot\lambda\cdot\frac{1}{2}\cdot\rho_w\cdot s_s^2 \tag{2-21}$$

The shear force of particles at the bottom (mechanical friction) is proportional to the submerged weight of the sludge layer, per unit of bed surface (see Figure 2-10):

$$\mathbf{f = \mu \cdot N = \mu \cdot (1-n) \cdot (\rho_q - \rho_w) \cdot g \cdot d} \quad \textbf{(2-22)}$$

In equilibrium the hydraulic shear equals the mechanical shear and the critical scour velocity can be calculated. The scour velocity for a specific grain with diameter $\mathbf{d_s}$, according to Huisman (1973-1995) and (1980) is:

$$\mathbf{s_s = \sqrt{\frac{8 \cdot \mu \cdot (1-n) \cdot (\rho_q - \rho_w) \cdot g \cdot d_s}{\lambda \cdot \rho_w}}} \quad \textbf{(2-23)}$$

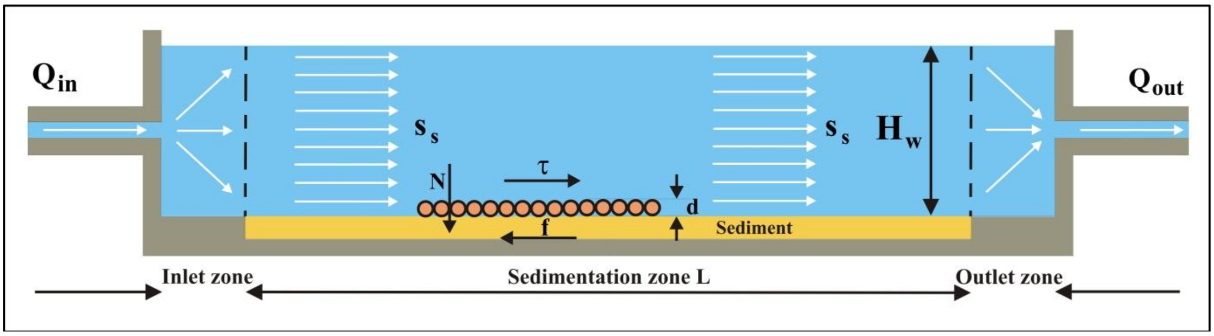

Figure 2-10: The equilibrium of forces on a particle.

With $\mathbf{\mu \cdot (1\text{-}n)=0.05}$ and $\mathbf{\lambda=0.03}$ this gives:

$$\mathbf{s_s = \sqrt{\frac{40 \cdot (\rho_q - \rho_w) \cdot g \cdot d_s}{3 \cdot \rho_w}}} \quad \textbf{(2-24)}$$

The particle diameter of particles that will not settle due to scour (and all particles with a smaller diameter) is:

$$\mathbf{d_s = \frac{3 \cdot \rho_w}{40 \cdot (\rho_q - \rho_w) \cdot g} \cdot s_s^2} \quad \textbf{(2-25)}$$

Knowing the diameter $\mathbf{d_s}$, the fraction $\mathbf{p_s}$ that will not settle due to scour can be found if the PSD of the sand is known. Equation (2-24) is often used for designing settling basins for drinking water. In such basins scour should be avoided, resulting in an equation with a safety margin. For the prediction of the erosion during the final phase of the settling process in TSHD's a more accurate prediction of the scour velocity is required, which will be discussed in another chapter. The settling efficiency $\mathbf{\eta_g}$, but this only occurs at the end of the loading cycle, can now be corrected for scour according to:

$$\mathbf{\eta_b = (1 - p_o) + \int_{p_s}^{p_o} \eta_g \cdot dp} \quad \textbf{(2-26)}$$

When $\mathbf{p_s > p_o}$ this results in:

$$\mathbf{\eta_b = (1 - p_s)} \quad \textbf{(2-27)}$$

Chapter 3: The Influence of Turbulence

For the ideal settlement basin laminar flow is assumed. Turbulent flow will reduce the settling velocity of the grains and thus the total settling efficiency. Whether turbulent flow occurs, depends on the Reynolds number of the flow in the basin. Using the hydraulic radius concept this number is:

$$\mathbf{Re} = \frac{\mathbf{Q_{in}}}{\boldsymbol{\nu} \cdot (\mathbf{W} + 2 \cdot \mathbf{H_w})} \tag{3-1}$$

For a given flow $\mathbf{Qi_n}$ and viscosity $\boldsymbol{\nu}$ the Reynolds number depends on the width $\mathbf{W}$ and the height $\mathbf{H_w}$ of the layer of fluid in the basin. A large width and height give a low Reynolds number. However this does not give an attractive shape for the basin from an economical point of view, which explains why the flow will be turbulent in existing basins.

Dobbins (1944) and Camp (1946) and (1953) use the two-dimensional turbulent diffusion equation to determine the resulting decrease of the settling efficiency.

$$\mathbf{s(z)} \cdot \frac{\partial \mathbf{c}}{\partial \mathbf{x}} = \boldsymbol{\varepsilon}_\mathbf{z} \cdot \frac{\partial^2 \mathbf{c}}{\partial \mathbf{z}^2} + \left(\mathbf{v(c)} + \frac{\partial \boldsymbol{\varepsilon}_\mathbf{z}}{\partial \mathbf{z}} \right) \cdot \frac{\partial \mathbf{c}}{\partial \mathbf{z}} + \boldsymbol{\varepsilon}_\mathbf{x} \cdot \frac{\partial^2 \mathbf{c}}{\partial \mathbf{x}^2} \tag{3-2}$$

Assuming a parabolic velocity distribution instead of the logarithmic distribution, neglecting diffusion in the x-direction and considering the settling velocity independent of the concentration reduces the equation to:

$$\left(\mathbf{s_t} - \mathbf{k} \cdot (\mathbf{h} - \mathbf{z})^2 \right) \cdot \frac{\partial \mathbf{c}}{\partial \mathbf{x}} = \boldsymbol{\varepsilon}_\mathbf{z} \cdot \frac{\partial^2 \mathbf{c}}{\partial \mathbf{z}^2} + \mathbf{v} \cdot \frac{\partial \mathbf{c}}{\partial \mathbf{z}} \tag{3-3}$$

Because of the parabolic velocity distribution, the turbulent diffusion coefficient $\boldsymbol{\varepsilon}_\mathbf{z}$ is a constant. A further simplification is obtained if the velocity $\mathbf{s}$ is assumed constant throughout the depth, meaning that the constant of the parabola $\mathbf{k}$ approaches zero. In this case the turbulent diffusion equation becomes:

$$\frac{\partial \mathbf{c}}{\partial \mathbf{t}} = \mathbf{s} \cdot \frac{\partial \mathbf{c}}{\partial \mathbf{x}} = \boldsymbol{\varepsilon}_\mathbf{z} \cdot \frac{\partial^2 \mathbf{c}}{\partial \mathbf{z}^2} + \mathbf{v} \cdot \frac{\partial \mathbf{c}}{\partial \mathbf{z}} \tag{3-4}$$

Huisman (1973-1995) in his lecture notes derives the diffusion-dispersion equation in a more general form, including longitudinal dispersion.

$$\frac{\partial \mathbf{c}}{\partial \mathbf{t}} + \frac{\partial (\mathbf{s} \cdot \mathbf{c})}{\partial \mathbf{x}} = \frac{\partial}{\partial \mathbf{x}} \cdot \left(\boldsymbol{\varepsilon}_\mathbf{x} \cdot \frac{\partial \mathbf{c}}{\partial \mathbf{x}} \right) + \frac{\partial}{\partial \mathbf{z}} \cdot \left(\mathbf{v} \cdot \mathbf{c} + \boldsymbol{\varepsilon}_\mathbf{z} \cdot \frac{\partial \mathbf{c}}{\partial \mathbf{z}} \right) \tag{3-5}$$

Assuming a steady and uniform flow, the longitudinal dispersion coefficient is independent of $\mathbf{x}$ and the settling velocity $\mathbf{v}$ independent of $\mathbf{z}$. This reduces the equation 18 to:

$$\mathbf{s} \cdot \frac{\partial \mathbf{c}}{\partial \mathbf{x}} = \boldsymbol{\varepsilon}_\mathbf{z} \cdot \frac{\partial^2 \mathbf{c}}{\partial \mathbf{z}^2} + \mathbf{v} \cdot \frac{\partial \mathbf{c}}{\partial \mathbf{z}} + \boldsymbol{\varepsilon}_\mathbf{x} \cdot \frac{\partial^2 \mathbf{c}}{\partial \mathbf{x}^2} \tag{3-6}$$

By means of computations Huisman (1973-1995) shows that the retarding effect of dispersion may be ignored for the commonly applied width to depth ratio 3 to 5. This reduces equation (3-5) to equation (3-2) of Dobbins and Camp.

Groot (1981) investigated the influence of hindered settling and the influence of different velocity distributions using the following equation:

$$\mathbf{s} \cdot \frac{\partial \mathbf{c}}{\partial \mathbf{x}} = \mathbf{v(c)} \cdot \frac{\partial \mathbf{c}}{\partial \mathbf{z}} + \mathbf{c} \cdot \frac{\partial \mathbf{v(c)}}{\partial \mathbf{c}} \cdot \frac{\partial \mathbf{c}}{\partial \mathbf{z}} + \frac{\partial}{\partial \mathbf{z}} \cdot \left(\boldsymbol{\varepsilon}(\mathbf{x}, \mathbf{z}) \cdot \frac{\partial \mathbf{c}}{\partial \mathbf{z}} \right) \tag{3-7}$$

The velocity distribution, the diffusion coefficient distribution and the distribution of the initial concentration did not have a significant influence on the computed results, but the results were very sensitive on the formulation of hindered settling. This formulation of course influences the settling velocity in general. Equation (3-6) can be solved analytically using separation of variables. The boundary conditions used by Camp and Dobbins describe the rate of vertical transport across the water surface and the sediment for **x=∞** and the concentration distribution at the inlet, these are:

$$\varepsilon \cdot \frac{\partial c}{\partial z} + v \cdot c = 0 \qquad \text{at the water surface} \qquad (3\text{-}8)$$

$$\varepsilon \cdot \frac{\partial c}{\partial z} + v \cdot c = 0 \qquad \text{at the sediment for } x=\infty\text{, for the no-scour situation} \qquad (3\text{-}9)$$

$$c = f(z) \qquad \text{at the entrance for } x=0 \qquad (3\text{-}10)$$

This method, resulting in Figure 3-1, Figure 3-2 and Figure 3-3, gives the removal ration due to turbulence for a single grain. The removal ratio can be determined by summation of a series.
Solving equation (3-7) gives ($v \cdot H/2 \cdot \varepsilon_z$) as the independent parameter on the horizontal axis and the removal ratio (v/v_o=settling efficiency) on the vertical axis. Using a parabolic velocity distribution this can be substituted by:

$$\frac{v \cdot H}{2 \cdot \varepsilon_z} = \frac{v}{s_o} \cdot \frac{3}{\kappa} \cdot \sqrt{\frac{8}{\lambda}} = 122 \cdot \frac{v}{s_o} \qquad \text{with: } \kappa=0.4 \text{ and } \lambda=0.03 \qquad (3\text{-}11)$$

Figure 3-1, Figure 3-2 and Figure 3-3 give the removal ratio or settling efficiency for individual particles for values of λ of 0.01, 0.02 and 0.03.

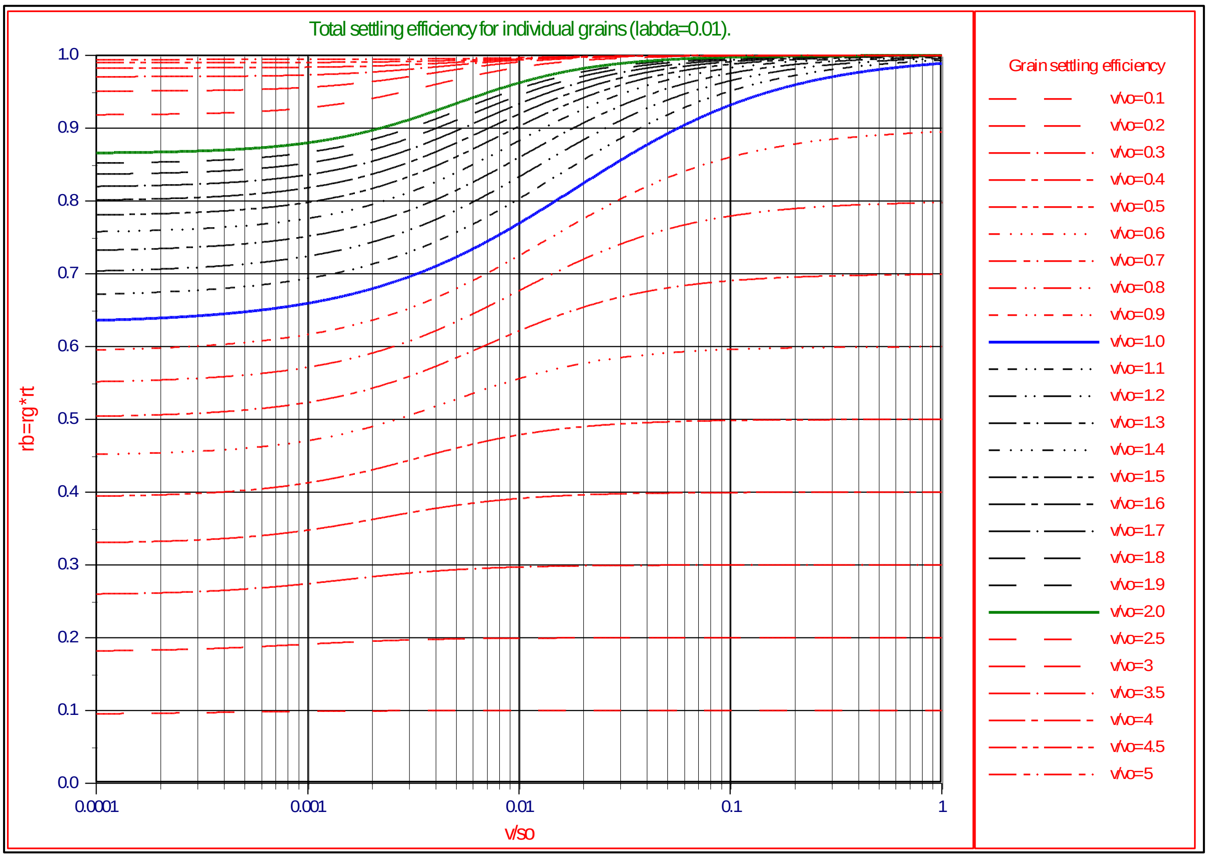

Figure 3-1: The total settling efficiency for λ=0.01.

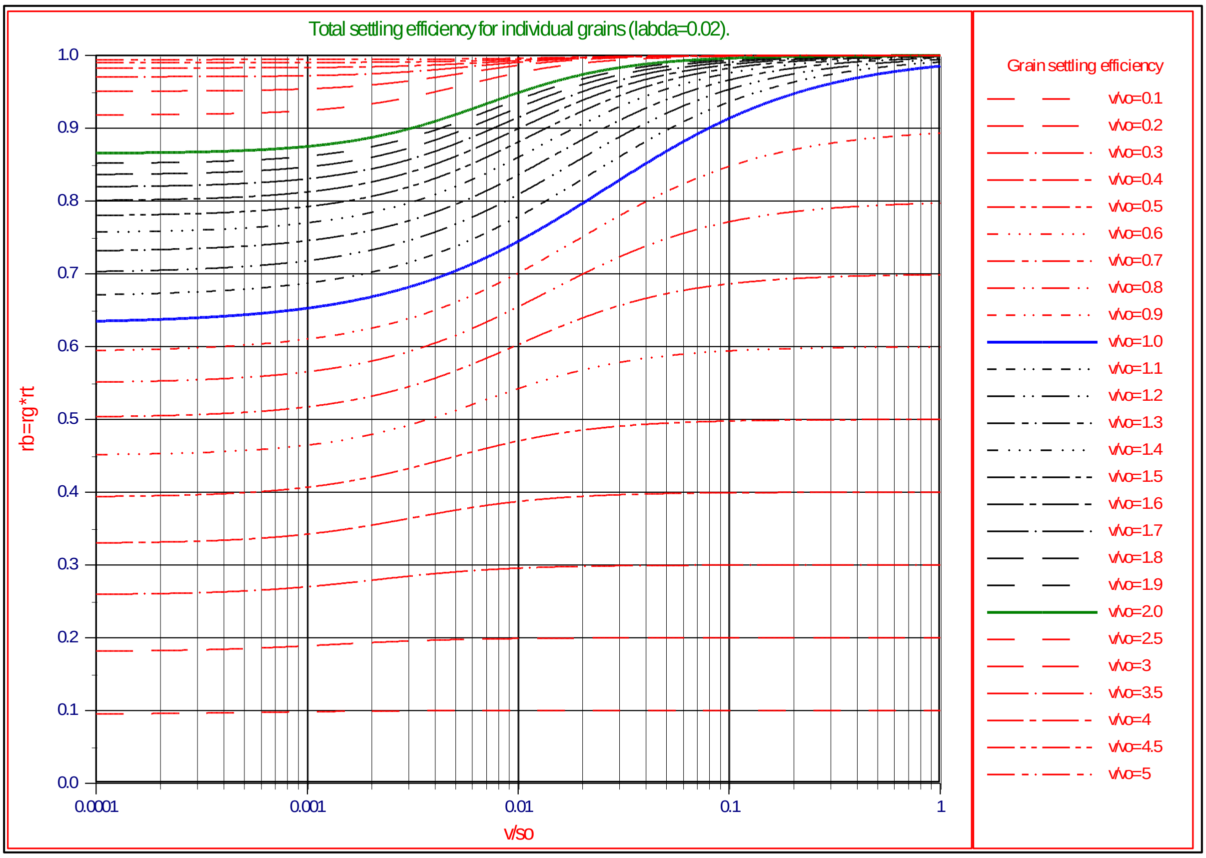

Figure 3-2: The total settling efficiency for λ=0.02.

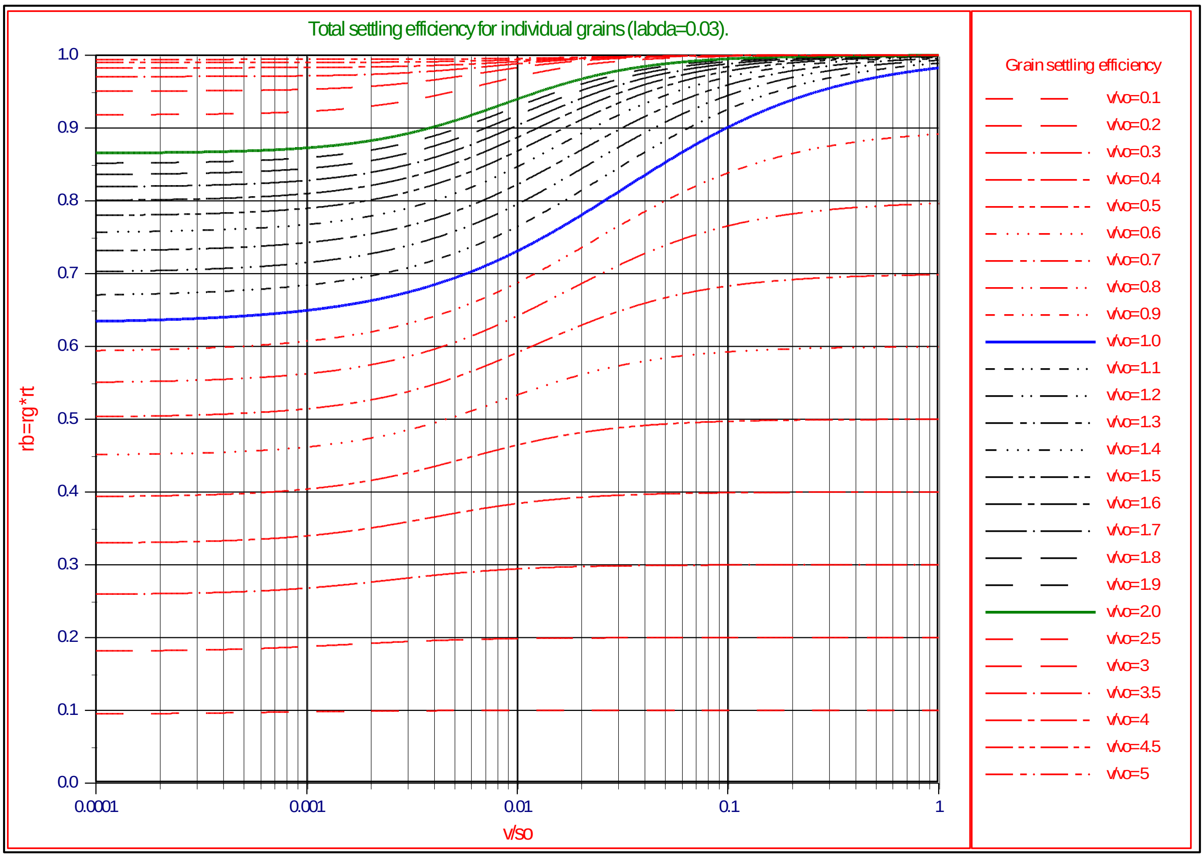

Figure 3-3: The total settling efficiency for λ=0.03.

The settling efficiency for $\mathbf{v/v_o<1}$ can be approximated by equation (3-12), while equation (3-13) gives a good approximation for the case $\mathbf{v/v_o>1}$:

$$\eta_t = \eta_g^0 \cdot \left(1 - .184 \cdot \eta_g^{+.885-.20\cdot\eta_g} \cdot \left(1 - \mathrm{TanH}\left(\eta_g^{-.13-.80\cdot\eta_g} \cdot \left(\mathrm{Log}\left(\frac{v}{s_o}\right) - .2614 - .5 \cdot \mathrm{Log}(\lambda) + \eta_g^{-.33-.94\cdot\eta_g}\right)\right)\right)\right) \tag{3-12}$$

$$\eta_t = \eta_g^{-1} \cdot \left(1 - .184 \cdot \eta_g^{-.69-.38\cdot\eta_g} \cdot \left(1 - \mathrm{TanH}\left(\eta_g^{+.77-.08\cdot\eta_g} \cdot \left(\mathrm{Log}\left(\frac{v}{s_o}\right) - .2614 - .5 \cdot \mathrm{Log}(\lambda) + \eta_g^{+1.01-.18\cdot\eta_g}\right)\right)\right)\right) \tag{3-13}$$

The effect of turbulence is taken into account by multiplying the settling efficiency with the turbulence efficiency $\boldsymbol{\eta_t}$ according to Miedema & Vlasblom (1996). Since the turbulence efficiency is smaller than 1 for all grains according to the equations (3-12) and (3-13), the basin settling efficiency can be determined with equation (3-14), where $\mathbf{p_s}$ equals 0 as long as scour does not occur. So the total settling efficiency is now:

$$\eta_b = \int_{p_s}^{1} \eta_g \cdot \eta_t \cdot dp \tag{3-14}$$

Chapter 4: The Terminal Settling Velocity of Grains

4.1 The General Terminal Settling Velocity Equation

The settling velocity of grains depends on the grain size, shape and specific density. It also depends on the density and the viscosity of the fluid the grains are settling in, and it depends upon whether the settling process is laminar or turbulent. Discrete particles do not change their size, shape or weight during the settling process (and thus do not form aggregates). A discrete particle in a fluid will settle under the influence of gravity. The particle will accelerate until the frictional drag force of the fluid equals the value of the gravitational force, after which the vertical (settling) velocity of the particle will be constant (Figure 4-1).

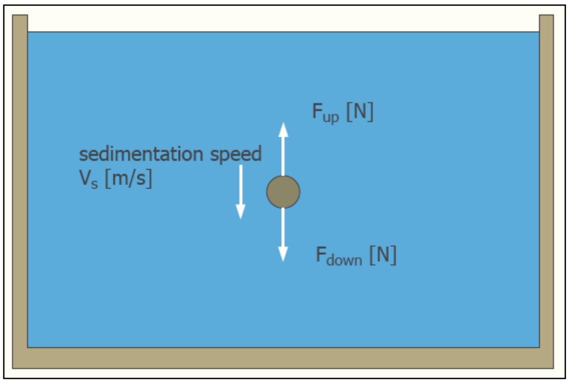

Figure 4-1: Forces on a settling particle.

The upward directed force on the particle, caused by the frictional drag of the fluid, can be calculated by:

$$\mathbf{F_{up} = C_D \cdot \frac{1}{2} \cdot \rho_w \cdot v_s^2 \cdot A} \tag{4-1}$$

The downward directed force, cause by the difference in density between the particle and the water can be calculated by:

$$\mathbf{F_{down} = (\rho_q - \rho_w) \cdot g \cdot V \cdot \psi} \tag{4-2}$$

In this equation a shape factor ψ is introduced to compensate for the shape of real sand grains. This shape factor is 1 for spheres and about 0.7 for real sand particles.

The projected surface of the particle is:

$$\mathbf{A = \frac{\pi}{4} \cdot d^2} \tag{4-3}$$

The volume of the particle is:

$$\mathbf{V = \frac{\pi}{6} \cdot d^3} \tag{4-4}$$

In general, the settling velocity $\mathbf{v_s}$ can now be determined with the following equation:

$$\mathbf{v_s = \sqrt{\frac{4 \cdot g \cdot (\rho_q - \rho_w) \cdot d \cdot \psi}{3 \cdot \rho_w \cdot C_d}}} \tag{4-5}$$

The settling velocity is thus dependent on:

- Density of particle and fluid
- Diameter (size) and shape (shape factor ψ) of the particle
- Flow pattern around particle.

The Reynolds number of the settling process determines whether the flow pattern around the particle is laminar or turbulent. The Reynolds number can be determined by:

$$\mathbf{Re_p = \frac{v_s \cdot d}{\nu}} \qquad \textbf{(4-6)}$$

The viscosity of the water is temperature dependent. If a temperature of 10° is used as a reference, then the viscosity increases by 27% at 0° and it decreases by 30% at 20° centigrade. Since the viscosity influences the Reynolds number, the settling velocity for laminar settling is also influenced by the viscosity. For turbulent settling the drag coefficient does not depend on the Reynolds number, so this settling process is not influenced by the viscosity. Other researchers use slightly different constants in these equations but, these equations suffice to explain the basics of the settling process in hopper dredges. For the viscosity the following equation is often used:

$$\mathbf{\nu = \frac{497 \cdot 10^{-6}}{(42.5 + T)^{1.5}}} \qquad \textbf{(4-7)}$$

The settling of particles occurs in one of 3 regions, the laminar region, a transitional region or the turbulent region.

The laminar region, $\mathbf{Re_p<1}$ (Stokes flow):

The upward flow of water along downward moving particles occurs under streamline conditions. The frictional resistance is only due to viscous forces and $\mathbf{C_d}$ varies inverse proportional to $\mathbf{Re_p}$.

The turbulent region, $\mathbf{Re_p>2000}$:

The flow of water along the settling particles takes place under fully developed turbulent conditions. Compared with the eddying resistance the viscous forces are negligible and $\mathbf{C_d}$ is virtually constant.

The transition region, $\mathbf{1<Re_p<2000}$:

The viscous and eddying resistances are of equal importance. And exact equation for $\mathbf{C_d}$ cannot be given, but there are several approximations, which will be discussed in the next chapters.

4.2 The Drag Coefficient

The drag coefficient $\mathbf{C_d}$ depends upon the Reynolds number according to:

The laminar region:

$$\mathbf{Re_p < 1 \quad \Rightarrow \quad C_d = \frac{24}{Re_p}} \qquad \textbf{(4-8)}$$

The transitional region:

$$\mathbf{1 < Re_p < 2000 \quad \Rightarrow \quad C_d = \frac{24}{Re_p} + \frac{3}{\sqrt{Re_p}} + 0.34} \qquad \textbf{(4-9)}$$

The turbulent region:

$$\mathbf{Re_p > 2000 \quad \Rightarrow \quad C_d = 0.445} \qquad \textbf{(4-10)}$$

As can be seen from the above equations, the $\mathbf{Re_p}$ number is not continuous at the transition points of $\mathbf{Re_p=1}$ and $\mathbf{Re_p=2000}$. To get a smooth continuous curve the following equations can be applied:

For the laminar region:

$$\mathbf{Re_p < 1} \qquad \Rightarrow \mathbf{C_d = Re_p \cdot (\frac{24}{Re_p} + \frac{3}{\sqrt{Re_p}} + 0.34) + (1\text{-}Re_p) \cdot \frac{24}{Re_p}} \tag{4-11}$$

The transitional region:

$$\mathbf{1 < Re_p < 10000} \qquad \Rightarrow \mathbf{C_d = \frac{24}{Re_p} + \frac{3}{\sqrt{Re_p}} + 0.34} \tag{4-12}$$

The turbulent region:

$$\mathbf{Re_p > 10000} \qquad \Rightarrow \mathbf{C_d = \frac{10000}{Re_p} \cdot (\frac{24}{Re_p} + \frac{3}{\sqrt{Re_p}} + 0.34) + (1 - \frac{10000}{Re_p}) \cdot 0.445} \tag{4-13}$$

Figure 4-2 shows the standard drag coefficient curve for spheres, for other shaped particles the drag coefficient will differ from this curve.

Another equation for the transitional region has been derived by Turton & Levenspiel (1986):

$$\mathbf{C_d = \frac{24}{Re_p} \cdot (1 + 0.173 \cdot Re_p^{0.657}) + \frac{0.413}{1 + 16300 \cdot Re_p^{-1.09}}} \tag{4-14}$$

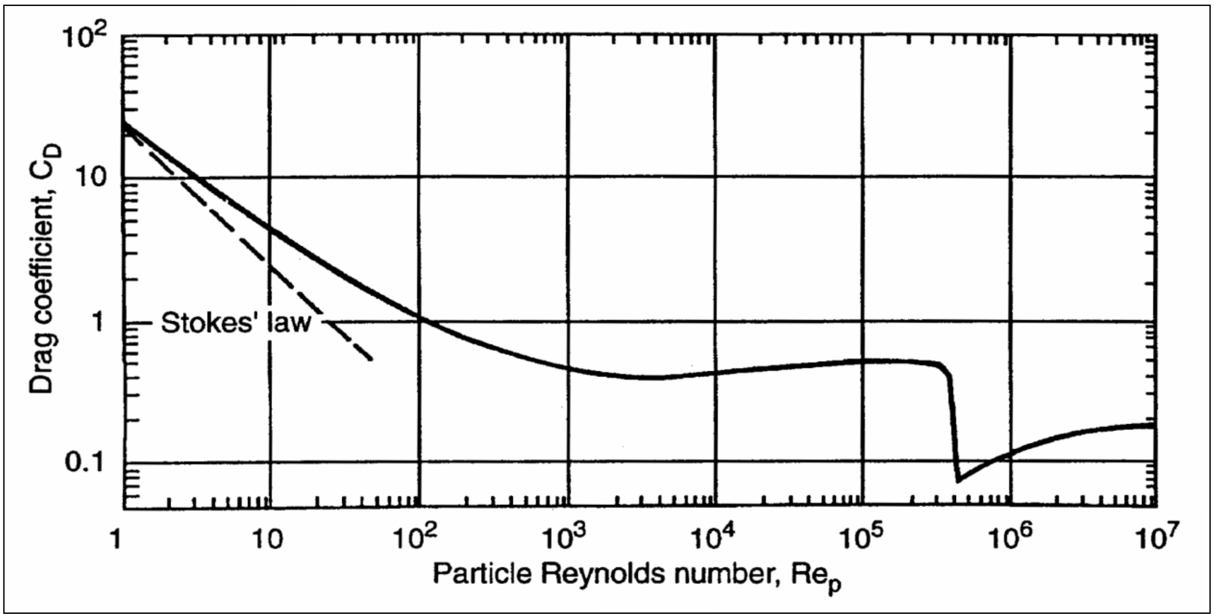

Figure 4-2: Standard drag coefficient curve for spheres.

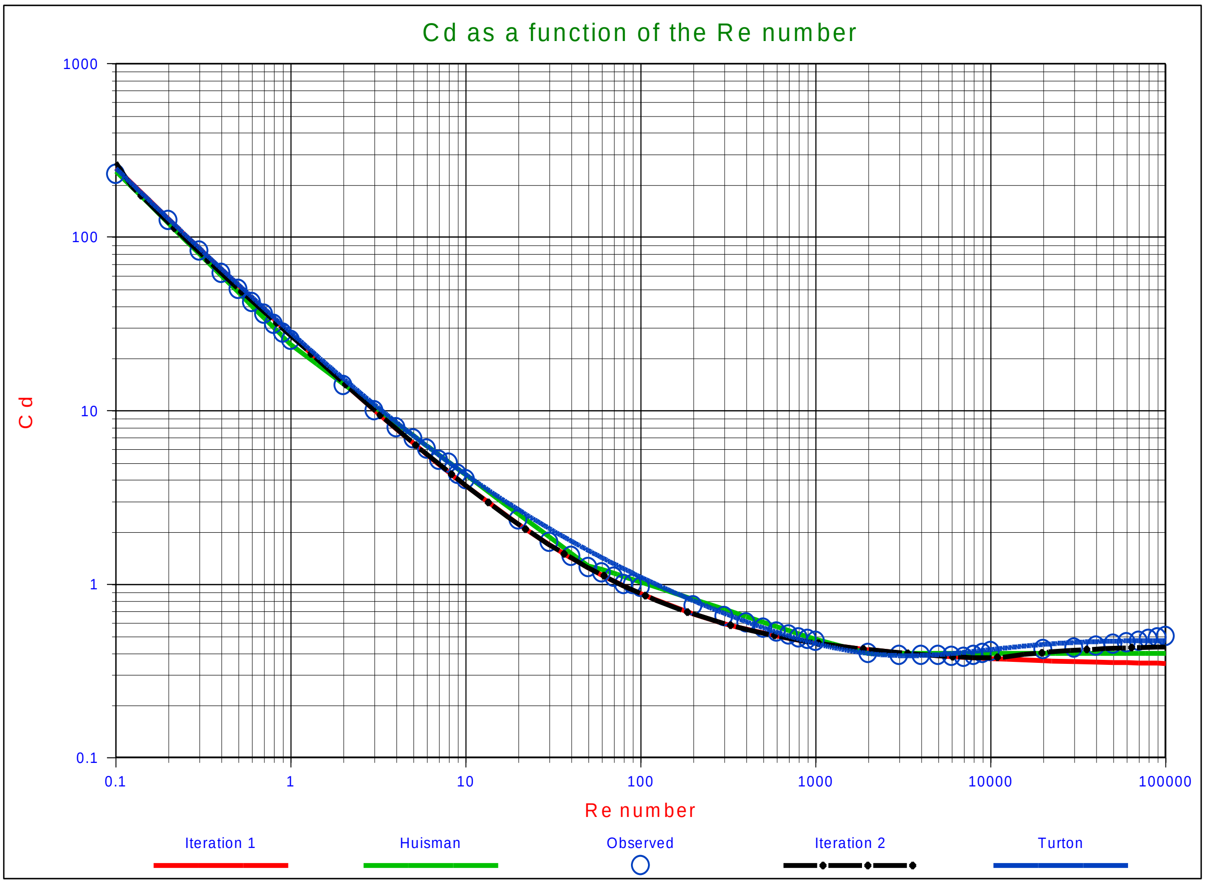

Figure 4-3: The drag coefficient as a function of the particle Reynolds number.

Figure 4-3 shows the $\mathbf{C_d}$ coefficient as a function of the $\mathbf{Re_p}$ number. In the transition area the equations are implicit. Iteration 1 shows the resulting $\mathbf{C_d}$ values based on equations (4-8), (4-9) and (4-10), while iteration 2 shows the results based on equations (4-11), (4-12) and (4-13). It is clear from this figure that iteration 2 matches the observed data better than iteration 1, but equation (4-14) of Turton & Levenspiel (1986) matches the best.

4.3 Terminal Settling Velocity Equations from Literature

Stokes, Budryck and Rittinger used these drag coefficients to calculate settling velocities for laminar settling (Stokes), a transition zone (Budryck) and turbulent settling (Rittinger) of real sand grains. This gives the following equations for the settling velocity:

Laminar flow, **d<0.1 mm**, according to Stokes.

$$\mathbf{v_s = 424 \cdot R_d \cdot d^2} \qquad \mathbf{(4\text{-}15)}$$

Transition zone, **d>0.1 mm** and **d<1 mm**, according to Budryck.

$$\mathbf{v_s = 8.925 \cdot \frac{\left(\sqrt{(1+95 \cdot R_d \cdot d^3)} - 1\right)}{d}} \qquad \mathbf{(4\text{-}16)}$$

Turbulent flow, **d>1 mm**, according to Rittinger.

$$\mathbf{v_s = 87 \cdot \sqrt{R_d \cdot d}} \qquad \mathbf{(4\text{-}17)}$$

With the relative density $\mathbf{R_d}$ defined as:

$$R_d = \frac{\rho_q - \rho_w}{\rho_w} \tag{4-18}$$

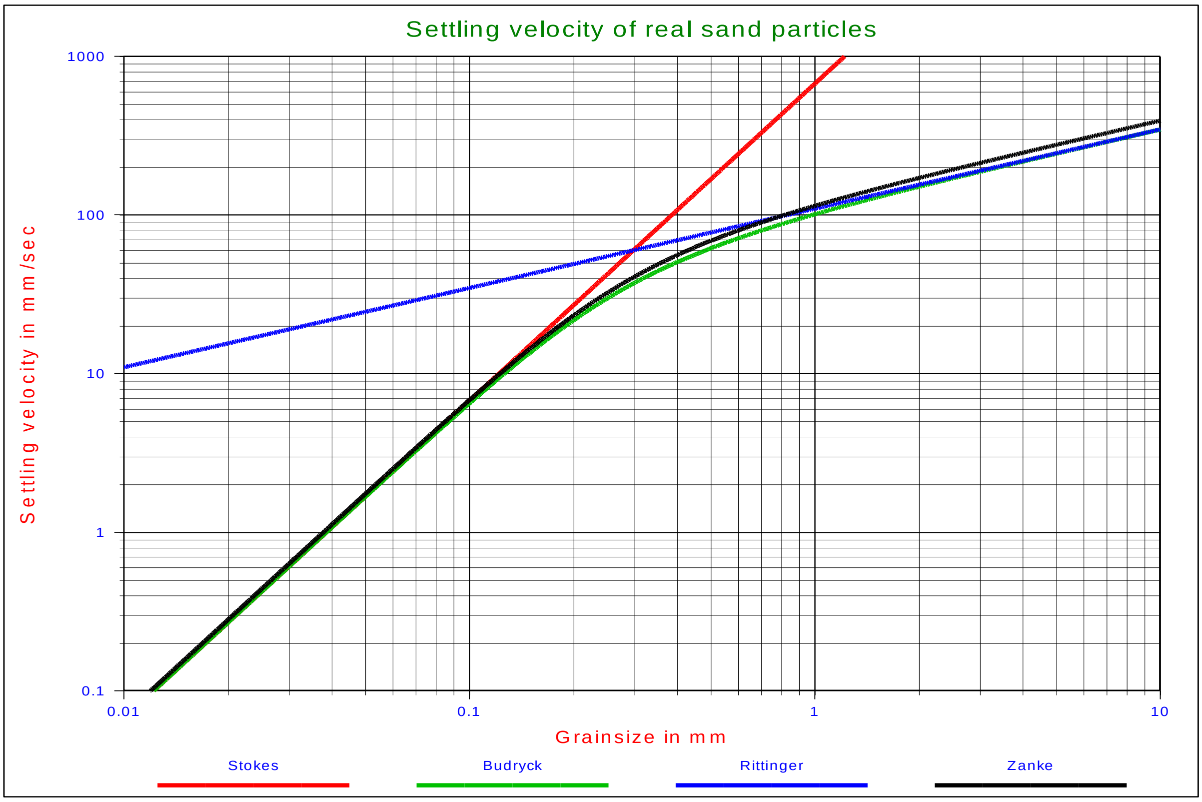

Figure 4-4: The settling velocity of individual particles.

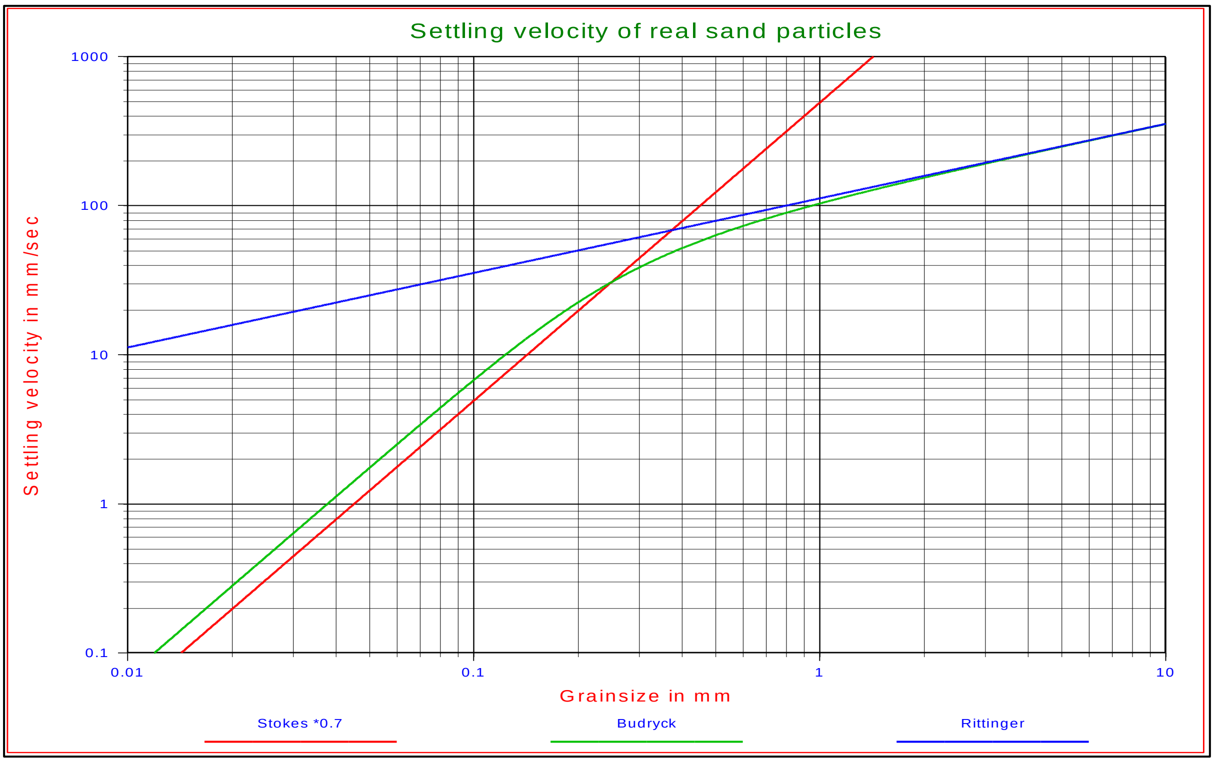

Figure 4-5: The settling velocity with the Stokes equation times 0.7.

In these equations the grain diameter is in mm and the settling velocity in mm/sec. Since the equations were derived for sand grains, the shape factor for sand grains is included for determining the constants in these equations. The shape factor was introduced into equation 2 by multiplying the mass of a sand particle with a shape factor ψ. For normal sands this shape factor has a value of 0.7. In chapter 4.6 the shape factor will be discussed in detail.

Another equation for the transitional region (in m and m/sec) has been derived by Ruby & Zanke (1977):

$$\mathbf{v_s = \frac{10 \cdot \nu}{d} \cdot \left(\sqrt{1 + \frac{R_d \cdot g \cdot d^3}{100 \cdot \nu^2}} - 1 \right)} \qquad \textbf{(4-19)}$$

Figure 4-4 shows the settling velocity as a function of the particle diameter for the Stokes, Budryck, Rittinger & Zanke equations.

Figure 4-6 shows the terminal settling velocity for the iterative method according to equations (4-11), (4-12) and (4-13) and the methods of Huisman (1973-1995) and Grace (1986) as described in chapters 4.4 and 4.5, using shape factors of 0.5 and 0.7. It can be seen that for small diameters these methods gives smaller velocities while for larger diameters larger velocities are predicted, compared with the other equations as shown in Figure 4-4. The iterative method gives larger velocities for the larger diameters, compared with the Huisman and Grace methods, but this is caused by the different way of implementing the shape factor. In the iterative method the shape factor is implemented according to equation 2, while with the Huisman and Grace methods the terminal settling velocity for spheres is multiplied by the shape factor according to equation (4-41). For the smaller grain diameters, smaller than 0.5mm, which are of interest here, the 3 methods give the same results.

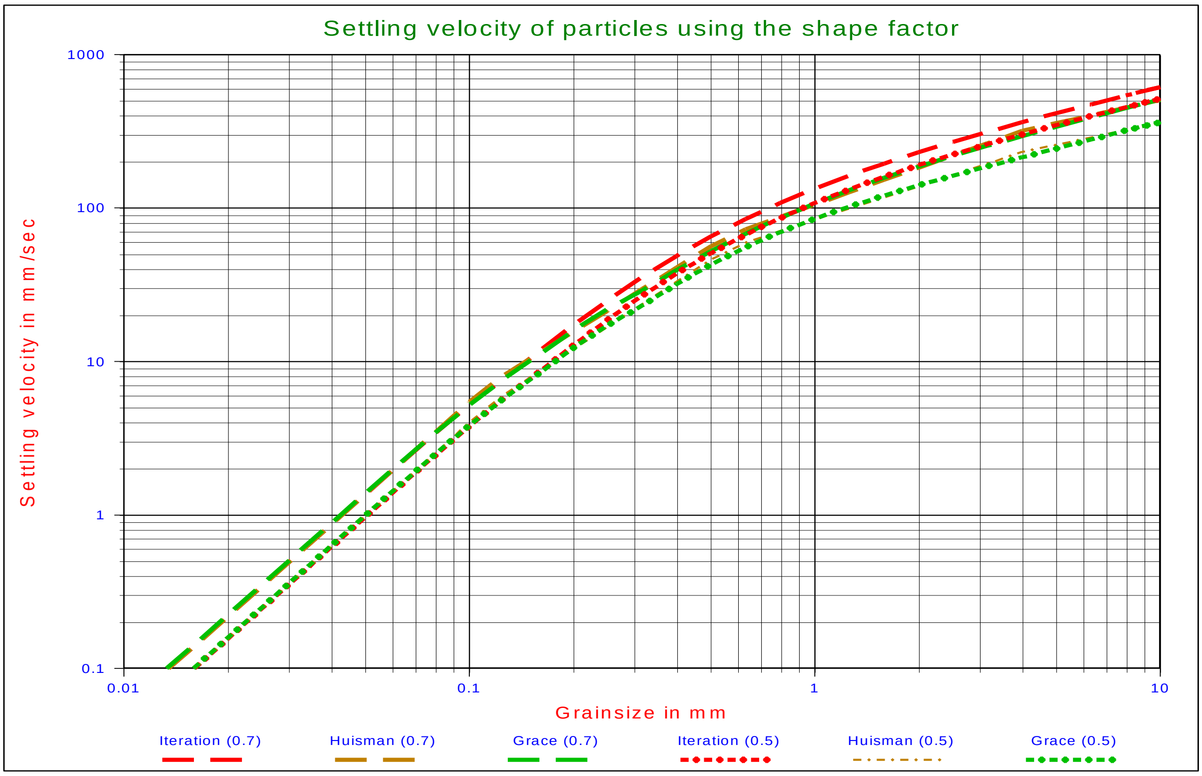

Figure 4-6: The settling velocity of individual particles using the shape factor.

4.4 The Huisman (1973-1995) Method

A better approximation and more workable equations for the drag coefficient $\mathbf{C_d}$ may be obtained by subdividing the transition region, for instance:

$$\mathbf{Re_p < 1} \qquad \mathbf{C_d = \frac{24}{Re_p^1}} \tag{4-20}$$

$$\mathbf{1 < Re_p < 50} \qquad \mathbf{C_d = \frac{24}{Re_p^{3/4}}} \tag{4-21}$$

$$\mathbf{50 < Re_p < 1620} \qquad \mathbf{C_d = \frac{4.7}{Re_p^{1/3}}} \tag{4-22}$$

$$\mathbf{1620 < Re_p} \qquad \mathbf{C_d = 0.4} \tag{4-23}$$

This power approximation is also shown in Figure 4-3. Substitution of these equations in equation (4-5) gives:

$$\mathbf{Re_p < 1} \qquad \mathbf{v_s = \frac{1}{18} \cdot \frac{g^1}{\nu^1} \cdot R_d^1 \cdot d^2} \tag{4-24}$$

$$\mathbf{1 < Re_p < 50} \qquad \mathbf{v_s = \frac{1}{10} \cdot \frac{g^{0.8}}{\nu^{0.6}} \cdot R_d^{0.8} \cdot d^{1.4}} \tag{4-25}$$

$$\mathbf{50 < Re_p < 1620} \qquad \mathbf{v_s = \frac{1}{2.13} \cdot \frac{g^{0.6}}{\nu^{0.2}} \cdot R_d^{0.6} \cdot d^{0.8}} \tag{4-26}$$

$$\mathbf{1620 < Re_p} \qquad \mathbf{v_s = 1.83 \cdot \frac{g^{0.5}}{\nu^0} \cdot R_d^{0.5} \cdot d^{0.5}} \tag{4-27}$$

These equations are difficult to use in an actual case because the value of $\mathbf{Re_p}$ depends on the terminal settling velocity. The following method gives a more workable solution.

Equation (4-5) can be transformed into:

$$\mathbf{C_d \cdot Re_p^2 = \frac{4}{3} \cdot R_d \cdot \frac{g}{\nu^2} \cdot d^3} \tag{4-28}$$

This factor can be determined from the equations above:

$$\mathbf{Re_p < 1} \qquad \mathbf{C_d \cdot Re_p^2 = 24 \cdot Re_p} \tag{4-29}$$

$$\mathbf{1 < Re_p < 50} \qquad \mathbf{C_d \cdot Re_p^2 = 24 \cdot Re_p^{5/4}} \tag{4-30}$$

$$\mathbf{50 < Re_p < 1620} \qquad \mathbf{C_d \cdot Re_p^2 = 4.7 \cdot Re_p^{5/3}} \tag{4-31}$$

$$\mathbf{1620 < Re_p} \qquad \mathbf{C_d \cdot Re_p^2 = 0.4 \cdot Re_p^2} \tag{4-32}$$

From these equations the equation to be applied can be picked and the value of $\mathbf{Re_p}$ calculated. The settling velocity now follows from:

$$\mathbf{v_s = Re_p \cdot \frac{\nu}{d}} \tag{4-33}$$

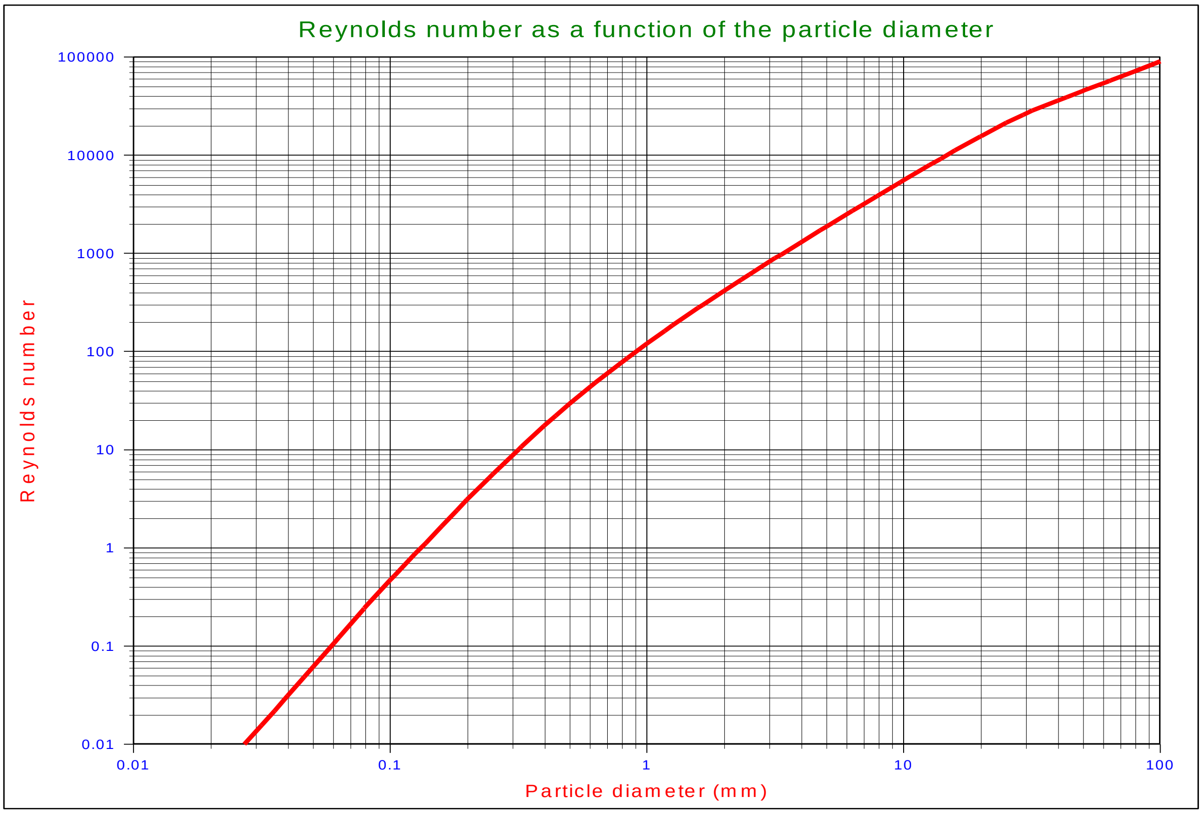

Figure 4-7: The Reynolds number as a function of the particle diameter.

4.5 The Grace Method (1986)

Following the suggestions of Grace (1986), it is found convenient to define a dimensionless particle diameter:

$$\mathbf{d^* = d \cdot \left[\frac{\rho_w^2 \cdot R_d \cdot g}{\nu^2} \right]^{1/3}} \tag{4-34}$$

And a dimensionless terminal velocity:

$$\mathbf{v_s^* = v_s \cdot \left[\frac{\rho_w}{\nu \cdot R_d \cdot g} \right]^{1/3}} \tag{4-35}$$

Those are mutually related as shown in Figure 4-8. Thus using the curve and rearranging gives directly the velocity $\mathbf{v_s}$ as a function of particle diameter **d**. No iteration is required.

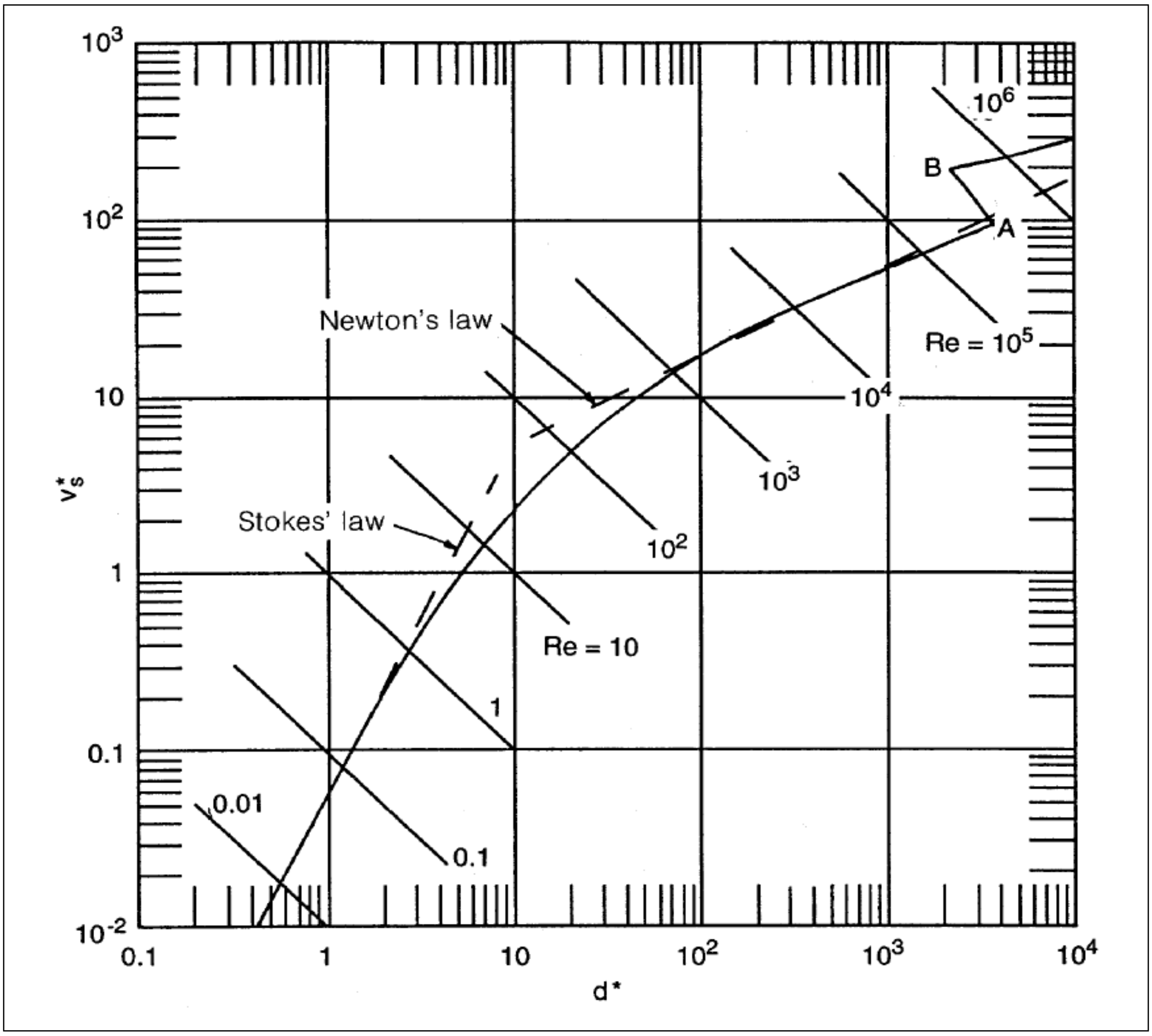

Figure 4-8: The dimensionless terminal settling velocity v_s* as a function of the dimensionless particle diameter d*, for rigid spheres, according to Grace (1986).

The curve in Figure 4-8 can be also described by analytic expressions appropriate for a computational determination of $\mathbf{v_s}$ according to Grace Method.

$$\mathbf{d^* < 3.8} \qquad \mathbf{v_s^* = \frac{d^{*2}}{18} - 3.1234 \cdot 10^{-4} \cdot d^{*5} + 1.6415 \cdot 10^{-6} \cdot d^{*8} - 7.278 \cdot 10^{-10} \cdot d^{*11}} \tag{4-36}$$

$$\mathbf{3.8 < d^* < 7.58} \qquad \mathbf{v_s^* = 10^{-1.5446 + 2.9162 \cdot \log(d^*) - 1.0432 \cdot \log(d^*)^2}} \tag{4-37}$$

$$\mathbf{7.58 < d^* < 227} \qquad \mathbf{v_s^* = 10^{-1.64758 + 2.94786 \cdot \log(d^*) - 1.09703 \cdot \log(d^*)^2 + 0.17129 \cdot \log(d^*)^3}} \tag{4-38}$$

$$\mathbf{227 < d^* < 3500} \qquad \mathbf{v_s^* = 10^{5.1837 - 4.51034 \cdot \log(d^*) + 1.687 \cdot \log(d^*)^2 - 0.189135 \cdot \log(d^*)^3}} \tag{4-39}$$

Now $\mathbf{v_s}$ can be computed according to:

$$\mathbf{v_s = v_s^* \cdot \left[\frac{\rho_w}{\nu \cdot R_d \cdot g} \right]^{-1/3}} \tag{4-40}$$

4.6 The Shape Factor

In the range of particle Reynolds numbers from roughly unity to about 100, which is the range of interest here, a particle orients itself during settling so as to maximize drag. Generally this means that an oblate or lenticular particle, i.e. a shape with one dimension smaller than the other two, will settle with its maximum area horizontal. The drag of fluid on the particle then depends most critically on this area. This is also the area seen if the particle lies in a stable position on a flat surface. Therefore, for estimation of drag, the non-spherical particle is characterized by the 'area equivalent diameter', i.e. the diameter of the sphere with the same projected area. For particles whose sizes are determined by sieving rather than microscopic analysis, the diameter is slightly smaller than the mesh size. However, unless the particles are needle shaped, the difference between the diameter and the screen opening is relatively small, generally less than 20%.

Although equation (4-2) contains a shape factor, basically all the equations in this chapter are derived for spheres. The shape factor ψ in equation (4-2) is one way of introducing the effect of the shape of particles on the terminal settling velocity. In fact equation (4-2) uses a shape factor based on the weight ratio between a real sand particle and a sphere with the same diameter. Another way is introducing a factor ξ according to:

$$\xi = \frac{v_s}{v_{ss}} \tag{4-41}$$

Where ξ equals the ratio of the terminal settling velocity of a non-spherical particle v_s and the terminal velocity v_{ss} of a spherical particle with the same diameter.
The shape of the particle can be described by the volumetric shape factor **K** which is defined as the ratio of the volume of a particle and a cube with sides equal to the particle diameter so that **K=0.524** for a sphere:

$$K = \frac{\text{volume of particle}}{d^3} \tag{4-42}$$

The shape factor ξ is a function of the volumetric form factor **K** and the dimensionless particle diameter **d*** according to equation (4-34).

$$\log(\xi) = -0.55 + K - 0.0015 \cdot K + 0.03 \cdot 1000^{K-0.524} + \frac{-0.045 + 0.05 \cdot K^{-0.6} - 0.0287 \cdot 55000^{K-0.524}}{\cosh(2.55 \cdot (\log(d^*) - 1.114)} \tag{4-43}$$

This equation takes a simpler form for sand shaped particles with **K=0.26**:

$$\log(\xi) = -0.3073 + \frac{0.0656}{\cosh(2.55 \cdot (\log(d^*) - 1.114)} \tag{4-44}$$

A value of **K=0.26** for sand grains would give a volume ratio of 0.26/0.524=0.496 and thus a factor ψ**=0.496** in equation (4-2), while often a factor ψ**=0.7** is used.

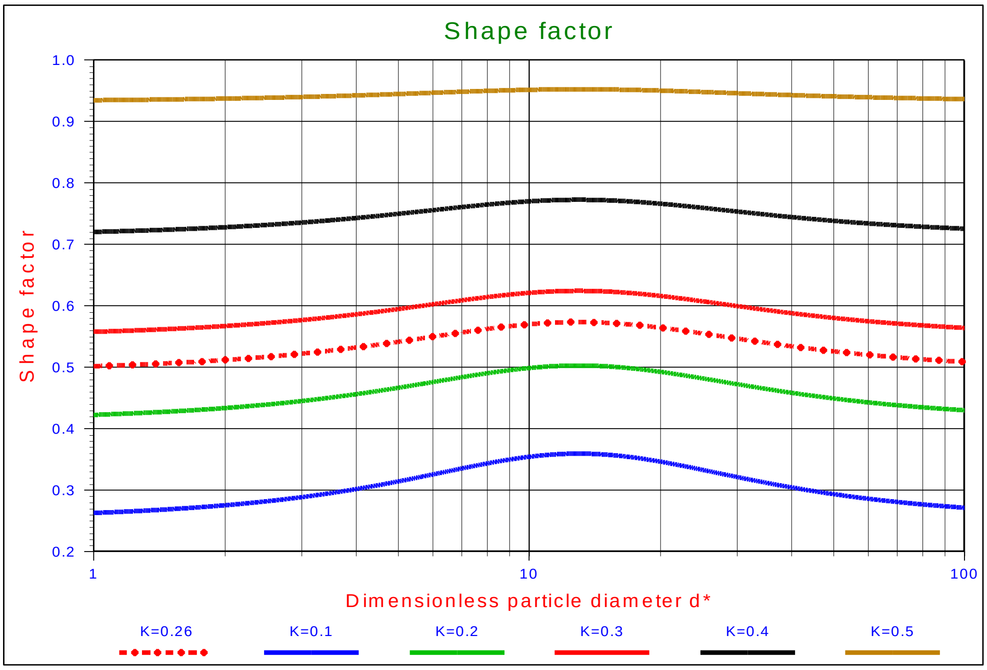

Figure 4-9: The shape factor ξ as a function of the dimensionless particle diameter d*.

Figure 4-9 shows the shape factor ξ as a function of the dimensionless particle diameter **d***, according to equation (4-43).

Figure 4-6 also shows the terminal settling velocity according to the methods of Huisman (1973-1995) and Grace (1986) using the shape factor according to equation (4-44). It can be seen clearly that both methods give the same results. One can see that the choice of the shape factor strongly determines the outcome of the terminal settling velocity.

4.7 Hindered Settling

The above equations calculate the settling velocities for individual grains. The grain moves downwards and the same volume of water has to move upwards. In a mixture, this means that, when many grains are settling, an average upwards velocity of the water exists. This results in a decrease of the settling velocity, which is often referred to as hindered settling. However, at very low concentrations the settling velocity will increase because the grains settle in each other's shadow. Richardson and Zaki (1954) determined an equation to calculate the influence of hindered settling for volume concentrations $\mathbf{C_v}$ between 0.05 and 0.65.
Theoretically, the validity of the Richardson & Zaki equation is limited by the maximum solids concentration that permits solids particle settling in a particulate cloud. This maximum concentration corresponds with the concentration in an incipient fluidized bed ($\mathbf{C_v}$ of about 0.57). Practically, the equation was experimentally verified for concentrations not far above 0.30. The exponent in this equation is dependent on the Reynolds number. The general equation yields:

$$\frac{v_c}{v_s} = \left(1 - C_v\right)^{\beta} \tag{4-45}$$

The following values for β should be used:

$$\begin{array}{ll} \mathbf{Re_p<0.2} & \beta = 4.65 \\ \mathbf{Re_p>0.2 \text{ and } Re_p<1.0} & \beta = 4.35 \cdot Re_p^{-0.03} \\ \mathbf{Re_p>1.0 \text{ and } Re_p<200} & \beta = 4.45 \cdot Re_p^{-0.1} \\ \mathbf{Re_p>200} & \beta = 2.39 \end{array} \tag{4-46}$$

However this does not give a smooth continuous curve. Using the following definition does give a continuous curve:

$$
\begin{array}{ll}
Re_p<0.1 & \beta = 4.65 \\
Re_p>0.1 \text{ and } Re_p<1.0 & \beta=4.35 \cdot Re_p^{-0.03} \\
Re_p>1.0 \text{ and } Re_p<400 & \beta=4.45 \cdot Re_p^{-0.1} \\
Re_p>400 & \beta=2.39
\end{array}
\tag{4-47}
$$

Other researchers found the same trend but sometimes somewhat different values for the power β. These equations are summarized below and shown in Figure 4-10.

According to Rowe (1987) this can be approximated by:

$$\beta = \frac{4.7 + 0.41 \cdot Re_p^{0.75}}{1 + 0.175 \cdot Re_p^{0.75}} \tag{4-48}$$

Wallis (1969) found an equation which matches Rowe (1987) for small Reynolds numbers and Garside & Al-Dibouni (1977) for the large Reynolds numbers:

$$\beta = \frac{4.7 \cdot (1 + 0.15 \cdot Re_p^{0.687})}{1 + 0.253 \cdot Re_p^{0.687}} \tag{4-49}$$

Garside & Al-Dibouni (1977) give the same trend but somewhat higher values for the exponent β.

$$\beta = \frac{5.1 + 0.27 \cdot Re_p^{0.9}}{1 + 0.1 \cdot Re_p^{0.9}} \tag{4-50}$$

Di Felici (1999) finds very high values for β but this relation is only valid for dilute mixtures (very low concentration, less than 5%).

$$\beta = \frac{6.5 + 0.3 \cdot Re_p^{0.74}}{1 + 0.1 \cdot Re_p^{0.74}} \tag{4-51}$$

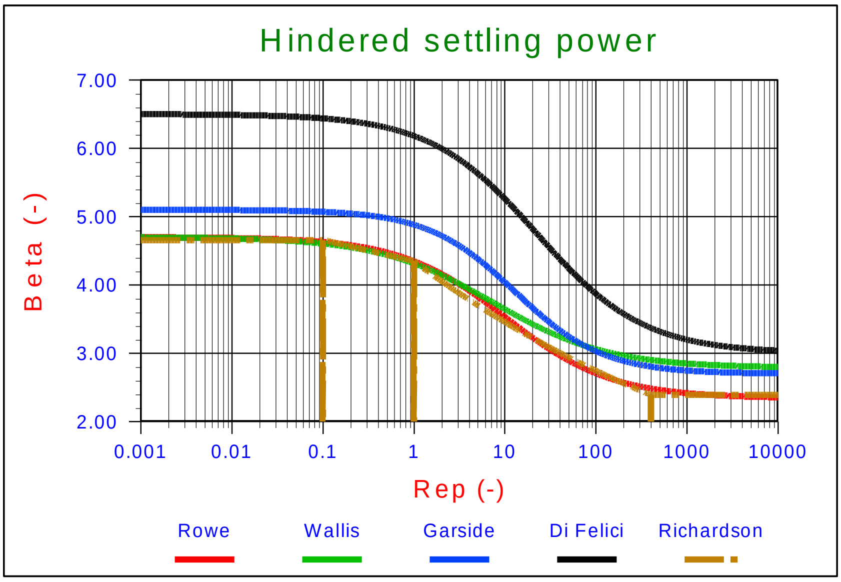

Figure 4-10: The hindered settling power according to several researchers.

Chapter 5: The Modified Hopper Load Parameter

The basic Camp theory assumes that the settled grains are removed constantly, resulting in a constant height $\mathbf{H_w}$ of the settlement zone. In the hopper of the TSHD this is not the case, resulting in a rising sediment zone and a decreasing height $\mathbf{H_w}$ during the sedimentation process. The rising sediment zone influences the effective or modified hopper load parameter $\mathbf{v_{oo}}$. This influence can be determined as follows (see also Figure 2-7 and equation (2-13)):

$$\frac{dH_w}{dt} \cdot L \cdot W \cdot c_{bed} = Q \cdot \left(c_{in} - c_{out}\right) \tag{5-1}$$

With the effective or modified settling efficiency $\boldsymbol{\eta_{gg}}$ of a grain, including the effect of the rising sediment zone:

$$\eta_{gg} = \frac{c_{in} - c_{out}}{c_{in}} \text{ thus: } c_{in} - c_{out} = \eta_{gg} \cdot c_{in} \text{ with: } \eta_{gg} = \left(\frac{v_s}{v_{oo}}\right) \tag{5-2}$$

The velocity at which the sediment zone is rising is:

$$\frac{dH_w}{dt} \cdot L \cdot W \cdot c_{bed} = Q \cdot \eta_{gg} \cdot c_{in}$$

thus: **(5-3)**

$$\frac{dH_w}{dt} = \frac{Q}{L \cdot W} \cdot \frac{c_{in}}{c_{bed}} \cdot \eta_{gg} = v_o \cdot \frac{c_{in}}{c_{bed}} \cdot \eta_{gg} = v_o \cdot \kappa \cdot \eta_{gg}$$

The time an element of mixture stays in the hopper is:

$$\Delta t = \frac{L}{s_o} = \frac{V}{Q} = \frac{L \cdot (H_w - 0.5 \cdot \Delta H) \cdot W}{Q} = \frac{L \cdot H_a \cdot W}{Q} \tag{5-4}$$

During the time an element of mixture stays in the hopper, the sediment level is raised by:

$$\Delta H = \frac{dH}{dt} \cdot \Delta t = v_o \cdot \kappa \cdot \eta_{gg} \cdot \frac{L \cdot H_a \cdot W}{Q} = H_a \cdot \kappa \cdot \eta_{gg} \tag{5-5}$$

The effective or modified hopper load parameter $\mathbf{v_{oo}}$, being the setting velocity of a grain that just reaches the (raised) sediment zone at the end of the hopper is now:

$$\frac{v_{oo}}{s_o} = \frac{H_w - \Delta H}{L} = \frac{H_a - 0.5 \cdot \Delta H}{L} = \frac{H_a}{L} \cdot \left(1 - 0.5 \cdot \kappa \cdot \eta_{gg}\right) \tag{5-6}$$

Substituting $\mathbf{s_o}$ in this equation gives:

$$v_{oo} = v_o \cdot \left(1 - 0.5 \cdot \kappa \cdot \eta_{gg}\right) \tag{5-7}$$

Now there are two cases, first the case where the settling velocity of a grain $\mathbf{v_s}$ is greater than or equal to the effective hopper load parameter $\mathbf{v_{oo}}$. In this case the effective settling efficiency is 1. This results in an effective hopper load parameter of:

$$v_{oo} = v_o \cdot \left(1 - 0.5 \cdot \kappa\right) \tag{5-8}$$

The second case is the case where the settling velocity of a grain $\mathbf{v_s}$ is smaller than the effective hopper load parameter $\mathbf{v_{oo}}$. In this case the effective settling efficiency will be smaller then 1, according to equation (5-2). This gives the following effective hopper load parameter:

$$\mathbf{v_{oo}=v_o\cdot\left(1-0.5\cdot\kappa\cdot\frac{v_s}{v_{oo}}\right)} \tag{5-9}$$

Since in this equation, the effective hopper load parameter $\mathbf{v_{oo}}$ depends on itself, this has to be solved as a quadratic equation, resulting in:

$$\mathbf{v_{oo}=\frac{1}{2}\cdot v_o+\sqrt{\frac{1}{4}\cdot v_o\left(v_o-2\cdot\kappa\cdot v_s\right)}}$$

With: $\mathbf{v_s=\alpha\cdot v_o}$ this gives: $\mathbf{v_{oo}=\frac{1}{2}\cdot v_o+\frac{1}{2}\cdot v_o\cdot\sqrt{1-2\cdot\kappa\cdot\alpha}}$ **(5-10)**

Now the question is, for which value of $\boldsymbol{\alpha}$ is the effective hopper load parameter $\mathbf{v_{oo}}$ equal to the settling velocity of the grain $\mathbf{v_s}$. At this value the effective settling efficiency $\boldsymbol{\eta_{gg}}$ equals 1. The following value for the effective hopper load parameter is valid.

$$\mathbf{v_{oo}=\alpha\cdot v_o}\ \text{ this gives: }\ \mathbf{\alpha=1-0.5\cdot\kappa=1-0.5\cdot\frac{c_{in}}{c_{bed}}}\ \text{ or }\ \mathbf{c_{in}=2\cdot c_{bed}\cdot\left(1-\alpha\right)} \tag{5-11}$$

This gives the following conditions for the settling efficiency to be smaller than 1:

$$\mathbf{\alpha<1-0.5\cdot\frac{c_{in}}{c_{bed}}}\ \text{ or }\ \mathbf{c_{in}<2\cdot c_{bed}\cdot\left(1-\alpha\right)} \tag{5-12}$$

In all other cases the effective settling efficiency equals 1, resulting in the following velocity of the rising sediment level:

$$\mathbf{\frac{dH_w}{dt}=\frac{Q}{L\cdot W}\cdot\kappa=v_o\cdot\kappa} \tag{5-13}$$

Figure 5-1, Figure 5-2, Figure 5-3, Figure 5-4, Figure 5-5 and Figure 5-6 show the resulting modified hopper load parameters and the settling velocities as a function of the relative concentration in a model hopper with **L=11.34 m**, **W=2.04 m**, **H=2 m** and **Q=0.1 m^3/sec** for grain diameters of 0.08, 0.10, 0.12, 0.14, 0.16 and 0.18 mm. It is clear from these figures that the modified hopper load parameter decreases linearly according to equation (5-9), with a settling efficiency of 1 as long as the modified hopper load parameter is smaller than the settling velocity. From the intersection point of the two curves to higher relative concentrations, the modified hopper load parameter increases again. The settling velocity $\mathbf{v_s}$ include the effects of hindered settling according to Richardson and Zaki (1954) with an exponent of 4.65 in the examples. The unmodified hopper load parameter is 4.3 mm/sec in these examples.

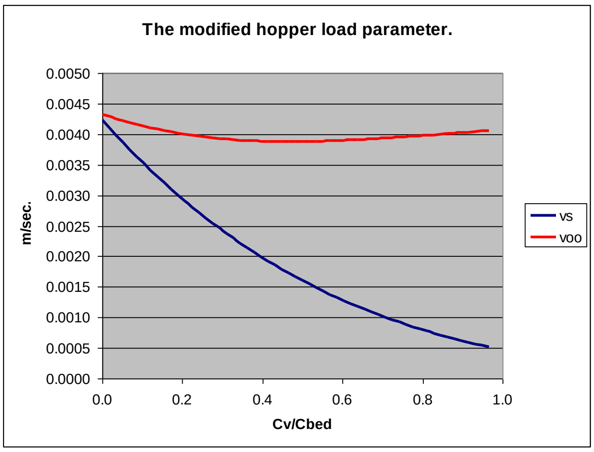

Figure 5-1: d=0.08 mm.

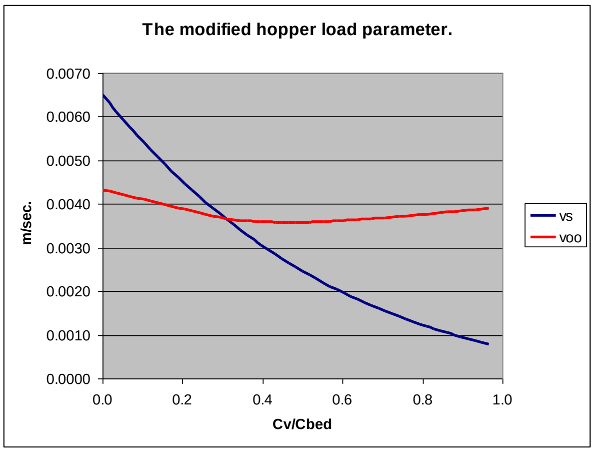

Figure 5-2: d=0.10 mm.

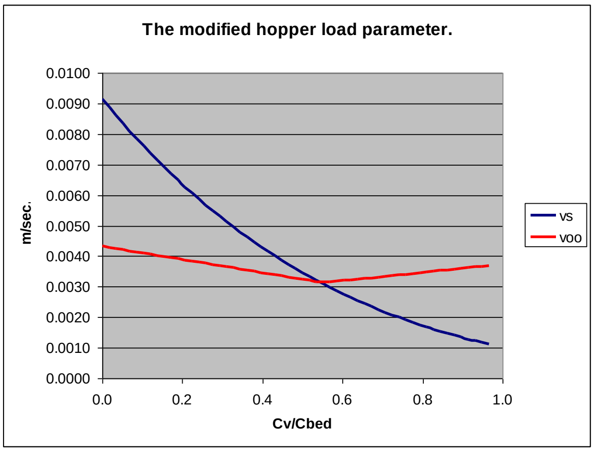

Figure 5-3: d=0.12 mm.

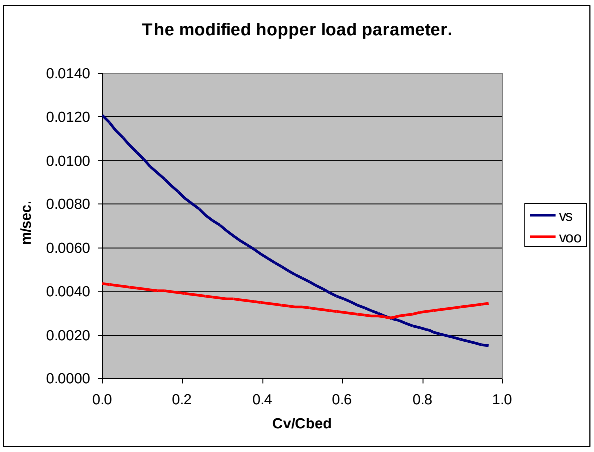

Figure 5-4: d=0.14mm.

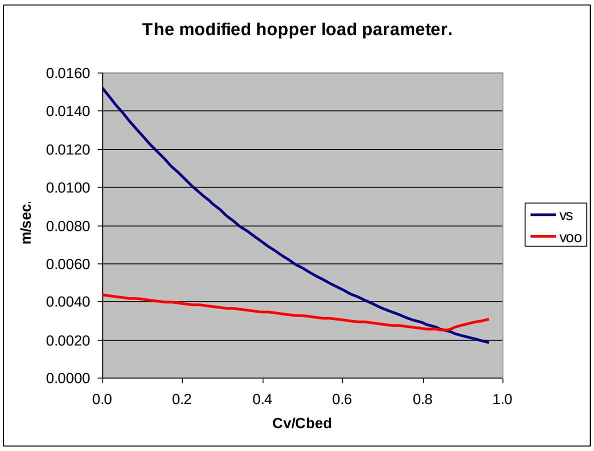

Figure 5-5: d=0.16 mm.

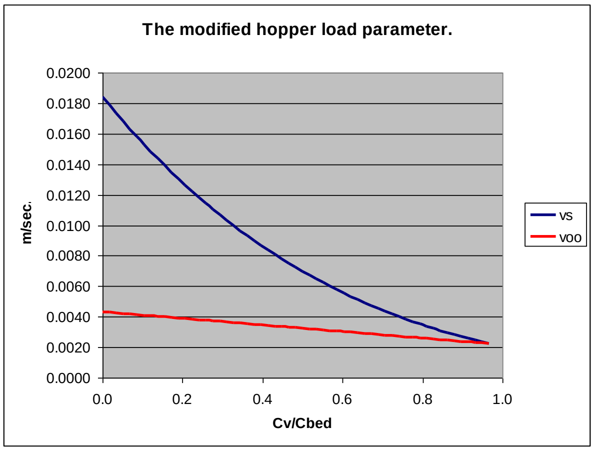

Figure 5-6: d=0.18 mm.

Figure 5-7 shows the sedimentation velocity $\mathbf{dH_w/dt}$ for grain diameters of 0.1, 0.15 and 0.2 mm. As can be seen the grain with a diameter of 0.2 mm gives a straight line, because the effective settling efficiency is equal to 1 for all concentrations. The grain with a diameter of 0.15 mm has a settling efficiency equal to 1 up to a relative concentration of about 0.65. Above this relative concentration the effect of hindered settling causes the sedimentation velocity to decrease. The grain with a diameter of 0.1 mm has a settling efficiency smaller than 1 from the beginning and the sedimentation velocity is determined by the hindered settling effect all the way.

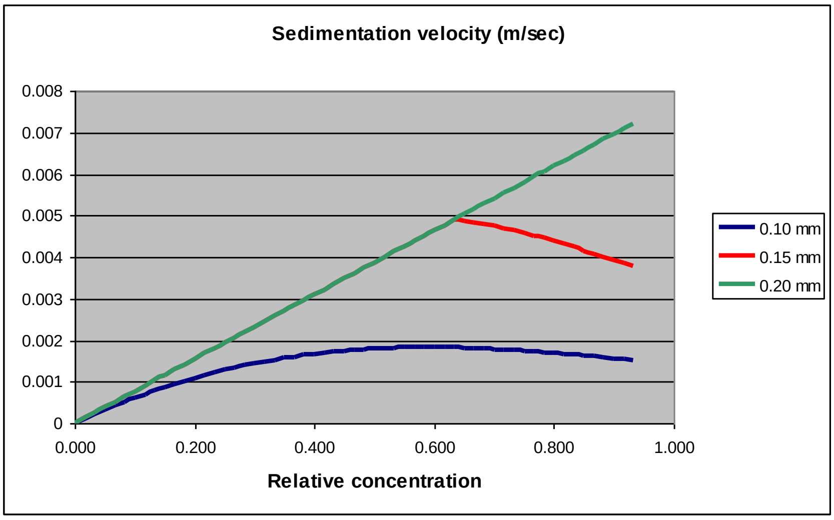

Figure 5-7: The sedimentation velocity dH_w/dt as a function of the relative concentration for 3 grain diameters.

Of course in the interpretation of the examples in this chapter one has to consider that real sand often consists of a graded PSD and not just one diameter. Still the examples show the influence of hindered settling on the modified hopper load parameter and they show that this effect should not be neglected. If a graded PSD is considered, the total settling efficiency should be used to determine the modified hopper load parameter. In Chapter 8: an analytical model will be derived to determine the settling efficiency for graded sand.

Chapter 6: The Influence of Hindered Settling on the Production

6.1 Theory

Hindered settling is the main cause for the settling efficiency and the sedimentation velocity to decrease with an increasing relative concentration for small grains as is shown in Figure 5-7. An interesting question is how does this influence de production of a TSHD, based on a full dredging cycle. First we define the production to be the total load in tons, divided by the total cycle time according to:

$$\mathbf{P} = \frac{\mathbf{W_{max}}}{\mathbf{T_{cycle}}} = \frac{\mathbf{W_f + W_l}}{\mathbf{T_s + T_f + T_l}} \qquad \textbf{(6-1)}$$

To simplify the cycle we divide it in 3 phases:

1. The sum of sailing time, dumping time, etc. $\mathbf{T_s}$.
2. The time to fill the hopper to the overflow level $\mathbf{T_{f,}}$, loading $\mathbf{W_f}$ tons.
3. The time to fill the hopper completely after the overflow level has been reached $\mathbf{T_l}$, loading $\mathbf{W_l}$ tons.

For this derivation it is assumed that we consider a CVS TSHD and it is assumed that the hopper can be filled completely with sand with a settling efficiency as derived before. The volume of sand loaded during phase 2 and the load and the time required are now:

$$\mathbf{V_f} = \frac{\mathbf{c_{in}}}{\mathbf{c_{bed}}} \cdot \mathbf{V_{max}} \;\text{ thus: }\; \mathbf{W_f} = \mathbf{V_f} \cdot \boldsymbol{\rho}_{\mathbf{bed}} \;\text{ and }\; \mathbf{T_f} = \frac{\mathbf{V_{max}}}{\mathbf{Q}} \qquad \textbf{(6-2)}$$

For the load and the volume during phase 3, now the following equations can be derived, assuming the hopper will be filled with a factor $\boldsymbol{\lambda}$:

$$\mathbf{W_l} = \mathbf{W_{max}} - \mathbf{W_f} \;\text{ and }\; \mathbf{V_l} = \boldsymbol{\lambda} \cdot \mathbf{V_{max}} - \mathbf{V_f} \;\text{ and }\; \mathbf{W_l} = \mathbf{V_l} \cdot \boldsymbol{\rho}_{\mathbf{bed}} \qquad \textbf{(6-3)}$$

The time to load this value can be simplified by assuming a certain average settling efficiency during this phase, being equal to the effective settling efficiency $\boldsymbol{\eta}_{\mathbf{gg}}$ as described earlier:

$$\mathbf{V_l} = \mathbf{Q} \cdot \frac{\mathbf{c_{in}}}{\mathbf{c_{bed}}} \cdot \boldsymbol{\eta}_{\mathbf{gg}} \cdot \mathbf{T_l} \;\text{ thus: }\; \mathbf{T_l} = \frac{\mathbf{V_l}}{\mathbf{Q} \cdot \frac{\mathbf{c_{in}}}{\mathbf{c_{bed}}} \cdot \boldsymbol{\eta}_{\mathbf{gg}}} = \frac{\mathbf{V_l}}{\mathbf{Q} \cdot \boldsymbol{\kappa} \cdot \boldsymbol{\eta}_{\mathbf{gg}}} \qquad \textbf{(6-4)}$$

Substituting the equations (6-2), (6-3) and (6-4) in equation (6-1) gives the following production:

$$\boxed{\mathbf{P} = \frac{\boldsymbol{\lambda} \cdot \mathbf{V_{max}} \cdot \boldsymbol{\rho}_{\mathbf{bed}}}{\mathbf{T_s} + \frac{\mathbf{V_{max}}}{\mathbf{Q}} \cdot \left\{ \frac{\boldsymbol{\lambda} - \boldsymbol{\kappa} \cdot \left(1 - \boldsymbol{\eta}_{\mathbf{gg}}\right)}{\boldsymbol{\kappa} \cdot \boldsymbol{\eta}_{\mathbf{gg}}} \right\}}} \qquad \textbf{(6-5)}$$

The calculations have been carried out for a 2500 m^3 hopper with a mixture flow $\mathbf{Q}$ of 3.33 m^3/sec and a total time $\mathbf{T_s}$ of 100 minutes. The settling efficiencies as derived with equation (5-7), including hindered settling, and as used in Figure 5-7, are also used to create Figure 6-1, Figure 6-2 and Figure 6-3.The A-curves are calculated with equation **Error! Reference source not found.**, while the B-curves are calculated with software, using a raded sand.

The figures clearly show a continuous increase of the production for the 0.1, 0.15 and 0.2 mm sand. The shape of the curve is determined by the mixture flow and the total delay time $\mathbf{T_s}$ in the denominator of equation **Error! eference source not found.**. Of course the shape of the curves depends strongly on the TSHD chosen, the total delay time and the mixture flow and should be determined with the right values for the different parameters involved.

Figure 6-1, Figure 6-2 and Figure 6-3 however prove that a decreasing sedimentation velocity as is shown in Figure 5-7, does not imply a decreasing final production when the effects of hindered settling are taken into account with an increasing relative concentration. The main reason for this is the fact that during the filling phase of the hopper up to overflow level, there are no losses. The figures show a clear increase in production at the smaller relative concentrations, while the productions are almost equal for the high productions. For example, at a relative concentration of 0.3, the 0.1 mm sand has a production of about 0.5 ton/sec, the 0.15 mm sand a production of about 0.55 ton/sec and the 0.2 mm sand a production of 0.56 ton/sec. Coarser sands will not have a much higher production since the main part of the PSD is above the hopper load parameter. Sands finer than the 0.1 mm sand will have a smaller production due to the increased overflow losses.

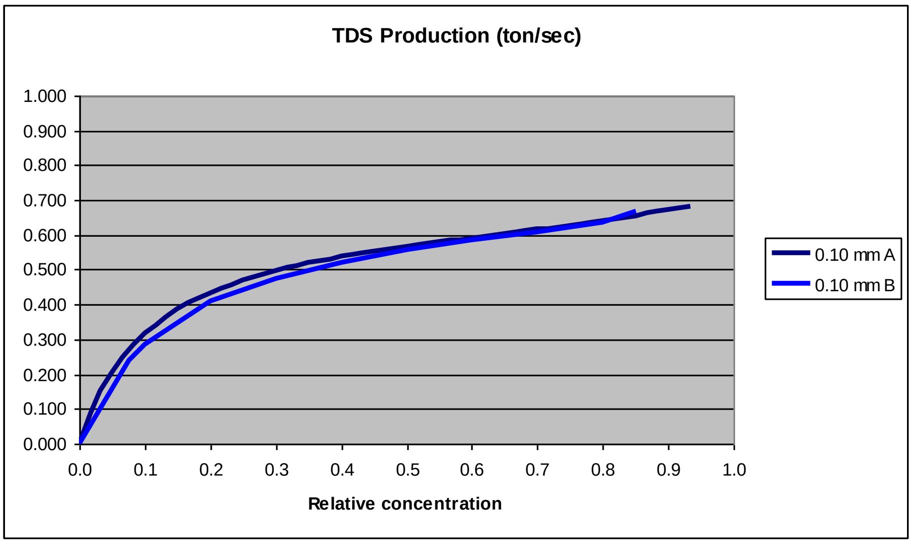

Figure 6-1: The production as a function of the relative concentration for an 0.10 mm grain diameter.

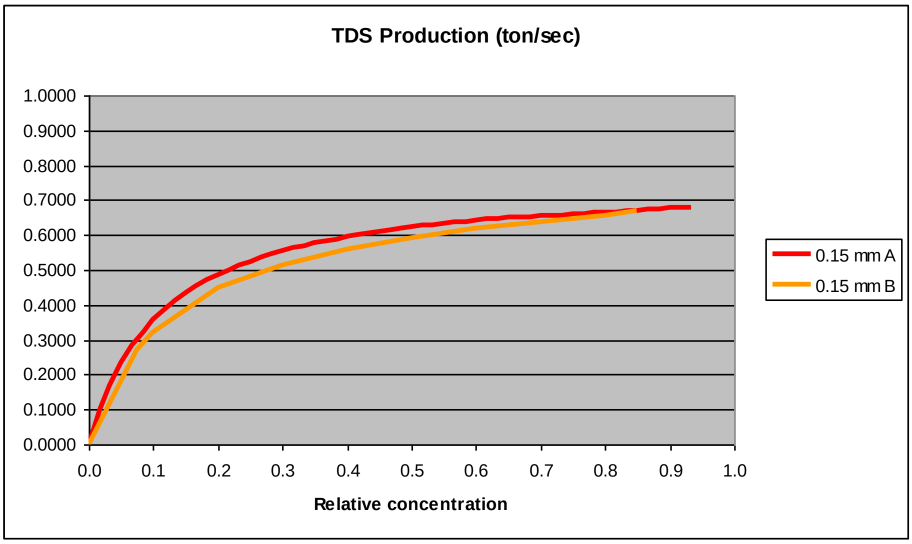

Figure 6-2: The production as a function of the relative concentration for an 0.15 mm grain diameter.

6.2 Implementation

The current simulation model is based on the theory as published in 3 publications and applied in some other publications. The basic theory was published in Terra et Aqua (Miedema (2008A)). Some special considerations and the one equation analytical model were published in the Journal of Dredging Engineering (Miedema (2009A)). Now how does this theory relate to reality? **Error! Reference source not found.** shows a easurement of the dredging cycle of a small TSHD using the Constant Volume System. In this figure the total load in the hopper, the total volume of the load in the hopper and the TDS in the hopper are shown, but many other signals like the density and the flow velocity were also available.

The measurements contain many turns and some other effects. After dumping, water is flowing back into the hopper, resulting in a partially filled hopper at the moment the real dredging starts. Due to a time delay between the registration of the density signal and the flow signal, the TDS (which is a derived signal) may become negative momentary. Due to some trim of the TSHD during the loading, it looks like the hopper volume is slightly increasing.

After the loading is stopped, the layer of water above the overflow has to flow away, resulting in a decrease of the total load and a decrease of the total volume. The measured decrease is bigger than would be expected. This is most probably caused by the Bernouilli effect when the TSHD starts sailing to the dump site. A higher sailing speed results in a smaller pressure measured by the transducers, resulting in an apparent decrease of the total load. When the TSHD approaches the dump site and reduces the sailing speed, the apparent load increases again.

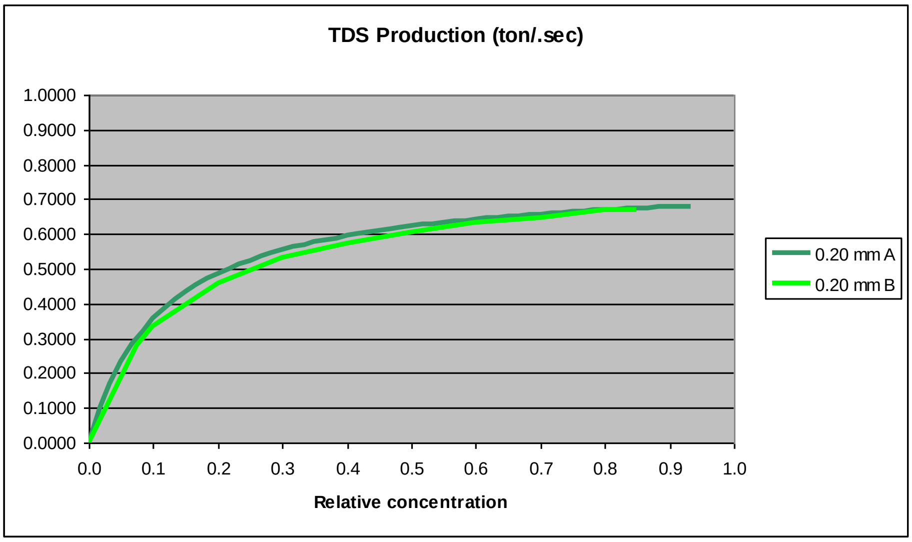

Figure 6-3: The production as a function of the relative concentration for an 0.20 mm grain diameter.

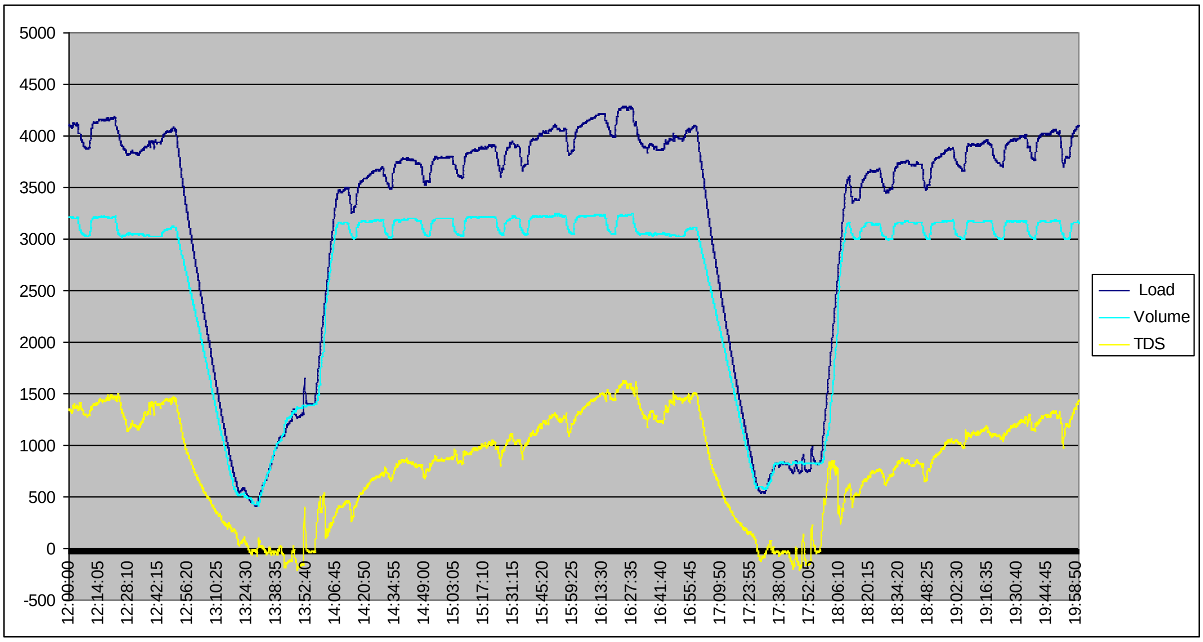

Figure 6-4: An example of a loading cycle of a TSHD with many turns.

The measurements were corrected for the effects of trim and time delays and compared with a simulation. To carry out the simulation it was important to reconstruct the input of the TSHD as accurately as possible. The input consisted of the density and flow signals. Figure 6-5 shows the corrected measurements (M) from Figure 6-4 and the results of the simulation (C). The first two lines to look at are the Total in (M) and (C), which show the total TDS going into the TSHD. All other signals are the result of what enters the hopper. It is clear that the measured Total in (M) is almost equal to the simulated Total in (C), although there are some small momentary deviations.
The other signals in Figure 6-5 are, the Total load (M) & (C), the Volume (M) & (C), the TDS (M) & (C) & buffered and finally the Overflow TDS (M) & (C) & buffered. From the figure it is clear that the simulations match the measurements very well and also that the buffered TDS and the buffered Overflow TDS match the measurements better than the un-buffered signals. It should be mentioned that the loading is stopped before erosion becomes important, so erosion behavior is not verified in these measurements. The behavior of flow

over a weir, which occurs each turn is simulated very well, while the cumulative overflow losses and thus also the TDS are simulated well by applying the time effect or buffer effect.

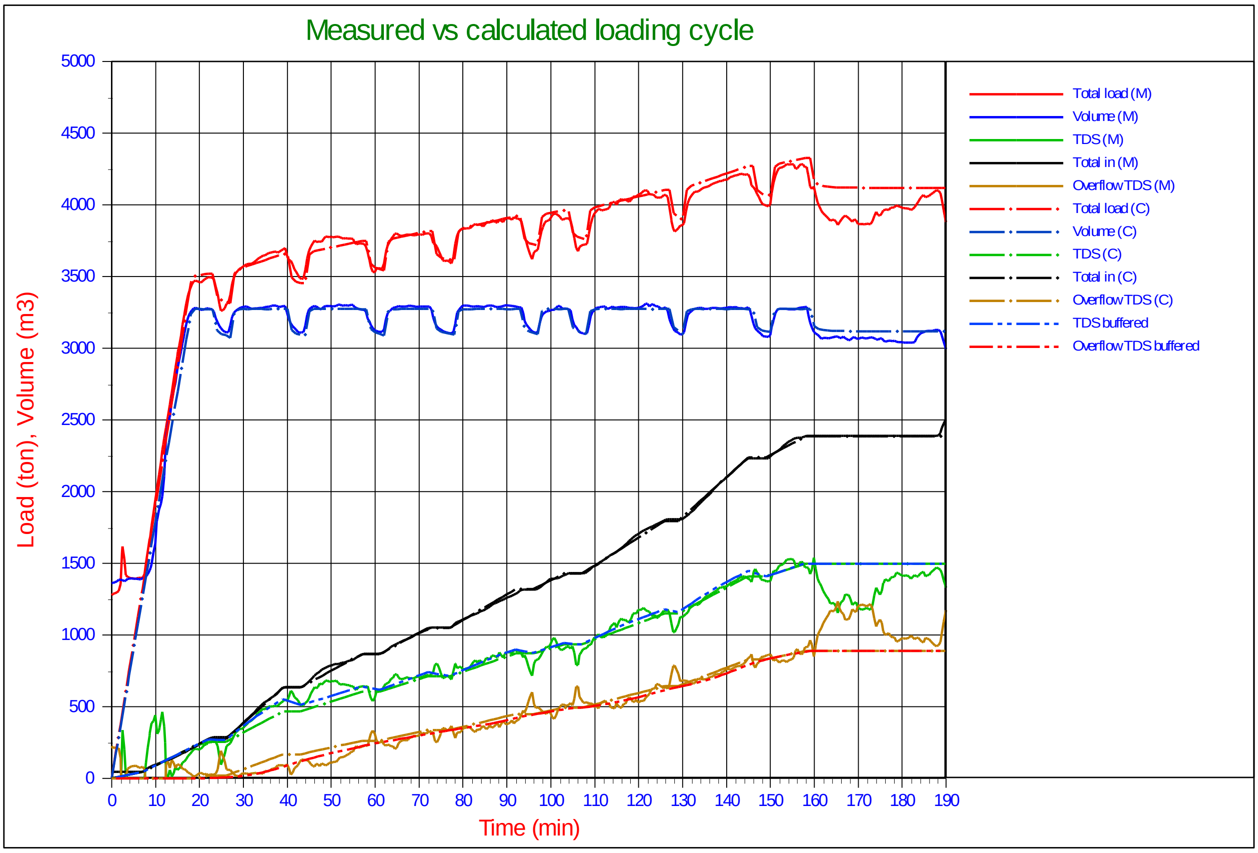

Figure 6-5: Simulation & measurement.

Figure 6-6 shows the cumulative overflow losses and efficiency as a function of the mixture concentration calculated with the one equation analytical model for 3 cases. The hopper was filled with water for 100% when the loading started, the hopper was filled for 50% and the hopper was empty, so 0% water. The cumulative efficiency, being the efficiency of one full cycle, continues to decrease with increasing concentration, due to the effect of hindered settling for the first case where we start with a 100% filled hopper. The sand used was an 0.1 mm sand, meaning that the sedimentation velocity is also decreasing with increasing concentration. When the hopper is filled for 50% or 0%, the efficiency decreases first, but increases later at the higher mixture concentrations. The reason is that it is assumed that the efficiency is 100% until the overflow level is reached and the influence of this becomes bigger at the higher concentrations.

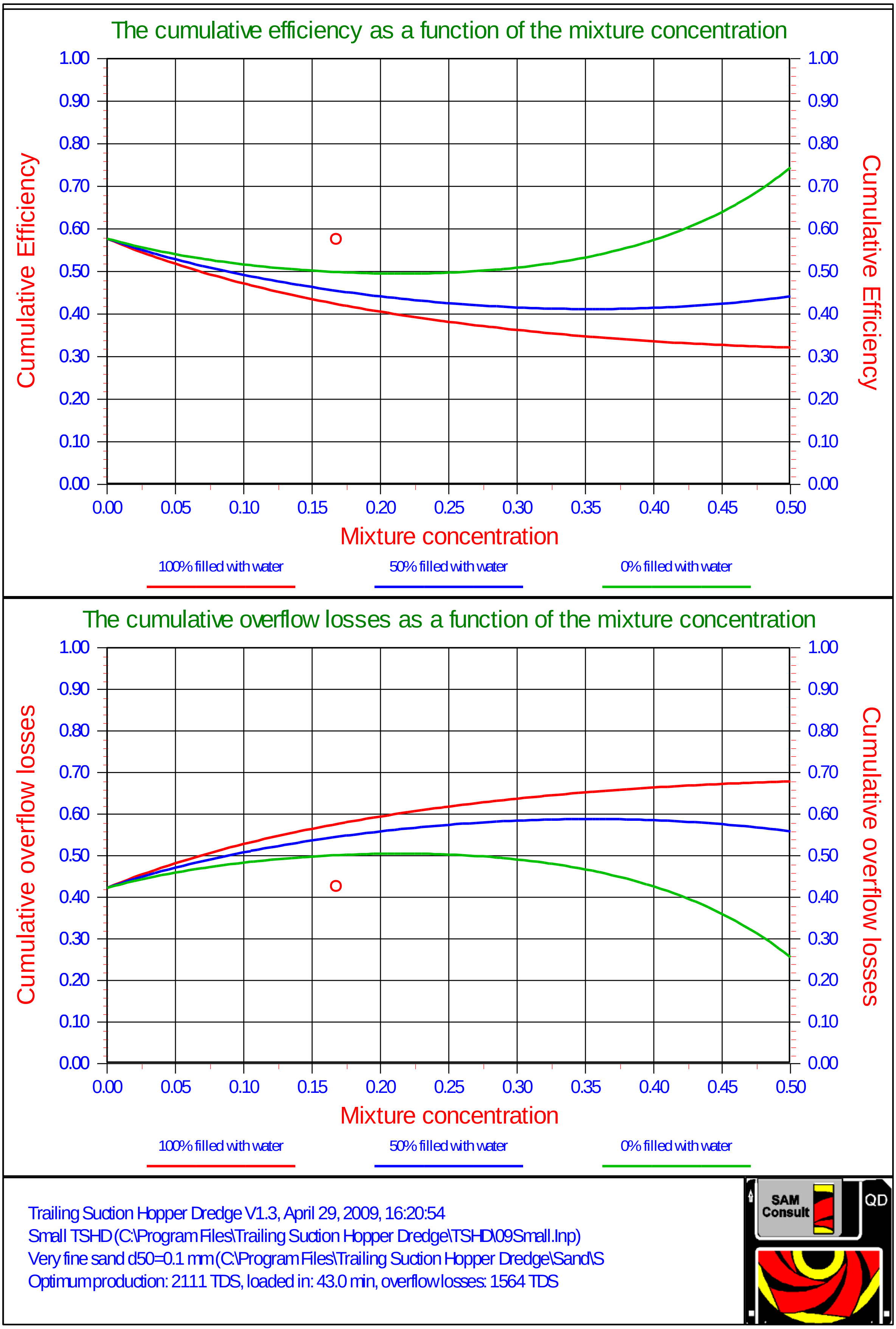

Figure 6-6: The overflow losses compared with an analytical model for the Small TSHD.

Chapter 7: Analytical Considerations

7.1 The Bed Rise or Sedimentation Velocity

Suppose a vertical element of the hopper with length and width equal to 1m consists of 3 layers. At the top a layer of water with a concentration of particles equal to zero, in the middle a layer of mixture with an average concentration $\mathbf{c_b}$ and at the bottom a layer of sediment with a concentration $\mathbf{c_{bed}}$. All the particles in the mixture layer have a vertical settling velocity $\mathbf{v_c}$ (including the hindered settling effect), while the sediment is moving up with a velocity $\mathbf{v_{sed}}$, the so-called sedimentation or bed rise velocity because of the sedimentation of the particles. Now the question is, what is the value of this sedimentation velocity if $\mathbf{c_b}$, $\mathbf{c_{bed}}$ and $\mathbf{v_c}$ are known and constant during a certain time interval.

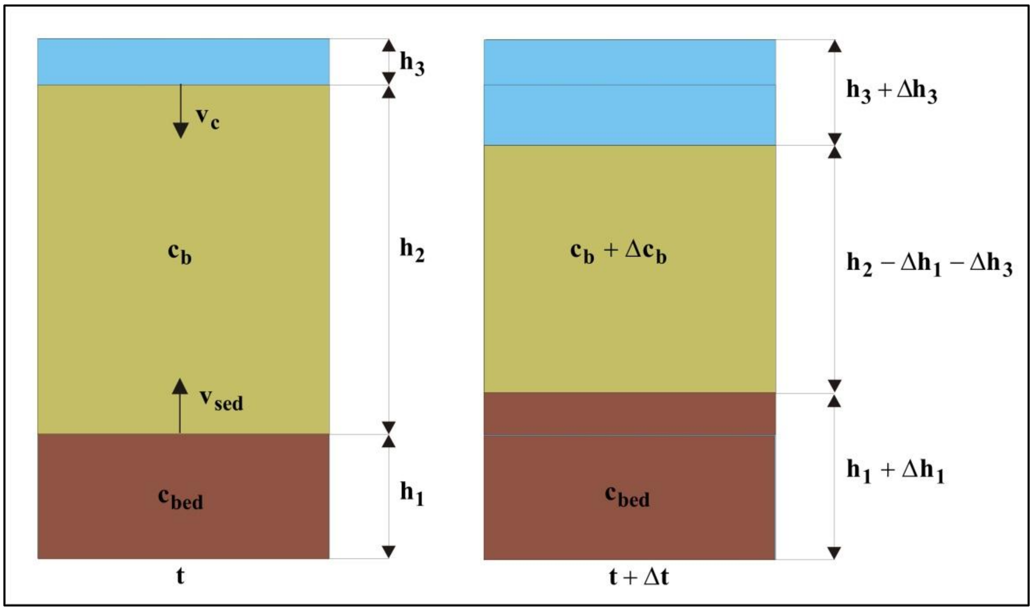

Figure 7-1: A segment of a hopper at 2 subsequent time steps.

Figure 7-1 shows the hopper at 2 subsequent time steps. During one time step, the mixture moves down with the settling velocity $\mathbf{v_c}$, causing the sediment to rise with the bed rise velocity $\mathbf{v_{sed}}$. There is no mass added during the time step, so the sum of the mixture mass and the sediment mass remains constant. At time **t** (left figure) the total mass in TDS in the hopper is:

$$\mathbf{TDS = h_1 \cdot c_{bed} + h_2 \cdot c_b} \tag{7-1}$$

A time step $\mathbf{\Delta t}$ later (right figure), if the total mass in TDS in the hopper is assumed to be constant:

$$\mathbf{TDS = (h_1 + \Delta h_1) \cdot c_{bed} + (h_2 - \Delta h_1 - \Delta h_3) \cdot (c_b + \Delta c_b)} \tag{7-2}$$

This gives:

$$\mathbf{\Delta h_1 \cdot c_{bed} + (-\Delta h_1 - \Delta h_3) \cdot c_b + (h_2 - \Delta h_1 - \Delta h_3) \cdot \Delta c_b = 0} \tag{7-3}$$

Neglecting the double derivatives this gives:

$$\mathbf{\Delta h_1 \cdot (c_{bed} - c_b) = \Delta h_3 \cdot c_b - h_2 \cdot \Delta c_b} \tag{7-4}$$

If the particles in the mixture layer all move downwards with the same settling velocity $\mathbf{v_c}$, then the increment of the concentration $\mathbf{\Delta c_b}$ in the second term on the right hand side equals zero, resulting in the following relation for the sedimentation or bed rise velocity:

$$\mathbf{v_{sed} = v_c \cdot \frac{c_b}{c_{bed} - c_b} \qquad with: \quad v_c = v_s \cdot \left(1 - C_v\right)^{\beta}} \tag{7-5}$$

$$\begin{aligned} \mathbf{With:} \quad & \mathbf{\Delta h_1 = v_{sed} \cdot \Delta t} \\ & \mathbf{\Delta h_3 = v_c \cdot \Delta t} \end{aligned} \tag{7-6}$$

Van Rhee (2002C) already derived this equation based on a finite element near the bed surface. If this equation is derived for a small element near the surface of the sediment, the concentration near the bed (the near bed concentration) does not have to be equal to the average concentration as used in the derivation above. Other researchers, Ooijens et al. (2001) and Braaksma et al. (2007), used this equation for determining the global overflow losses and just like van Rhee use the concentration of the dredged mixture $\mathbf{c_{in}}$ as a first approximation for the near bed concentration $\mathbf{c_b}$. This may lead however to results that are physically impossible.

7.2 The Dimensionless Overflow Rate

Based on the conservation of mass it can be proven that in general the near bed concentration $\mathbf{c_b}$ and the mixture concentration $\mathbf{c_{in}}$ are not equal.

If the increase of the sand mass in the sediment (bed) is considered as:

$$\mathbf{Q_{m_{bed}} = v_{sed} \cdot c_{bed} \cdot W \cdot L} \tag{7-7}$$

Then the total sand mass in the hopper at the end of the loading process, assuming a constant sedimentation velocity, after a time **T** equals to:

$$\mathbf{TDS_{bed} = Q_{m_{bed}} \cdot T = v_{sed} \cdot c_{bed} \cdot W \cdot L \cdot T} \tag{7-8}$$

The total mass of TDS that has entered the hopper during this time equals to:

$$\mathbf{TDS_{in} = Q_{m_{in}} \cdot T = Q_{in} \cdot c_{in} \cdot T} \tag{7-9}$$

The cumulative overflow losses are equal to the amount of mass that entered the hopper, minus the amount that has settled, divided by the amount that has entered the hopper, according to:

$$\mathbf{ov_{cum} = 1 - \eta_{cum} = \frac{TDS_{in} - TDS_{bed}}{TDS_{in}} = \frac{Q_{in} \cdot c_{in} \cdot T - v_{sed} \cdot c_{bed} \cdot W \cdot L \cdot T}{Q_{in} \cdot c_{in} \cdot T} = 1 - \frac{W \cdot L}{Q_{in}} \cdot v_{sed} \cdot \frac{c_{bed}}{c_{in}}} \tag{7-10}$$

Using the unmodified hopper load parameter $\mathbf{v_o = Q_{in}/W \cdot L}$ and equation (7-5) for the sedimentation velocity, this gives:

$$\mathbf{ov_{cum} = 1 - \eta_{cum} = 1 - \frac{W \cdot L}{Q_{in}} \cdot v_c \frac{c_b}{c_{bed} - c_b} \cdot \frac{c_{bed}}{c_{in}} = 1 - \frac{v_c}{v_o} \cdot \frac{c_b}{c_{in}} \cdot \frac{c_{bed}}{c_{bed} - c_b}} \tag{7-11}$$

Ooijens et al. (2001) uses this equation for determining the cumulative overflow losses. Van Rhee (2002C) defined a dimensionless overflow rate **S***, based on the sedimentation velocity according to equation (7-5):

$$\mathbf{S^* = \frac{v_o}{v_c} \cdot \frac{c_{in}}{c_b} \cdot \frac{c_{bed} - c_b}{c_{bed}} = H^* \cdot \frac{c_{in}}{c_b} \cdot \frac{c_{bed} - c_b}{c_{bed}} \quad and \quad S'^* = H^* \cdot \frac{c_{bed} - c_{in}}{c_{bed}}} \tag{7-12}$$

The second equation for **S'*** is valid if $\mathbf{c_b = c_{in}}$. This however has no physical meaning. Substituting equation (7-12) in equation (7-11) gives a relation between the cumulative overflow losses $\mathbf{ov_{cum}}$ and the dimensionless overflow rate **S***:

$$\mathbf{ov_{cum}=1-\frac{1}{S^*}} \qquad \text{or} \qquad \mathbf{\eta_{cum}=\frac{1}{S^*}} \tag{7-13}$$

Since the overall settling efficiency can never be greater than 1, this means that **S*** should always be greater or equal to 1. Besides, the name dimensionless overflow rate does not seem to be appropriate, because **S*** equals to the reciprocal of the cumulative settling efficiency and not to the cumulative overflow losses.

7.3 The Near Bed Concentration

Both van Rhee (2002C) and Ooijens et al. (2001) state that making the near bed concentration $\mathbf{c_b}$ equal to the mixture concentration $\mathbf{c_{in}}$, is a good first approximation. For course particles with a settling velocity $\mathbf{v_c}$ higher than the unmodified hopper load parameter $\mathbf{v_o}$, equation (7-11) leads to negative overflow losses and equation (7-12) will gives an **S*** smaller than 1. This leads to the conclusion that for an overall approach, the near bed concentration should not be chosen equal to the mixture concentration. From equation (7-11), the following equation can be derived for the overall settling efficiency:

$$\eta_{cum}=\frac{v_c}{v_o}\cdot\frac{c_b}{c_{in}}\cdot\frac{c_{bed}}{c_{bed}-c_b} \tag{7-14}$$

From this equation, an equation for the near bed concentration $\mathbf{c_b}$ can be derived:

$$c_b=\frac{\eta_{cum}\cdot c_{bed}}{\left(\eta_{cum}+\frac{v_c}{v_o}\cdot\frac{c_{bed}}{c_{in}}\right)}=\frac{\eta_{cum}\cdot c_{bed}\cdot c_{in}}{\left(\eta_{cum}\cdot c_{in}+\frac{v_c}{v_o}\cdot c_{bed}\right)}=c_{bed}\cdot\frac{\eta_{cum}\cdot\frac{c_{in}}{c_{bed}}}{\left(\eta_{cum}\cdot\frac{c_{in}}{c_{bed}}+\frac{v_c}{v_o}\right)} \tag{7-15}$$

Thus:

$$\frac{c_b}{c_{bed}}=\frac{\eta_{cum}\cdot\frac{c_{in}}{c_{bed}}}{\left(\eta_{cum}\cdot\frac{c_{in}}{c_{bed}}+\frac{v_c}{v_o}\right)}=\frac{\eta_{cum}\cdot\kappa}{\left(\eta_{cum}\cdot\kappa+\frac{v_c}{v_o}\right)} \tag{7-16}$$

$$\textbf{With :} \qquad \kappa=\frac{c_{in}}{c_{bed}}$$

Now two cases can be considered:
1. There are hardly any overflow losses, which means that the particle settling velocity is much higher then the hopper load parameter.
2. The particle settling velocity is smaller than the hopper load parameter.

In both cases it is assumed that the loading process starts with a hopper full of water, otherwise the filling of the hopper up to overflow level is part of the cumulative settling efficiency, while there are no overflow losses during this phase, so a to high settling efficiency is found. If the loading process starts with an empty hopper or a partially filled hopper, this part of the filling process should not be considered when determining the cumulative settling efficiency, for the purpose of determining the correct near bed concentration.

Case 1: **η=1**

$$\frac{c_b}{c_{bed}}=\frac{\kappa}{\left(\kappa+\frac{v_c}{v_o}\right)} \tag{7-17}$$

Since in this case the velocity ratio $\mathbf{v_c/v_o}$ is always greater than 1, the near bed concentration $\mathbf{c_b}$ will always be smaller than the mixture concentration $\mathbf{c_{in}}$. The greater the settling velocity of the particle, the smaller the near bed concentration. In other words, the ratio c_b/c_{bed} will always be smaller than κ the ratio c_{in}/c_{bed}. Physically this means that the particles settle faster than they are supplied by the inflow of mixture.

Case 2: $\eta_p = \frac{v_c}{v_o} < 1$

$$\frac{c_b}{c_{bed}} = \frac{\eta_{cum} \cdot \kappa}{\left(\eta_{cum} \cdot \kappa + \eta_p\right)} \tag{7-18}$$

If the PSD is very narrow graded, the cumulative settling efficiency η_{cum} is equal to the settling efficiency of the particle considered η_p leading to the following equation:

$$\frac{c_b}{c_{bed}} = \frac{\kappa}{\left(\kappa + 1\right)} \tag{7-19}$$

The near bed concentration c_b in this case is always smaller than the mixture concentration c_{in}. Physically this is caused by the overflow losses.

If the PSD is not narrow graded, the cumulative settling efficiency η_{cum} can be smaller of greater than the particle settling efficiency η_p, where it is assumed that the particle efficiency for the d_{50} is chosen.
If the PSD is steep for the grains smaller than the d_{50} and well graded for the grains larger than the d_{50}, the cumulative settling efficiency η_{cum} will be greater than the particle settling efficiency η_p. Figure 7-2 shows that in this case the near bed concentration c_b is greater than the mixture concentration c_{in} for small mixture concentrations and smaller than the mixture concentration for high mixture concentrations. Physically this is caused by the fact that the larger particles dominate the settling efficiency. For example, the cumulative settling efficiency in Figure 7-2 is chosen 0.8. For a particle settling efficiency η_p of 0.6, the ratio λ is greater than 1 for a value of κ smaller than 0.25. The ratio λ between the near bed concentration c_b and the mixture concentration c_{in} is:

$$\lambda = \frac{c_b}{c_{bed} \cdot \kappa} = \frac{c_b}{c_{in}} = \frac{\eta_{cum}}{\left(\eta_{cum} \cdot \kappa + \eta_p\right)} \tag{7-20}$$

If the PSD is steep for the grains larger than the d_{50} and well graded for the grains smaller than the d_{50}, the cumulative settling efficiency η_{cum} will be smaller than the particle settling efficiency η_p for the d_{50} resulting in a ratio λ that is always smaller then 1, so the near bed concentration c_b is always smaller than the mixture concentration c_{in}. Physically this is caused by the fact that the smaller particles dominate the cumulative settling efficiency.

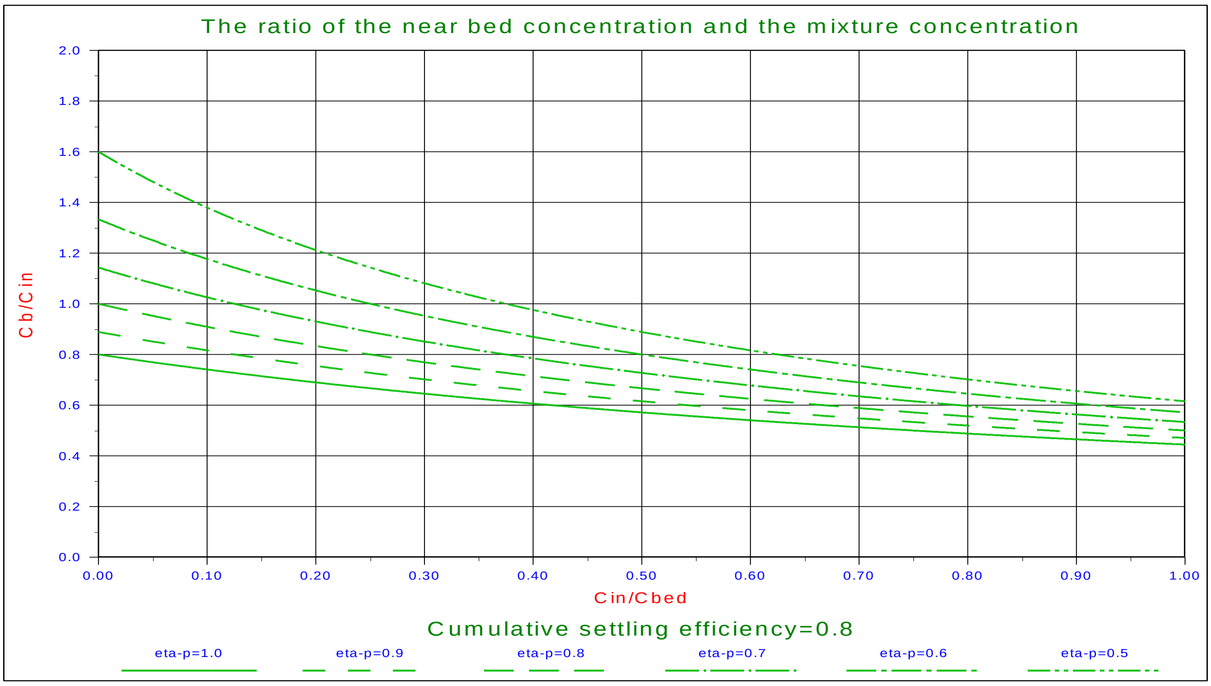

Figure 7-2: The ratio between c_b and c_{in}.

7.4 The Overall Bed Rise or Sedimentation Velocity

Based on the conservation of mass it has been proven that the near bed concentration $\mathbf{c_b}$ should not be chosen equal to the mixture concentration. In fact the near bed concentration $\mathbf{c_b}$ can be smaller or greater than the mixture concentration $\mathbf{c_{in}}$, depending on the PSD of the sand. The loading process considered, should start at the moment the overflow level is reached, otherwise a to high cumulative settling efficiency is chosen. If equation (7-16) is substituted in equation (7-5), the following equation for the sedimentation or bed rise velocity is found:

$$\mathbf{v_{sed} = v_c \cdot \frac{c_b}{c_{bed} - c_b} = v_c \cdot \frac{c_{in} \cdot \dfrac{\eta_{cum}}{\eta_{cum} \cdot \kappa + \dfrac{v_c}{v_o}}}{c_{bed} - c_{in} \cdot \dfrac{\eta_{cum}}{\eta_{cum} \cdot \kappa + \dfrac{v_c}{v_o}}} = v_o \cdot \eta_{cum} \cdot \kappa} \qquad \textbf{(7-21)}$$

In other words:

$$\mathbf{L \cdot W \cdot v_{sed} \cdot c_{bed} = Q \cdot c_{in} \cdot \eta_{cum}}$$

$$\mathbf{With: \quad v_o = \frac{Q}{L \cdot W}} \qquad \textbf{(7-22)}$$

$$\mathbf{\kappa = \frac{c_{in}}{c_{bed}}}$$

From the point of view of conservation of mass this is logic, so the circle is round again. The derivation is for the whole loading cycle, from the moment the overflow level is reached to the moment the hopper is economically full. Some aspects of the loading process however are not taken into account:

1. The filling of the hopper up to the overflow level. Since it is assumed that there are no overflow losses during this phase, this will increase the cumulative settling efficiency and thus the bed rise velocity. This also gives a higher near bed concentration, which is valid for the whole loading cycle, but not realistic for the loading after the overflow level has been reached.
2. The occurrence of scour at the end of the loading cycle. This will decrease the average sedimentation velocity resulting in a lower cumulative settling efficiency. The calculated near bed concentration will also decrease, which is not representative for the main part of the loading cycle. Fortunately the scour does not occur very long if the loading stops at the most economical point, so this influence is not very important.

Equation (7-13) implies that the factor **S*** should always be greater than 1. Van Rhee ((2002C), page 72 and page 205) however found values for **S*** between 0.5 and 1 with the approximation that the near bed concentration $\mathbf{c_b}$ equals the mixture concentration $\mathbf{c_{in}}$. For this case he found the following empirical relation between the cumulative overflow losses and the dimensionless overflow rate:

$$\mathbf{ov_{cum} = 0.39 \cdot (S'^{*} - 0.43)} \tag{7-23}$$

To explain this, the example from chapter 8 of van Rhee (2002C) will be reproduced. Van Rhee used the TSHD Cornelia, a hopper with **L=52m**, **W=11.5m**, **H=8.36m**, $\mathbf{Q=5.75m^3/sec}$, $\mathbf{c_{bed}=0.54}$, $\mathbf{c_{in}=0.15}$, $\mathbf{\eta_{cum}=0.92}$ and $\mathbf{d_{50}=0.235mm}$. This gives $\mathbf{v_c=14.8mm/sec}$ including the hindered settling effect, $\mathbf{v_o=9.6mm/sec}$, $\mathbf{\kappa=0.278}$, **H*=0.648**, **S*=0.47** and $\mathbf{ov_{cum}=0.015}$ if $\mathbf{c_b=c_{in}}$.
From equation (7-16) it can be seen however that $\mathbf{c_b=0.513 \cdot c_{in}}$. This gives **S*=1.09** according to equation (7-12) and (7-13), which in fact is a self-fulfilling prophecy and $\mathbf{ov_{cum}=0.259}$ according to equation (7-23) using **S*=1.09**. The real cumulative overflow losses were 0.08, so the empirical equation (7-23) for the overflow losses is not very accurate. In fact using the approximation of $\mathbf{c_b=c_{in}}$ does not match the conservation of mass principle and should only be applied as a first approximation.

Equation (7-23) has been derived by van Rhee ((2002C) , page 72) based on a set of model tests, see Table 7-1. Recalculating the values for $\mathbf{c_b}$ with equation (7-16) and **S*** with equation (7-12) gives a new relation between the cumulative overflow losses $\mathbf{ov_{cum}}$ and **S***. This gives a 100% correlation matching equation (7-12), but this is a self-fulfilling prophecy, since the near bed concentration has been derived from the cumulative overflow losses. Table 7-1, Figure 7-3 and Figure 7-4 show the original data from van Rhee (2002C), while Figure 7-5 shows the results of the recalculation.

The original equation (7-5) for the bed rise velocity however is still valid for a small element of sediment and mixture at a certain moment of the loading process if the correct near bed concentration $\mathbf{c_b}$ is used. For the overall approach equation (7-21) should be used to calculate the average bed rise velocity.

Table 7-1: The model tests as carried out by van Rhee (2002C).

Test	ρ_{in}	c_{in}	Q	v_o	d_{50}	ov_{cum}	H*	S'* ($c_b=c_{in}$)	c_b	S* (c_b<>c_{in})
1	1310	0.18	0.099	2.75	0.140	0.01	0.75	0.50	0.105	1.01
2	1210	0.11	0.139	3.86	0.146	0.02	0.70	0.55	0.068	1.02
4	1460	0.27	0.100	2.78	0.147	0.04	1.25	0.62	0.201	1.04
5	1350	0.20	0.100	2.78	0.102	0.25	1.60	1.00	0.165	1.33
6	1420	0.24	0.137	3.81	0.107	0.42	2.60	1.43	0.218	1.72
7	1100	0.05	0.140	3.89	0.089	0.23	1.10	1.00	0.037	1.30
8	1500	0.29	0.075	2.08	0.103	0.25	2.20	1.02	0.255	1.33
9	1260	0.14	0.138	3.83	0.096	0.27	1.62	1.18	0.130	1.37
10	1310	0.18	0.101	2.81	0.105	0.18	1.30	0.88	0.139	1.22
11	1290	0.16	0.137	3.81	0.106	0.21	1.60	1.12	0.149	1.27
12	1480	0.28	0.101	2.81	0.105	0.32	2.55	1.22	0.255	1.47
13	1480	0.28	0.102	2.83	0.104	0.29	2.60	1.24	0.264	1.41
15	1370	0.21	0.138	3.83	0.101	0.35	2.35	1.43	0.203	1.54
16	1130	0.06	0.141	3.92	0.103	0.23	1.00	0.88	0.046	1.30
17	1290	0.16	0.142	3.94	0.104	0.29	1.75	1.22	0.148	1.40
18	1280	0.16	0.140	3.89	0.111	0.28	1.48	1.05	0.128	1.38
19	1180	0.10	0.100	2.78	0.100	0.11	0.85	0.70	0.063	1.12

Ooijens et al. (2001) also published data of research carried out to validate the model of the sedimentation velocity. He used equation (7-5) with $\mathbf{c_b=c_{in}}$. Figure 7-6 shows the measurements and prediction of Ooijens et al. (2001) and the prediction using the near bed concentration according to equation (7-16). The cumulative efficiency $\mathbf{\eta_{cum}}$, required in equation (7-16) has been calculated using the modified Camp model of Miedema and Vlasblom (1996). It is obvious that using the near bed concentration according to equation (7-16) results in a better match with the measured data. Ooijens et al. (2001) used a hopper with **L=11.34m**, **W=2.0m**, **H=1.4-2.4m**, $\mathbf{Q=0.1m^3/sec}$, $\mathbf{d_{50}=0.1mm}$ and densities up to 1.6 ton/m^3. For the calculations a bed concentration $\mathbf{c_{bed}}$ of 0.55 has been used.

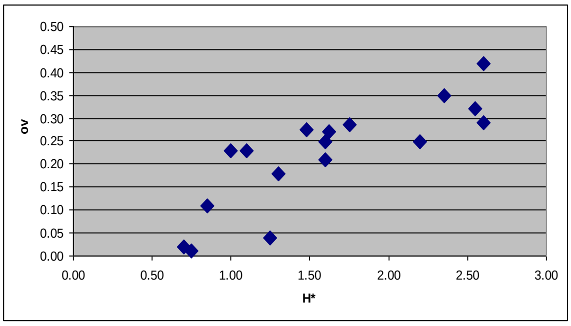

Figure 7-3: Overflow losses vs H*.

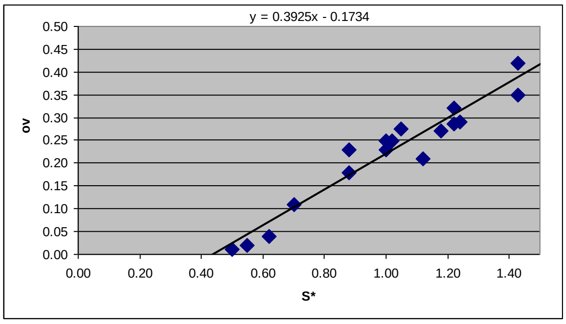

Figure 7-4: Overflow losses vs S'*.

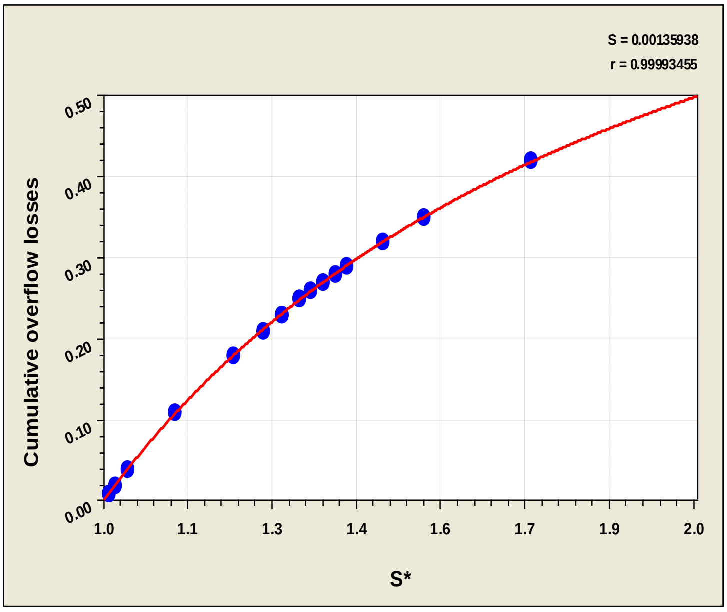

Figure 7-5: The cumulative overflow losses vs S*, c_b re-calculated.

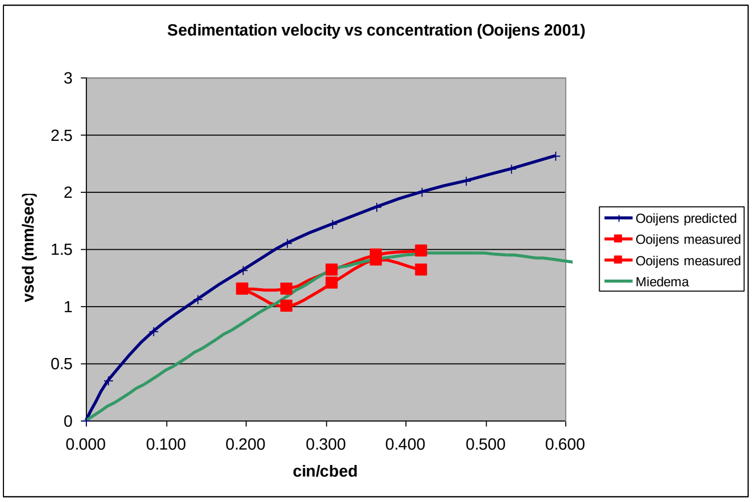

Figure 7-6: The sedimentation velocity measured by Ooijens et al. (2001).

7.5 The Concentrations during the Loading Cycle

Equation (7-16) gives the average near bed concentration, averaged during the total loading process. In fact the concentration calculated with equation (7-16) equals the average mixture concentration above the bed. The momentary near bed concentration however may differ from the average. If a hopper with a height **H** and a sediment level **h** is considered, the following equation can be derived based on the conservation of mass principle, starting with a hopper full of water at t=0, and assuming a uniform concentration distribution with concentration $\mathbf{c_b(t)}$ above the sediment level and a concentration $\mathbf{c_{bed}}$ in the sediment.

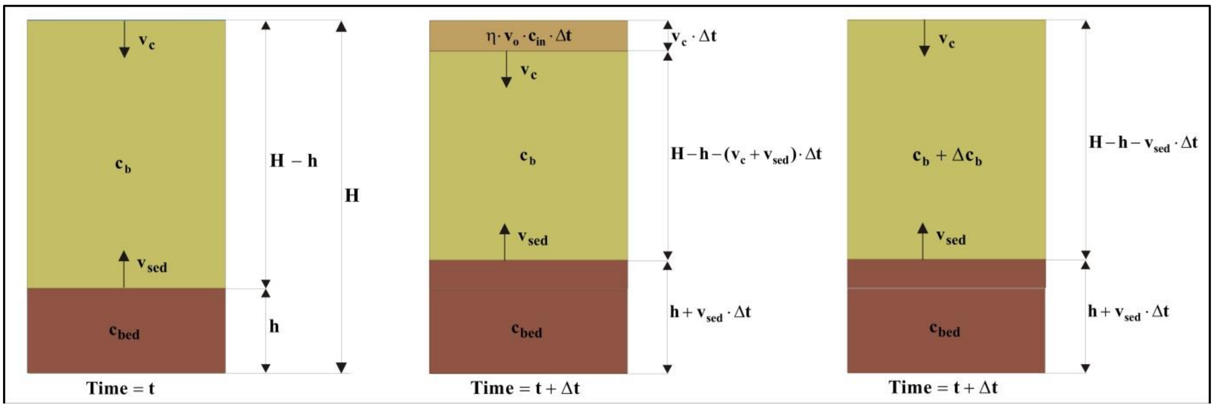

Figure 7-7: The concentrations during the loading cycle.

Further assuming a hopper with a width and a length of 1 m, the total mass TDS in the hopper at any moment of time equals the amount of TDS that has entered the hopper and stayed in the hopper during this time, assuming a constant settling efficiency **η**:

$$\mathbf{h \cdot c_{bed} + (H-h) \cdot c_b = \eta \cdot v_o \cdot c_{in} \cdot t} \quad \textbf{(7-24)}$$

The left hand side shows the amount of mass in the sediment ($\mathbf{h \cdot c_{bed}}$) and above the sediment ($\mathbf{(H-h)\cdot c_b}$), while the right hand side shows the amount of mass that has entered the hopper ($\mathbf{\eta \cdot v_o \cdot c_{in} \cdot t}$) at a time **t** after the loading has started. This can be rewritten as:

$$\mathbf{h \cdot (c_{bed} - c_b) + H \cdot c_b = \eta \cdot v_o \cdot c_{in} \cdot t} \quad \textbf{(7-25)}$$

Taking the derivative with respect to time gives:

$$\mathbf{\left(c_{bed} - c_b\right) \cdot \frac{dh}{dt} + \left(H-h\right) \cdot \frac{dc_b}{dt} = \eta \cdot v_o \cdot c_{in}} \quad \textbf{(7-26)}$$

With the sedimentation velocity according to equation 5:

$$\mathbf{\frac{dh}{dt} = v_{sed} = v_c \cdot \frac{c_b}{c_{bed} - c_b}} \quad \textbf{(7-27)}$$

This gives for the derivative of the near bed concentration:

$$\mathbf{\frac{dc_b}{dt} = \frac{\eta \cdot v_o \cdot c_{in} - v_c \cdot c_b}{H-h}} \quad \textbf{(7-28)}$$

Or:

$$\mathbf{\left(H-h\right) \cdot \frac{dc_b}{dt} + v_c \cdot c_b - \eta \cdot v_o \cdot c_{in} = 0} \quad \textbf{(7-29)}$$

Solving equation (7-29) for a constant sediment level **h** gives:

$$\frac{c_b}{c_{in}} = \eta \cdot \frac{v_o}{v_c} \cdot \left(1 - e^{-\frac{v_c}{H-h} \cdot t}\right) \qquad (7\text{-}30)$$

Now an expression has been found for the average near bed concentration (equation (7-16)) and an expression for the momentary near bed concentration (equation (7-30)).
For the case of the Cornelia, as discussed before, equations (7-27) and (7-28) have been solved numerically. The results are shown in Figure 7-8 and Figure 7-9 it is obvious that the near bed concentration has to build up, causing a time delay in the momentary sediment level, with respect to the sediment entered in the hopper. The vertical distance between the momentary sediment level and the level of the sediment in, is the amount of sediment still in suspension.
It should be noted here that the near bed concentration is assumed to be the concentration of all the mixture above the sediment. Although this is not in accordance with the definition of van Rhee (2002C), it gives more insight in the loading process.

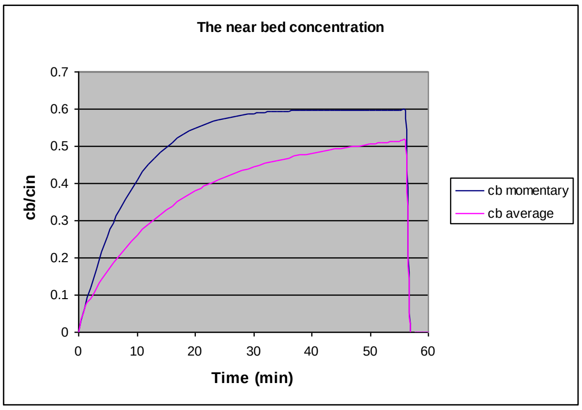

Figure 7-8: The near bed concentration, v_c=14.8 mm/sec.

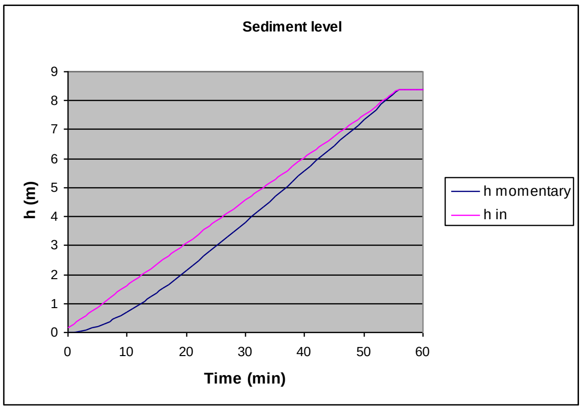

Figure 7-9: The sediment level, v_c=14.8 mm/sec.

The case considered in Figure 7-8 and Figure 7-9, has a sand with a settling velocity of 14.8 mm/sec, so a rather course sand. It is interesting to see what these figures would look like for finer sands. If two other cases are considered, sand with a settling velocity of 9.6 mm/sec (equal to the hopper load parameter) and sand with 50% of this settling velocity, 4.8 mm/sec, including the hindered settling effect. This gives values for the **S*** of 0.72 and 1.44 (assuming c_b=c_{in}). The estimated overflow losses according to equation (7-23) are now 11.31% and 39.39%, but since the estimation was 6.5% too low for the sand with a settling velocity of 14.8 mm/sec, as discussed before, this 6.5% is added to the estimation, giving 17.8% and 45.9%. So the settling efficiencies are estimated to 0.822 and 0.541.

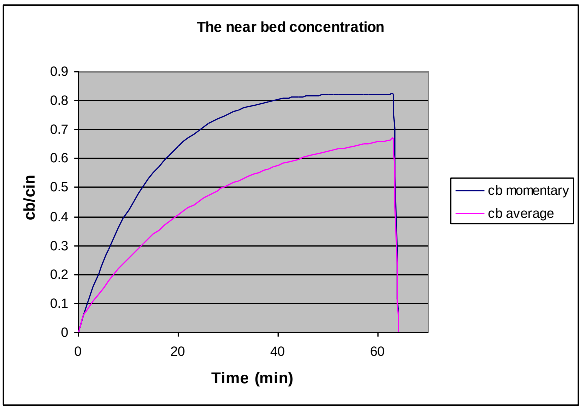

Figure 7-10: The near bed concentration, vc=9.6 mm/sec.

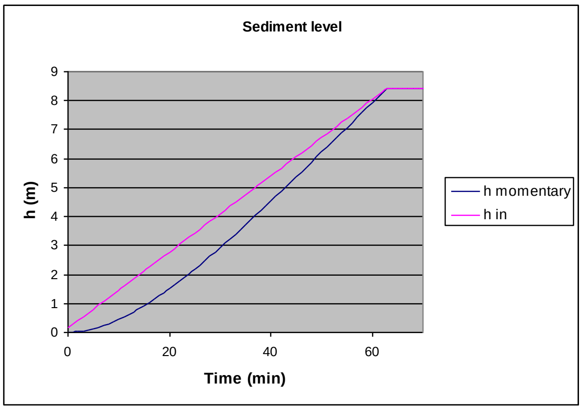

Figure 7-11: The sediment level, vc=9.6 mm/sec.

From these figures it can be seen that a smaller grain with a smaller settling velocity will result in a higher near bed concentration as also was concluded from Figure 7-2 and equation (7-20). The smallest grain gives a momentary near bed concentration which is higher than the incoming mixture concentration at the end of the loading process, while the average near bed concentration is still below the incoming mixture concentration. Another conclusion that can be drawn and also makes sense, is that the time required for the mixture to settle increases when the settling velocity decreases. This is in accordance with equation (7-30).

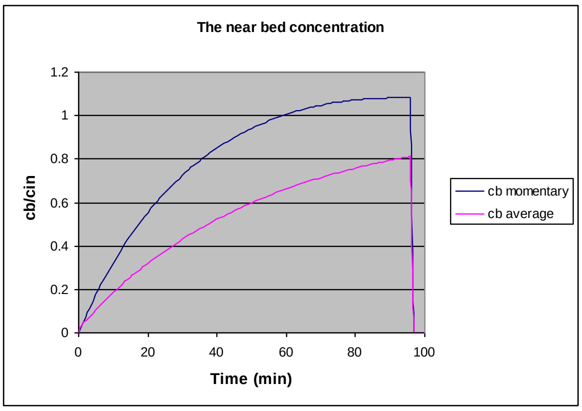

Figure 7-12: The near bed concentration, vc=4.8 mm/sec.

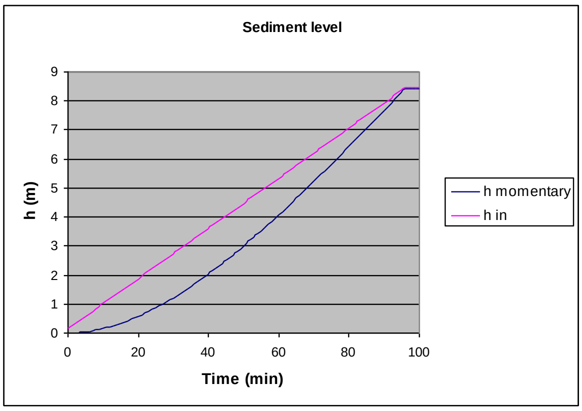

Figure 7-13: The sediment level, vc=4.8 mm/sec.

The fact that the near bed concentration (here it is the average concentration in the hopper above the bed) is different from the incoming mixture concentration also implies that this near bed concentration should be used for determining the hindered settling effect. In most cases this will result in a near bed concentration smaller than the incoming mixture concentration, but in specific cases the near bed concentration is higher.

Chapter 8: Analytical Model to Predict the Overflow Losses

8.1 The Analytical Model

After discussing the empirical equation (7-23) of van Rhee (2002C), it is interesting to see if there is a more theoretical background behind this equation. Of course equation (7-13) has been found, but using it in combination with the near bed concentration according to equation (7-16), is a self-fulfilling prophecy. Equation (7-23) at least gives a first estimate of the overflow losses, although some questions can be asked about the validity as already mentioned by van Rhee (2002C).
One of the omissions of equation (7-23) is, that it is based on tests with a certain grading of the sand, so the question would be, how accurate is this equation if sand with another grading is used. To investigate this, an old analytical model of Miedema (Miedema S. , The flow of dredged slurry in and out hoppers and the settlement process in hoppers, 1981) is used. The model is based on the Camp (1946) approach and published by Miedema and Vlasblom (Miedema & Vlasblom, Theory of Hopper Sedimentation, 1996). The settling efficiency $\boldsymbol{\eta_b}$ at a certain moment of the hopper loading process is defined as:

$$\eta_b = (1-p_o) + \int_{p_{fs}}^{p_o} \frac{v_c}{v_o} \cdot dp \tag{8-1}$$

One should read Miedema & Vlasblom (1996) for the derivation of this equation. Basically, there are 3 areas in this equation. The area from 0 to $\mathbf{p_{fs}}$ are the particles that will not settle due to scour, or because they are to small (fines), the area from $\mathbf{p_{fs}}$ to $\mathbf{p_o}$, which are the particles that settle partially, some reach the sediment but some don't and leave the hopper through the overflow, and last but not least the area above $\mathbf{p_o}$ which are the particles that settle 100%. To find an analytical solution for this equation, the PSD should be approximated by a straight line according to:

$$\log(d) = a \cdot p - b \tag{8-2}$$

A number of examples of PSD's according to equation (8-2) are shown in Figure 8-1. Equation (8-2) can also be written as:

$$p = \frac{\log(d) + b}{a} \tag{8-3}$$

Now the grains that cause overflow losses are usually grains that settle in the Stokes region, according to:

$$v_s = 424 \cdot R_d \cdot \mu \cdot d^2 \tag{8-4}$$

Hindered settling can be taken into account with the well-known Richardson and Zaki equation:

$$v_c = 424 \cdot R_d \cdot \mu \cdot d^2 \cdot (1 - C_v)^{\beta} \tag{8-5}$$

This can be rewritten as equation (8-6) to show the grain diameter as a function of the settling velocity.

$$d = \left(\frac{v_c}{424 \cdot R_d \cdot \mu \cdot (1 - C_v)^{\beta}} \right)^{1/2} \tag{8-6}$$

The number 424 is based on the original Stokes equation but can be changed using the variable $\boldsymbol{\mu}$. The particle diameter that matches the hopper load parameter $\mathbf{v_o}$, the particle that will just settle 100% is now:

$$d_o = \left(\frac{v_o}{424 \cdot R_d \cdot \mu \cdot (1 - C_v)^{\beta}} \right)^{1/2} \tag{8-7}$$

This gives for the fraction of the particles that will settle 100%, $\mathbf{p_o}$:

$$p_o = \frac{\log(d_o)+b}{a} \tag{8-8}$$

For the particles that settle partially the second term on the right hand side of equation (8-1) has to be solved according to:

$$p_1 = \int_{p_{fs}}^{p_o} \frac{v_c}{v_o} \cdot dp = \int_{p_{fs}}^{p_o} \frac{424 \cdot R_d \cdot \mu \cdot d^2 \cdot (1-C_v)^{\beta}}{v_o} \cdot dp = \int_{p_{fs}}^{p_o} \frac{424 \cdot R_d \cdot \mu \cdot (1-C_v)^{\beta} \cdot e^{2\cdot(a\cdot p-b)\cdot \ln(10)}}{v_o} dp \tag{8-9}$$

$$p_1 = \frac{1}{2 \cdot a \cdot \ln(10)} \cdot \frac{424 \cdot R_d \cdot \mu \cdot (1-C_v)^{\beta}}{v_o} \cdot e^{-2\cdot b \cdot \ln(10)} \cdot \left(e^{2\cdot a \cdot p_o \cdot \ln(10)} - e^{2\cdot a \cdot p_{fs} \cdot \ln(10)}\right) \tag{8-10}$$

This gives for the settling efficiency of the whole PSD:

$$\eta = (1-p_o)+p_1 \tag{8-11}$$

Equation (8-11) does not include the turbulence effect as described by Miedema & Vlasblom (Miedema & Vlasblom, Theory of Hopper Sedimentation, 1996), because here it is the aim to find a simple equation to predict overflow losses. Of course this will give an error, but the magnitude of the settling efficiency found will be correct. The derivation until now assumes that the loading process starts with a hopper full of water, so from the beginning of the loading process the settling efficiency is active. In reality though, it is possible that the loading process starts with an empty hopper or a partially filled hopper. When the hopper at the start of the loading process has to be partially filled with mixture for a fraction $\boldsymbol{\alpha}$, and it is assumed that all the particles that enter the hopper before the overflow level has been reached will settle, then the sediment level will already reach a fraction $\boldsymbol{\varepsilon}$ of the height of the hopper when the overflow level has been reached. This fraction $\boldsymbol{\varepsilon}$ can be calculated with:

$$\varepsilon = \alpha \cdot \left(\frac{\rho_{in} - \rho_w}{\rho_{bed} - \rho_w} \right) \tag{8-12}$$

Since this has an effect on the cumulative settling efficiency $\boldsymbol{\eta_{cum}}$, the settling efficiency has to be corrected by:

$$ov_{cum} = \frac{ov \cdot (1-\varepsilon)}{1-\varepsilon \cdot ov} \tag{8-13}$$

The cumulative overflow losses are now:

$$\eta_{cum} = 1 - ov_{cum} \tag{8-14}$$

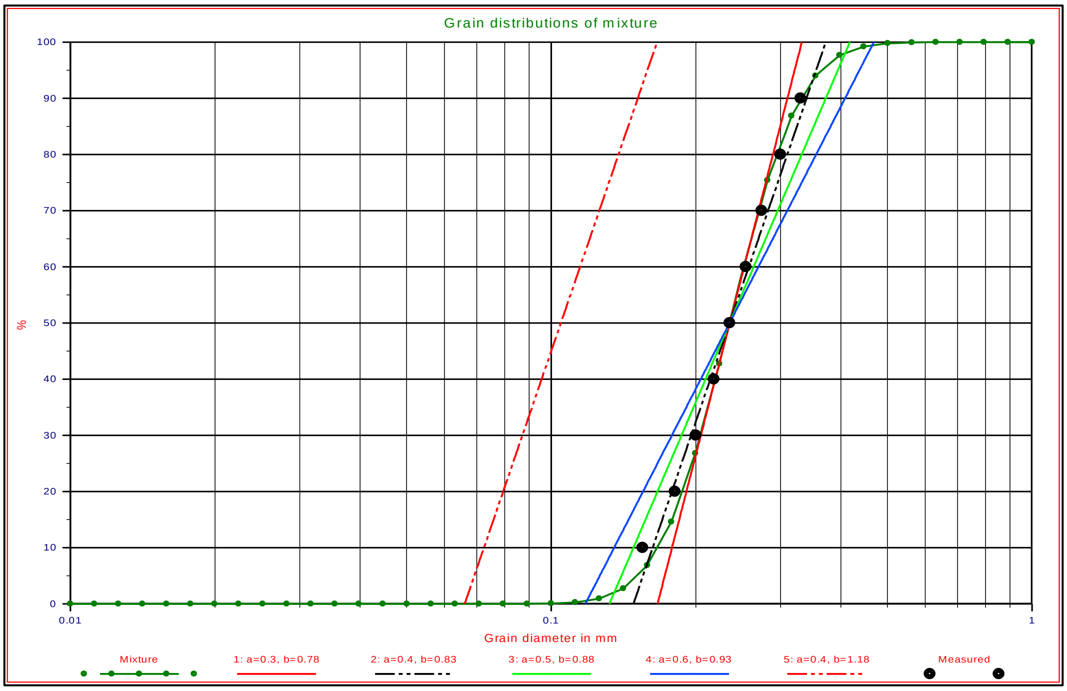

Figure 8-1: The PSD's as used in the examples.

8.2 Verification of the Analytical Model

The analytical model found has been verified using the data from van Rhee (2002C), as given in Table 7-1. Figure 8-2 shows the cumulative overflow losses of the analytical model, the empirical equation (7-23) and the measured data of Table 7-1, as a function of the dimensionless overflow rate **S*** assuming $\mathbf{c_b=c_{in}}$, as a function of the concentration and as a function of the dimensionless overflow rate **S*** with $\mathbf{c_b}$ calculated according to equation (7-16).

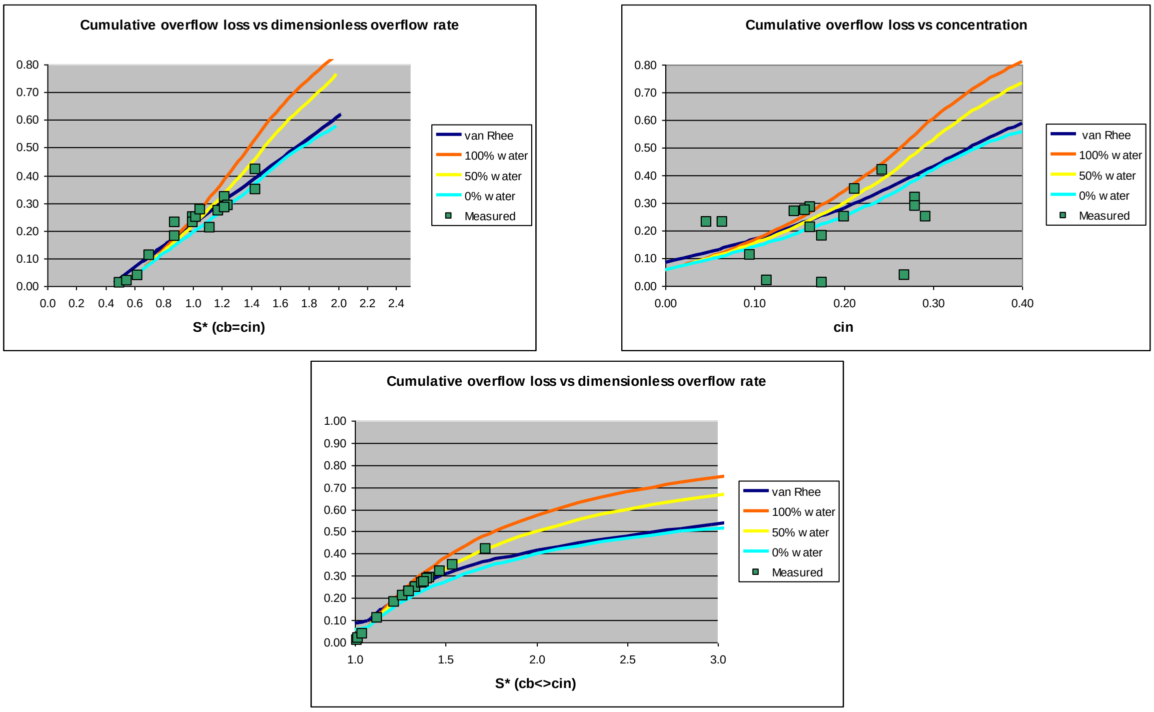

Figure 8-2: Comparing van Rhee (chapter 4) with the analytical model.
(Q=0.125, L=12, W=3, H=2, d_{50}=0.105, a=0.4, b=1.18, β=4.47, n=0.4, μ=1)

The analytical model has been computed for a hopper filled with 0%, 50% and 100% water at the start of the loading process. It should be noted that the measurements of van Rhee (2002C) from Table 7-1 are carried out with a hopper with about 50% of water at the start of the loading process. So the analytical model for 50% initial hopper filling should be compared with the empirical equation (7-23). It is obvious that the analytical model matches the empirical equation (7-23) up to a value of **S*** of 1.2 in the top left graph, up to a concentration $\mathbf{c_{in}}$ of 0.2 in the top right graph and up to a value of **S*** of 1.5 in the bottom graph. For these computations, the settling velocity has been calculated using the iterative method based on the drag coefficient and using the Richardson and Zaki equation for hindered settling. Van Rhee (2002C) however states that the hindered settling process is more complicated for well graded sand. In the experiments sand according to Figure 8-1 sand number 5 has been used. In such sand there is interaction between smaller and larger particles regarding the hindered settling effect. If this is taken into account by the principle of hindered density, which means, that the larger particles settle in a heavier mixture of the smaller particles according to:

$$\rho_f = \frac{C_v}{2}\cdot\rho_q + \left(1-\frac{C_v}{2}\right)\cdot\rho_w \tag{8-15}$$

Giving a relative density $\mathbf{R_d}$ of:

$$R_d = \frac{\rho_q - \rho_f}{\rho_f} \tag{8-16}$$

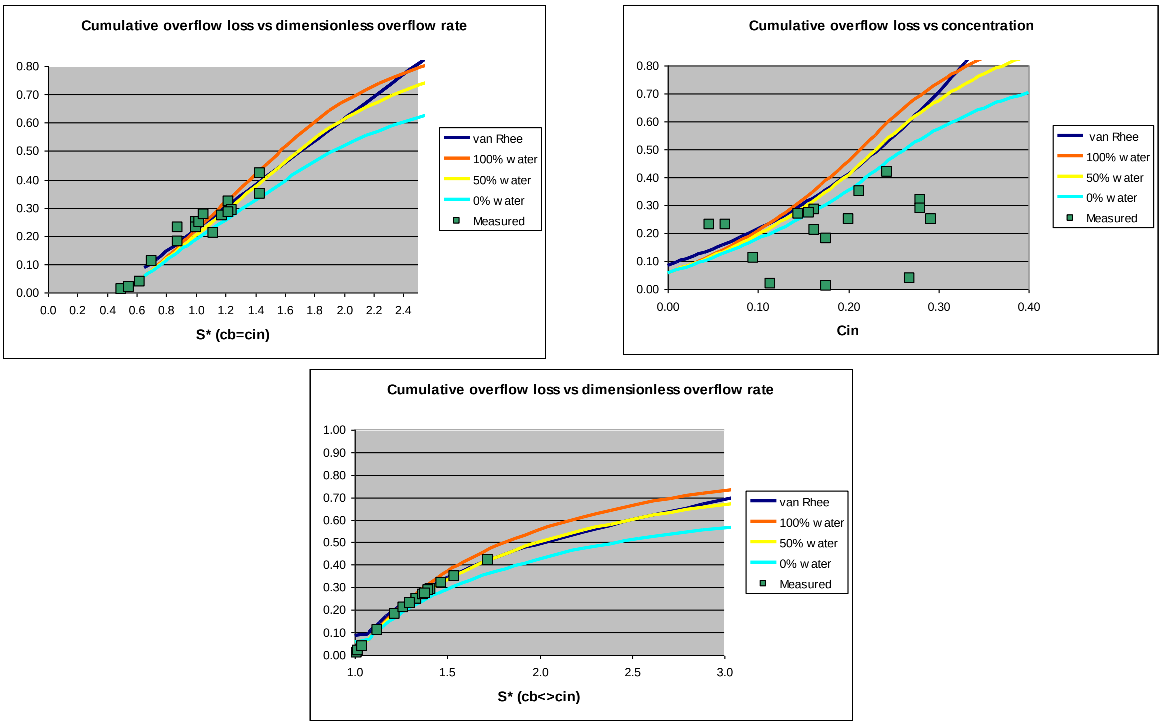

Figure 8-3: Comparing van Rhee (chapter 4) with the analytical model, including the hindered density effect.
(Q=0.125, L=12, W=3, H=2, d_{50}=0.105, a=0.4, b=1.18, β=4.47, n=0.4, μ=1)

Using equation (8-15) in the equations (8-7) and (8-10), gives an improved result according to Figure 8-3. It is obvious from this figure that the analytical model with 50% filling at the start of the loading process matches the empirical equation perfectly. Which proves the validity of the analytical model derived and gives a more physical background to the empirical equation of van Rhee (2002C). Now the question is, does the analytical model give good predictions in other cases. Van Rhee (2002C) tested equation (7-23) on the measurements of the Cornelia as mentioned before and found cumulative overflow losses of 1.5%, while the measurements gave cumulative overflow losses of 8%. One of the reasons for this might be that the model tests on which equation (7-23) is based are carried out with sand with a certain grading, see Figure 8-1 sand number 5. The tests with the Cornelia used sand with another grading. First the overflow losses are computed with the same grading as in the model tests which is sand number 2 in Figure 8-1.

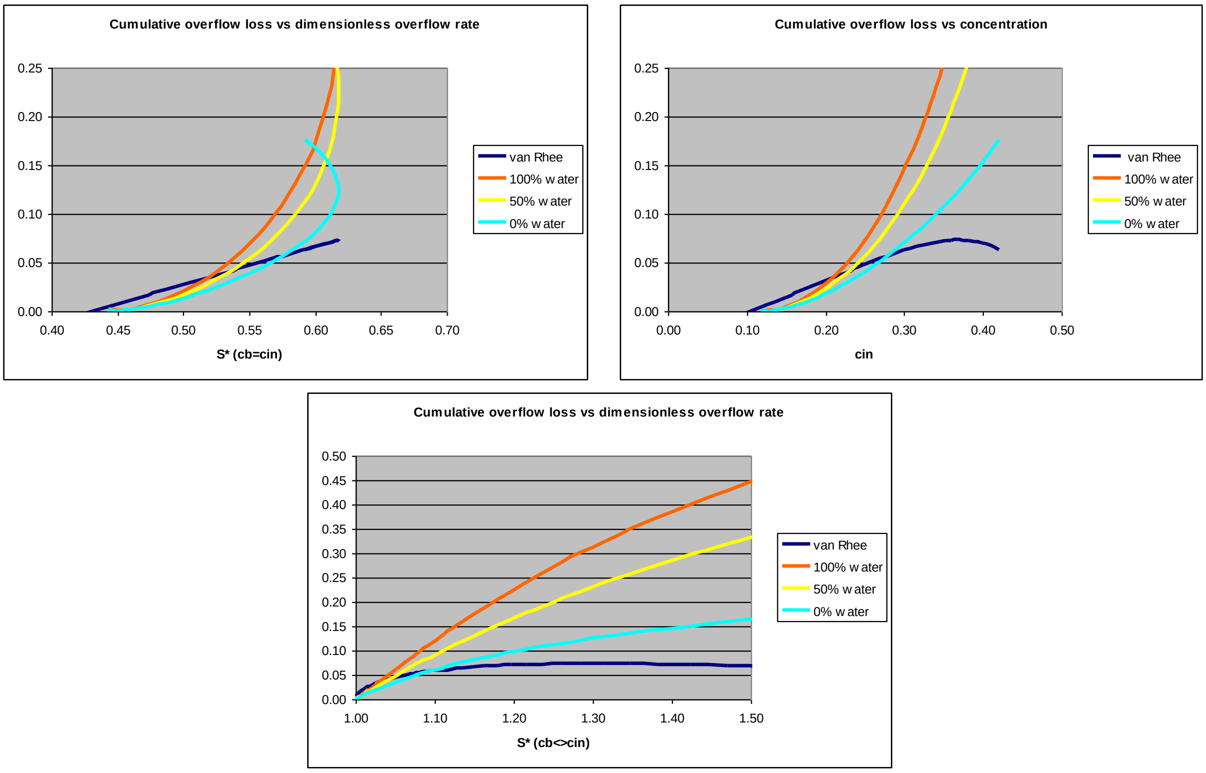

Figure 8-4: Comparing van Rhee (chapter 8) with the analytical model (a=0.3, b=0.78).
(Q=6, L=52, W=11.5, H=8.36, d_{50}=0.235, a=0.3, b=0.779, β=3.7, n=0.46, μ=0.725)

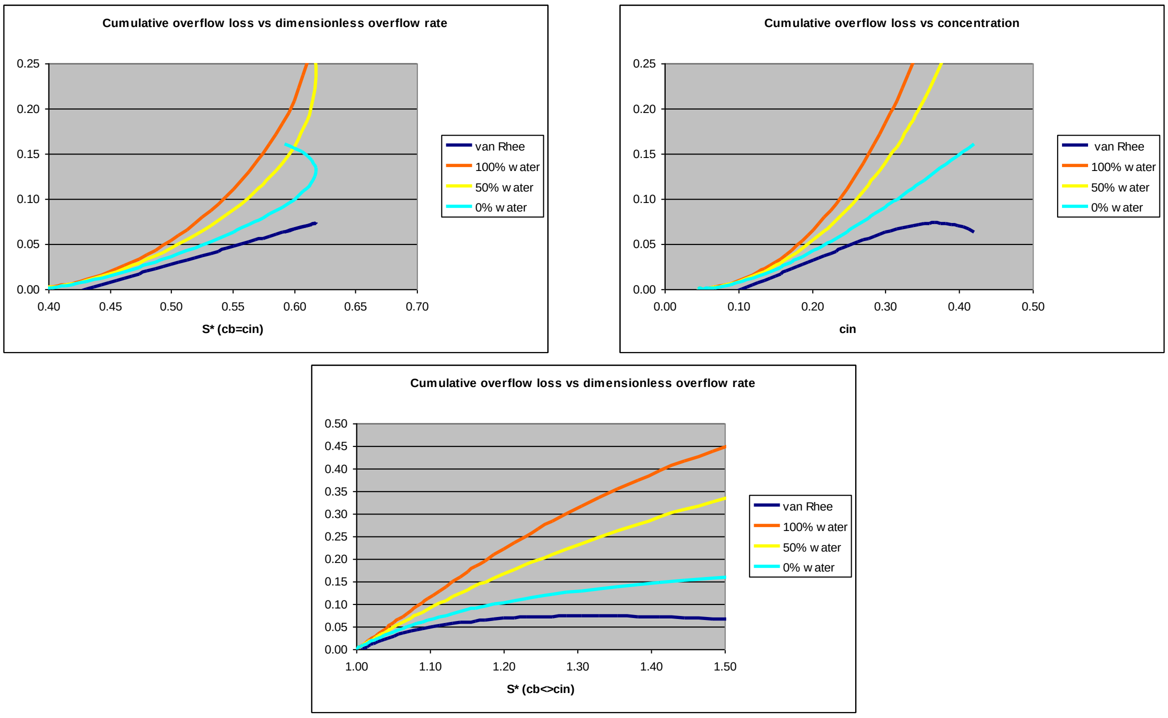

Figure 8-5: Comparing van Rhee (chapter 8) with the analytical model (a=0.4, b=0.83).
(Q=6, L=52, W=11.5, H=8.36, d_{50}=0.235, a=0.4, b=0.829, β=3.7, n=0.46, μ=0.725)

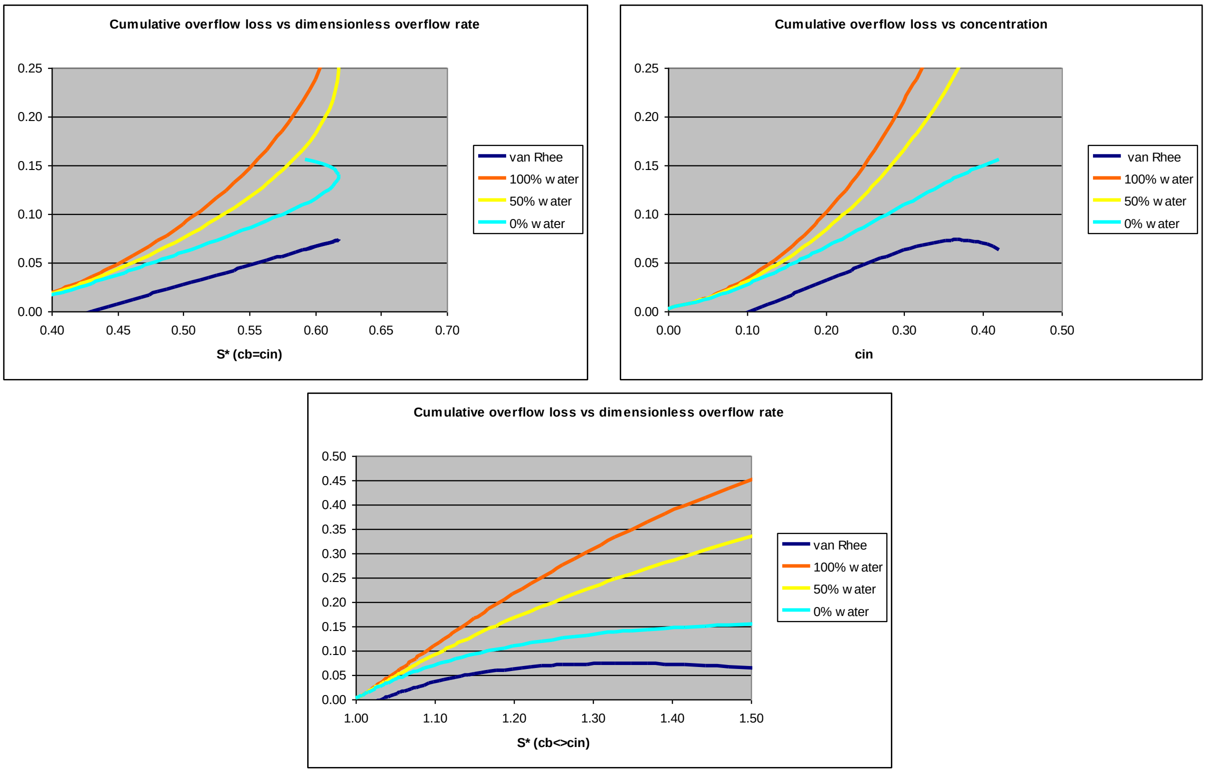

Figure 8-6: Comparing van Rhee (chapter 8) with the analytical model (a=0.5, b=0.88).
(Q=6, L=52, W=11.5, H=8.36, d_{50}=0.235, a=0.5, b=0.879, β=3.7, n=0.46, μ=0.725)

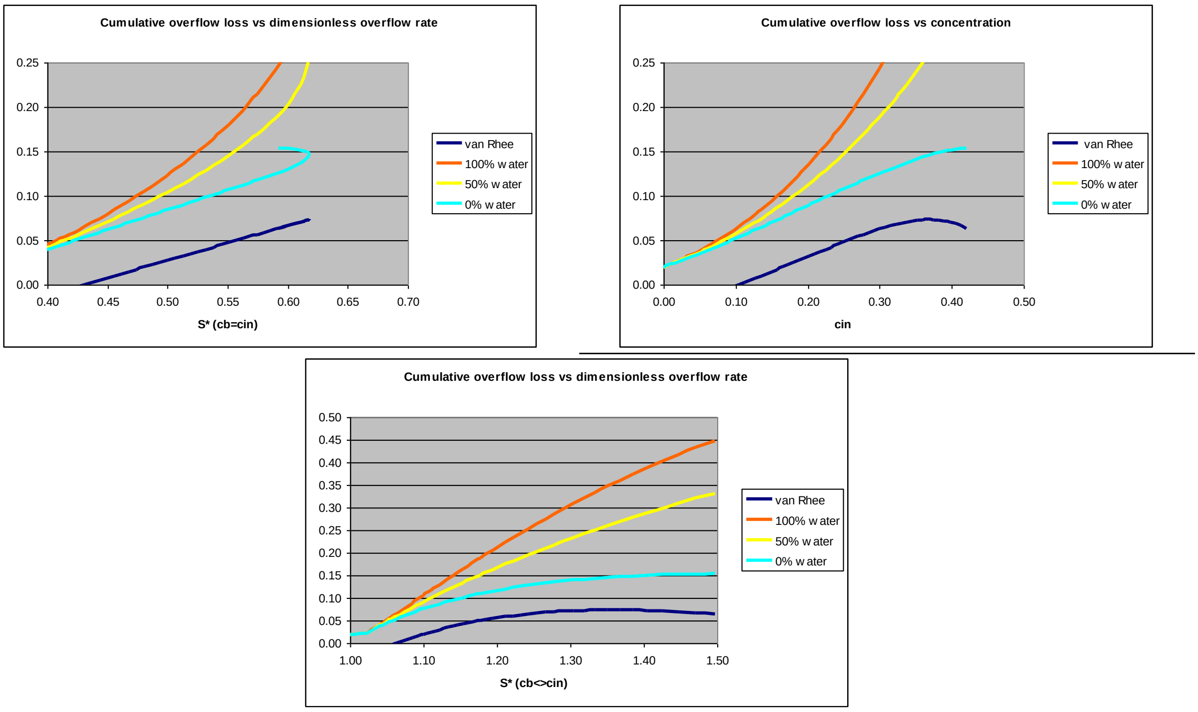

Figure 8-7: Comparing van Rhee (chapter 8) with the analytical model (a=0.6, b=0.93).
(Q=6, L=52, W=11.5, H=8.36, d_{50}=0.235, a=0.6, b=0.929, β=3.7, n=0.46, μ=0.725)

The results of this computation are shown in Figure 8-5. The top left figure shows the results according to equation (7-23) with $\mathbf{c_b=c_{in}}$. Now cumulative overflow losses are found of about 2% at **S*=0.47**, similar to the 1.5% of van Rhee (2002C). In these calculations, the hindered density effect has not been used because of the narrow grading of the PSD.

From Figure 8-1 it can be seen however that the fines are not taken into account properly and it is the fines that cause the higher cumulative overflow losses. If sand number 4 is used however, taking into account the fines, Figure 8-7 is the result giving cumulative overflow losses of about 8% for **S*=0.47** in the top left graph. It is clear that finding the right model PSD is difficult and sand number 4 is a little bit jumping to conclusions, but it is also clear that using a PSD that matches the real sand closer will result in a better prediction of the overflow losses.

Chapter 9: Comparing the Miedema and the van Rhee Model

9.1 Introduction

This chapter is based on Miedema & van Rhee (2007).
In the past two decades the size of TSHD's has tripled and there are plans for TSHD's in the range of 50.000 m^3. When enlarging hoppers there are some limitations like the draught of the vessel and the line velocity in the suction lines. It's interesting to compare the influences of length, width, height ratio's, flow capacity and some other parameters on the production and the overflow losses of TSHD's. To do so, mathematical models have been developed to simulate the sedimentation process in the hopper. Two models will be used and compared, first the model of Vlasblom/Miedema (1995), Miedema/Vlasblom (1996) and Miedema (2008A) and second the more sophisticated 2DV model of van Rhee (2002C), which is verified and validated with model and prototype tests. Both models are explained briefly. With the two models 3 cases are analyzed, a 2316 m^3, a 21579 m^3 and a 36842 m^3 hopper. The results of the case studies give the following conclusions and recommendations:

- The two models give the same magnitude for the overflow losses, but the shape of the curves is different due to the differences in the physical modeling of the processes.
- Due to the lower losses the computed optimal loading time will be shorter for the Vlasblom /Miedema approach.
- The strong point of the van Rhee model is the accurate physical modeling, giving the possibility to model the geometry of the hopper in great detail, but also describing the physical processes in more detail.
- The van Rhee model is verified and validated with model and prototype tests and can be considered a reference model for other models.
- The strong point of the Miedema/Vlasblom model is the simplicity, giving a transparent model where result and cause are easily related.

From a scientific point of view it is interesting to compare the sophisticated van Rhee model with the simplified models and to do so, the van Rhee (2002C) model is compared with the Miedema (2008A) model. The comparison consists of a number of cases regarding real TSHD's. The following TSHD's will be compared:

Table 9-1: The data of the TSHD's used.

Hopper	Load	Volume	Length	Width	Empty height	Flow	Hopper load v_0	Mixture density
	ton	m^3	m	m	m	m^3/sec	m/sec	ton/m^3
Small	4400	2316	44.0	11.5	4.577	4	0.0079	1.3
Jumbo	41000	21579	79.2	22.4	12.163	14	0.0079	1.3
Mega	70000	36842	125.0	30.0	9.825	19	0.0051	1.3

Further it is assumed that all 3 TSHD's have a design density of 1.9 ton/m^3 and they operate according to the CVS system (no adjustable overflow). This gives a sand fraction of 0.54 and a porosity of 0.46. For the calculations a sand with a $\mathbf{d_{50}}$ of 0.4 mm is chosen, according to figure 1. The particle size distribution is chosen in such a way that there is a reasonable percentage of fines in order to have moderate overflow losses.

9.2 Case Studies with the Camp/Miedema Model

The calculations according to the modified Camp/Miedema model as developed by Miedema (1981) and published by Vlasblom & Miedema (1995), Miedema & Vlasblom (1996) and Miedema (2008A) are carried out with the program TSHD (developed by Miedema). The effects of hindered settling, turbulence and scour and an adjustable overflow are implemented in this program as described previously.
The program assumes that first the hopper is filled with mixture up to the overflow level and all the grains entering the hopper during this phase will stay in the hopper, so the overflow losses are 0 during this phase. The table below shows the filling time, the total load and the TDS at the end of this phase.

Table 9-2: The hopper content after the filling phase.

Hopper	Load	Volume	Flow	Filling time	Total load	TDS	Overflow losses	Mixture density
	ton	m^3	m^3/sec	min	ton	ton	%	ton/m^3
Small	4400	2316	4	9.65	3011	1039	20.0	1.3
Jumbo	41000	21579	14	25.69	28053	9678	20.0	1.3
Mega	70000	36842	19	32.32	47895	16523	16.6	1.3

After this phase the program will determine the total settling efficiency and based on this the increase of the sediment and the overflow losses in time steps of 1 minute. Each time step the program checks whether or not scour occurs and if so which fraction of the PSD will not settle due to scour. Usually first there is a phase where scour does not occur. The overflow losses are determined by the settling efficiency according to the equations (3-12) and (3-13). If the hopper has a CTS system, each time the necessary overflow level is calculated and the overflow level is adjusted. In the cases considered a CVS system is assumed, so the overflow level is fixed. When the sediment level is so high that the velocity above the bed is very high, scour starts. This will happen at the end of the loading process. In the calculations the loading process is continued for a while, so the effect of scour is clearly visible. The results of the calculations are show in Figure 9-2, Figure 9-3 and Figure 9-4 for the Small, Jumbo and Mega hopper. The initial overflow losses of 20, 20 and 16.6% match the values of the hopper load parameter as mentioned in Table 9-1. The Mega hopper has a smaller hopper load parameter and thus also smaller initial overflow losses (without scour).

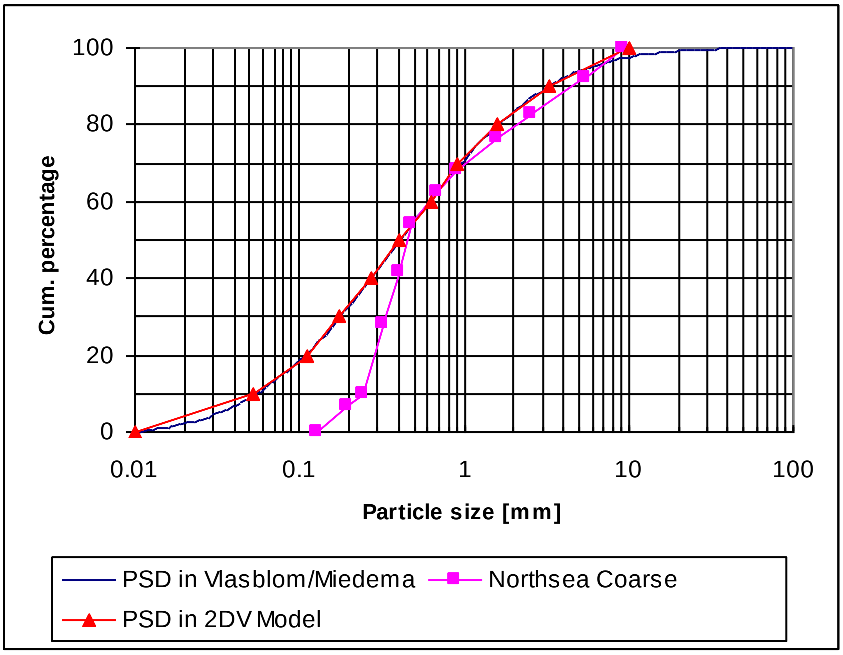

Figure 9-1: The 0.4 mm grain distribution.

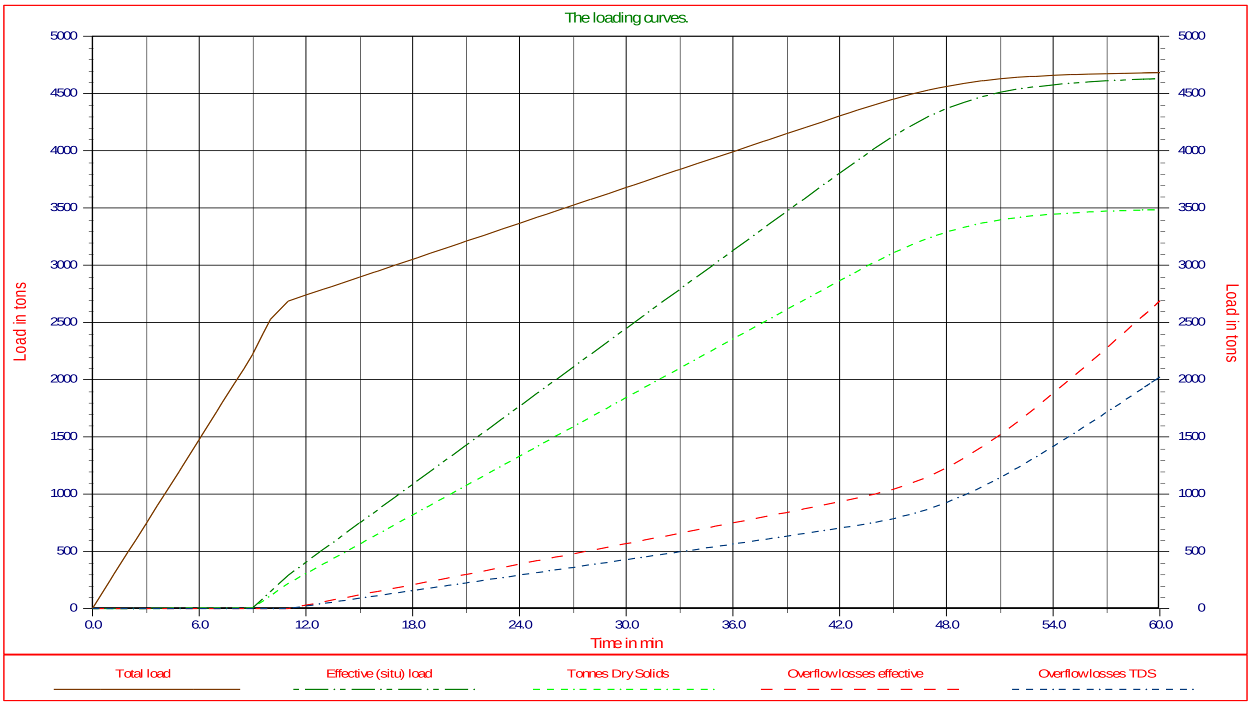

Figure 9-2: The loading curves of the Small TSHD.

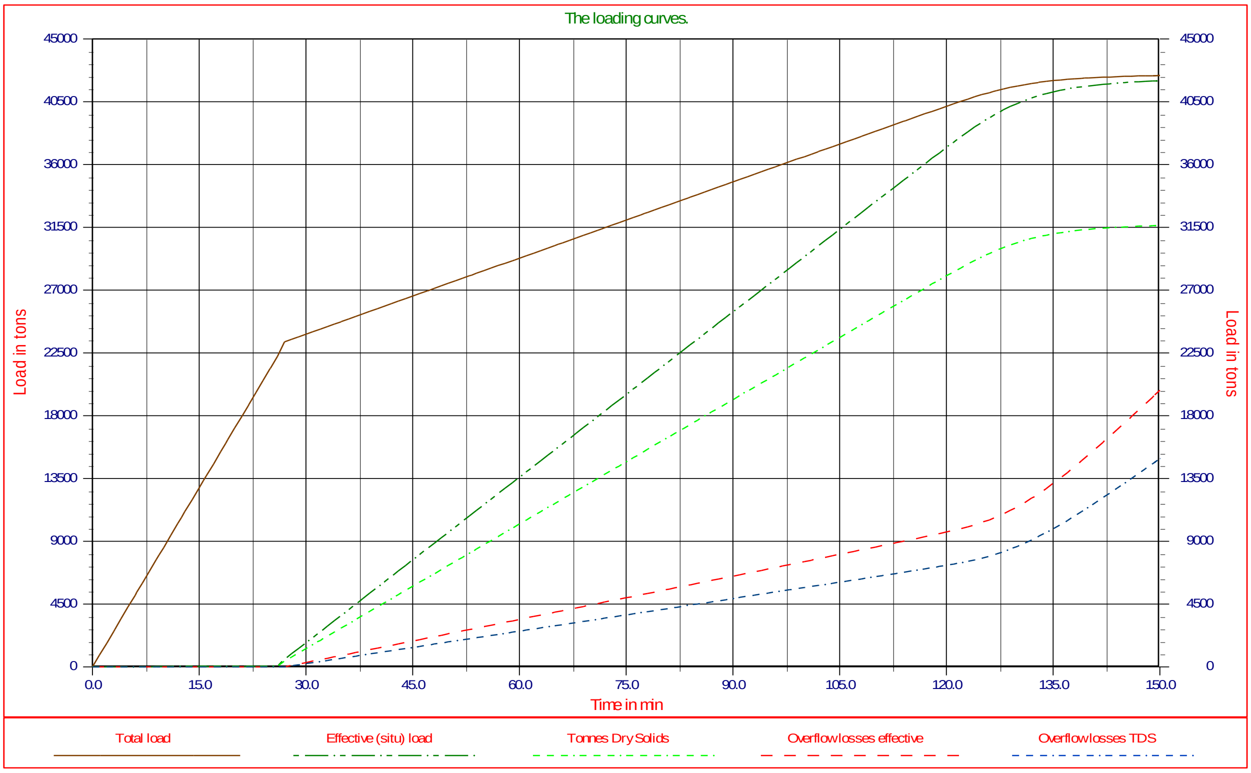

Figure 9-3: The loading curves of the Jumbo TSHD

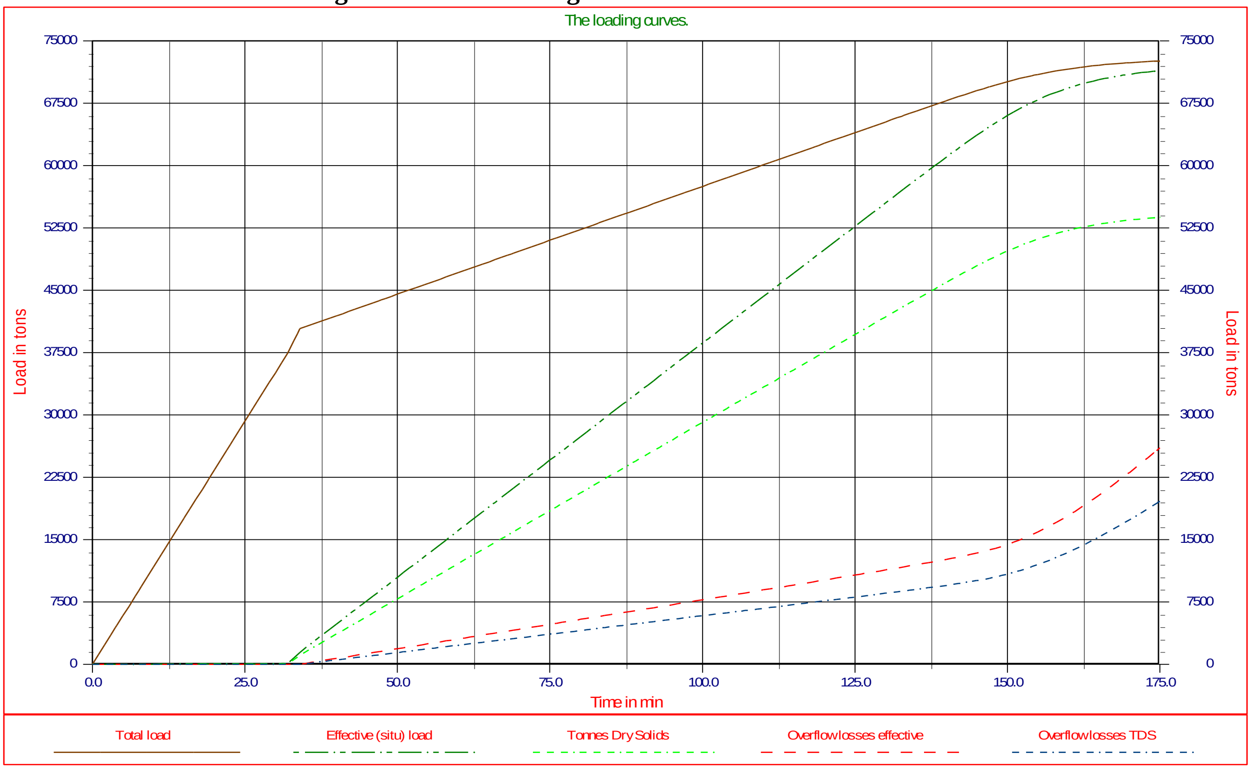

Figure 9-4: The loading curves of the Mega TSHD

It should be noted that the optimum loading time, the loading time with the maximum production, depends on the total cycle, including sailing times, dumping time, etc. Since the calculations with the 2DV model start with a hopper full of water, also here first the hopper is filled with water, so the two models can be compared.

9.3 The 2DV Model

The settlement model described above provides a good approximation of the overflow losses. The influence of grain size, discharge, concentration and hopper geometry can be taken into account. Some influences however are not included in the model. For instance the influence of the inflow location, variation of water level at the start of dredging is not included. To overcome these limitations the 2DV hopper sedimentation model was developed (Van Rhee (2002A)). The model is based on the Reynolds Averaged Navier Stokes equations with a k-epsilon turbulence model. The model includes the influence of the overflow level of the hopper (moving water surface) and a moving sand bed due to the filling of the hopper. The influence of the particle size distribution (PSD) is included in the sediment transport equations. A summary of the model is described in Van Rhee (2002C). The total model is based on three modules (see Figure 9-5).

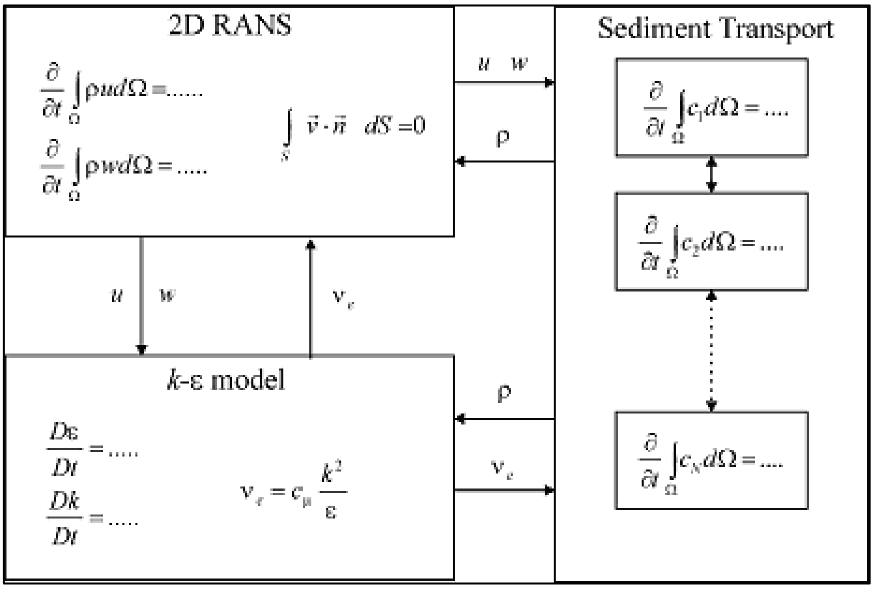

Figure 9-5: Overview of the 2DV model.

In the 2D RANS module the Reynolds Averaged Navier Stokes equations are solved (the momentum equations). The sediment transport module computes the distribution of suspended sediment in the hopper while the k-epsilon module is necessary for the turbulent closure. The modules have to be solved simultaneously because the equations are strongly coupled. In the momentum equations the density is present which follows from the sediment transport equations. The diffusive transport of sediment is governed by turbulence predicted by the k-epsilon model. The turbulence on the other hand is influenced by the density gradients computed in the sediment transport module.

Boundary conditions

The partial differential equations can be solved in case boundary conditions are prescribed. Different boundaries can be distinguished: Walls (sediment bed and side walls), water surface, inflow section and outflow section. At the walls the normal flow velocity is zero. The boundary condition for the flow velocity at the wall is computed using a so-called wall function (Rodi (1993), Stansby (1997)). The boundary conditions for the turbulent energy **k** en dissipation rate **ε** are consistent with this wall function approach. For the sediment transport equations the fluxes through vertical walls and water surface is equal to zero since no sediment enters or leaves the domain at these boundaries. At the sand bed for every fraction the sedimentation flux $\mathbf{S_i}$ is prescribed (the product of the near bed concentration and vertical particle velocity of a certain fraction). The influence of the bottom shear stress on the sedimentation is modeled using a reduction factor **R**.

$$\mathbf{S_i = R \cdot c_i \cdot w_{zj}}$$

$$\mathbf{R} = \begin{cases} 1-\dfrac{\theta}{\theta_0} & \theta < \theta_0 \\ 0 & \theta \geq \theta_0 \end{cases} \qquad \mathbf{(9\text{-}1)}$$

This simple relation between the reduction factor and Shields parameter **θ** is based on flume tests (Van Rhee (2002B)). The critical value for the Shields parameter proved to be independent of the grain size for the sands tested (d50 < 300 μm). It will be clear that this approach can only be used when overall sedimentation (like in a hopper of a TSHD) will take place. When the Shields value exceeds the critical value no sedimentation will take place, but sediment already settled will not be picked up with this approach. Hence net erosion is not (yet) possible in the model.

At the inflow section the velocity and concentration is prescribed. The outflow boundary is only active when overflow is present, so when the mixture level in the hopper exceeds the overflow level. In that case the outflow velocity is prescribed, and follows simply from the ratio of the overflow discharge and the difference between the hopper and overflow level. For the other quantities the normal gradients are equal to zero (Neumann condition).
At the water surface a rigid-lid assumption is used since surface wave phenomena are not important for the subject situation. A rigid-lid can be regarded as a smooth horizontal plate covering the water surface in the hopper. Depending on the total volume balance inside the hopper this "plate" will be moved up and down.

Numerical approach
The momentum and sediment transport equations are solved using the Finite Volume Method to ensure conservation. The transport equations for the turbulent quantities k and are solved using the Finite Difference method. A Finite Difference Method is allays implemented on a rectangular (Cartesian) grid. Although a Finite Volume Method can be applied on any grid it is advantageous to use a Cartesian approach for this method as well especially when a staggered arrangement of variables is used. In general the flow domain is however not rectangular. The water surface can be considered horizontal on the length scale considered, but a sloping bottom will not coincide with the gridlines. Different approaches are possible. The first method is to use a Cartesian grid and to adjust the bottom cells (cut-cell method). Another method is to fit the grid at the bottom. In that case a boundary fitted non-orthogonal grid can be used. A third method is using grid transformation. By choosing an appropriate transformation the equations are solved on a Cartesian domain in transformed co-ordinates. Although this transformation allows for a good representation of a curved topography the method has the disadvantage that due to truncation errors in the horizontal momentum equation artificial flows will develop when a steep bottom encounters density gradients. These unrealistic flows can be partly suppressed when the diffusion terms are locally discretized in a Cartesian grid (Stelling (1994)). Since however in a hopper both large density gradients as steep bottom geometry can be present it was decided to develop the model in Cartesian co-ordinates with a cut-cell approach at the bed.
The computational procedure can only be outlined here very roughly. The flow is not stationary hence the system is evaluated in time. The following steps are repeated during time:

- Update the velocity field to time $\mathbf{t_{n+1}}$ by solving the NS-equations together with the continuity equation using a pressure correction method (SIMPLE-method (Patankar (1980)) using the density and eddy viscosity of the old time step $\mathbf{t_n}$.
- Update the turbulent quantities and to time $\mathbf{t_{n+1}}$ using the velocity field of $\mathbf{t_{n+1}}$. Compute the eddy-viscosity for the new time.
- Use the flow field of $\mathbf{t_{n+1}}$ to compute the grain velocities for the next time and update the concentrations for all fractions and hence the mixture density to time $\mathbf{t_{n+1}}$.
- Compute the new location for the bed level and mixture surface in the hopper

Results
The 2DV model is used to simulate the loading process for the three different cases. At the start of the simulation the hopper is filled with water. The results are shown in Figure 9-6, Figure 9-7 and Figure 9-8. In these figures the TDS in the hopper (settled in the bed and in suspension) and the cumulative overflow losses are plotted versus loading time.

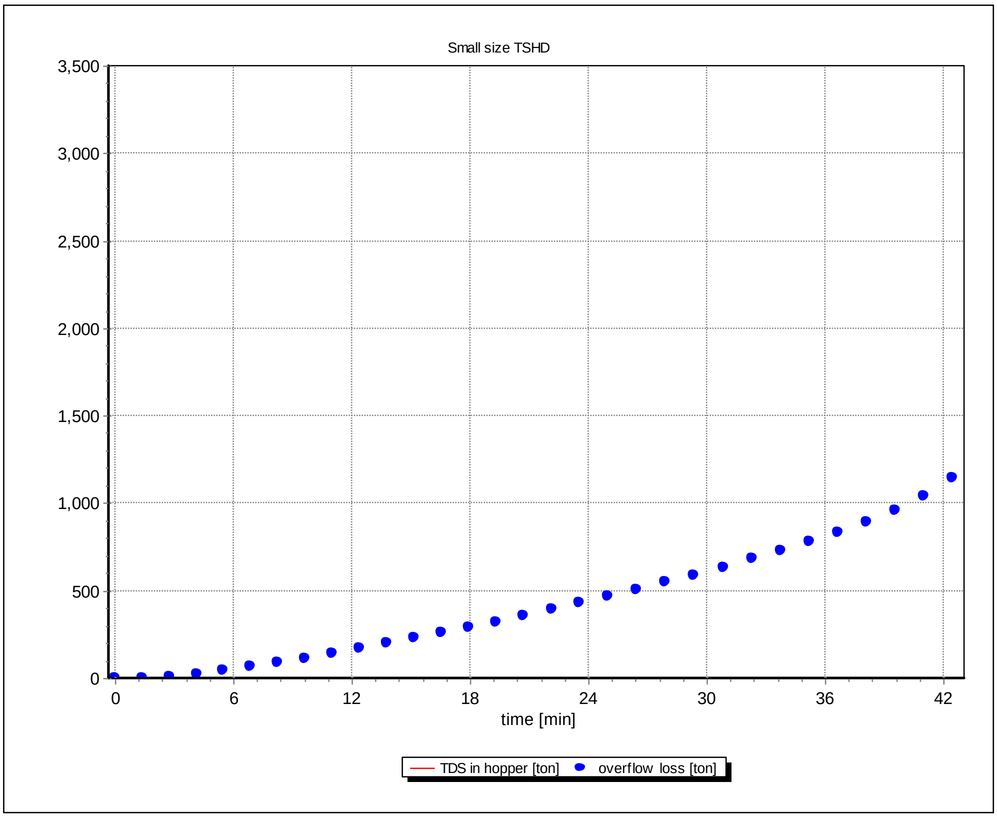

Figure 9-6: Loaded TDS and overflow losses as a function of time for a Small size TSHD.

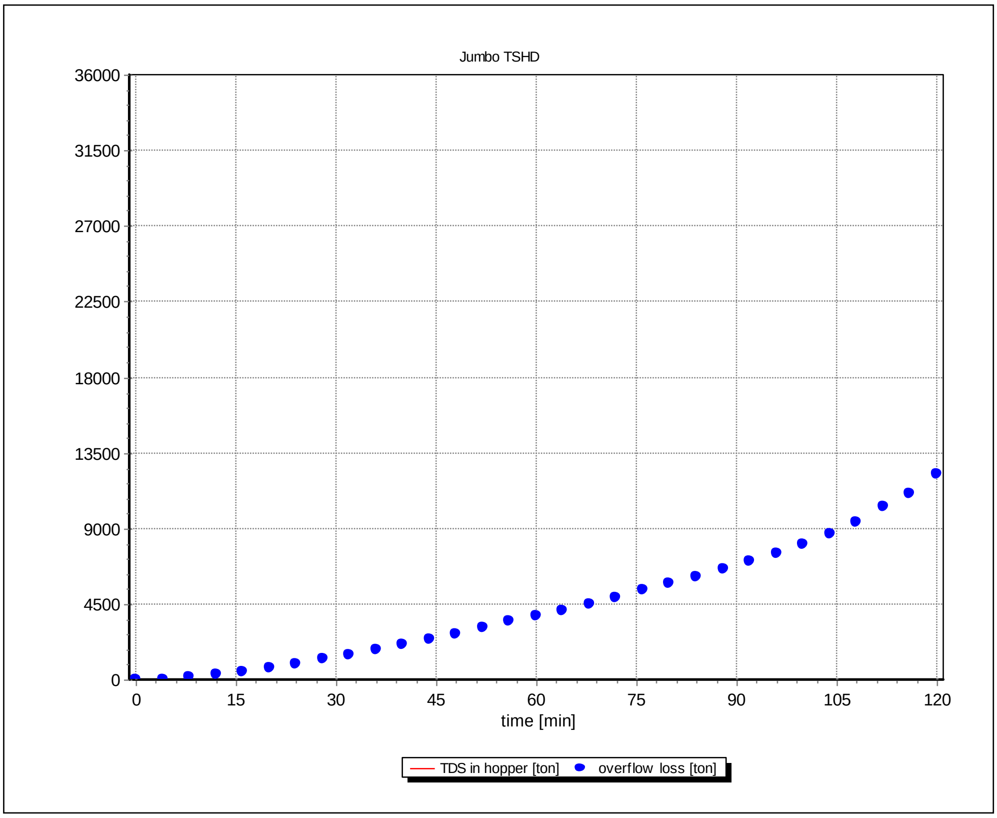

Figure 9-7: Loaded TDS and overflow losses as a function of time for Jumbo TSHD.

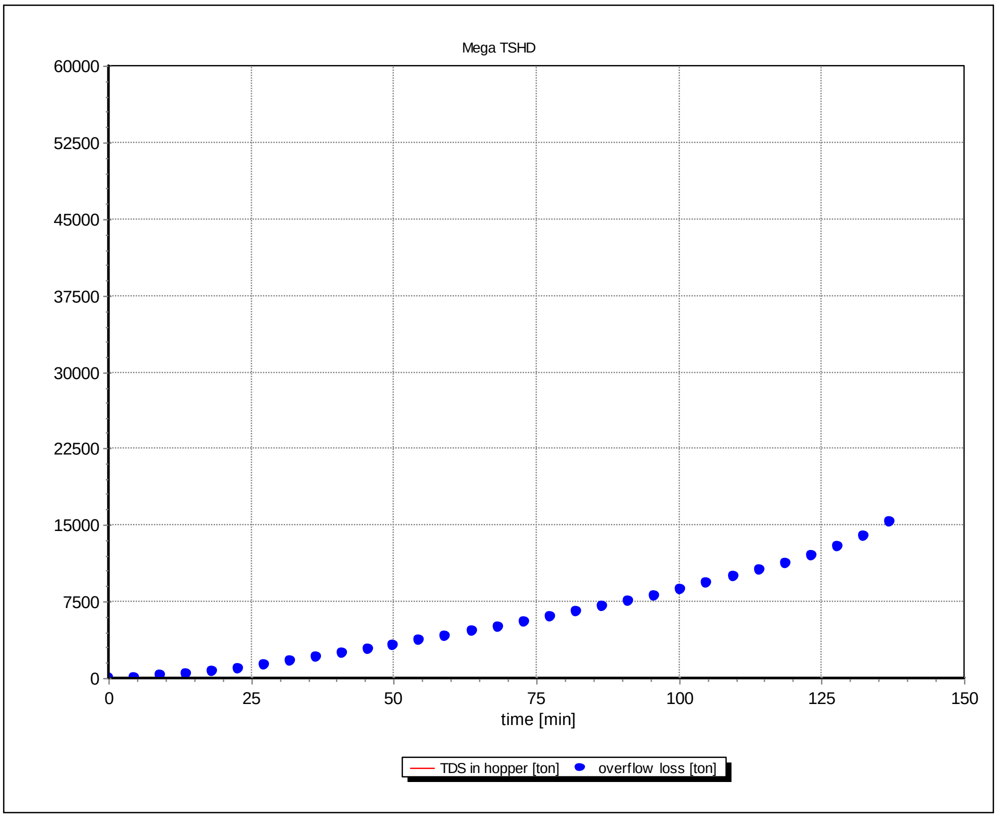

Figure 9-8: Loaded TDS and overflow losses as a function of time for a mega TSHD.

9.4 Comparison of the Two Models

To compare the results of the two methods, first the differences in the models are summarized:

1. The physical modeling of the two methods is different; Miedema/Vlasblom/Camp is based on the Camp approach, while the 2DV model is based on the Reynolds Averaged Navier Stokes equations.
2. The van Rhee model starts with a hopper full of water, while the Miedema/Vlasblom/Camp model starts with an empty hopper.
3. The Miedema/Vlasblom/Camp model assumes 100% settling of the grains during the filling phase of the hopper.
4. The van Rhee model includes a layer of water above the overflow level, while the Miedema/Vlasblom/Camp model doesn't by default. But to compare the two models the height of the overflow level has been increased by the thickness of this layer of water and the results are shown in the Figure 9-9, Figure 9-10 and Figure 9-11. With the layer thickness according to: $\mathbf{H_l = \left(\frac{Q}{1.72 \cdot b}\right)^{2/3}}$, where the constant 1.72 may vary. The width **W** is chosen for the width of the overflow **b** in the calculations. This gives a layer thickness of 34 cm for the small hopper and 51 cm for the Jumbo and the Mega hopper.

The results of the Small hopper and the Jumbo hopper are similar due to the same hopper load parameter of 0.0079 m/sec. The Mega hopper has a smaller hopper load parameter of 0.0051 m/sec, resulting in relatively smaller overflow losses. To compare the two models the graphs of the two models are combined and similarities and differences are discussed:

Similarities:

1. The overflow rate seems to be quite similar for all 3 hoppers, until the Miedema/Vlasblom/Camp approach reaches the scour phase. From this moment on the overflow rate increases rapidly.
2. It is obvious that at the end of the loading both models find the same amount of sand in all cases, since this matches the maximum loading capacity of the hopper in question. This observation explains the fact that the overflow losses of both models are almost the same at the time where the van Rhee simulation stops (42 minutes for the Small hopper, 112 minutes for the Jumbo hopper and 137 minutes for the Mega hopper).

Differences:

1. The overflow losses in the van Rhee model are lower in the first phase, because in the Miedema/Vlasblom/Camp approach this occurs instantly, while the van Rhee approach considers the time the mixture needs to flow through the hopper and the effect of scour is very limited because a uniform flow velocity distribution over depth is assumed (leading to very low horizontal flow velocities) in this model. Only at the end of the loading stage the effect of the horizontal flow velocity on sedimentation becomes noticeable. For instance for the Small hopper the TDS loading curve is a straight line from the start of overflow up to 33 min after start dredging. After that time the loading rate decreases as a result of the increasing horizontal velocity. At t = 45 min the hopper is completely filled. Hence the influence of the velocity during the final loading stage is present for about 12 minutes.
2. In the 2DV model velocity distribution is not prescribed, but is determined by physics and depends on the inflow conditions. In general, due to the large density difference between the inflowing mixture and fluid already present in the hopper, density currents will develop. This will lead to a larger velocity close to the sand bed surface. Hence the effect of the flow velocity on sedimentation will be present from the start of dredging. This influence does not increase much during loading. The effect is more spread out over the loading cycle. The loading rate decreases gradually, but remains on a reasonable level unto the moment that the hopper is fully loaded. In the Miedema/Vlasblom/Camp loading rate reduces to zero at full load..
3. If optimum loading time is considered, the two models differ in that the van Rhee model gives 43, 112 and 137 minutes, while this will be around 38, 99 and 120 minutes in the Miedema/Vlasblom/Camp approach. Both models start with a hopper full of water, so this should be considered. The overflow losses in the final phase of the loading process are similar for both models.

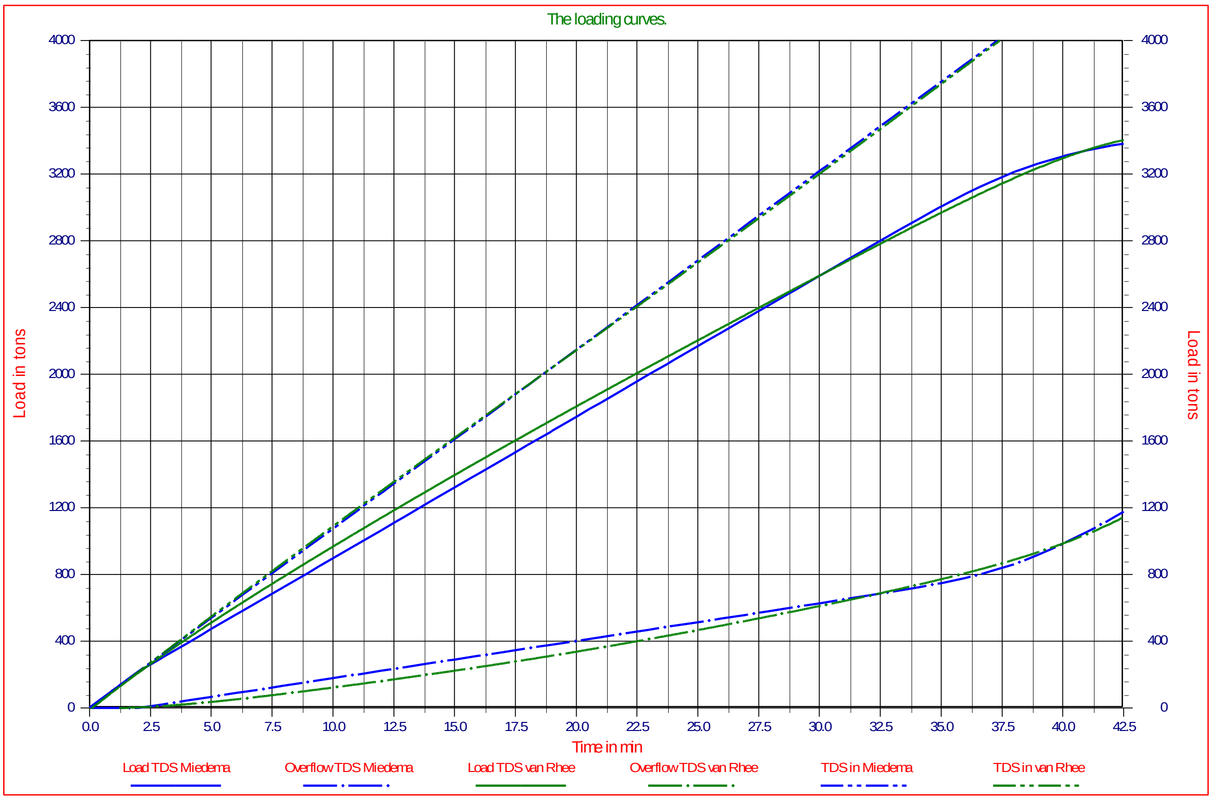

Figure 9-9: Comparison of the two models for the Small hopper.

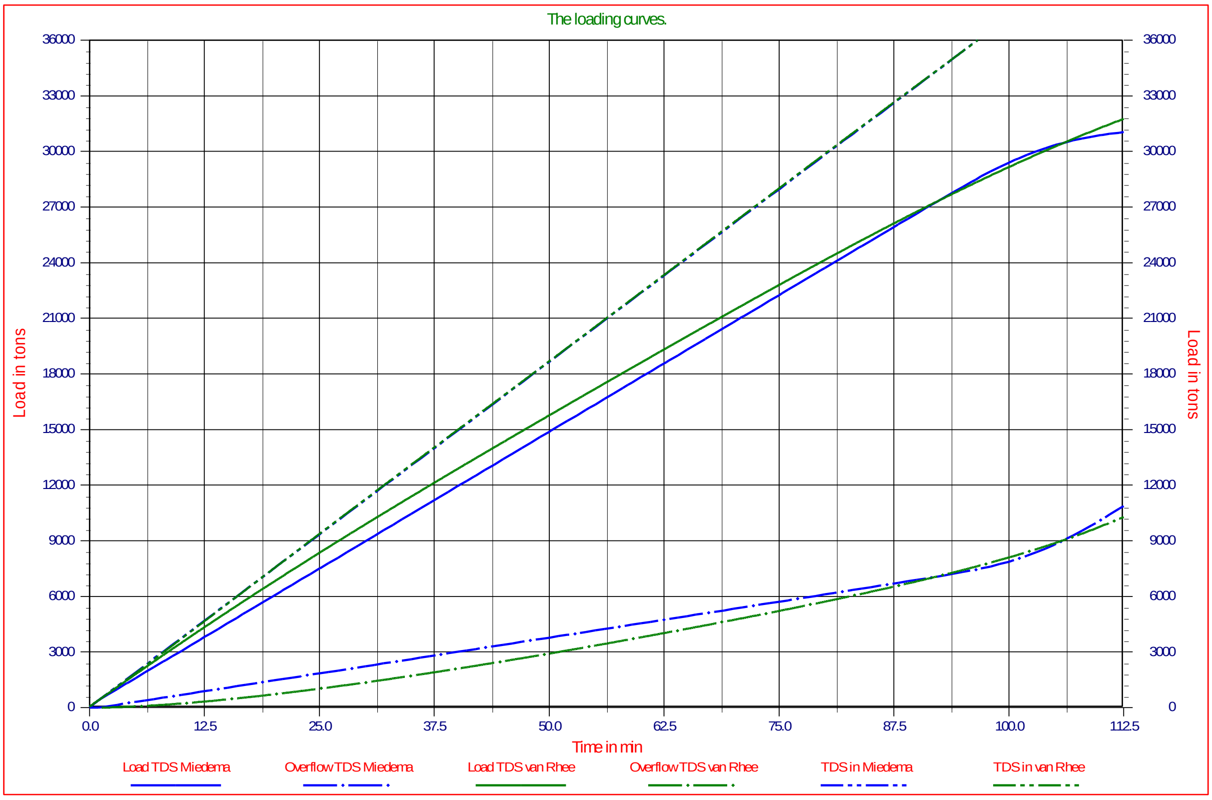

Figure 9-10: Comparison of the two models for the Jumbo hopper.

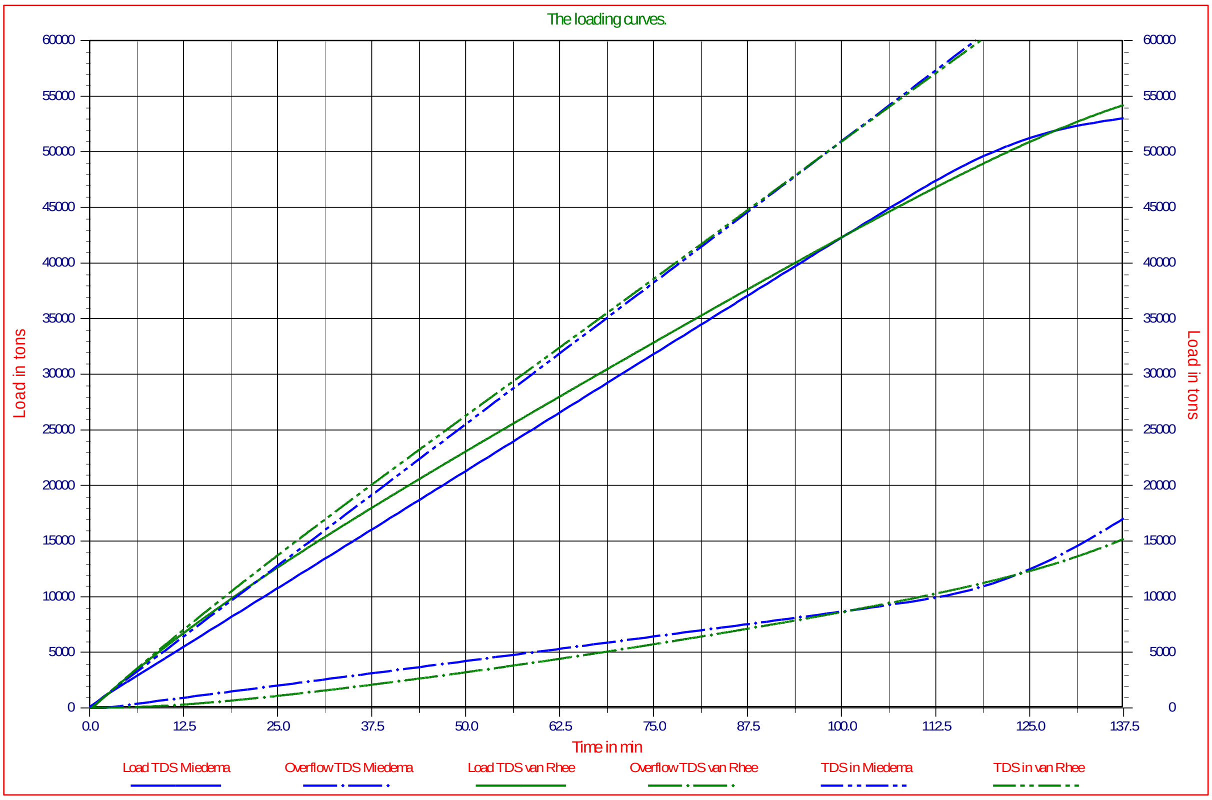

Figure 9-11: Comparison of the two models for the Mega hopper.

9.5 Conclusions

- The two models give the same magnitude for the overflow losses, but the shapes of the curves are different due to the differences in the physical modeling of the processes.
- Due to the lower losses the computed optimal loading time will be shorter for the Miedema/Vlasblom /Camp approach.
- The strong point of the van Rhee model is the accurate physical modeling, giving the possibility to model the geometry of the hopper in great detail, but also describing the physical processes in more detail.
- The van Rhee model is verified and validated with model and prototype tests and can be considered a reference model for other models.
- The strong point of the Miedema/Vlasblom/Camp model is the simplicity, giving a transparent model where result and cause are easily related.

Chapter 10: A Sensitivity Analysis of the Scaling of TSHS's

The loading process of TSHD's contains a number of non-linearity's:

1. The real hopper load parameter will vary during the loading process.
2. The turbulence settling efficiency.
3. The behavior of the layer of water above the overflow.
4. The behavior of hindered settling.
5. The effective concentration in the hopper.
6. The so called storage effect.

Based on all these non-linearity's it is not expected that TSHD's can be scaled easily, however the research in this paper shows that with the right choice of scale laws the TSHD's can be scaled rather well.
4 TSHD's are chosen, derived from Miedema & van Rhee (2007), but adapted to the scale laws. With each of these TSHD's simulations are carried out in 4 types of sand, 400 µm, 250 µm, 150 µm and 100 µm sand.

10.1 Scale Laws

To compare TSHD's of different dimensions scale laws have to be applied in order to create identical loading processes. Scale laws should be based on the physical and the operational processes that occur. Further the shape of the hopper should be identical and the relation with the flow should match. It is however also important to decide which parameter or parameters to choose for the comparison of the TSHD's. When can the conclusion be drawn that two hoppers with different dimensions behave identical. The main parameter that is chosen for this comparison are the cumulative overflow losses. The cumulative overflow losses are the overflow losses expressed as TDS (Tonnes Dry Solids) divided by the total amount of TDS that has entered the hopper, from the start of the loading process until the moment of optimum loading.
The first important parameter to consider is the hopper load parameter (HLP) as described in equation (10-1). Here the hopper load parameter without the effect of the bed rise velocity is considered, because the bed rise velocity changes during the loading process and would result in changing scale laws. As stated before, the hopper load parameter is the settling velocity of a grain that will settle for 100%. Larger grains will also settle for 100%, but smaller grains will settle with a smaller percentage.

$$\mathbf{v_o = s_o \cdot \frac{H_w}{L} = \frac{Q_{in}}{W \cdot L}} \qquad \mathbf{(10\text{-}1)}$$

If two TSHD's with different dimensions have the same hopper load parameter, it can be expected that under similar conditions, the momentary overflow losses are equal and thus also the cumulative overflow losses. However the hopper load parameter does not take into consideration the effects of turbulence efficiency, hindered settling, and the storage effect and so on.

A second scale law could be that the ratios between Length, Width and Height are identical. If a length scale $\boldsymbol{\lambda}$ is considered this gives:

$$\mathbf{\lambda = \frac{L_1}{L_2} = \frac{W_1}{W_2} = \frac{H_1}{H_2} \quad and \quad \frac{HLP_1}{HLP_2} = 1 \quad and \quad \frac{Q_1}{Q_2} = \lambda^2 \quad and \quad \frac{T_{f1}}{T_{f2}} = \frac{V_1 / Q_1}{V_2 / Q_2} = \lambda} \qquad \mathbf{(10\text{-}2)}$$

Because the hopper load parameter is considered to be a constant, the flow $\mathbf{Q}$ will scale with the square of the length scale $\boldsymbol{\lambda}$. The filling time $\mathbf{T_f}$, which is the time to fill the hopper up to the overflow level also scales with the length scale $\boldsymbol{\lambda}$. To have similar processes for determining the optimum loading time, the travelling time, which is the sum of the sailing time to and from the dump area and the dumping time, should also be scaled with the length scale, assuming that the loading time is proportional to the filling time. Since the horizontal flow velocity in the hopper equals the flow $\mathbf{Q}$ divided by the width $\mathbf{W}$ and the height $\mathbf{H}$ of the hopper, the horizontal flow velocity is a constant and does not depend on the length scale. This also follows from the fact that the hopper load parameter is a constant. If it is assumed that the maximum line velocity in the suction pipes is a constant, for example 7 m/s and because the line velocity equals the flow velocity divided by 2 and divided by the cross section of one pipe, this implies that the pipe diameter should be proportional to the square root of the flow and thus be proportional to the length scale $\boldsymbol{\lambda}$.
Because sand is difficult to scale and in reality the sand will be the same independent of the TSHD used, it is assumed that the sand is the same for all hopper sizes. This implies that the settling velocities are the same and looking at the equations (3-12) and (3-13) this means that the grain settling efficiency $\boldsymbol{\eta_g}$ does not depend on the

hopper size and the ratio v_s/s_o does not depend on the hopper size, since the horizontal flow velocity s_o does not depend on the hopper size. The resulting turbulence efficiency as calculated with equations (3-12) and (3-13) is thus not dependent on the hopper size, although it will change during the loading process.

10.2 The TSHD'S used

Based on the scale laws and based on Miedema & van Rhee (2007), 4 TSHD's are chosen in a range from small to Mega. The main dimensions and additional parameters of these hoppers can be found in table 1 and 2.

Table 10-1: The main dimensions of the 4 TSHD's.

Hopper	Length (m)	Width (m)	Empty height (m)	Volume (m^3)	Design density (ton/m^3)	Maximum load (ton)	HLP (m/sec)
Small	40	10	5.0	2000	1.5	3000	0.008
Large	60	15	7.5	6750	1.5	10125	0.008
Jumbo	80	20	10.0	16000	1.5	24000	0.008
Mega	100	25	12.5	31250	1.5	46875	0.008

Table 10-2: Additional and derived quantities.

Hopper	Flow (m^3/sec)	Pipe diameter (m)	Filling time (min)	Sailing time (min)	Hydraulic diameter (m)	Reynolds number	Mixture density (ton/m^3)
Small	3.2	0.54	10.4	104	10	$0.64*10^6$	1.3
Large	7.2	0.81	15.6	156	15	$0.96*10^6$	1.3
Jumbo	12.8	1.08	20.8	208	20	$1.28*10^6$	1.3
Mega	20.0	1.35	26.0	260	25	$1.60*10^6$	1.3

Table 10-1 and Table 10-2 show a wide range of TSHD's from Small (2000 m^3) to Mega (31250 m^3) . As can be noted in the tables, the hopper load parameters are constant at 0.008 m/sec, which is the settling velocity of a grain a bit bigger than 100 µm. The design density of the TSHD's is chosen at 1.5 ton/m^3, which implies that the loading process will follow the Constant Tonnage Loading process. The total sailing and dumping time is chosen 10 times the filling time, which of course is arbitrary, but the resulting sailing times seem to be representative for the reality. The mixture density is chosen at 1.3 ton/m^3, which is high enough to take the influence of hindered settling into account. It should be noted that the Reynolds numbers of the horizontal flow in the hopper are not constant; the Reynolds numbers are proportional to the length scale $\boldsymbol{\lambda}$. The question is whether or not this will influence the loading process. As stated before, it does not influence the turbulent settling efficiency, but it could influence the scour in the final phase of the loading process. Scour is influenced by the viscous friction of the fluid flowing over the bed. This friction depends on the relative roughness and the Reynolds number. The roughness of the sediment has the magnitude of the grain diameter which is in the range of 0.1-0.5 mm, while the hydraulic diameters of the 4 TSHD's are in the magnitude of 10-25 m. The largest relative roughness would occur for a 0.5 mm grain and a hydraulic diameter of 10 m, giving 0.0005/10=0.00005. The friction coefficient will be between 0.0175 and 0.0171, which hardly has an effect on the scour. Although there will always be some effect, it is not expected that this effect will have a big influence on the similarity of the loading processes of the 4 TSHD's. The sediment density is chosen at 1.9 ton/m^3, which means that the TDS is about 76% of the weight of the wet sediment.

For carrying out the simulations 4 grain distributions are chosen. All 4 grain distributions have a $\mathbf{d_{15}}$ for grains with a settling velocity smaller than the hopper load parameter in order to be sure there will be significant overflow losses. If grain distributions were chosen with almost 100% of the grains having a settling velocity above the hopper load parameter, this would result in very small cumulative overflow losses and a good comparison would be difficult.
Table 10-3 gives the $\mathbf{d_{15}}$, $\mathbf{d_{50}}$ and $\mathbf{d_{85}}$ of the 4 grain distributions, while figure 12 shows the full PSD's.

Table 10-3: The characteristics of the 4 grain distributions.

	400 µm	250 µm	150 µm	100 µm
d_{15}	70 µm	80 µm	80 µm	50 µm
d_{50}	400 µm	250 µm	150 µm	100 µm
d_{85}	2000 µm	750 µm	300 µm	200 µm

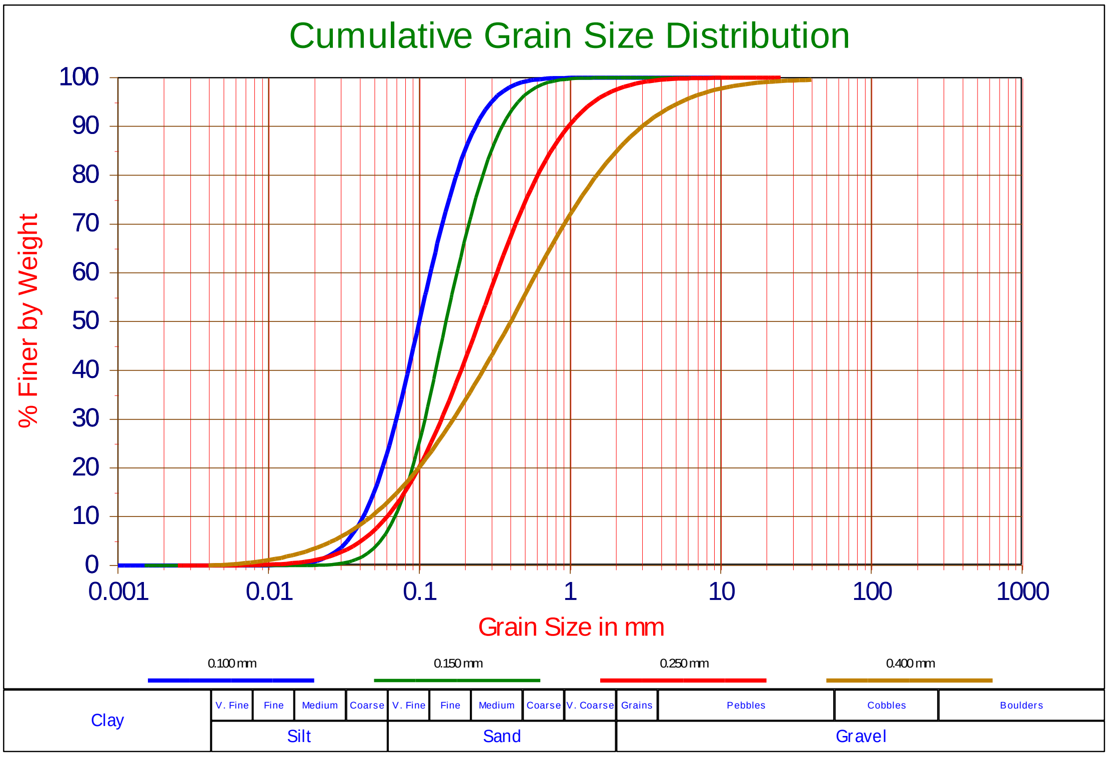

Figure 10-1: The 4 grain distributions.

10.3 Simulation Results

The simulations of the loading process of the 4 TSHD's are carried out with software based on the model published by Miedema (2008A), including turbulence efficiency, hindered settling, the storage effect, the layer of water above the overflow and more. The results of these simulations are summarized in Table 10-4, Table 10-5, Table 10-6 and Table 10-7.

Table 10-4: The simulation results with the 0.400 mm sand.

400 µm sand	Loading time (min)	TDS (ton)	Overflow losses TDS (ton)	Cumulative overflow losses (%)	Production (ton/min)
Small	31.0	2174	476	18.0%	16.1
Large	46.5	7349	1594	17.8%	36.2
Jumbo	62.0	17440	3758	17.7%	64.5
Mega	77.5	34089	7313	17.7%	100.9

Table 10-5: The simulation results with the 0.250 mm sand.

250 µm sand	Loading time (min)	TDS (ton)	Overflow losses TDS (ton)	Cumulative overflow losses (%)	Production (ton/min)
Small	31.0	2146	503	19.0%	15.9
Large	46.5	7258	1685	18.8%	35.8
Jumbo	61.8	17218	3923	18.6%	63.7
Mega	77.3	33662	7651	18.5%	99.7

Table 10-6: The simulation results with the 0.150 mm sand.

150 µm sand	Loading time (min)	TDS (ton)	Overflow losses TDS (ton)	Cumulative overflow losses (%)	Production (ton/min)
Small	32.2	2104	645	23.5%	15.4
Large	48.2	7114	2149	23.2%	34.8
Jumbo	64.2	16887	3923	23.0%	62.0
Mega	80.3	33030	7651	23.0%	96.9

Table 10-7: The simulation results with the 0.100 mm sand.

100 µm sand	Loading time (min)	TDS (ton)	Overflow losses TDS (ton)	Cumulative overflow losses (%)	Production (ton/min)
Small	43.0	2111	1564	42.6%	14.3
Large	64.7	7145	5292	42.6%	32.3
Jumbo	86.0	16952	12452	42.3%	57.6
Mega	107.7	33149	24368	42.4%	90.1

To visualize the simulations, the graphs of the simulations of the Small TSHD and the Mega TSHD can be found in the Figure 10-2, Figure 10-3, Figure 10-4, Figure 10-5, Figure 10-6, Figure 10-7, Figure 10-8 and Figure 10-9. From these graphs and the above tables it will be clear that the cumulative overflow losses do not depend on the size of the TSHD in quantity and in shape op de loading and overflow curves. To understand the above tables and the following figures, they will be explained and discussed each.

Table 10-4, Table 10-5, Table 10-6 and Table 10-7 show the loading times in the second column, it is clear that the loading times are almost proportional to the length scale **λ** and they increase with increasing overflow losses. The finer the sand, the longer the loading time. The third column gives the TDS at the point of optimum loading. The TDS of a hopper filled with sediment is about 76% of the weight of the sediment, but since there is still some water on top of the sediment at the moment of optimum loading the TDS is a bit less. This means that the maximum TDS of the Small TSHD is 2280 tons, for the Large TSHD 7695 tons, for the Jumbo TSHD 18240 tons and for the Mega TSHD 35625 tons, so the assumption is correct. The TDS does not depend on the type of sand. The fourth column gives the overflow losses in tons TDS. Again TDS means, only the weight of the solids, excluding the pore water and the water on top of the sediment. The fifth column gives the cumulative overflow losses, which are almost constant for each type of sand. For the 400 µm sand about 17.8%, for the 250 µm about 18.7%, for the 150 µm sand about 23.2% and for the 100 µm sand about 42.4%. These cumulative overflow losses are the overflow losses in TDS, divided by the total amount of TDS that has entered the hopper. It is clear that the cumulative overflow losses do not seem to depend on the size of the TSHD, given the scale laws applied in the simulations. Apparently the scale laws applied are the correct scale laws for scaling TSHD's in order to get similar loading and sedimentation processes. It is interesting however to compare the cumulative overflow losses with the grain size distribution curves of the sands used. The hopper load parameter of 0.008 m/s matches a grain with a diameter of 0.112 mm. If the percentage of grains smaller than this diameter is considered and compared we the overflow losses, the following numbers are found. For the 400 µm sand, about 20% smaller than 0.112 mm and cumulative overflow losses of 17.8%, for the 250 µm sand, about 20% smaller than 0.112 mm and 18.7% cumulative overflow losses, for the 150 µm sand, about 26% smaller than 0.112 mm and 23.2% cumulative overflow losses and for the 100 µm sand, about 52% smaller than 0.112 mm and 42.4% cumulative overflow losses. Apparently, but not unexpected, the cumulative overflow losses have a strong relation with the percentage of the grains smaller than the grain diameter matching the hopper load parameter. There is however not a fixed relation, because the grains smaller than the diameter matching the hopper load parameter will still settle partially and this depends strongly on the steepness of the cumulative grain size distribution. In the examples given it is clear that the 400 µm sand and the 250 µm sand, both have about 20% smaller and both have a cumulative overflow loss of about 20%. The simulations however also take hindered settling, the effect of the concentration on the settling velocity, into account and in reality the TSHD might make turns, resulting in a more complicated loading process. The overflow losses will also depend on the concentration as will be discussed later. The last column shows the production and of course the production is decreasing if the cumulative overflow losses are increasing.

Figure 10-2 and Figure 10-3 give the loading curves of the Small and the Mega TSHD in order to see if not only the cumulative overflow losses are independent of the size of the TSHD, but also the shape of the loading curves. To understand these graphs the different curves are explained. The loading process starts with an empty hopper, so there is no water in the hopper. First for 10.4 minutes for the Small hopper and 26.0 minutes for the Mega hopper, the hopper is filled with mixture of 1.3 ton/m3. After that the loading continues until after about 22.4 minutes for the Small hopper and 57 minutes for the Mega hopper, the maximum load is reached as can be found in table 1, seventh column. After reaching the maximum load, the loading continues while the overflow is lowered in such a way that the total load in the hopper remains constant, replacing water above the sediment with sediment. After about 40 minutes for the Small hopper and about 100 minutes for the Mega hopper, the sediment level is so high and the layer of water above the sediment is so thin, that very high flow velocities occur above the sediment, preventing the grains the settle and resulting in scour. After a short while hardly any grains will settle and the optimum loading point is reached. Continuing after this point will result in a decrease of production and is thus useless.

The black solid line at the top is the total load in the hopper and it is obvious that this line stays at the maximum load once this is reached. The blue solid line is the total volume in the hopper, it can be seen that after reaching the maximum load, the total volume is decreasing because the overflow is lowered. The dashed red line shows the tangent method to determine the optimum loading point. The dashed brown line shows the weight of the sediment in the hopper, including the weight of the pore water. At the end of the loading this line is just below the maximum load line, because there is still a layer of water above the sediment, which does not count in the sediment weight. The black solid straight line gives the amount of TDS that enters the hopper, so the sum of sediment TDS and overflow TDS should be equal to this line. The highest solid brown line is the amount of TDS in the hopper, while the lowest solid brown line is the sediment volume. Finally the solid red line gives the overflow losses in TDS. It can be seen that until the mixture in the hopper reaches the overflow level, there are no overflow losses. After the hopper is filled the overflow losses follow an almost straight line, which curves to a steeper line when scour starts to occur.
Although the scales of Figure 10-2 and Figure 10-3 are different, it is clear that the different loading curves have similar shapes, so not only the cumulative overflow losses are independent of the size of the hopper, also the momentary overflow losses are.

Figure 10-4 and Figure 10-5 show the loading curves including the storage effect. So what exactly is this storage effect? When grains enter the hopper, it can already be calculated which fraction of the grains will settle and which fraction of the grains will leave the hopper through the overflow. Figure 10-2 and Figure 10-3 are based on such a calculation. Grains that will leave through the overflow however, first have to travel through the hopper before they actually leave the hopper through the overflow. One can say that these grains are temporary stored in the hopper, the so called storage effect. This means that if suddenly the loading process would stop before the optimum is reached, there are more grains and thus TDS in the hopper then would follow from the Figure 10-2 and Figure 10-3. It also means that the overflow losses at such a moment would be less. The amount of grains that will leave the hopper, but are still inside, depends on the time it takes for a particle to move from the entrance to the overflow and this depends on the flow velocity. The flow velocity will increase when the sediment level increases and at the end of the loading cycle this velocity is so high that the storage effect can be neglected. In the Figure 10-4 and Figure 10-5 the top thick solid black lines show the amount of TDS in the hopper (compare with Figure 10-2 and Figure 10-3, these contain the same lines but solid brown). Just above the thick solid black lines are the thin solid green lines. The difference between the thick solid black line and the thin solid green line is the amount of TDS that will leave through the overflow, but has not yet left. The thin solid brown line below the thick solid black line show how many grains have already settled, the difference between the two lines is the amount of grains that will settle, but has not yet settled. Finally the thick solid black line at the bottom gives the overflow losses as have already been shown in Figure 10-2 and Figure 10-3. The thin red line, below this line give the amount of TDS that have already left the hopper.

Figure 10-6 and Figure 10-7 show the grain distribution curves of the 100 μm for the Small and the Mega TSHD. The original distribution is the lines with the dots. Left from these are the red lines which give the distribution of the grains leaving the overflow, on average from the start of the loading until the optimum loading point. Right from the original distribution is the solid green line, showing the average distribution in the hopper. It can be concluded that the grain distributions are similar for the Small and the Mega TSHD.

Figure 10-8 and Figure 10-9 show the influence of the concentration and the amount of water in the hopper at the moment the loading starts, on the cumulative overflow losses and the cumulative efficiency. The dot in both graphs shows the result of the simulation carried out. It is obvious that Figure 10-8 and Figure 10-9 show similar graphs. The lines in the graphs are determined by an equation, derived as an attempt to predict the overflow losses with just one equation. The green solid line shows the cumulative overflow losses when the hopper is completely empty at the start of the loading process. The blue line when the hopper is filled with 50% water and the red line when its filled with 100% water. The graph shows the overflow losses as a function of the mixture concentration. These graphs are still experimental, but give good tendencies of the overflow losses.

10.4 Conclusions & Discussion

The question before this research started, was how do the cumulative overflow losses behave when TSHD's are scaled from small to very big. The second question was, are that scale laws that should be applied when scaling TSHD's in order to create similar or maybe even identical processes.

First the answer on the second question, there are scale laws that should be applied and the main law is, to keep the hopper load parameter constant and from there derive the scale laws for the flow and other dimensions, but don't scale the sand.
If the scale laws are applied correctly, the simulations show that scaling the TSHD has hardly any influence on the cumulative overflow losses and the loading processes are similar.
The overflow losses however depend strongly on the position of the grain diameter match the hopper load parameter in the particle size distribution diagram. The fraction of the sand with diameters smaller than this diameter has a very strong relation with the cumulative overflow losses.

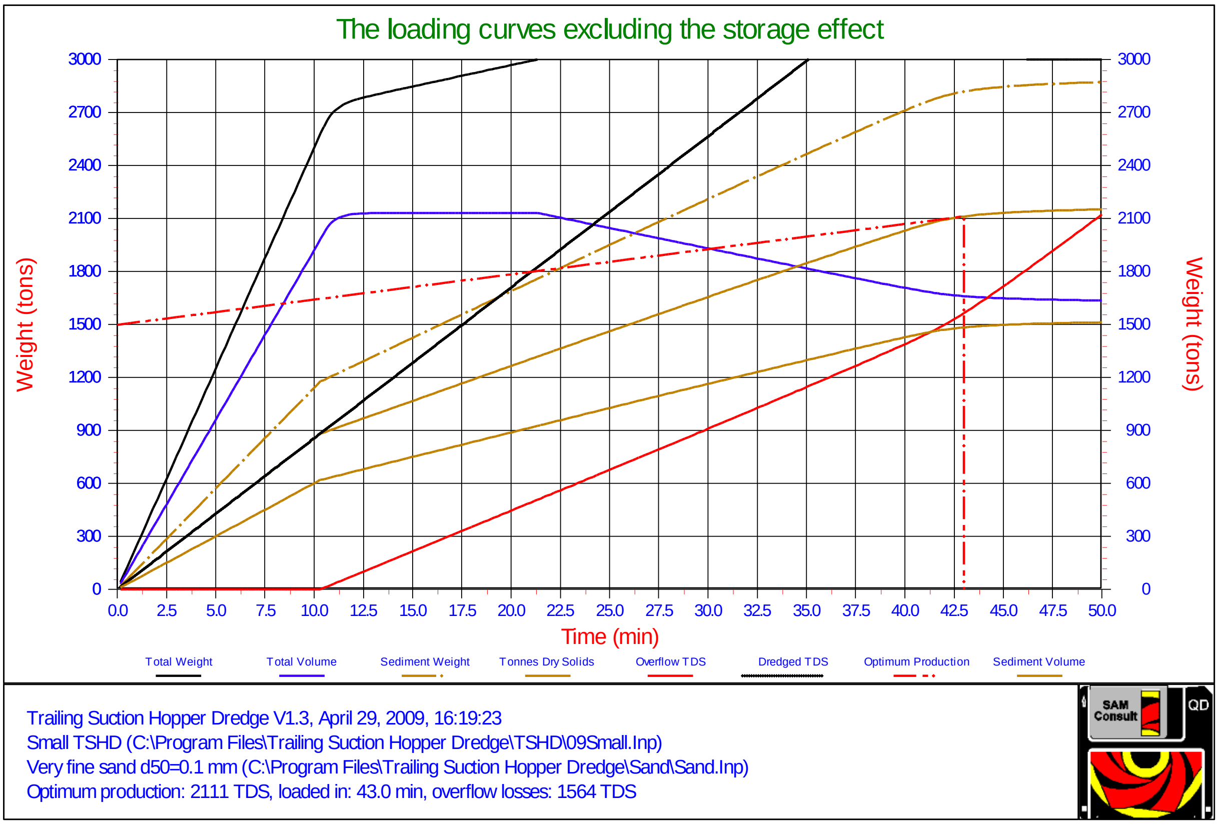

Figure 10-2: The loading curves for the Small TSHD.

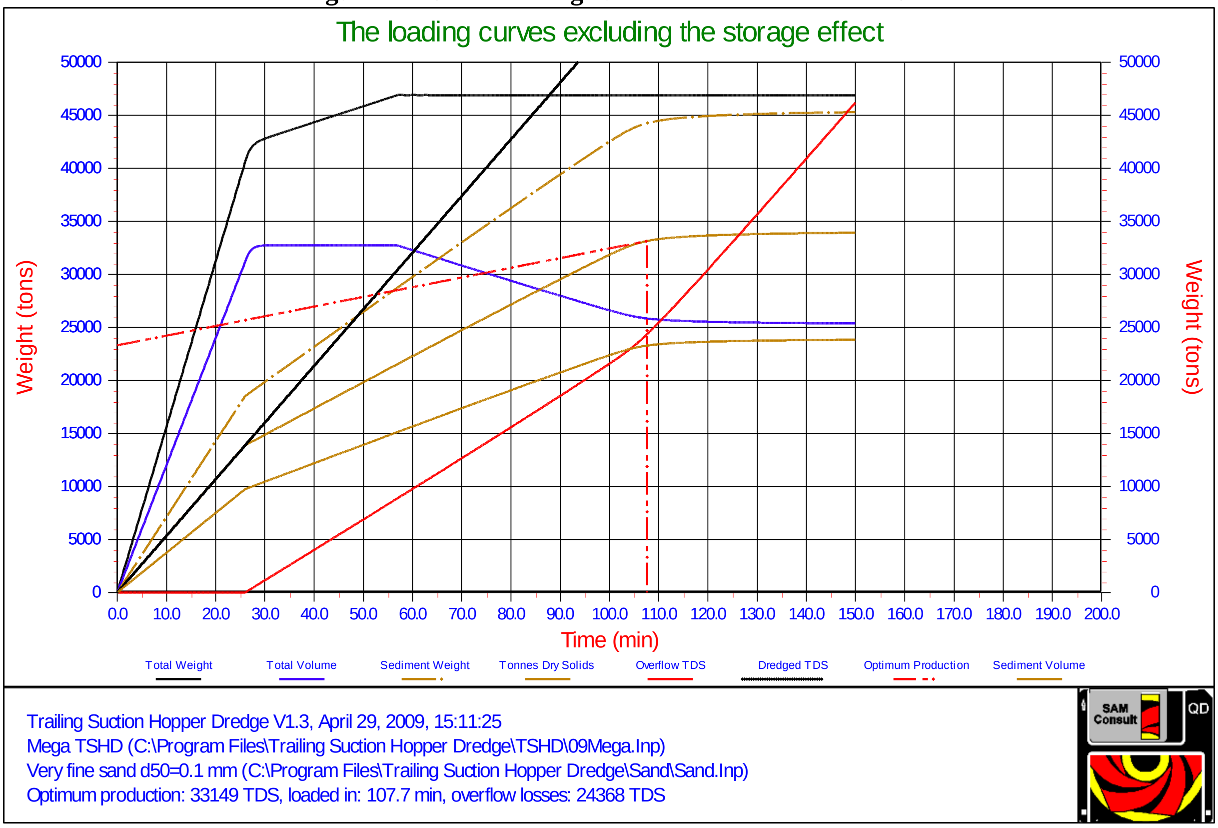

Figure 10-3: The loading curves for the Mega TSHD.

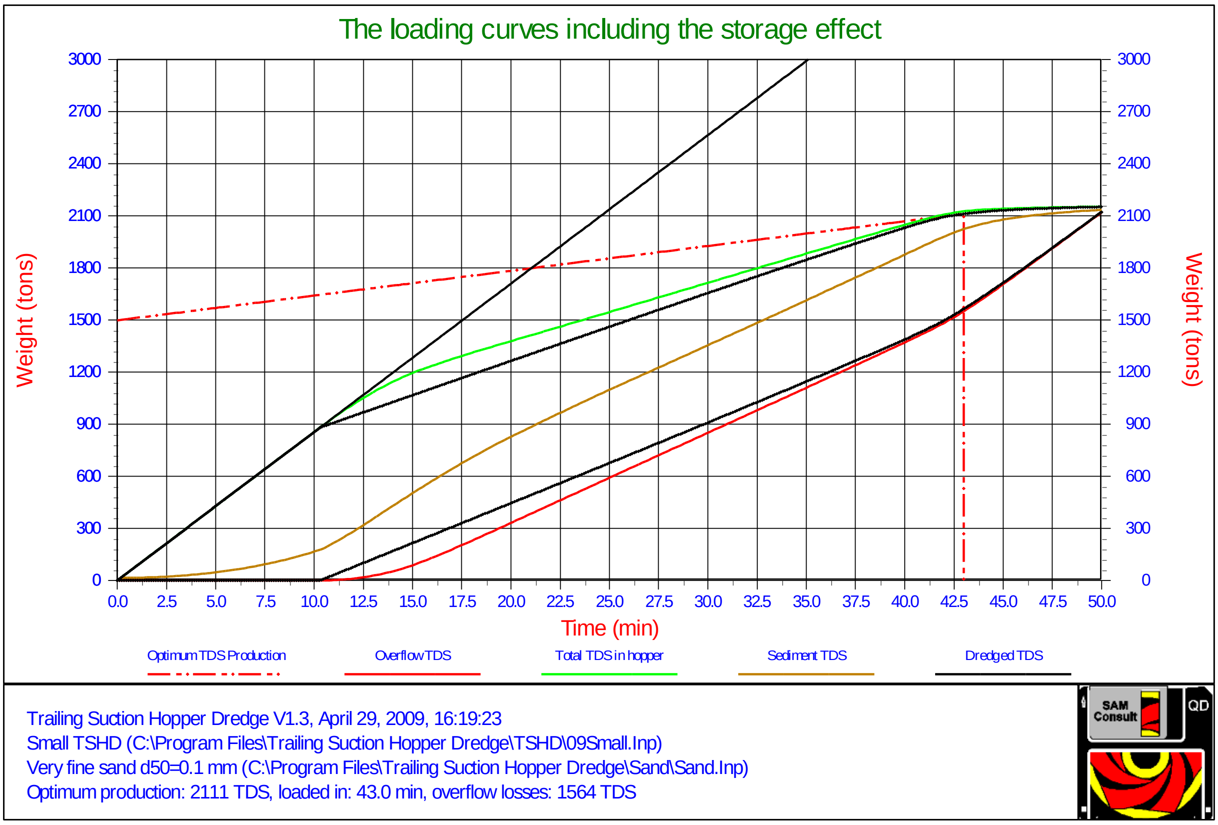

Figure 10-4: The loading curves including the storage effect for the Small TSHD.

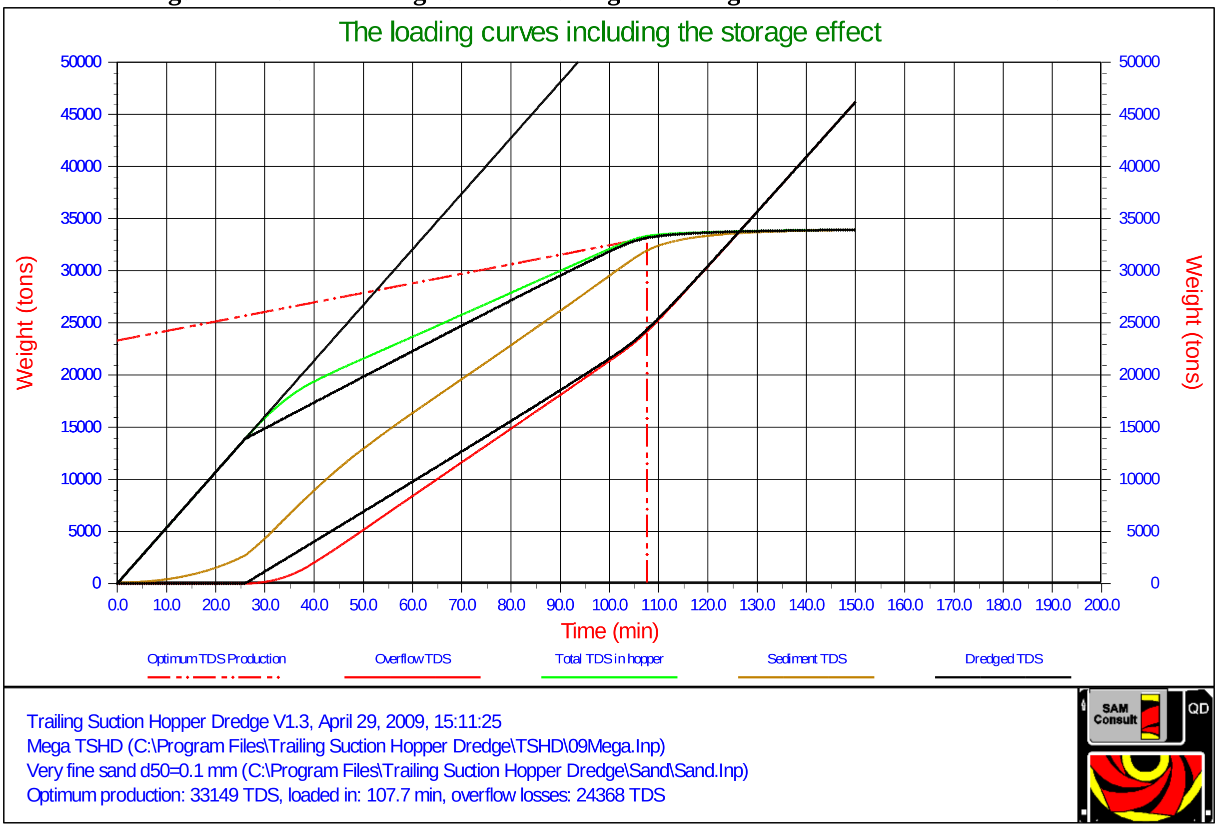

Figure 10-5: The loading curves including the storage effect for the Mega TSHD.

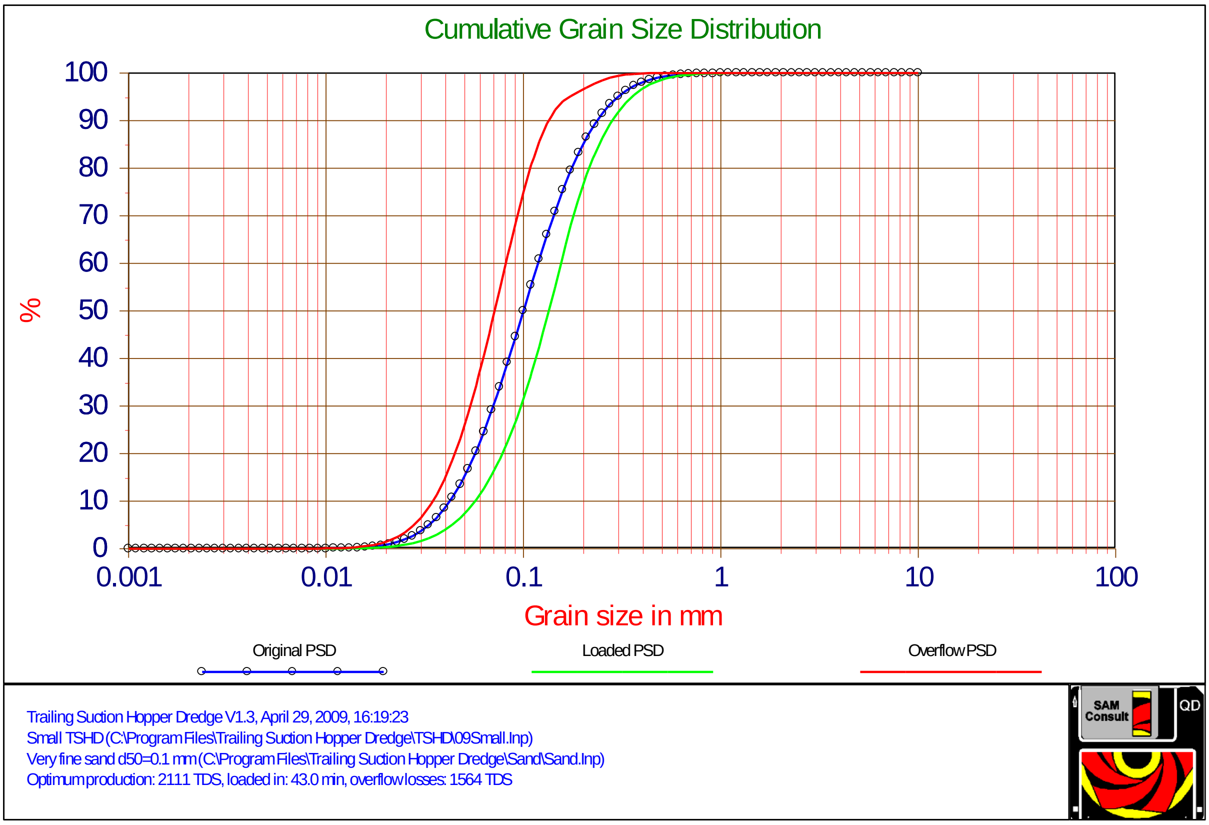

Figure 10-6: The grain distribution curves, original, overflow losses and sediment for the Small TSHD.

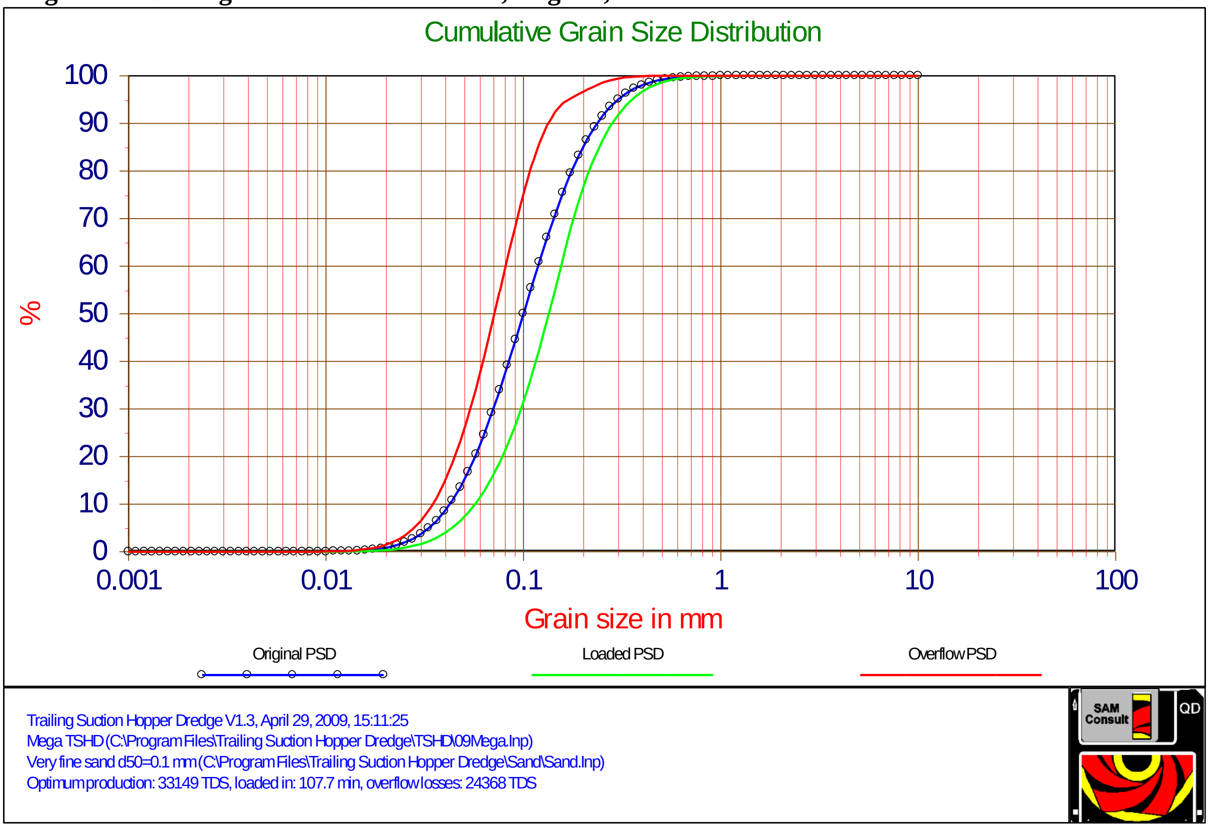

Figure 10-7: The grain distribution curves, original, overflow losses and sediment for the Mega TSHD.

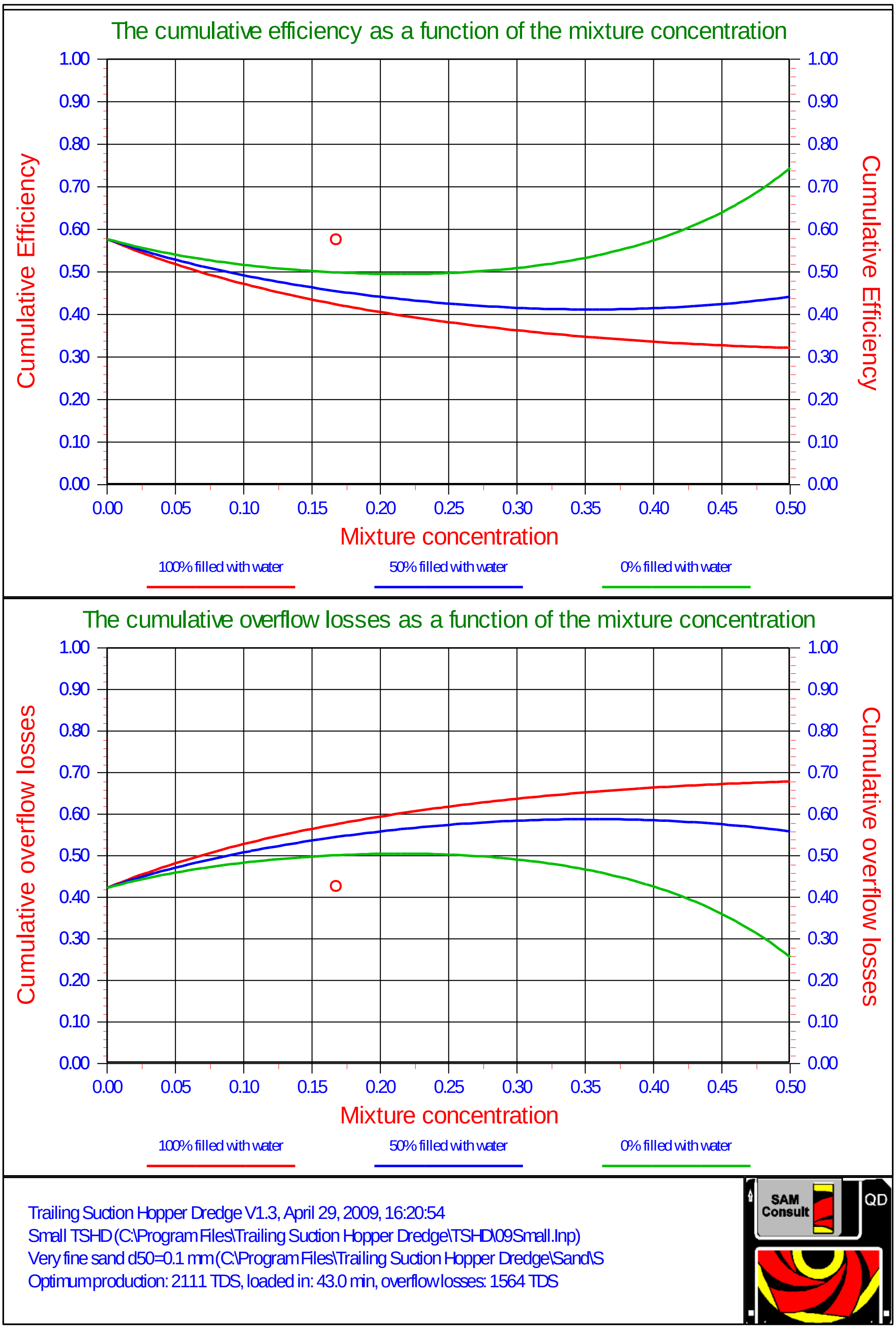

Figure 10-8: The overflow losses compared with an analytical model for the Small TSHD.

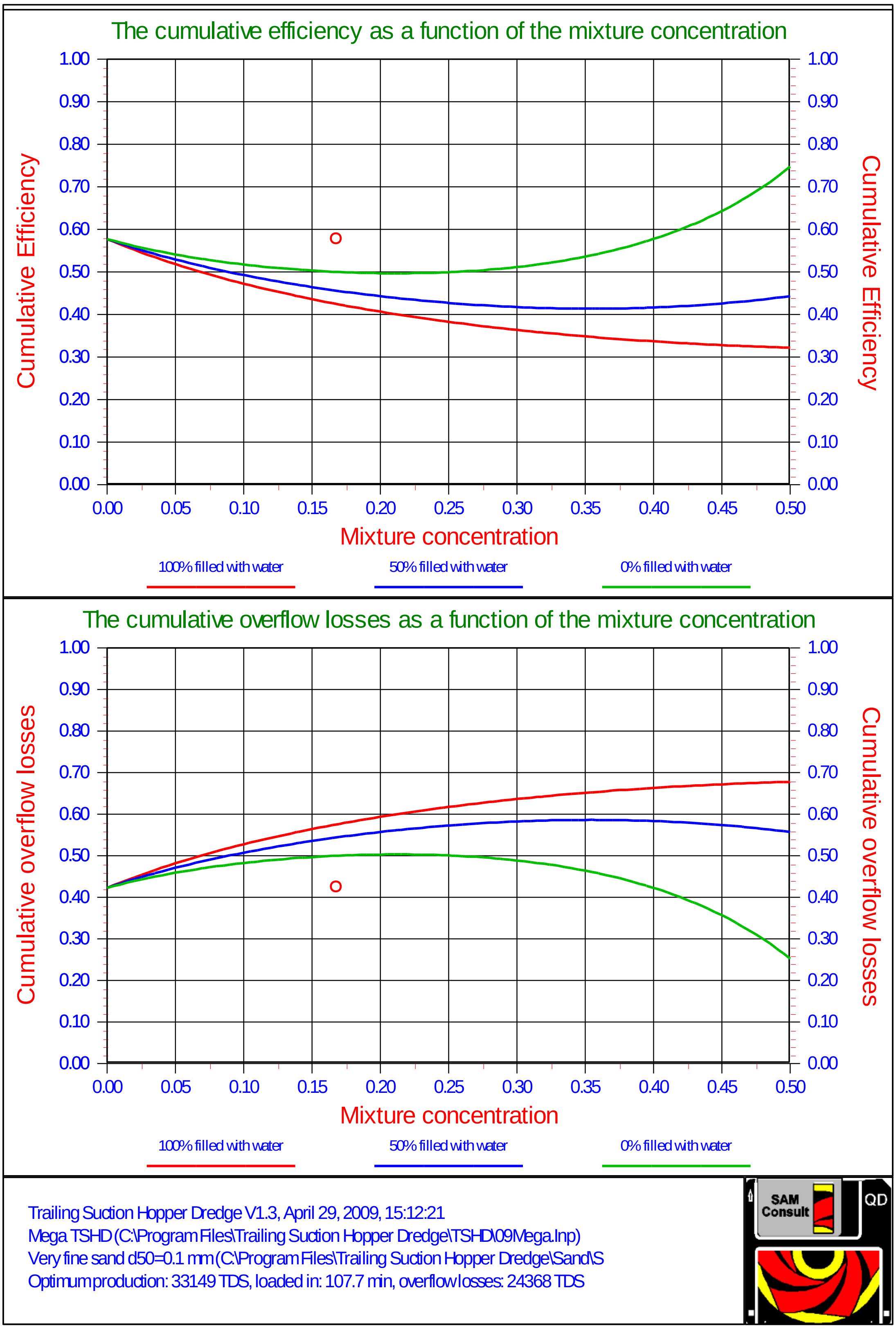

Figure 10-9: The overflow losses compared with an analytical model for the Mega TSHD.

Chapter 11: Steady Uniform Flow in Open Channels

This chapter is written with a view to bottom scour. The main outcome is the scour velocity as a function of the particle diameter. The coordinate system applied in this chapter is shown in Figure 11-1. This chapter is based on lecture notes of Liu (2001).

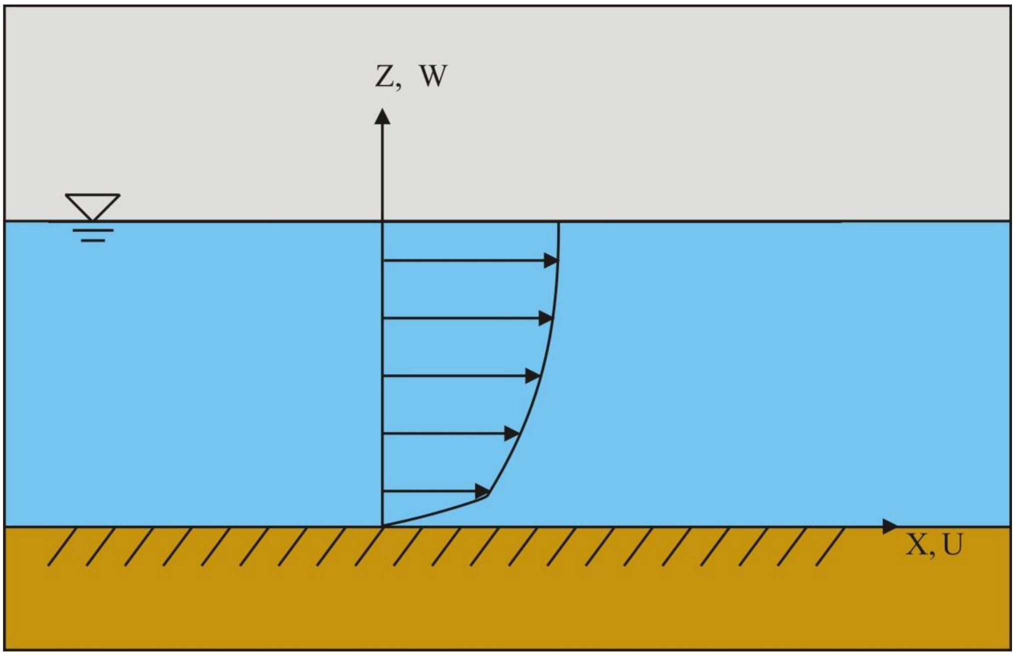

Figure 11-1: Coordinate system for the flow in open channels.

11.1 Types of flow

Description of various types of flow are given in the following.

Laminar versus turbulent

Laminar flow occurs at relatively low fluid velocity. The flow is visualized as layers which slide smoothly over each other without macroscopic mixing of fluid particles. The shear stress in laminar flow is given by Newton's law of viscosity:

$$\tau_v = \rho \cdot \nu \cdot \frac{du}{dz} \tag{11-1}$$

Where ρ is density of water and ν kinematic viscosity (ν = 10−6 m^2/s at 200˚C). Most flows in nature are turbulent. Turbulence is generated by instability in the flow, which trigger vortices. However, a thin layer exists near the boundary where the fluid motion is still laminar. A typical phenomenon of turbulent flow is the fluctuation of velocity

$$U = u + u' \qquad W = w + w' \tag{11-2}$$

Where: **U** and **W** are instantaneous velocities, in **x** and **z** directions respectively
u and **w** time-averaged velocities, in **x** and **z** directions respectively
u' and **w'** instantaneous velocity fluctuations, in **x** and **z** directions respectively

Turbulent flow is often given as the mean flow, described by **u** and **w**. In turbulent flow the water particles move in very irregular paths, causing an exchange of momentum from one portion of fluid to another, and hence, the turbulent shear stress (Reynolds stress). The turbulent shear stress, given by time-averaging of the Navier-Stokes equation, is:

$$\tau_t = -\rho \cdot \overline{u' \cdot w'} \tag{11-3}$$

Note that $\overline{\mathbf{u'}\cdot\mathbf{w'}}$ is always negative. In turbulent flow both viscosity and turbulence contribute to shear stress. The total shear stress is:

$$\tau = \tau_{\mathbf{v}} + \tau_{\mathbf{t}} = \rho \cdot \nu \cdot \frac{\mathbf{du}}{\mathbf{dz}} + \rho \cdot \overline{\mathbf{u'}\cdot\mathbf{w'}} \tag{11-4}$$

Steady versus unsteady

A flow is steady when the flow properties (e.g. density, velocity, pressure etc.) at any point are constant with respect to time. However, these properties may vary from point to point. In mathematical language:

$$\frac{\partial(\mathbf{any\ flow\ property})}{\partial \mathbf{t}} = \mathbf{0} \tag{11-5}$$

In the case of turbulent flow, steady flow means that the statistical parameters (mean and standard deviation) of the flow do not change with respect to time. If the flow is not steady, it is unsteady.

Uniform versus non-uniform

A flow is uniform when the flow velocity does not change along the flow direction, see Figure 11-2. Otherwise it is non-uniform flow.

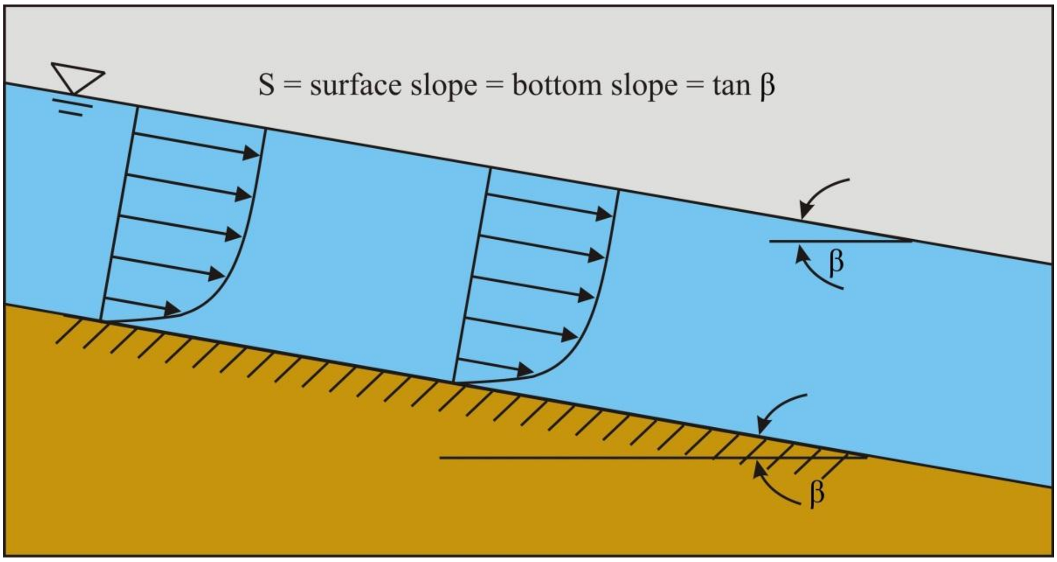

Figure 11-2: Steady uniform flow in a open channel.

Boundary layer flow

Prandtl developed the concept of the boundary layer. It provides an important link between ideal-fluid flow and real-fluid flow. Here is the original description.

For fluids having small viscosity, the effect of internal friction in the flow is appreciable only in a thin layer surrounding the flow boundaries.

However, we will demonstrate that the boundary layer fulfill the whole flow in open channels. The boundary layer thickness **δ** is defined as the distance from the boundary surface to the point where **u = 0.995·U**. The boundary layer development can be expressed as:

Laminar flow $$\frac{\delta}{\mathbf{x}} = 5 \cdot \left(\frac{\mathbf{U}\cdot\mathbf{x}}{\nu}\right)^{-0.5} \quad \text{when:} \quad \mathbf{Re_x} = \frac{\mathbf{U}\cdot\mathbf{x}}{\nu} < 5 \cdot 10^5 \tag{11-6}$$

Turbulent flow $$\frac{\delta}{\mathbf{x}} = 0.4 \cdot \left(\frac{\mathbf{U}\cdot\mathbf{x}}{\nu}\right)^{-0.2} \quad \text{when:} \quad \mathbf{Re_x} = \frac{\mathbf{U}\cdot\mathbf{x}}{\nu} > 5 \cdot 10^5 \tag{11-7}$$

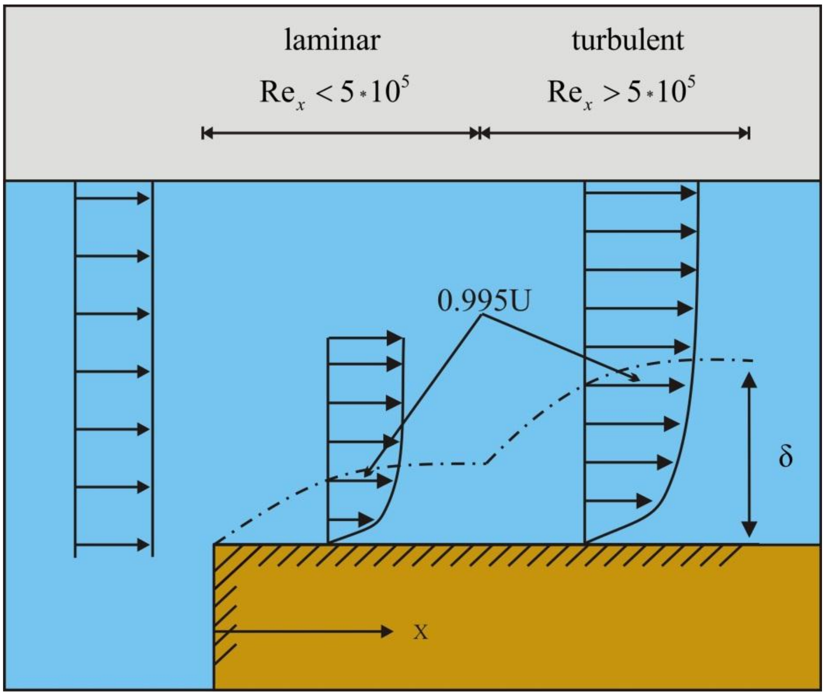

Figure 11-3: Development of the boundary layer.

11.2 Prandtl's Mixing Length Theory

Prandtl introduced the mixing length concept in order to calculate the turbulent shear stress. He assumed that a fluid parcel travels over a length $\boldsymbol{\ell}$ before its momentum is transferred.

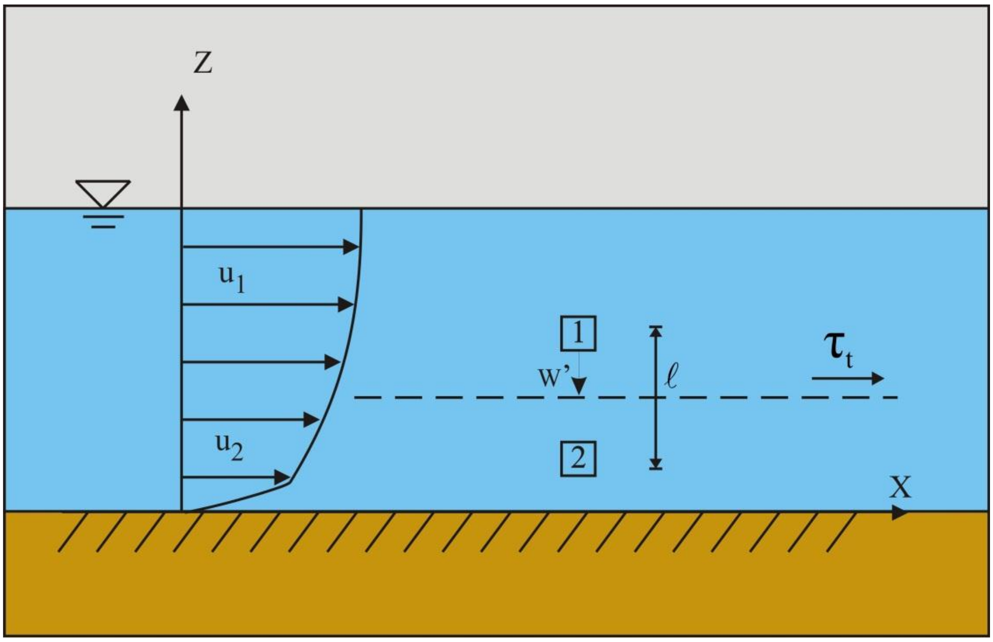

Figure 11-4: Prandtl's mixing length theory.

Figure 11-4 shows the time-averaged velocity profile. The fluid parcel, located in layer 1 and having the velocity $\mathbf{u_1}$, moves to layer 2 due to eddy motion. There is no momentum transfer during movement, i.e. the velocity of the fluid parcel is still $\mathbf{u_1}$ when it just arrives at layer 2, and decreases to $\mathbf{u_2}$ some time later by the momentum exchange with other fluid in layer 2. This action will speed up the fluid in layer 2, which can be seen as a turbulent shear stress $\boldsymbol{\tau_t}$ acting on layer 2 trying to accelerate layer 2. The horizontal instantaneous velocity fluctuation of the fluid parcel in layer 2 is:

$$\mathbf{u'=u_1-u_2=\ell\cdot\frac{du}{dz}} \tag{11-8}$$

Assuming the vertical instantaneous velocity fluctuation having the same magnitude:

$$\mathbf{w'=-\ell\cdot\frac{du}{dz}} \tag{11-9}$$

Where the negative sign is due to the downward movement of the fluid parcel, the turbulent shear stress now becomes:

$$\mathbf{\tau_t=-\rho\cdot u'\cdot w'=\rho\cdot\ell^2\cdot\left(\frac{du}{dz}\right)^2} \tag{11-10}$$

If we define kinematic eddy viscosity as:

$$\mathbf{\varepsilon=\ell^2\cdot\frac{du}{dz}} \tag{11-11}$$

The turbulent shear stress can be expressed in a way similar to viscous shear stress:

$$\mathbf{\tau_t=\rho\cdot\varepsilon\cdot\frac{du}{dz}} \tag{11-12}$$

11.3 Fluid Shear Stress and Friction Velocity

Fluid shear stress

The forces on a fluid element with unit width are shown in Figure 11-5. Because the flow is uniform (no acceleration), the force equilibrium in x-direction reads:

$$\mathbf{\tau_z\cdot\Delta x=\rho\cdot g\cdot(h-z)\cdot\Delta x\cdot\sin(\beta)} \tag{11-13}$$

For small slope we have $\mathbf{\sin(\beta)\approx\tan(\beta)=S}$. Therefore:

$$\mathbf{\tau_z=\rho\cdot g\cdot(h-z)\cdot S} \tag{11-14}$$

The bottom shear stress is:

$$\mathbf{\tau_b=\tau_{z=0}=\rho\cdot g\cdot h\cdot S} \tag{11-15}$$

Bottom shear stress

In the case of arbitrary cross section, the shear stress acting on the boundary changes along the wetted perimeter, cf. Fig.5. Then the bottom shear stress means actually the average of the shear stress along the wetted perimeter. The force equilibrium reads:

$$\mathbf{\tau_b\cdot O\cdot\Delta x=\rho\cdot g\cdot A\cdot\Delta x\cdot\sin(\beta)} \tag{11-16}$$

Where **O** is the wetted perimeter and **A** the area of the cross section. By applying the hydraulic radius (**R = A/O**) we get:

$$\mathbf{\tau_b=\rho\cdot g\cdot R\cdot S} \tag{11-17}$$

In the case of wide and shallow channel, **R** is approximately equal to **h** and equation (11-15) is identical to equation (11-17).

Friction velocity

The bottom shear stress is often represented by friction velocity, defined by:

$$\mathbf{u_* = \sqrt{\frac{\tau_b}{\rho}}} \qquad \mathbf{(11\text{-}18)}$$

The term *friction velocity* comes from the fact that $\sqrt{\tau_b/\rho}$ has the same unit as velocity and it has something to do with friction force. Inserting equation (11-17) into equation (11-18), gives:

$$\mathbf{u_* = \sqrt{g \cdot R \cdot S}} \qquad \mathbf{(11\text{-}19)}$$

Viscous shear stress versus turbulent shear stress

Equation (11-15) states that the shear stress in flow increases linearly with water depth see Figure 11-6.

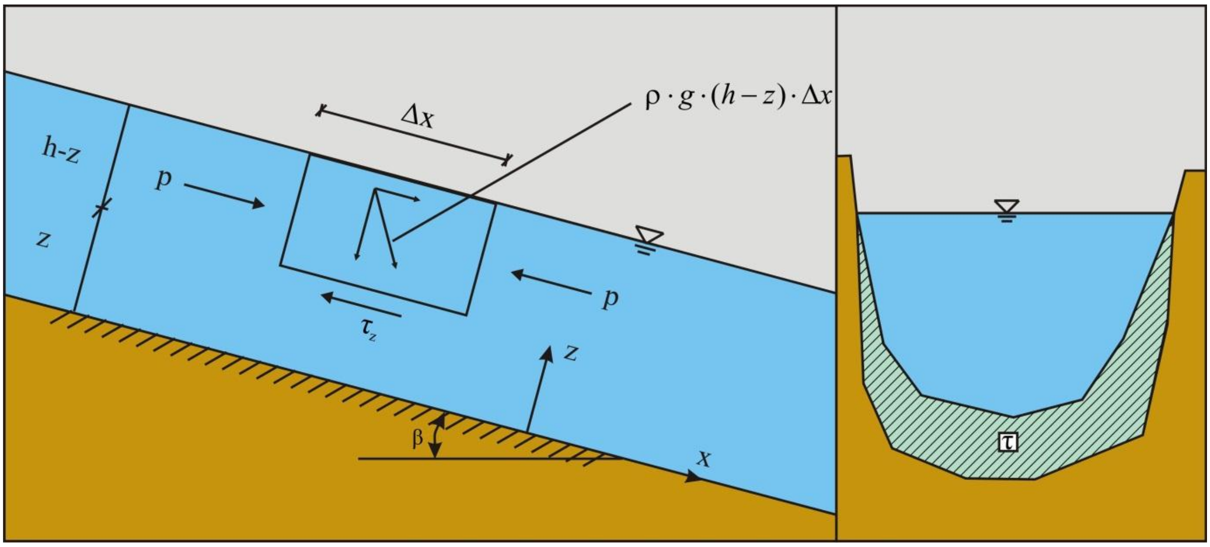

Figure 11-5: Fluid force and bottom shear stress.

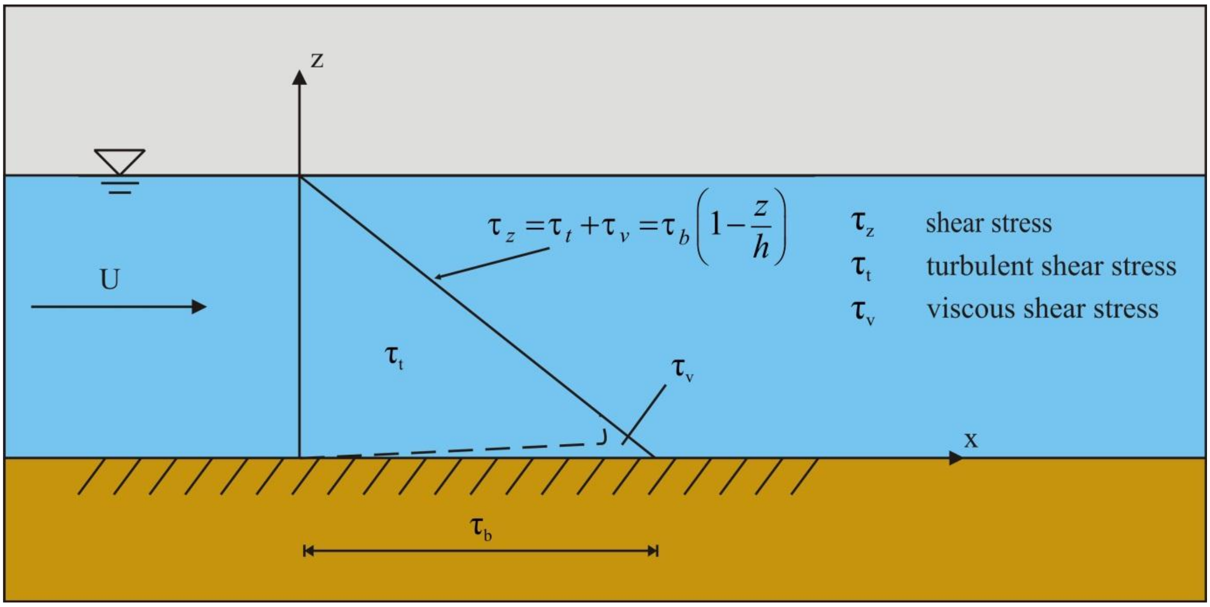

Figure 11-6: Shear stress components and distribution.

As the shear stress is consisted of viscosity and turbulence, we have:

$$\tau_z = \tau_v + \tau_t = \rho \cdot g \cdot (h - z) \cdot S \tag{11-20}$$

On the bottom surface, there is no turbulence (**u=w=0**, **u'=w'=0**), the turbulent shear stress:

$$\tau_t = -\rho \cdot \overline{u' \cdot w'} = 0 \tag{11-21}$$

Therefore, in a very thin layer above the bottom, viscous shear stress is dominant, and hence the flow is laminar. This thin layer is called viscous sub layer. Above the viscous sub layer, i.e. in the major part of flow, the turbulent shear stress dominates, see Figure 11-6. The measurement shows the shear stress in the viscous sub layer is constant and equal to the bottom shear stress, not increasing linearly with depth as indicated by Figure 11-6.

11.4 Classification of Flow Layers

Scientific classification

Figure 11-7 shows the classification of flow layers. Starting from the bottom we have:

1. Viscous sub layer: a thin layer just above the bottom. In this layer there is almost no turbulence. Measurement shows that the viscous shear stress in this layer is constant. The flow is laminar. Above this layer the flow is turbulent.
2. Transition layer: also called buffer layer, viscosity and turbulence are equally important.
3. Turbulent logarithmic layer: viscous shear stress can be neglected in this layer. Based on measurement, it is assumed that the turbulent shear stress is constant and equal to bottom shear stress. It is in this layer where Prandtl introduced the mixing length concept and derived the logarithmic velocity profile.
4. Turbulent outer layer: velocities are almost constant because of the presence of large eddies which produce strong mixing of the flow.

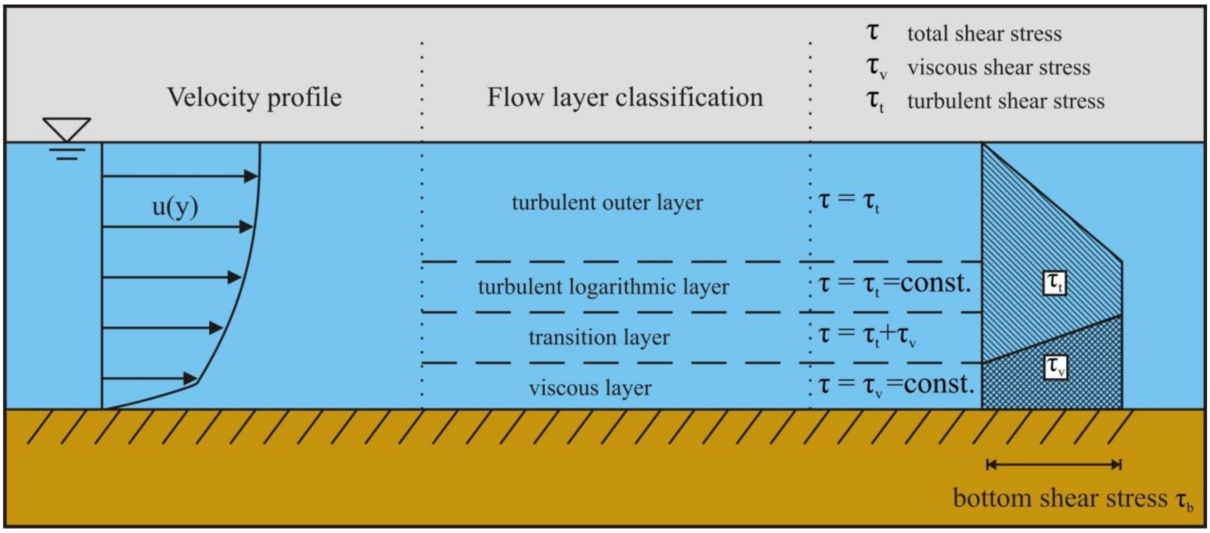

Figure 11-7: Scientific classification of flow region
(Layer thickness is not to scale, turbulent outer layer accounts for 80% - 90% of the region).

Engineering classification

In the turbulent logarithmic layer the measurements show that the turbulent shear stress is constant and equal to the bottom shear stress. By assuming that the mixing length is proportional to the distance to the bottom (**$\ell=\kappa \cdot z$**), Prandtl obtained the logarithmic velocity profile.

Various expressions have been proposed for the velocity distribution in the transitional layer and the turbulent outer layer. None of them are widely accepted. However, by the modification of the mixing length assumption, see next section, the logarithmic velocity profile applies also to the transitional layer and the turbulent outer layer. Measurement and computed velocities show reasonable agreement.

Therefore in engineering point of view, a turbulent layer with the logarithmic velocity profile covers the transitional layer, the turbulent logarithmic layer and the turbulent outer layer, see Figure 11-8.

As to the viscous sub layer, the effect of the bottom (or wall) roughness on the velocity distribution was first investigated for pipe flow by Nikuradse. He introduced the concept of equivalent grain roughness $\mathbf{k_s}$ (Nikuradse roughness, bed roughness). Based on experimental data, it was found

1. Hydraulically smooth flow for $\frac{\mathbf{u_* \cdot k_s}}{\mathbf{\nu}} \leq \mathbf{5}$, bed roughness is much smaller than the thickness of viscous sub layer. Therefore, the bed roughness will not affect the velocity distribution.
2. Hydraulically rough flow for $\frac{\mathbf{u_* \cdot k_s}}{\mathbf{\nu}} \geq \mathbf{70}$, bed roughness is so large that it produces eddies close to the bottom. A viscous sub layer does not exist and the flow velocity is not dependent on viscosity.
3. Hydraulically transitional flow for $\mathbf{5} \leq \frac{\mathbf{u_* \cdot k_s}}{\mathbf{\nu}} \leq \mathbf{70}$, the velocity distribution is affected by bed roughness and viscosity.

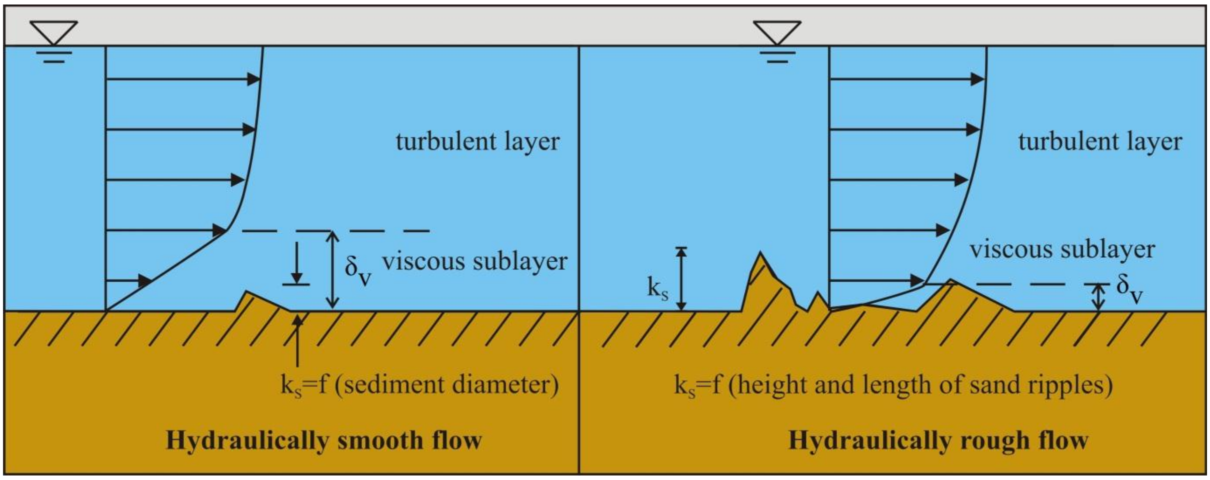

Figure 11-8: Engineering classification of flow region (Layer thickness is not to scale).

11.5 Velocity Distribution

Turbulent layer

In the turbulent layer the total shear stress contains only the turbulent shear stress. The total shear stress increases linearly with depth (equation (11-15) or Figure 11-6), i.e.

$$\tau_t(z) = \tau_b \cdot \left(1 - \frac{z}{h}\right) \tag{11-22}$$

By Prandtl's mixing length theory:

$$\tau_t = \rho \cdot \ell^2 \left(\frac{du}{dz}\right)^2 \tag{11-23}$$

Now assuming the mixing length:

$$\ell = \kappa \cdot z \cdot \left(1 - \frac{z}{h}\right)^{0.5} \tag{11-24}$$

With $\mathbf{\kappa}$ the Von Karman constant ($\mathbf{\kappa=0.4}$) and $\mathbf{h>>z}$, we get:

$$\frac{du}{dz} = \frac{1}{\kappa \cdot z} \cdot \sqrt{\frac{\tau_b}{\rho}} = \frac{u_*}{\kappa \cdot z} \tag{11-25}$$

Integration of the equation gives the famous logarithmic velocity profile:

$$u(z) = \frac{u_*}{\kappa} \cdot \ln\left(\frac{z}{z_0}\right) \tag{11-26}$$

Where the integration constant z_0 is the elevation corresponding to zero velocity ($u_{z=z0}=0$), given by Nikuradse by the study of the pipe flows.

$$z_0 = 0.11 \cdot \frac{\nu}{u_*} \quad \text{Hydraulically smooth flow} \quad \frac{u_* \cdot k_s}{\nu} \leq 5 \tag{11-27}$$

$$z_0 = 0.033 \cdot k_s \quad \text{Hydraulically rough flow} \quad \frac{u_* \cdot k_s}{\nu} \geq 70 \tag{11-28}$$

$$z_0 = 0.11 \cdot \frac{\nu}{u_*} + 0.033 \cdot k_s \quad \text{Hydraulically transition flow} \quad 5 < \frac{u_* \cdot k_s}{\nu} < 70 \tag{11-29}$$

It is interesting to note that the friction velocity u_*, which, by definition, has nothing to do with velocity, is the flow velocity at the elevation $z=z_0 . e^{\kappa}$, thus:

$$u_{z=z_0 \cdot e^{\kappa}} = u_* \tag{11-30}$$

In the study of sediment transport, it is important to know that the friction velocity is the fluid velocity very close to the bottom, see Figure 11-9.

Viscous sub layer

In the case of hydraulically smooth flow there is a viscous sub layer. Viscous shear stress is constant in this layer and equal to the bottom shear stress, i.e.

$$\tau_\nu = \rho \cdot \nu \cdot \frac{du}{dz} = \tau_b \tag{11-31}$$

Integrating and applying $u_{z=0}=0$ gives:

$$u(z) = \frac{\tau_b}{\rho} \cdot \frac{z}{\nu} = \frac{u_*^2}{\nu} \cdot z \tag{11-32}$$

Thus, there is a linear velocity distribution in the viscous sub layer. The linear velocity distribution intersects with the logarithmic velocity distribution at the elevation $z=11.6\nu/u_*$, yielding a theoretical viscous sub layer thickness:

$$\delta_\nu = 11.6 \cdot \frac{\nu}{u_*} \tag{11-33}$$

The velocity profile is illustrated in Figure 11-9, with the detailed description of the fluid velocity near the bottom.

Bed roughness

The bed roughness k_s is also called the equivalent Nikuradse grain roughness, because it was originally introduced by Nikuradse in his pipe flow experiments, where grains are glued to the smooth wall of the pipes. The only situation where we can directly obtain the bed roughness is a flatbed consisting of uniform spheres, where k_s = diameter of sphere.
But in nature the bed is composed of grains with different size. Moreover, the bed is not flat, various bed forms, e.g. sand ripples or dunes, will appear depending on grain size and current. In that case the bed roughness can be obtained indirectly by the velocity measurement.

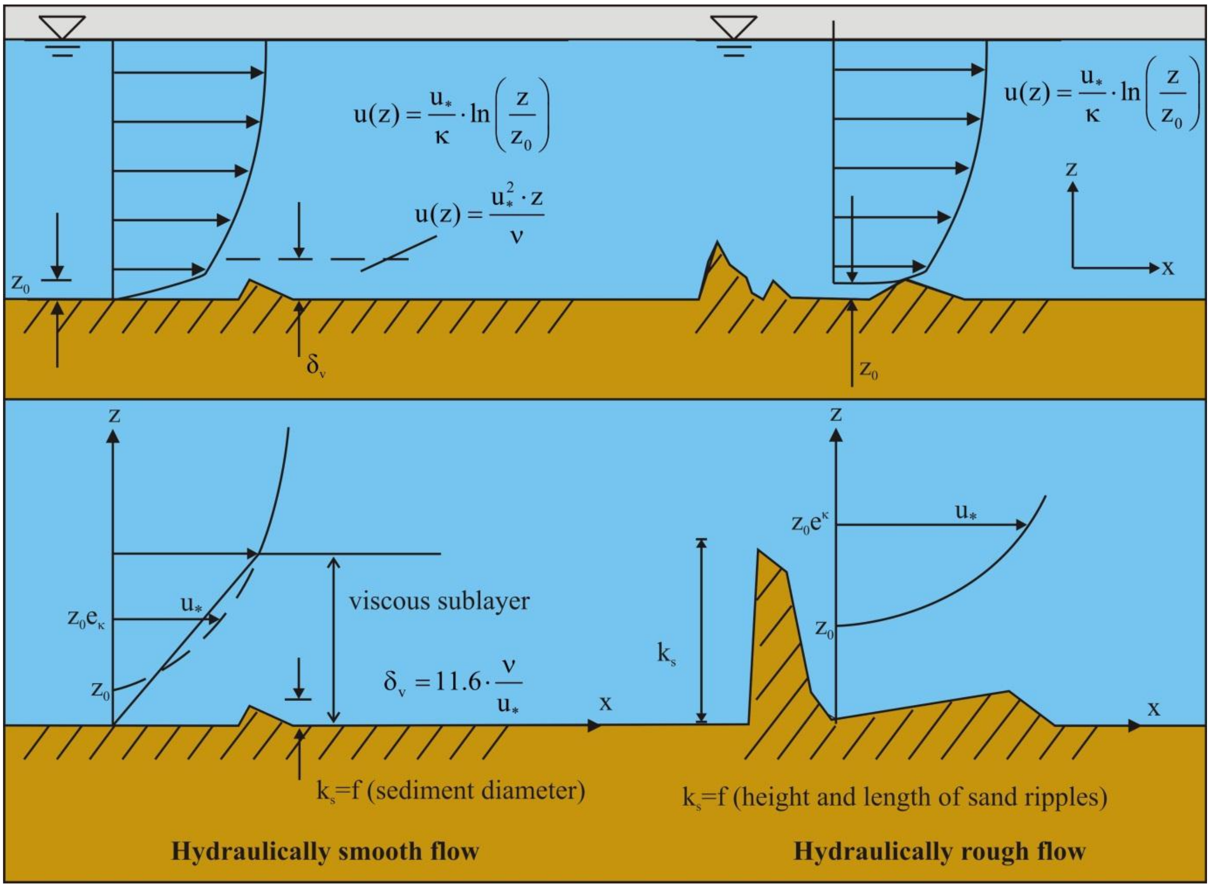

Figure 11-9: Illustration of the velocity profile in hydraulically smooth and rough flows.

11.6 Chézy Coefficient

Chézy proposed an empirical formula for the average velocity of steady uniform channel flow:

$$\mathbf{U = C \cdot \sqrt{R \cdot S}} \tag{11-34}$$

Where: R - Hydraulic radius, i.e. area of cross section divided by wetted perimeter
S - Bed slope
C - Empirical coefficient called Chézy coefficient. **C** was originally thought to be constant. Various formulas for **C** have been proposed.

Here we will see that **C** can be theoretically determined by averaging the logarithmic velocity profile. Recalling that the friction velocity is (equation (11-19)) and applying it into equation (11-34), we get the expression of **C**:

$$\mathbf{C = \frac{U}{u_*} \cdot \sqrt{g}} \tag{11-35}$$

Averaging the logarithmic velocity profile gives:

$$\mathbf{U = \frac{1}{h} \cdot \int_{z_0}^{h} u(z) \cdot dz = \frac{u_*}{\kappa \cdot h} \cdot \int_{z_0}^{h} \ln\left(\frac{z}{z_0}\right) \cdot dz} \tag{11-36}$$

$$\mathbf{U = \frac{u_*}{\kappa} \cdot \left(\ln\left(\frac{h}{z_0}\right) - 1 + \frac{z_0}{h} \right) \approx \frac{u_*}{\kappa} \cdot \ln\left(\frac{h}{z_0 \cdot e}\right)} \tag{11-37}$$

Inserting the above equation into equation 5.35 gives:

$$\mathbf{C}=\frac{\sqrt{\mathbf{g}}}{\kappa}\cdot\mathbf{ln}\left(\frac{\mathbf{h}}{\mathbf{z_0}\cdot\mathbf{e}}\right)=\mathbf{2.3}\cdot\frac{\sqrt{\mathbf{g}}}{\kappa}\cdot\mathbf{log}\left(\frac{\mathbf{h}}{\mathbf{z_0}\cdot\mathbf{e}}\right) \tag{11-38}$$

$$\mathbf{C}=\mathbf{2.3}\cdot\frac{\sqrt{\mathbf{g}}}{\kappa}\cdot\mathbf{log}\left(\frac{\mathbf{h}}{\left(\mathbf{0.11}\cdot\frac{\nu}{\mathbf{u_*}}+\mathbf{0.033}\cdot\mathbf{k_s}\right)\cdot\mathbf{e}}\right)=\mathbf{18}\cdot\mathbf{log}\left(\frac{\mathbf{11.14}\cdot\mathbf{h}}{\mathbf{3.33}\cdot\frac{\nu}{\mathbf{u_*}}+\mathbf{k_s}}\right) \tag{11-39}$$

This can be approximated by:

$$\mathbf{C}\approx\mathbf{18}\cdot\mathbf{log}\left(\frac{\mathbf{12}\cdot\mathbf{h}\cdot\mathbf{u_*}}{\mathbf{3.3}\cdot\nu}\right)\qquad\text{Hydraulically smooth flow}\qquad\frac{\mathbf{u_*}\cdot\mathbf{k_s}}{\nu}\leq\mathbf{5} \tag{11-40}$$

$$\mathbf{C}\approx\mathbf{18}\cdot\mathbf{log}\left(\frac{\mathbf{12}\cdot\mathbf{h}}{\mathbf{k_s}}\right)\qquad\text{Hydraulically rough flow}\qquad\frac{\mathbf{u_*}\cdot\mathbf{k_s}}{\nu}\geq\mathbf{70} \tag{11-41}$$

Where the expression for $\mathbf{z_0}$ has been used and **ln** has been converted to **log**. Moreover the inclusion of $\mathbf{g=9.8m/s^2}$ means that **C** has the unit **√m/s.**

Hydraulic roughness is expressed in terms of the Chézy (**C**), Manning-Strickler (**n**), Darcy-Weisbach (**λ**). The relation between **C** and **λ** is:

$$\mathbf{C}^2=\frac{\mathbf{8}\cdot\mathbf{g}}{\lambda} \tag{11-42}$$

Equation (11-39) is often written as a function of the theoretical viscous sub layer thickness $\boldsymbol{\delta_\nu}$ (equation (11-33)) and the hydraulic radius (**R=A/O**):

$$\mathbf{C}=\mathbf{18}\cdot\mathbf{log}\left(\frac{\mathbf{12}\cdot\mathbf{R}}{\delta_\nu/\mathbf{3.5}+\mathbf{k_s}}\right) \tag{11-43}$$

Note that the hydraulic radius does not equal half the hydraulic diameter, but one fourth, since the hydraulic diameter **D=4·A/O**. The hydraulic diameter concept matches pipe flow, where the hydraulic diameter equals the pipe diameter for around pipe, where the hydraulic radius concept matches river flow, where for a wide river; the hydraulic radius equals the depth of the river.

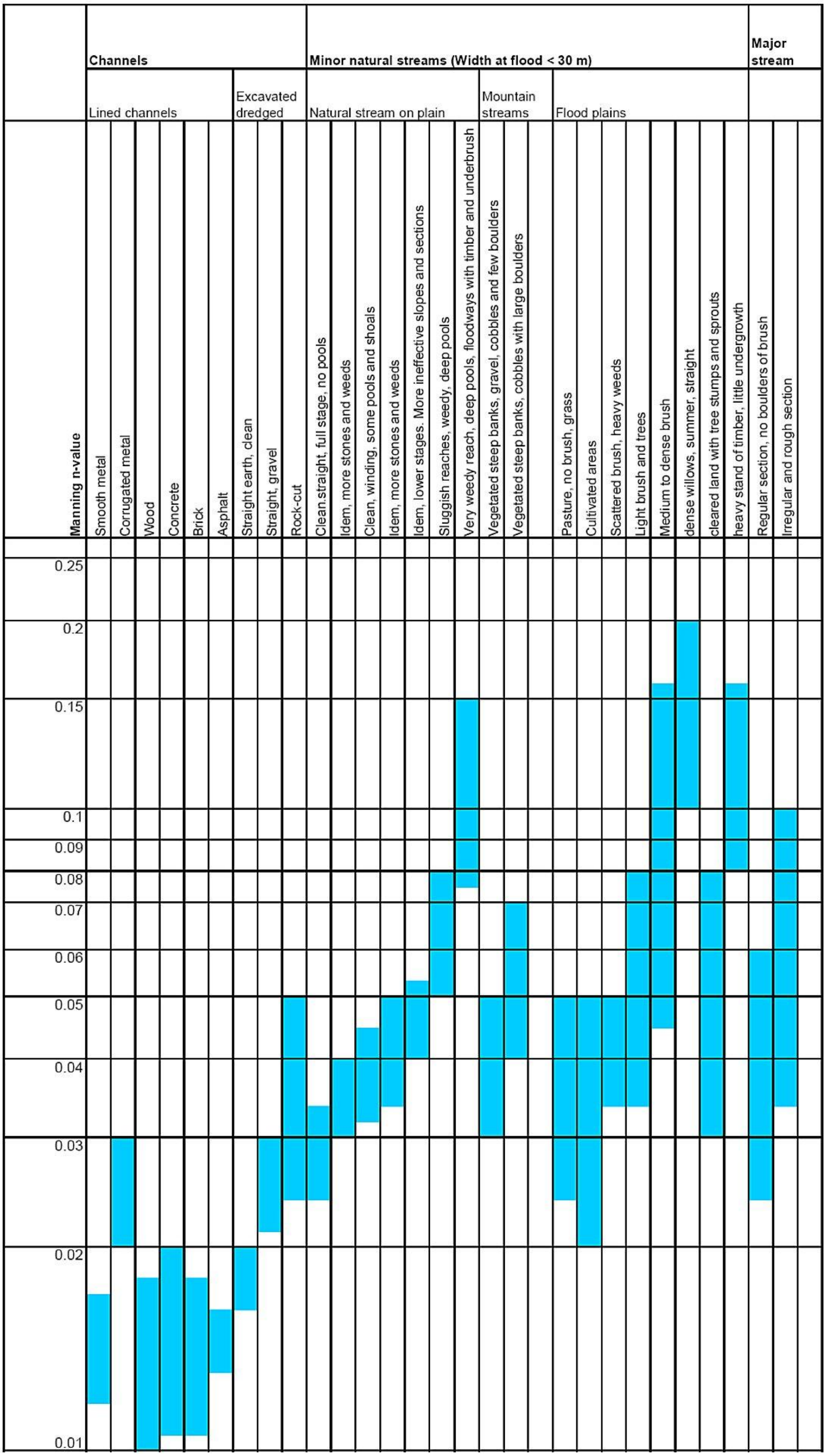

Figure 11-10: Range of values of the roughness coefficient n for different types of channels.

In these equations $\mathbf{k_s}$ is the equivalent sand roughness according to Nikuradse. For an alluvial bed the value of $\mathbf{k_s}$ varies strongly with the flow conditions. In rivers the flow regime will often be hydraulically rough ($\mathbf{k_s}$>>$\mathbf{d}$). According to Strickler the Chézy coefficient is:

$$\mathbf{C} = \left(\frac{\mathbf{R}}{\mathbf{k_s}}\right)^{\mathbf{1/6}} \tag{11-44}$$

Most often used, and linked with Strickler's equation, is the Manning roughness formula (or Manning-Strickler roughness formula). The relation between Manning's roughness coefficient **n** and the Chézy coefficient **C** is (with **R** in meters):

$$\mathbf{C} = \frac{\mathbf{R^{1/6}}}{\mathbf{n}} \tag{11-45}$$

Figure 11-10 gives an overview of Manning's roughness coefficient **n** for different types of channels. Chapter 12.5 will go into detail regarding the Darcy-Weisbach friction coefficient.

11.7 Drag Coefficient, Lift Coefficient and Friction Coefficient

Drag and lift coefficients

A real fluid moving past a body will exert a drag force on the body, see Figure 11-11.

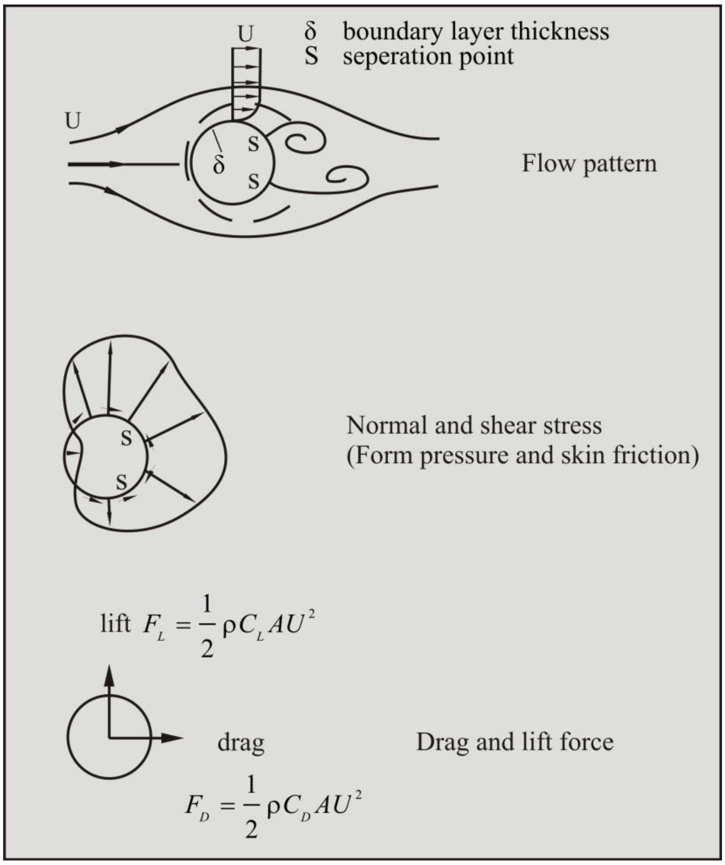

Figure 11-11: Drag force and lift force.

Drag force is consisted of friction drag and form drag, the former comes from the projection of skin friction force in the flow direction, and the latter from the projection of the form pressure force in the flow direction. The total drag is written as:

$$\mathbf{F_D} = \mathbf{C_D} \cdot \frac{1}{2} \cdot \rho \cdot \mathbf{U^2} \cdot \mathbf{A} \tag{11-46}$$

The lift force is written in the same way:

$$\mathbf{F_L = C_L \cdot \tfrac{1}{2} \cdot \rho \cdot U^2 \cdot A} \tag{11-47}$$

Where: **A -** Projected area of the body to the plane perpendicular to the flow direction.
C_D, C_L - Drag and lift coefficients, depend on the shape and surface roughness of the body and the Reynolds number. They are usually determined by experiments

Friction coefficient

Figure 11-12 illustrates fluid forces acting on a grain resting on the bed. The drag force:

$$\mathbf{F_D = C_D \cdot \tfrac{1}{2} \cdot \rho \cdot (\varsigma \cdot U)^2 \cdot A} \tag{11-48}$$

Where **ζ** is included because we do not know the fluid velocity past the grain, but we can reasonably assume that it is the function of the average velocity and other parameters.

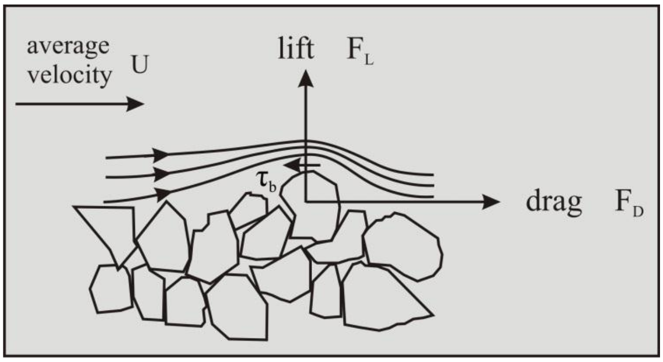

Figure 11-12: Fluid forces acting on a grain resting on the bed.

We can also say that the grain exerts a resistant force **F_D** on the flow. If **A'** is the projected area of the grain to the horizontal plane, the bottom shear stress is:

$$\mathbf{\tau_b = \frac{F_D}{A'} = \left(C_D \cdot \varsigma^2 \cdot \frac{A}{A'} \right) \cdot \tfrac{1}{2} \cdot \rho \cdot U^2 = f \cdot \tfrac{1}{2} \cdot \rho \cdot U^2 = \frac{\lambda}{4} \cdot \tfrac{1}{2} \cdot \rho \cdot U^2} \tag{11-49}$$

Where: **f** is the Fanning friction (**4·f=λ**) coefficient of the bed, which is a dimensionless parameter. By applying the Chézy coefficient we get:

$$\mathbf{C^2 = \frac{2 \cdot g}{f}} \tag{11-50}$$

$$\mathbf{f \approx \frac{0.06}{\left(\log\left(\frac{12 \cdot h \cdot u_*}{3.3 \cdot \nu} \right) \right)^2}} \quad \text{Hydraulically smooth flow} \quad \mathbf{\frac{u_* \cdot k_s}{\nu} \leq 5} \tag{11-51}$$

$$\mathbf{f \approx \frac{0.06}{\left(\log\left(\frac{12 \cdot h}{k_s} \right) \right)}} \quad \text{Hydraulically rough flow} \quad \mathbf{\frac{u_* \cdot k_s}{\nu} \geq 70} \tag{11-52}$$

Chapter 12: Scour/Erosion in the Hopper

During the final phase of the loading cycle the sediment level in the hopper is rising due to sedimentation, the flow velocity above the sediment increases, resulting in scour. This is the cause of rapidly increasing overflow losses. Figure 12-1 shows this situation. From literature a number of approaches can be found, the Camp approach for sedimentation tanks and the Shields and Hjulstrøm approaches for erosion in rivers. In general erosion is defined as the pickup of particles because of the flow of water above the particles. During the final phase of the loading cycle of a TSHD however, there is a high density mixture flowing above the bed and not just water. This may influence the way and the moment scour occurs. To find a solution to this problem, the physics of erosion will be analyzed. This is based on Miedema (2008B).

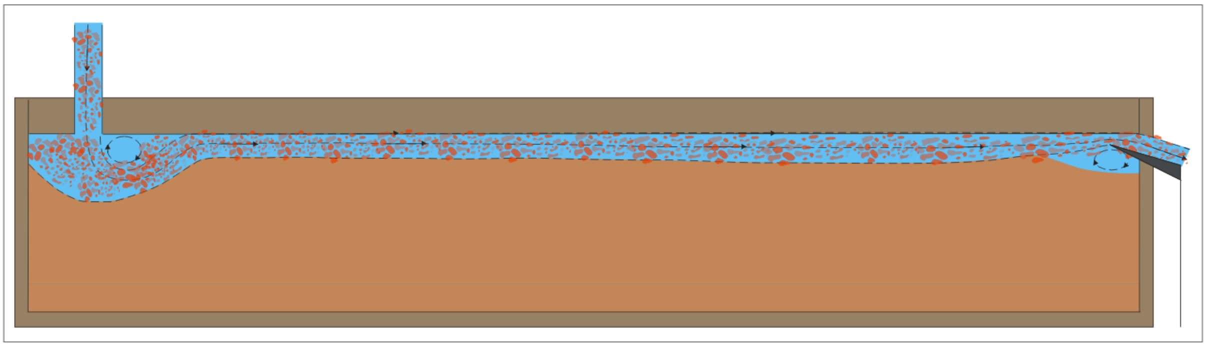

Figure 12-1: The final phase of the loading cycle.

12.1 The Camp Approach

When the height of the sediment increases and the hopper load parameter remains constant, the horizontal flow velocity above the sediment also increases. Grains that have already settled will be re-suspended and leave the basin through the overflow. This is called scouring.
First the small grains will not settle or erode and when the level increases more, also the bigger grains will stop settling, resulting in a smaller settling efficiency.

The shear force of water on a spherical particle is:

$$\tau = \frac{1}{4} \cdot \lambda \cdot \frac{1}{2} \cdot \rho_w \cdot s_s^2 \tag{12-1}$$

The shear force of particles at the bottom (mechanical friction) is proportional to the submerged weight of the sludge layer, per unit of bed surface (see Figure 2-10):

$$f = \mu \cdot N = \mu \cdot (1-n) \cdot (\rho_q - \rho_w) \cdot g \cdot d \tag{12-2}$$

In equilibrium the hydraulic shear equals the mechanical shear and the critical scour velocity can be calculated. The scour s_s velocity for a specific grain with diameter d_s, according to Huisman (1995) and Camp (1946) is:

$$s_s = \sqrt{\frac{8 \cdot \mu \cdot (1-n) \cdot (\rho_q - \rho_w) \cdot g \cdot d_s}{\lambda \cdot \rho_w}} \tag{12-3}$$

Grains that are re suspended due to scour, will not stay in the basin and thus have a settling efficiency of zero. In this equation, λ is the viscous friction coefficient mobilized on the top surface of the sediment and has a value in the range of 0.01-0.03, depending upon the Reynolds number and the ratio between the hydraulic radius and the grain size (surface roughness). The porosity **n** has a value in the range 0.4-0.5, while the friction coefficient μ depends on the internal friction of the sediment and has a value in the range of 0.1-1.0 for sand grains.

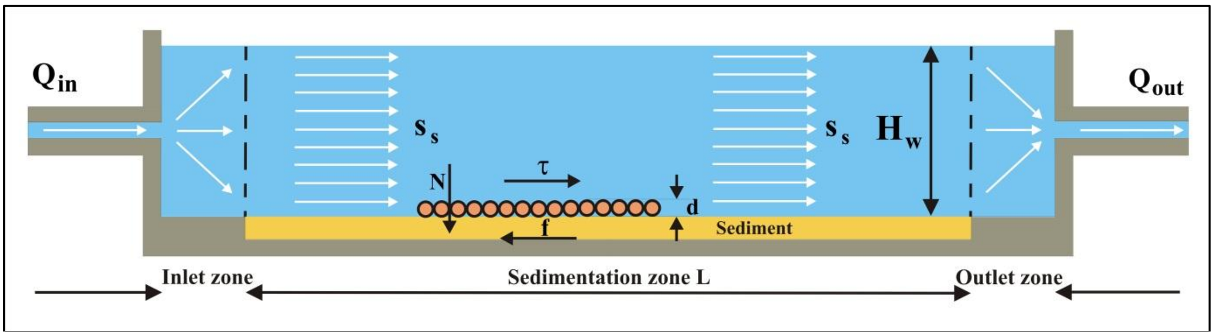

Figure 12-2: The equilibrium of forces on a particle.

With $\mu\cdot(1\text{-}n)=0.05$ and $\lambda=0.03$ this gives:

$$\mathbf{s_s = \sqrt{\frac{40\cdot(\rho_q - \rho_w)\cdot g\cdot d_s}{3\cdot\rho_w}}} \quad \textbf{(12-4)}$$

The particle diameter of particles that will not settle due to scour (and all particles with a smaller diameter) is:

$$\mathbf{d_s = \frac{3\cdot\rho_w}{40\cdot(\rho_q - \rho_w)\cdot g}\cdot s_s^2} \quad \textbf{(12-5)}$$

Knowing the diameter $\mathbf{d_s}$, the fraction $\mathbf{p_s}$ that will not settle due to scour can be found if the PSD of the sand is known. Equation (12-4) is often used for designing settling basins for drinking water. In such basins scour should be avoided, resulting in an equation with a safety margin. For the prediction of the erosion during the final phase of the settling process in TSHD's a more accurate prediction of the scour velocity is required.

12.2 The Shields Approach

Let us consider the steady flow over the bed composed of cohesion less grains. The forces acting on the grain is shown in Figure 12-3. The driving force is the flow drag force on the grain, assuming that part of the surface of the particle is hiding behind other particles and only a fraction $\boldsymbol{\beta}$ is subject to drag and lift:

$$\mathbf{F_D = C_D\cdot\tfrac{1}{2}\cdot\rho_w\cdot(\alpha\cdot u_*)^2\cdot\beta\cdot\frac{\pi\cdot d^2}{4}} \quad \textbf{(12-6)}$$

The lift force is written in the same way:

$$\mathbf{F_L = C_L\cdot\tfrac{1}{2}\cdot\rho_w\cdot(\alpha\cdot u_*)^2\cdot\beta\cdot\frac{\pi\cdot d^2}{4}} \quad \textbf{(12-7)}$$

The submerged weight of the particle is:

$$\mathbf{F_w = (\rho_q - \rho_w)\cdot g\cdot\frac{\pi\cdot d^3}{6}} \quad \textbf{(12-8)}$$

At equilibrium:

$$\mathbf{F_D = \mu\cdot(F_w - F_L)} \quad \textbf{(12-9)}$$

Where the friction velocity $\mathbf{u_*}$ is the flow velocity close to the bed. $\boldsymbol{\alpha}$ is a coefficient, used to modify $\mathbf{u_*}$ so that $\boldsymbol{\alpha}\mathbf{u_*}$ forms the characteristic flow velocity past the grain. The stabilizing force can be modeled as the friction force acting on the grain. If $\mathbf{u_{*,c}}$, critical friction velocity, denotes the situation where the grain is about to move, then the drag force is equal to the friction force, so:

$$\mathbf{C_D \cdot \tfrac{1}{2} \cdot \rho_w \cdot (\alpha \cdot u_{*,c})^2 \cdot \beta \cdot \frac{\pi \cdot d^2}{4} = \mu \cdot \left((\rho_q - \rho_w) \cdot g \cdot \frac{\pi \cdot d^3}{6} - C_L \cdot \tfrac{1}{2} \cdot \rho_w \cdot (\alpha \cdot u_{*,c})^2 \cdot \beta \cdot \frac{\pi \cdot d^2}{4} \right)} \qquad \text{(12-10)}$$

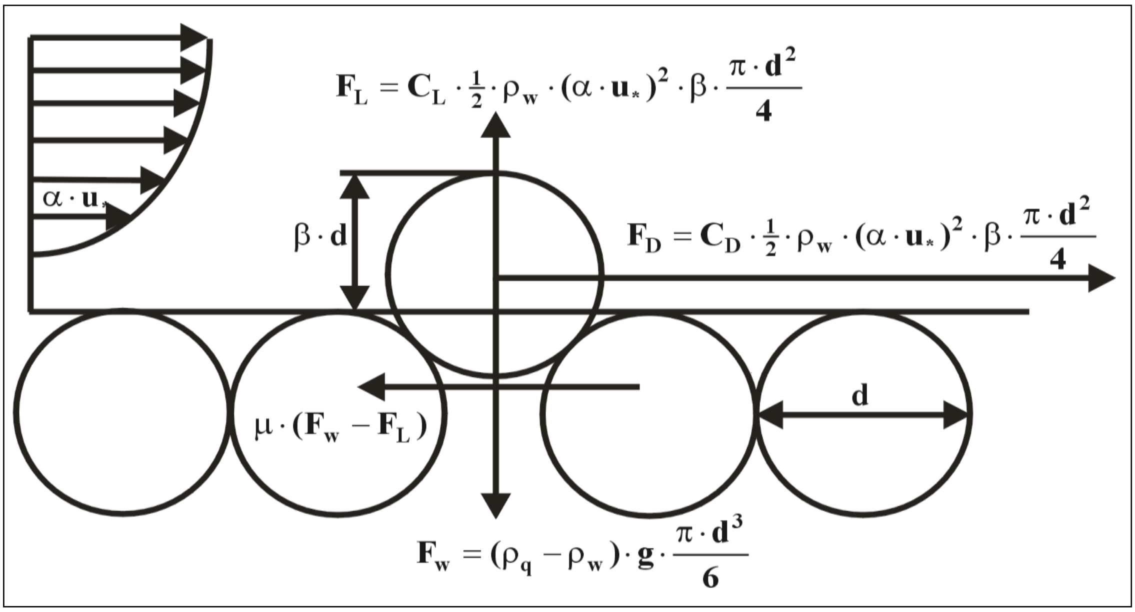

Figure 12-3: Forces acting on a grain resting on the bed.

This can be re-arranged into:

$$\mathbf{\frac{u_{*,c}^2}{R_d \cdot g \cdot d} = \frac{4}{3} \cdot \frac{1}{\alpha^2} \cdot \frac{\mu}{\beta \cdot C_D + \mu \cdot \beta \cdot C_L}} \qquad \text{(12-11)}$$

The Shields parameter is now defined as:

$$\mathbf{\theta_c = \frac{u_{*,c}^2}{R_d \cdot g \cdot d}} \qquad \text{(12-12)}$$

Re-arranging gives a simple equation for the Shields parameter:

$$\mathbf{\theta_c = \frac{u_{*,c}^2}{R_d \cdot g \cdot d} = \frac{4}{3} \cdot \frac{\mu}{\beta} \cdot \frac{1}{\alpha^2} \cdot \frac{1}{C_D + \mu \cdot C_L}} \qquad \text{(12-13)}$$

Since $\mathbf{C_D}$ normally depends on the boundary Reynolds number $\mathbf{Re_*}$, the Shields $\boldsymbol{\theta_c}$ number will be a function of the boundary Reynolds number $\mathbf{Re_* = u_* \cdot d / \nu}$. Carrying out an equilibrium of moments around the contact point of a particle with the particle its resting on, results in the same equation. One can discuss which equation to use for the $\mathbf{C_D}$ value and the $\mathbf{C_L}$ value, since the particles are not free from the surface as with the determination of the settling velocity for individual particles. Now the question is what such a function would look like. Figure 12-4 shows the relation between the Shields parameter and the boundary Reynolds number as is shown in Shields (1936).

It is however interesting to investigate if this curve can be determined in a more fundamental way. Based on the theory in this chapter the following can be derived.

Case 1: Hydraulically smooth flow (very low Re$_*$).

First let's assume a very small particle in a viscous laminar boundary layer. The particle is hiding for **(1- β)** behind other particles, which also means that **β** of the surface is subject to drag, assume **β** is about 0.5, which means the changes in drag area are about proportional with **β**. The velocity **u(z)** in the viscous sub layer at **β** times the diameter **d** height is equal to:

$$\mathbf{u}(\beta \cdot \mathbf{d}) = \frac{\mathbf{u}_*^2}{\nu} \cdot \beta \cdot \mathbf{d} \tag{12-14}$$

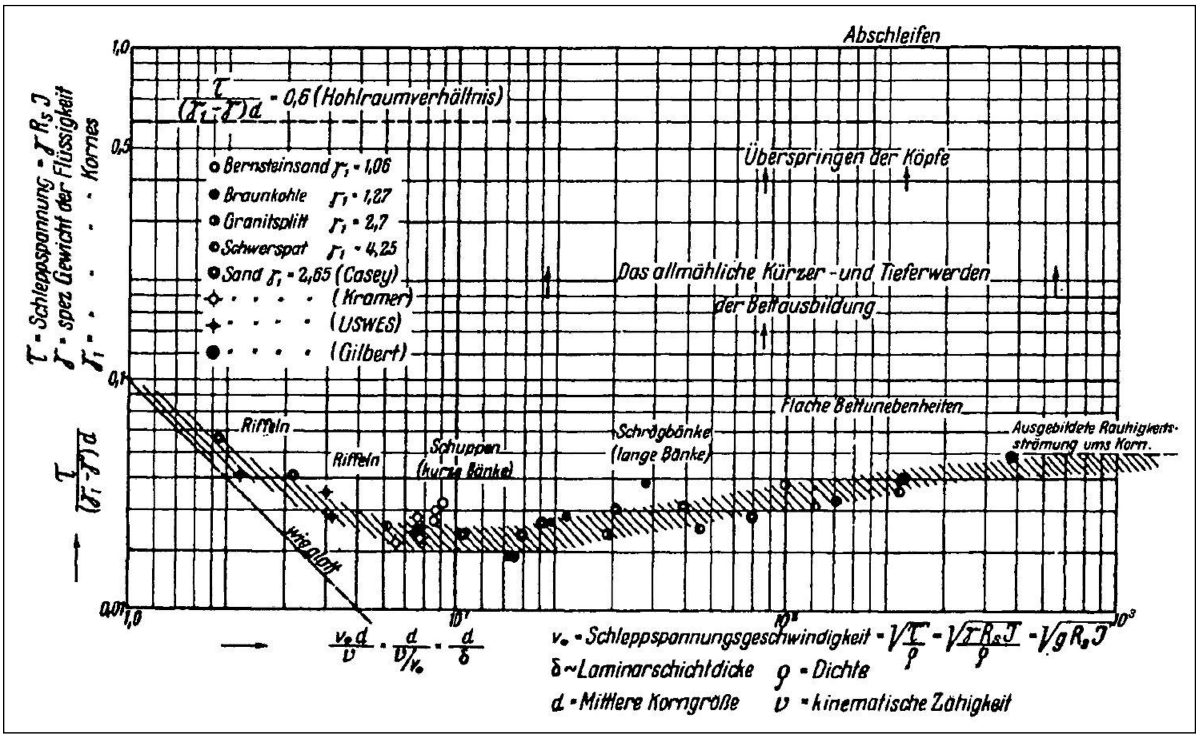

Figure 12-4: The original Shields (1936) curve.

Since the velocity develops linear with **z**, the drag force exerted on the particle, has to be found by integration of the velocity squared over the surface that is subject to the drag, but since the shape of the particle is not a square, but irregular, an effective velocity of $\frac{1}{3} \cdot \sqrt{3} = 0.577$ of the velocity at the top of the particle is chosen. This gives for the effective velocity on the particle:

$$\mathbf{u}_{\mathbf{eff}} = \frac{1}{3} \cdot \sqrt{3} \cdot \mathbf{u}(\beta \cdot \mathbf{d}) = \frac{1}{3} \cdot \sqrt{3} \cdot \frac{\mathbf{u}_*^2}{\nu} \cdot \beta \cdot \mathbf{d} = \frac{1}{3} \cdot \sqrt{3} \cdot \beta \cdot \frac{\mathbf{u}_*^2}{\nu} \cdot \mathbf{d} \tag{12-15}$$

With:

$$\mathbf{u}_{\mathbf{eff}} = \alpha \cdot \mathbf{u}_* = \frac{1}{3} \cdot \sqrt{3} \cdot \beta \cdot \frac{\mathbf{u}_*}{\nu} \cdot \mathbf{d} \cdot \mathbf{u}_* \tag{12-16}$$

So the coefficient **α** is equal to:

$$\alpha = \frac{1}{3} \cdot \sqrt{3} \cdot \beta \cdot \frac{\mathbf{u}_*}{\nu} \cdot \mathbf{d} = \frac{1}{3} \cdot \sqrt{3} \cdot \beta \cdot \mathbf{Re}_* \tag{12-17}$$

The Reynolds number for the flow around the particle is, assuming the hydraulic diameter of the particle equals 4 times the area that is subject to drag, divided by the wetted perimeter equals **d**:

$$\mathbf{Re}_{\mathbf{p}} = \frac{\mathbf{u}_{\mathbf{eff}} \cdot \mathbf{d}}{\nu} = \frac{1}{3} \cdot \sqrt{3} \cdot \beta \cdot \left(\frac{\mathbf{u}_* \cdot \mathbf{d}}{\nu}\right)^2 = \frac{1}{3} \cdot \sqrt{3} \cdot \beta \cdot \mathbf{Re}_*^2 = \alpha \cdot \mathbf{Re}_* \tag{12-18}$$

The drag coefficient in this Stokes area equals:

$$\mathbf{C_D = \frac{24}{Re_p}} \qquad \textbf{(12-19)}$$

Substituting this in equation (12-13) gives for the Shields parameter:

$$\mathbf{\theta_c = \frac{4}{3} \cdot \frac{\mu}{\beta} \cdot \left(\frac{1}{\frac{1}{3} \cdot \sqrt{3} \cdot \beta \cdot Re_*} \right)^2 \cdot \frac{\frac{1}{3} \cdot \sqrt{3} \cdot \beta \cdot Re_*^2}{24} = \frac{\sqrt{3}}{18} \cdot \frac{\mu}{\beta^2}} \qquad \textbf{(12-20)}$$

Let's assume a mechanical friction coefficient of **μ=0.5** and a surface factor **β=0.5** (meaning that 50% of the particle is subject to drag)**.** This would give a Shields parameter of 0.19. Soulsby & Whitehouse (1997) assume there is a maximum of 0.3, but as can be concluded from equation (12-20), there must be a certain bandwidth depending on the mechanical friction coefficient **μ** and the fraction of the surface of the particle that is subject to drag **β**. Using the transition region for $\mathbf{C_D}$, gives:

$$\mathbf{\theta_c = \frac{4}{3} \cdot \frac{\mu}{\beta} \cdot \left(\frac{1}{\frac{1}{3} \cdot \sqrt{3} \cdot \beta \cdot Re_*} \right)^2 \cdot \frac{1}{\frac{24}{\frac{1}{3} \cdot \sqrt{3} \cdot \beta \cdot Re_*^2} + \frac{3}{\left(\frac{1}{3} \cdot \sqrt{3} \cdot \beta \cdot Re_*^2 \right)^{0.5}} + 0.34}} \qquad \textbf{(12-21)}$$

Case 2: Hydraulically rough flow (very high Re*).

Now let's consider a very course particle in turbulent flow. According to equation 5.26 the velocity equals to:

$$\mathbf{u(z) = \frac{u_*}{\kappa} \cdot \ln\left(\frac{z}{0.033 \cdot k_s} \right)} \qquad \textbf{(12-22)}$$

Assuming a roughness $\mathbf{k_s}$ about equal to **β** times the particle diameter **d**, gives:

$$\mathbf{u(\beta \cdot d) = \frac{u_*}{\kappa} \cdot \ln\left(\frac{1}{0.033} \right) = 8.53 \cdot u_*} \qquad \textbf{(12-23)}$$

The effective velocity will be smaller, but since the particle is subject to turbulent flow in a logarithmic velocity field, equation (12-22) should be used to determine the effective velocity the part of the particle subject to drag, with respect to drag. For a logarithmic velocity field this is 0.764 times the velocity at the top of the particle, giving a velocity coefficient **α=6.5,** resulting in an effective velocity of:

$$\mathbf{u_{eff} = 6.5 \cdot u_*} \qquad \textbf{(12-24)}$$

And a particle Reynolds number of:

$$\mathbf{Re_p = \frac{u_{eff} \cdot d}{\nu} = 6.5 \cdot \frac{u_* \cdot d}{\nu} = 6.5 \cdot Re_* = \alpha \cdot Re_*} \qquad \textbf{(12-25)}$$

The drag coefficient $\mathbf{C_D}$ has a constant value of 0.445 for turbulent flow. Substituting this in equation (12-13) gives:

$$\mathbf{\theta_c = \frac{4}{3} \cdot \frac{\mu}{\beta} \cdot \frac{1}{6.5^2} \cdot \frac{1}{0.445} = 0.0709 \cdot \frac{\mu}{\beta}} \qquad \textbf{(12-26)}$$

If the mechanical friction coefficient **μ** and the area coefficient **β** are chosen equal, this results in a Shields parameter $\mathbf{\theta_c}$ of about 0.071 for the very high Reynolds $\mathbf{Re_*}$ numbers. In literature a value of 0.055-0.060 is found, but measurements show a certain bandwidth. Using a mechanical friction coefficient **μ** of 0.45 and an area factor **β** of 0.55, results in a Shields parameter $\mathbf{\theta_c}$ of 0.058, which matches literature. Values smaller than 0.5 for the area factor **β** are unlikely, because the Shields parameters predicts the beginning of erosion/scour of the entire sediment and there will always be particles with a higher area factor **β** up to about 0.75. Using this maximum area factor with a mechanical friction coefficient μ of 0.45, gives a Shields parameter θ_c of about 0.0425. Using the transition region, gives:

$$\theta_c = \frac{4}{3} \cdot \frac{\mu}{\beta} \cdot \left(\frac{1}{6.5}\right)^2 \cdot \frac{1}{\frac{24}{(6.5 \cdot Re_*)} + \frac{3}{(6.5 \cdot Re_*)^{0.5}} + 0.34} \tag{12-27}$$

Case 3: Transitional flow (medium Re*).

In the transitional area, both the linear velocity profile of the viscous sub layer and the logarithmic profile play a role in the forces on a particle. The transitional area has no fixed boundaries, but roughly it's from **Re_*=0.5** to **Re_*=20.** For the transitional area an empirical equation can be used for the velocity profile, according to:

$$\begin{aligned} \alpha &= A - B \cdot e^{-C \cdot Re_*^{D}} \\ A &= 5.62 + 0.70 \cdot \beta \\ B &= 5.62 + 0.68 \cdot \beta \\ C &= 0.063 - 0.0237 \cdot \beta \\ D &= 1.488 - 0.1183 \cdot \beta \end{aligned} \tag{12-28}$$

With:

$$Re_p = \alpha \cdot Re_* \tag{12-29}$$

Equation (12-28) has been derived in such a way that the resulting curves match the data measured by Julien (1995) as is shown in Figure 12-6. Using the transition region for C_D, and equation (12-13), the Shields curve can be determined. Figure 12-5 shows the estimated curves for values of β of 0.475, 0.525, 0.6, 0.7, 0.8, 0.9 and 1.0, with in the back ground the original Shields curve, while Figure 12-7 shows these, with in the background measured values of the Shields parameter from Julien (1995). The estimated curves are calculated with a friction coefficient **μ=0.45** and a lift coefficient **C_L=0.25**. It is very well possible that in reality this coefficient may have a higher value. It is also possible that this coefficient depends on the particle diameter or the particle Reynolds number.

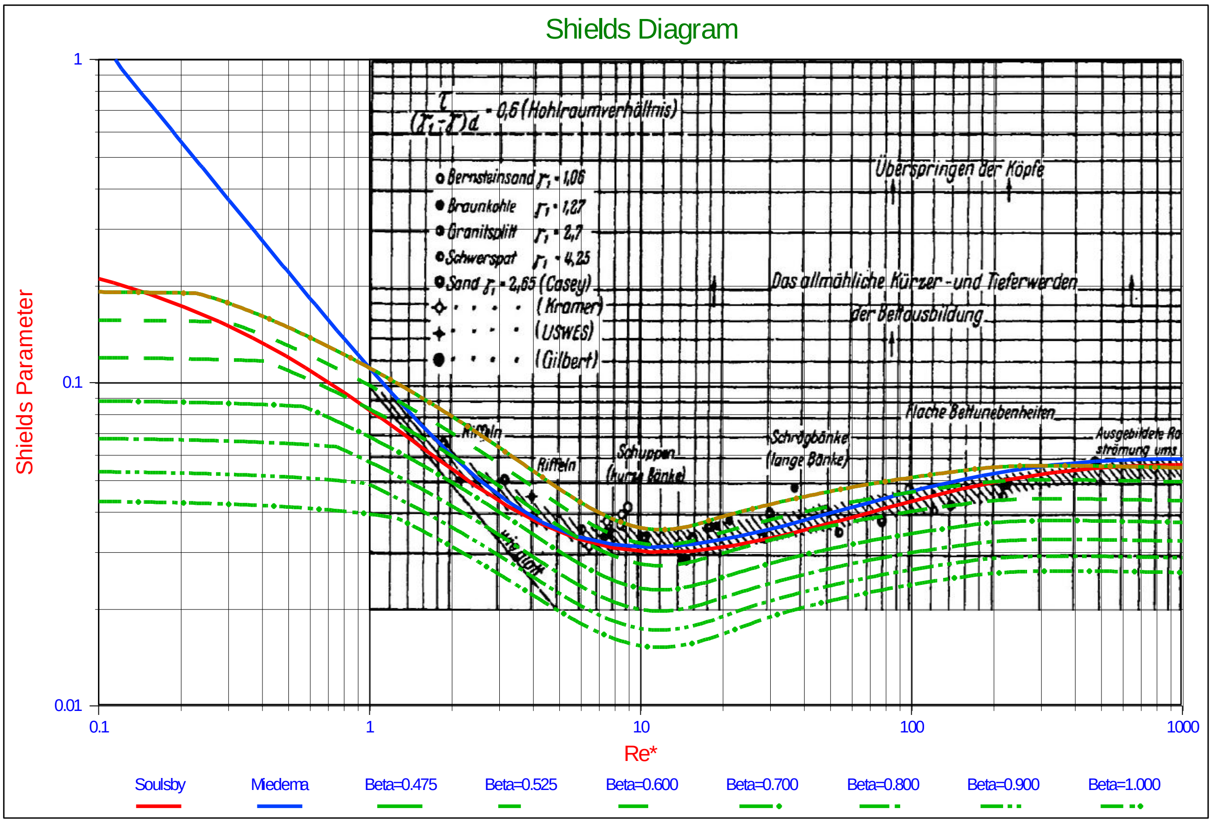

Figure 12-5: The estimated Shields curves versus the original Shields curve.

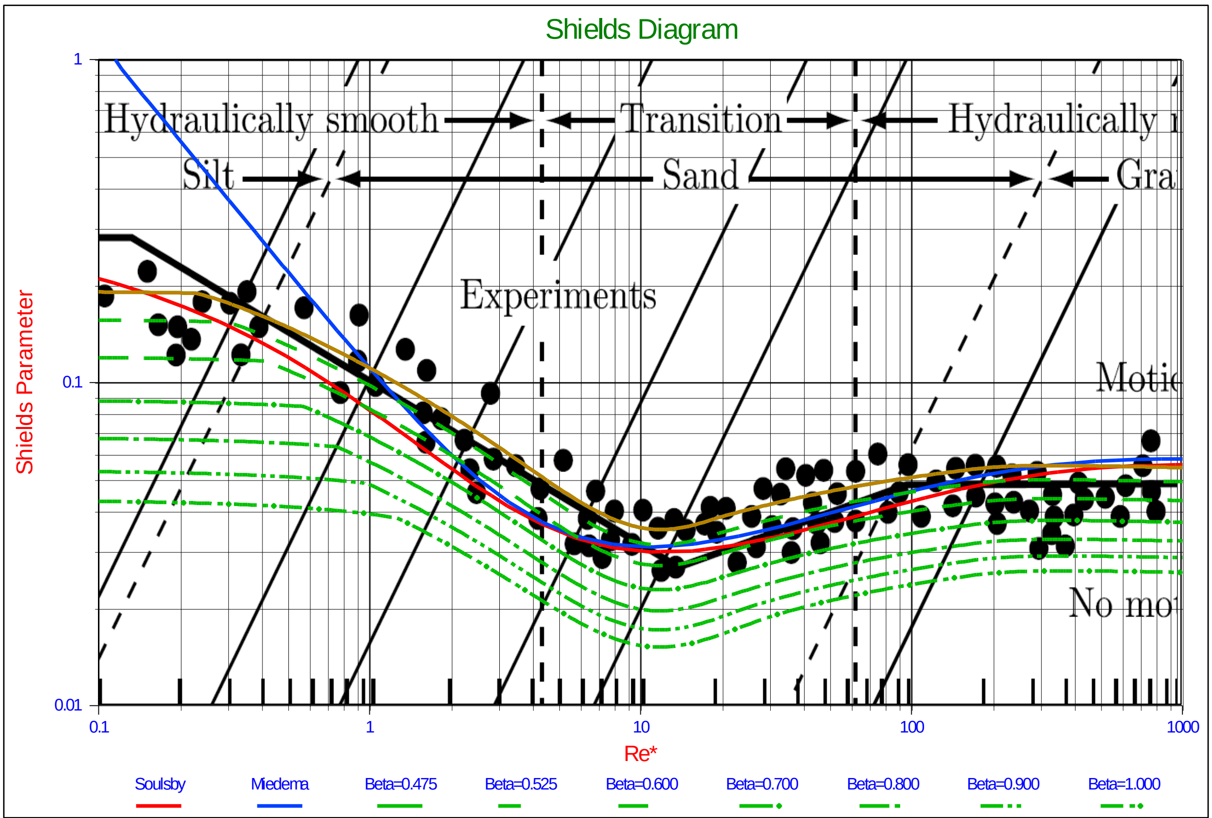

Figure 12-6: The estimated Shields curves for different values of β.

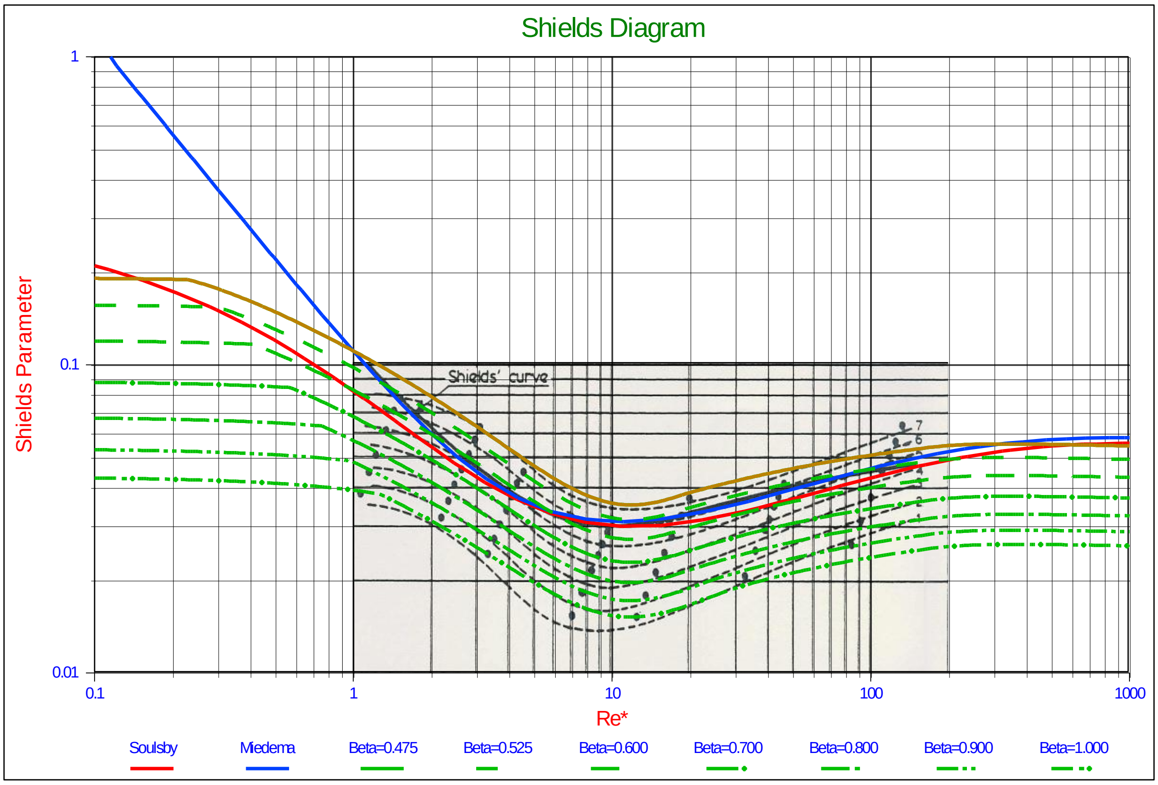

Figure 12-7: The 7 levels of erosion according to Delft Hydraulics (1972).

The Delft Hydraulics (1972) defined 7 levels of erosion according to:
1. Occasional particle movement at some locations.
2. Frequent particle movement at some locations.
3. Frequent particle movement at many locations.
4. Frequent particle movement at nearly all locations.
5. Frequent particle movement at all locations.
6. Permanent particle movement at all locations.
7. General transport (initiation of ripples).

As can be seen from Figure 12-7, the curves with the 7 values for **β** match closely with the 7 levels according to Delft Hydraulics (1972), although there are differences. Since the factor **β** is the fraction of a particle that is subject to drag, this seems plausible. In a normal sediment, there will be a few particles that lay on top of the bed and that are subject to drag for 100%. These particles will be the first to move (erode), so this is level 1. Particles that are embedded for 50% will be much harder to move and form level 5 or higher.

12.3 Shields Approximation Equations

Many researchers created equations to approximate the Shields curve. The original Shields graph however is not convenient to use, because both axis contain the shear velocity $\mathbf{u_*}$ and this is usually an unknown, this makes the graph an implicit graph. To make the graph explicit, the graph has to be transformed to another axis system. In literature often the dimensionless grain diameter $\mathbf{D_*}$ is used. This dimensionless diameter has already been used for the Grace (1986) method for determining the settling velocity, assuming the water density equals 1. This dimensionless diameter also called the Bonneville parameter is:

$$\mathbf{D_* = d \cdot \sqrt[3]{\frac{R_d \cdot g}{\nu^2}}} \qquad \textbf{(12-30)}$$

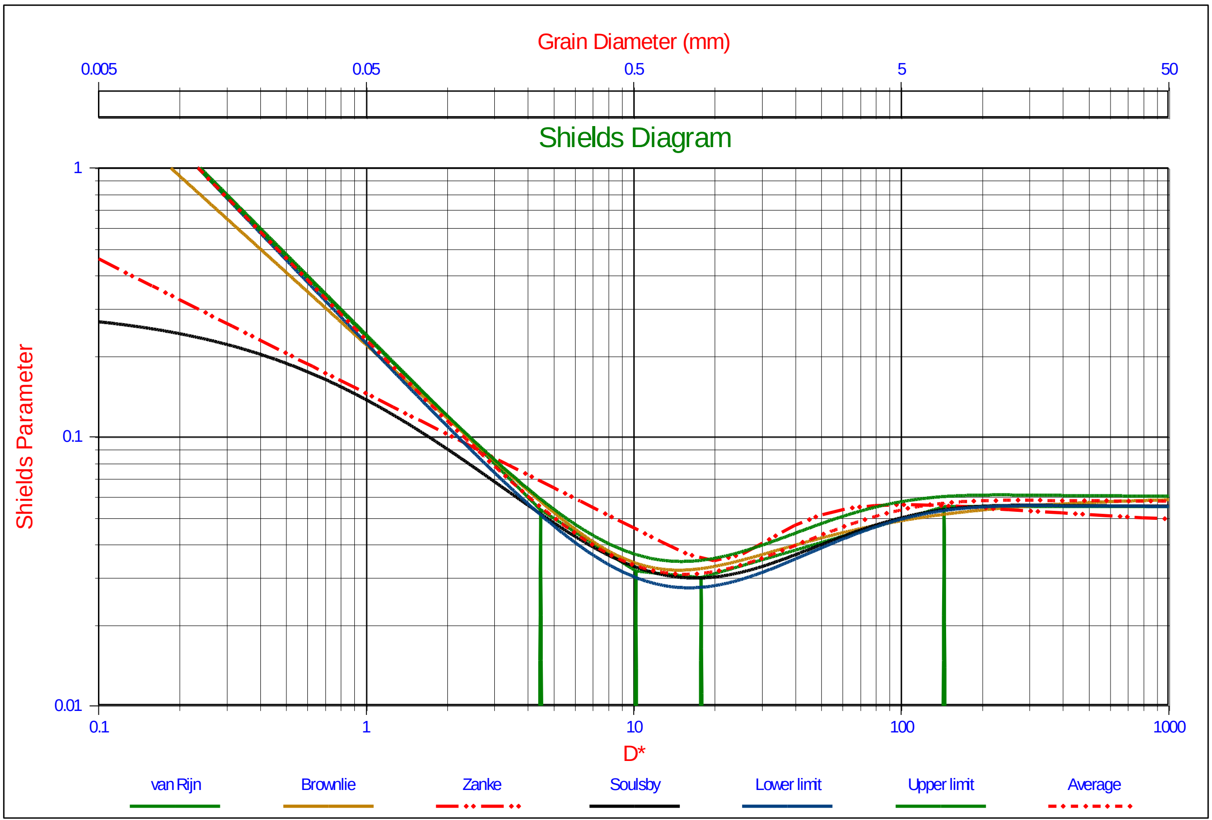

Figure 12-8: The Shields parameter as a function of the dimensionless diameter.

With the normal values for the water density, the relative density and the viscosity, the dimensionless diameter is about 20.000 times the particle diameter, or 20 times the particle diameter in mm. Figure 12-8 & Figure 12-9 show the Shields approximations of van Rijn (1993), Brownlie (1981), Zanke (2003), Soulsby & Whitehouse (1997) completed with a lower limit, upper limit and average approximation derived for these lecture notes by the author. It is interesting to see that the van Rijn and Brownlie equations result in a continuously increasing Shields parameter with a decreasing dimensionless diameter, the Zanke approach does this also, but less steep, while the Soulsby & Whitehouse approach has a limit of 0.3 for very small particles, matching the model as described in the previous chapter. Only Soulsby & Whitehouse take the linear velocity profile in the viscous sub layer, resulting in a constant Shields parameter at very low Reynolds numbers, into account.

From the definition of the Shields parameter, the relation between the Shields parameter and the Bonneville parameter can be derived, the Shields parameter is:

$$\theta_{cr} = \frac{u_*^2}{R_d \cdot g \cdot d} \tag{12-31}$$

The grain Reynolds number **Re$_*$**, which defines the transition between hydraulic smooth and rough conditions for which grains protrude into the flow above the laminar sub layer **δ** at **Re*=11.63** as:

$$Re_* = \frac{u_* \cdot d}{\nu} = \frac{\sqrt{\theta} \cdot \sqrt{R_d \cdot g \cdot d} \cdot d}{\nu} \tag{12-32}$$

Using equation (12-30), this gives:

$$Re_* = \sqrt{\theta} \cdot D_*^{1.5} \tag{12-33}$$

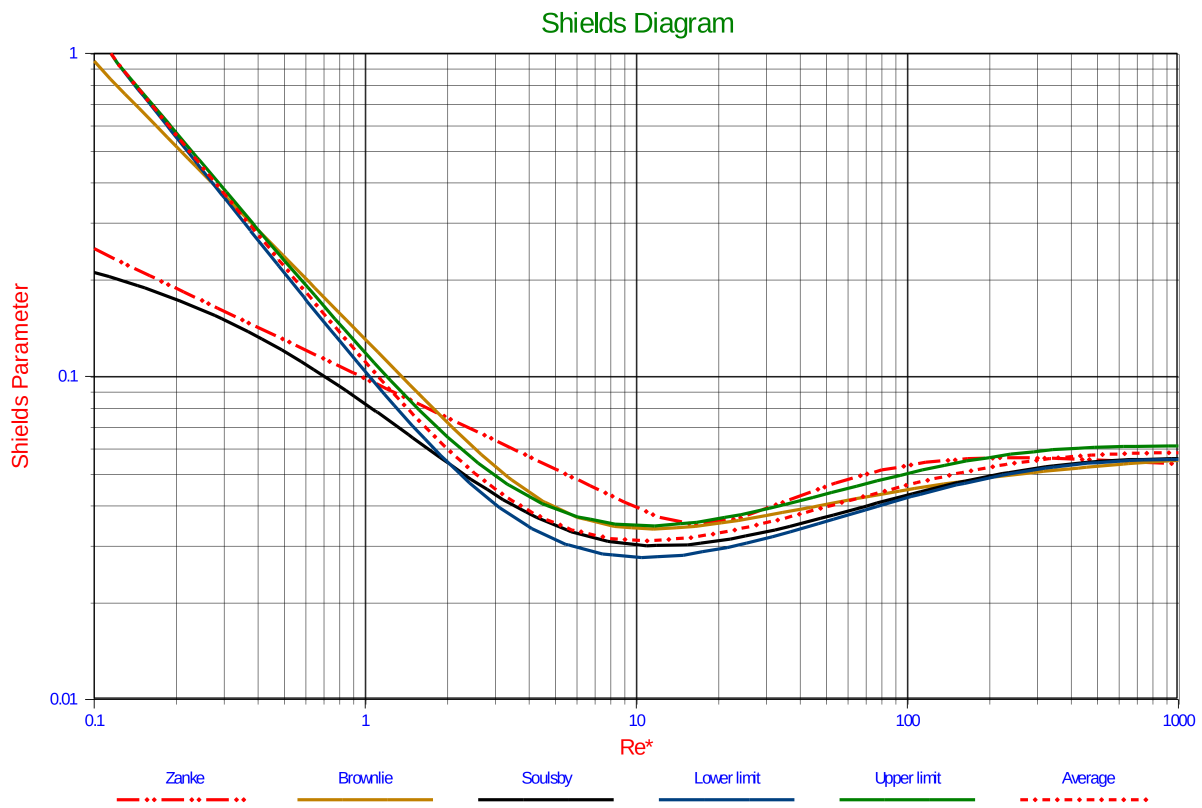

Figure 12-9: The Shields parameter as a function of the boundary Reynolds number.

So the Bonneville parameter is a function of the Shields number and the boundary Reynolds number according to:

$$\mathbf{D_* = \left(\frac{Re_*}{\sqrt{\theta}}\right)^{2/3}} \tag{12-34}$$

Another parameter that is often used for the horizontal axis is the so called Grant and Madsen (1976) parameter or sediment fluid parameter, see Figure 12-10:

$$\mathbf{S_* = \frac{\sqrt{R_d \cdot g \cdot d} \cdot d}{4 \cdot \nu} = \frac{D_*^{1.5}}{4} = \frac{Re_*}{4 \cdot \sqrt{\theta}}} \tag{12-35}$$

The factor of 4 appears in the definition of $\mathbf{S_*}$ to render the numerical values of $\mathbf{S_*}$ comparable with the $\mathbf{Re_*}$ values in the traditional Shields diagram. This is done merely for convenience and has no physical significance.

Which differs a factor 4 from the particle Reynolds number $\mathbf{Re_p}$:

$$\mathbf{Re_p = \frac{\sqrt{R_d \cdot g \cdot d} \cdot d}{\nu} = D_*^{1.5} = \frac{Re_*}{\sqrt{\theta}}} \tag{12-36}$$

This particle Reynolds number can be derived , omitting the constants and assuming turbulent settling with a constant drag coefficient $\mathbf{C_D}$.

Figure 12-11 shows the relation between the boundary or grain Reynolds number, the Bonneville parameter (dimensionless grain diameter) and the Grant & Madsen parameter.

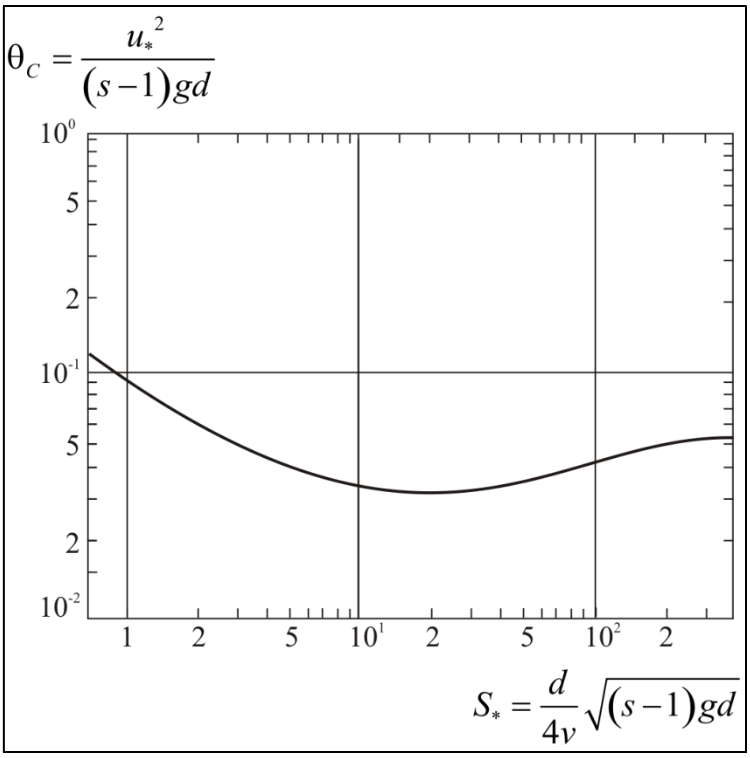

Figure 12-10: Modified Shields diagram, Madsen & Grant (1976).

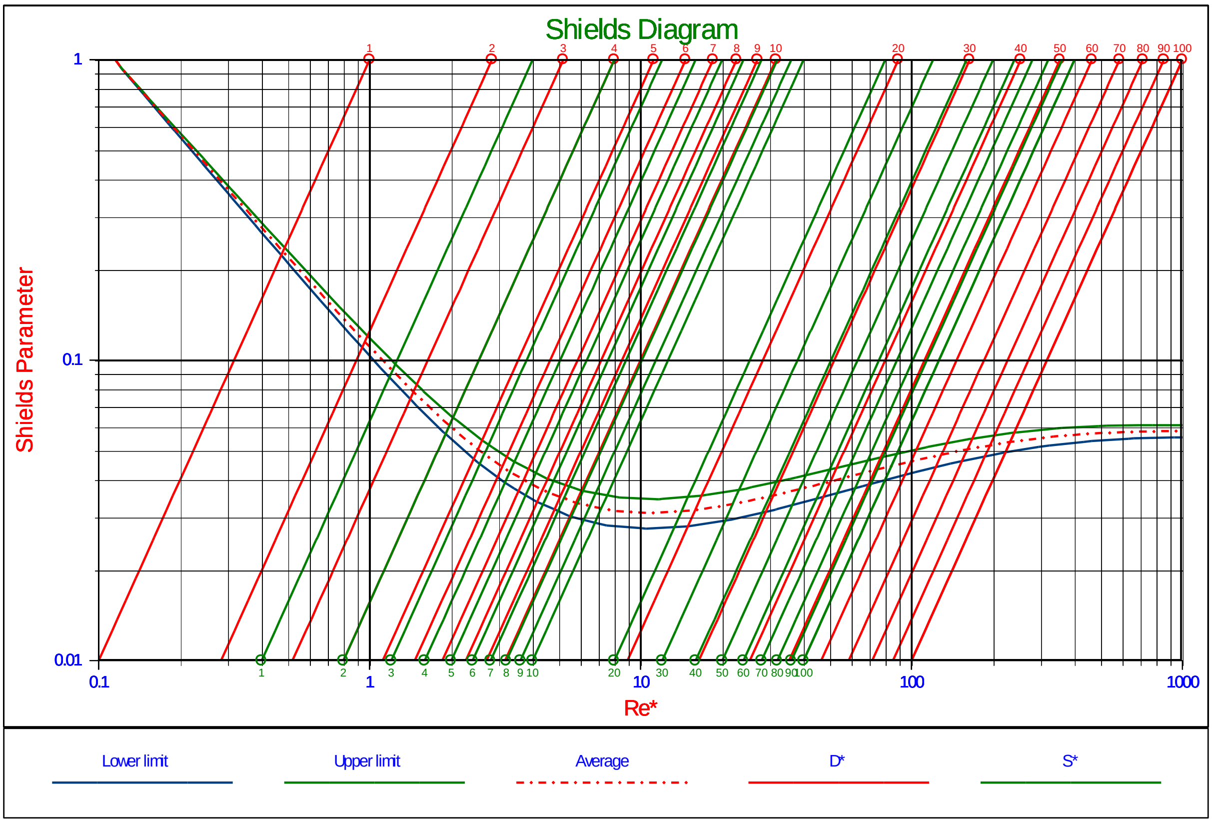

Figure 12-11: The relation between the boundary Reynolds number, the Bonneville parameter and the Grant and Madsen parameter.

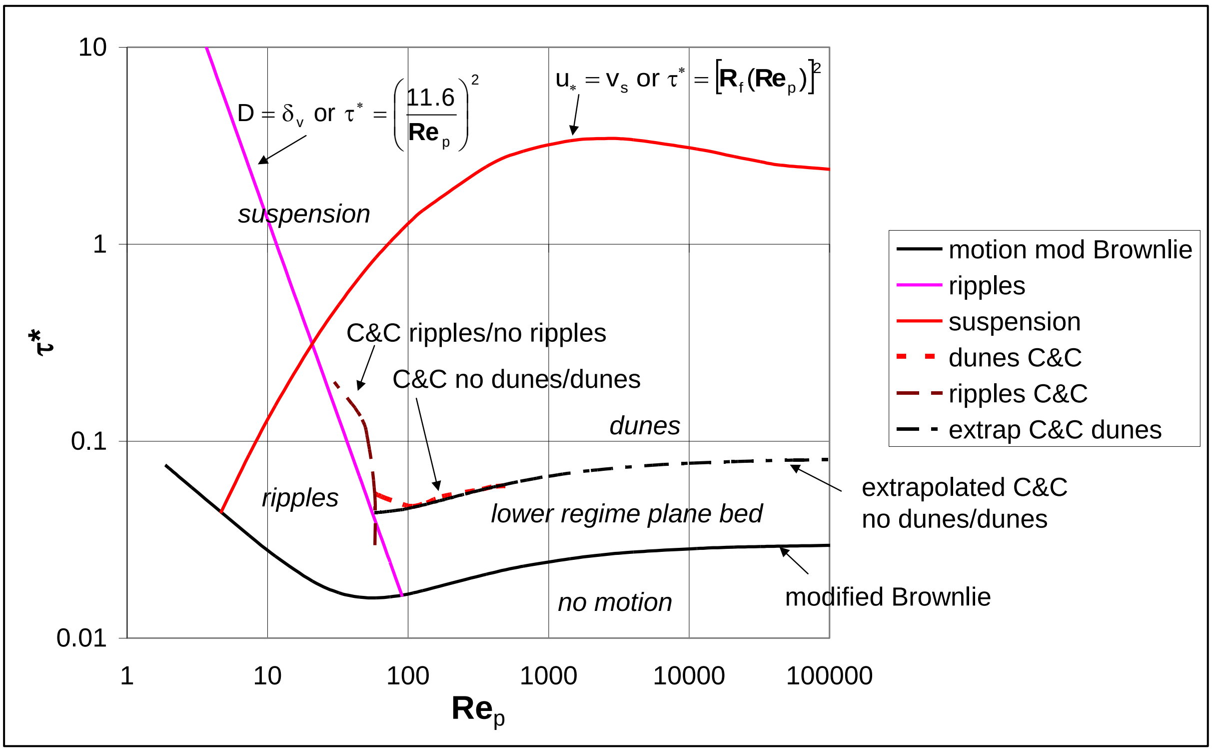

Figure 12-12: Modified Shields diagram using Re_p (equation (12-36)), (Chabert and Chauvin (1963)).

The different approximation equations are summarized below.

Table 12-1: Shields approximation equations.

$\theta_{cr} = \frac{0.30}{(1+1.2 \cdot D_*)} + 0.055 \cdot \left(1 - e^{-0.02 \cdot D_*}\right)$	Soulsby & Whitehouse	**(12-37)**
$\theta_{cr} = \frac{0.22}{D_*^{0.9}} + 0.06 \cdot 10^{-7.7 \cdot D_*^{-0.9}}$	Brownlie	**(12-38)**
$\theta_{cr} = \frac{0.24}{D_*}$ $\quad D_* < 4.5$ $\theta_{cr} = \frac{0.14}{D_*^{0.64}}$ $\quad 4.5 < D_* < 10.2$ $\theta_{cr} = \frac{0.04}{D_*^{0.1}}$ $\quad 10.2 < D_* < 17.9$ $\theta_{cr} = 0.013 \cdot D_*^{0.29}$ $\quad 17.9 < D_* < 145$ $\theta_{cr} = 0.055$ $\quad 145 < D_*$	van Rijn	**(12-39)**
$\theta_{cr} = \frac{0.145}{D_*^{0.5}} + 0.045 \cdot 10^{-1100 \cdot D_*^{-2.25}}$	Zanke	**(12-40)**
$\theta_{cr} = \frac{0.2220}{D_*^{1.04}} + 0.0550 \cdot \left(1 - e^{-0.0200 \cdot D_*}\right)$	Miedema lower limit	**(12-41)**
$\theta_{cr} = \frac{0.2350}{D_*^{1.00}} + 0.0600 \cdot \left(1 - e^{-0.0250 \cdot D_*}\right)$	Miedema upper limit	**(12-42)**
$\theta_{cr} = \frac{0.2285}{D_*^{1.02}} + 0.0575 \cdot \left(1 - e^{-0.0225 \cdot D_*}\right)$	Miedema average	**(12-43)**

12.4 The Hjulstrom Approach

The **Hjulstrøm curve** is a graph used by hydrologists to determine whether a river will erode, transport or deposit sediment. The graph takes sediment size and channel velocity into account. The x-axis shows the size of the particles in mm. The y-axis shows the velocity of the river in cm/s. The tree lines on the diagram show when different sized particles will be deposited, transported or eroded. The Curve uses a double logarithmic scale.
The curve shows several key ideas about the relationships between erosion, transportation and deposition. The Hjulstrøm Curve shows that particles of a size around 1mm require the least energy to erode, as they are sands that do not coagulate. Particles smaller than these fine sands are often clays which require a higher velocity to produce the energy required to split the small clay particles which have coagulated. Larger particles such as pebbles are eroded at higher velocities and very large objects such as boulders require the highest velocities to erode. When the velocity drops below this velocity called the line of critical velocity, particles will be deposited or transported, instead of being eroded, depending on the river's energy. It should be noted however that there is a difference between the line of critical velocity for erosion and deposition. Between the two particles will be transported as bed load. Figure 12-13 and Figure 12-16 give examples of Hjulstrøm graphs found on internet.

Threshold of Motion
Grains forming the boundary between a fluid and sediment possess a finite weight and finite coefficient of friction. When the applied shear stress is low they are not brought into motion. As applied shear stress is increased, a critical shear stress is reached at which grains will begin to move. The value of the critical stress will depend primarily on the size and density of the particles and secondarily on their shape and packing and the cohesive forces acting between particles.

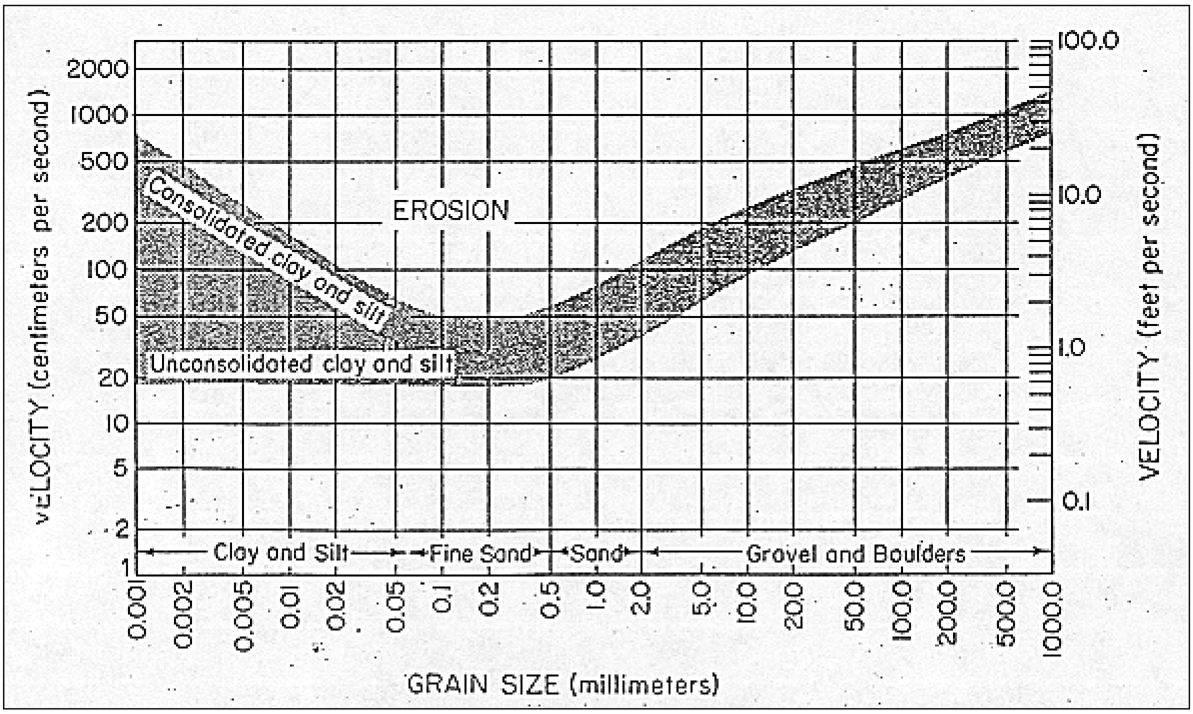

Figure 12-13: An example of the Hjulstrøm graph.

One the critical stress is just exceeded, particles will advance in the direction of flow due to irregular jumps or less commonly rolls. This mode of transport is termed the bed load and conceptually can be thought of as being deterministic, that is the behavior of a particle once in motion is dominated by the gravity force. As the stress is further increased, particles will also begin to be suspended in solution and subject to turbulent forces. This mode of transport is termed the suspended load. Due to these two modes of transport there will be a flux of material across a plane perpendicular to the flow. Our ultimate goal is to determine this mass flux by integrating the product of the velocity profile and concentration profile.

The Critical Stress
The motion of sediment can be parameterized in a number of ways. The oldest of these is due to Hjulstrom who summarized observational data in terms of fluid velocity and grain size. There are a number of variants of the

Hjulstrom diagram, using grain diameter as one parameter and some measure of the stress as the other (via the quadratic stress law: u, u_{100} or stress itself: u_*).

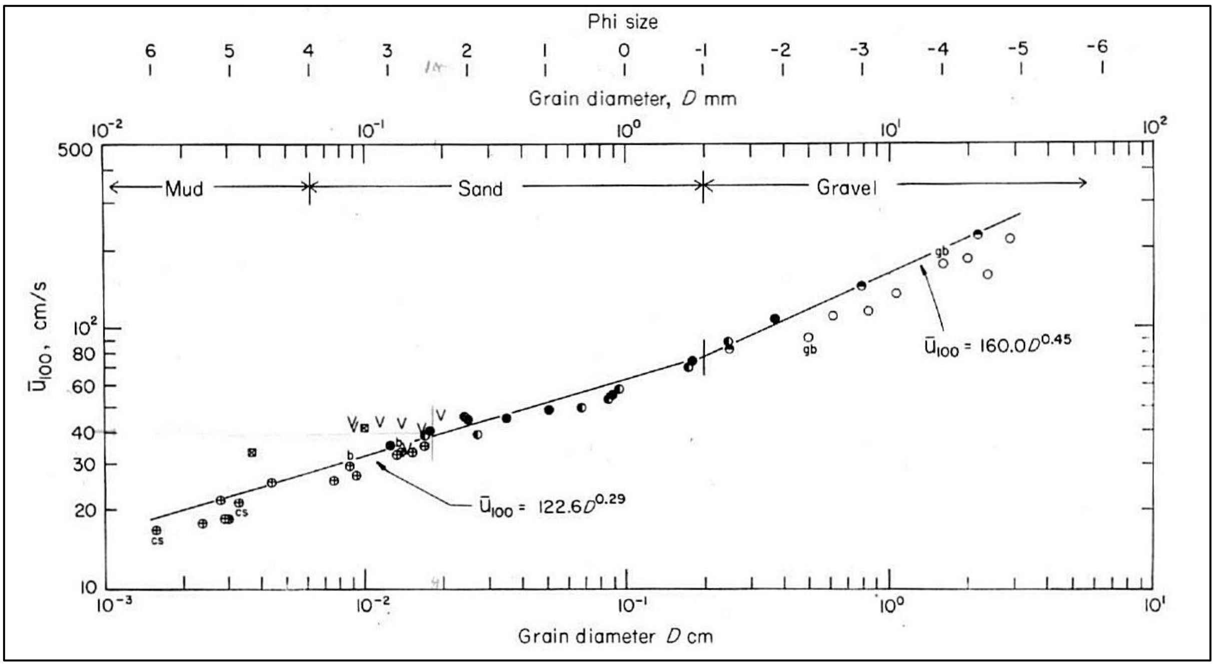

Figure 12-14: The grain diameter versus the flow velocity, Sundborg (1956).

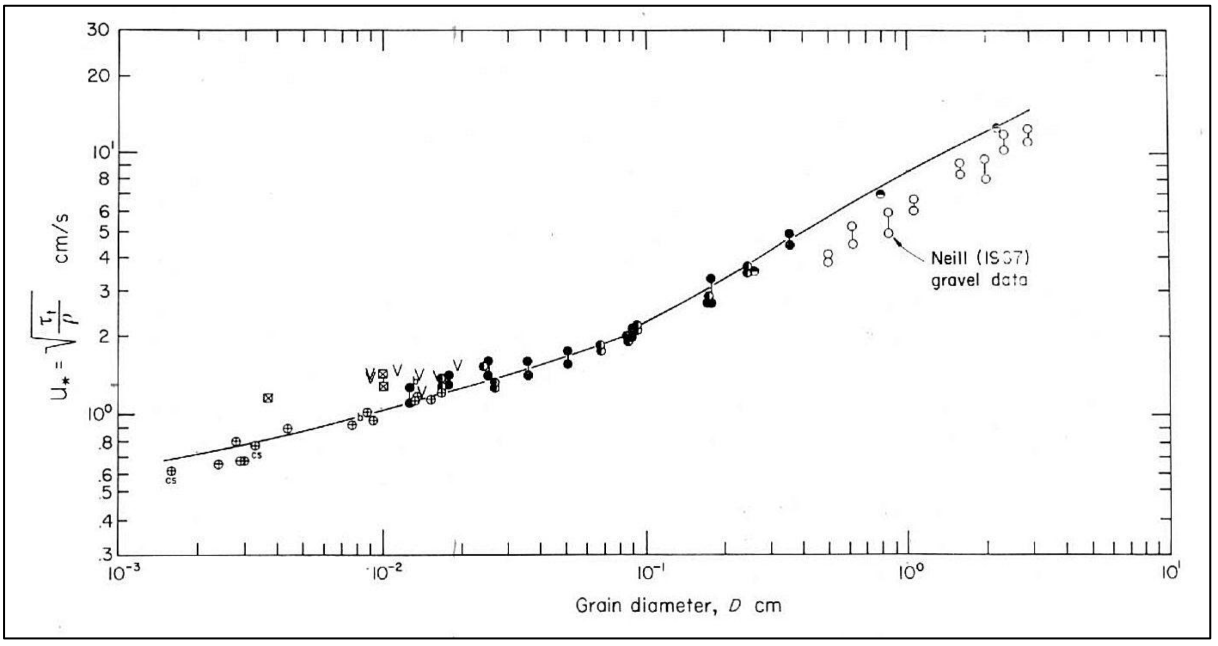

Figure 12-15: The grain diameter versus the friction velocity, Sundborg (1956).

In several of these figures there is a envelope of values for small particles, contrasting unconsolidated and consolidated/cohesive sediment. This reflects the importance of inter particle forces because of the higher ratio of surface area to volume. Sundborg (1956) added more detail, and dealt with consolidation in fine-grained end.
Figure 12-19 shows the Hjulstrøm curves, normalized for 100cm water depth and compared with Shields curves. In this graph, 3 Shields curves are plotted, first the Soulsby curve, equation (12-37), second the Miedema curve, equation (12-42) and third the Brownlie curve, equation (12-38). Since the Shields curves are derived for non-cohesive soils, they should be more or less horizontal for the very fine particles. The Brownlie and Miedema curves match this, while the Soulsby curve is descending with a decreasing particle diameter. From the analysis in the previous paragraph, this is what should be expected based on equation (12-20).

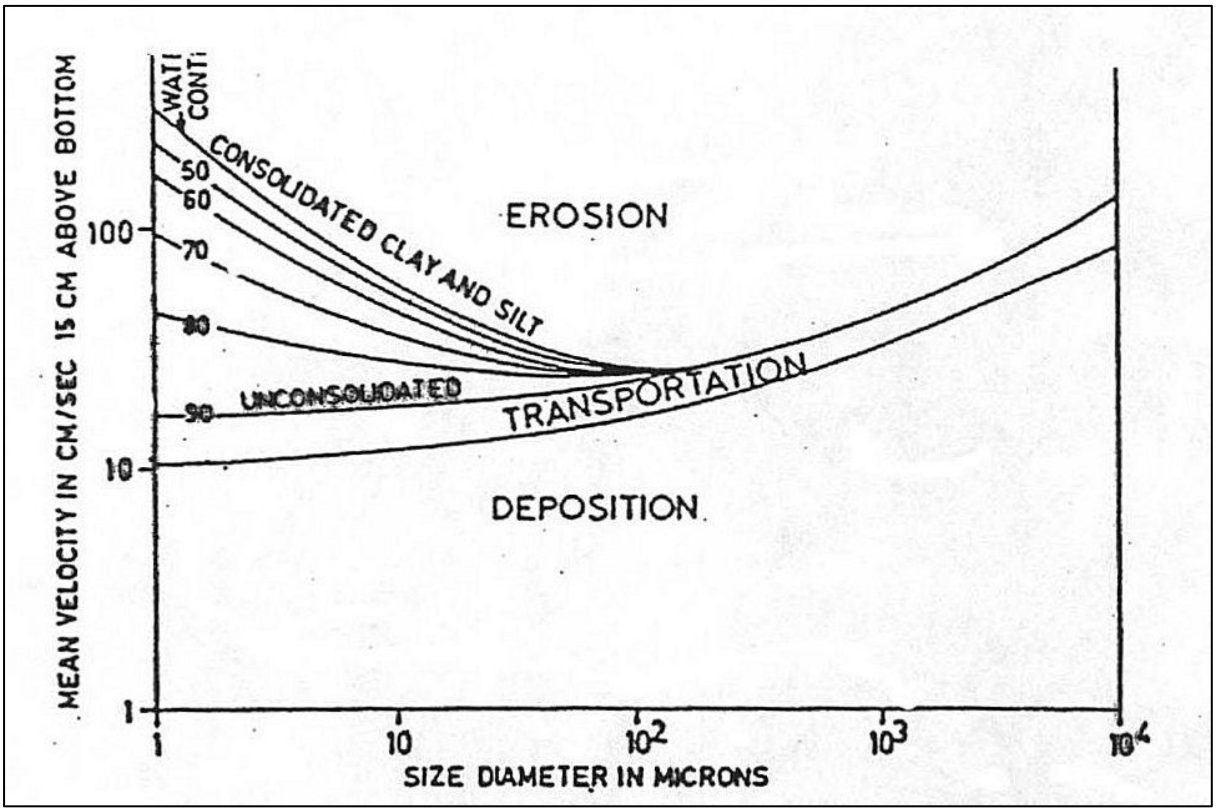

Figure 12-16: A Hjulstrøm graph showing bed load transportation.

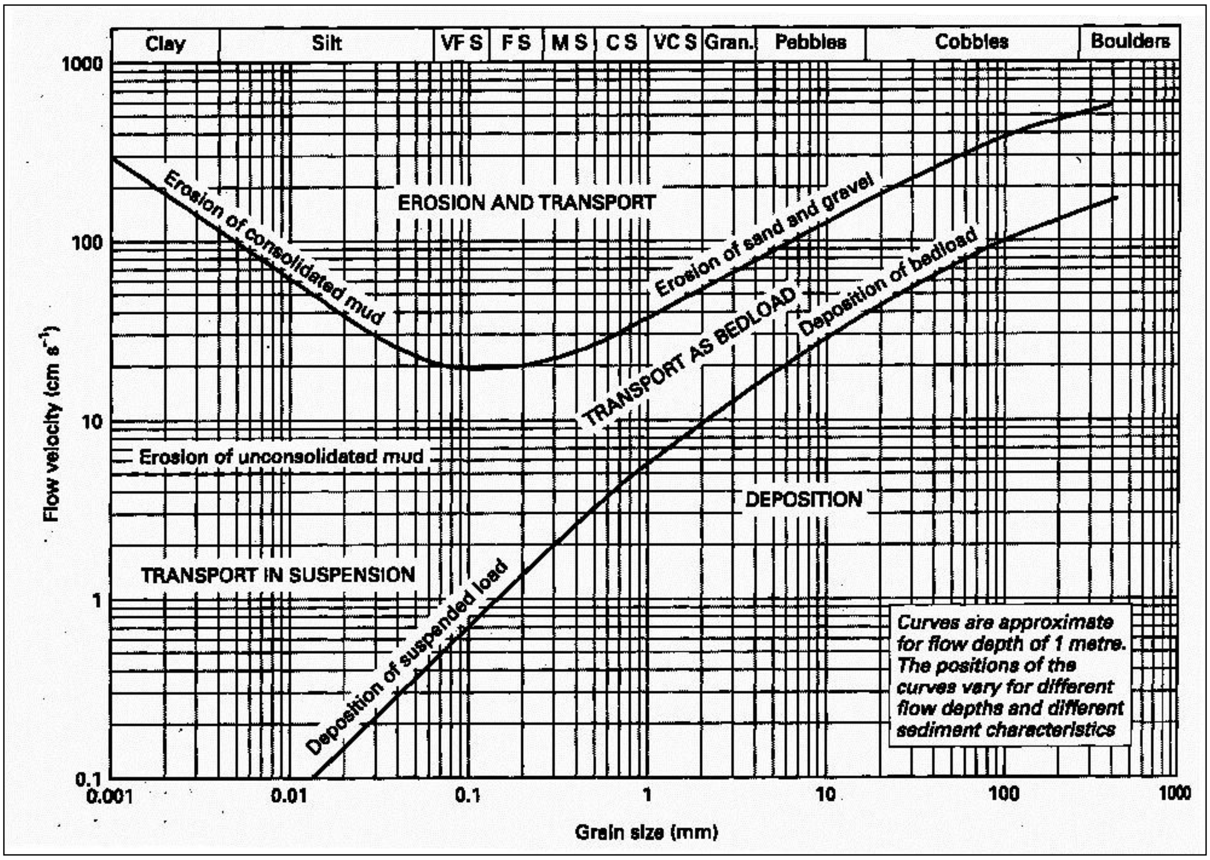

Figure 12-17: A Hjulstrøm graph showing the deposition line.

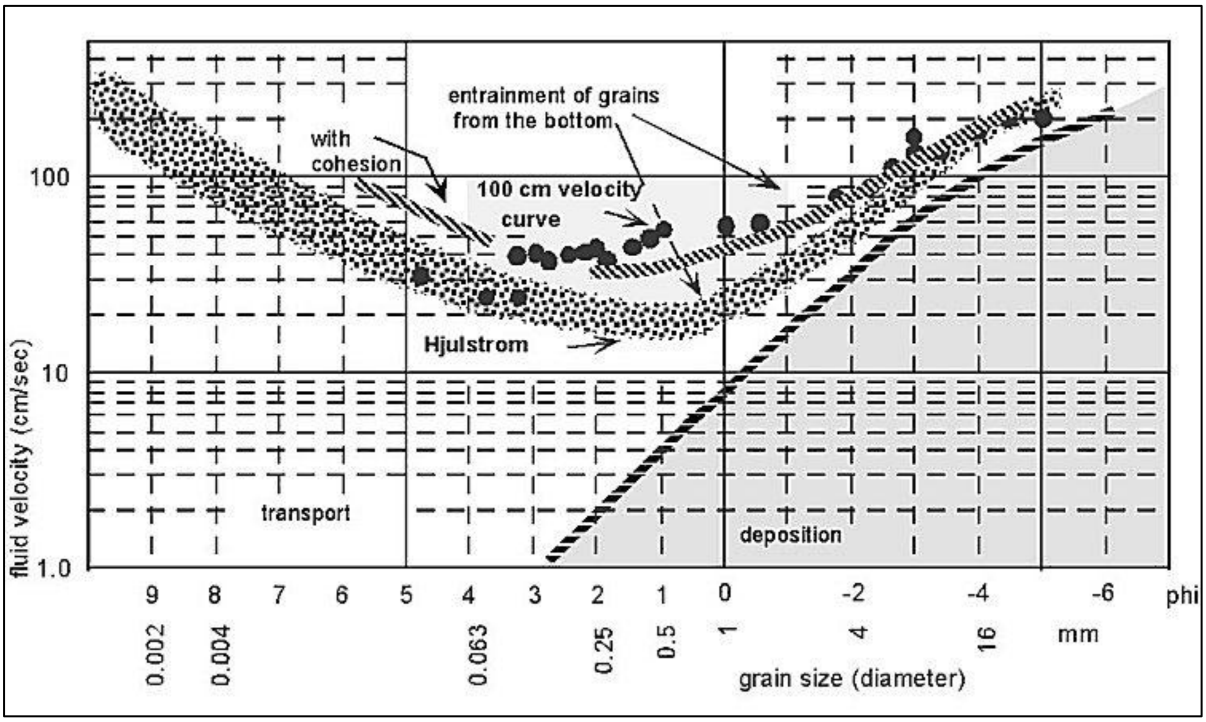

Figure 12-18: A Hjulstrøm graph showing the bandwidth.

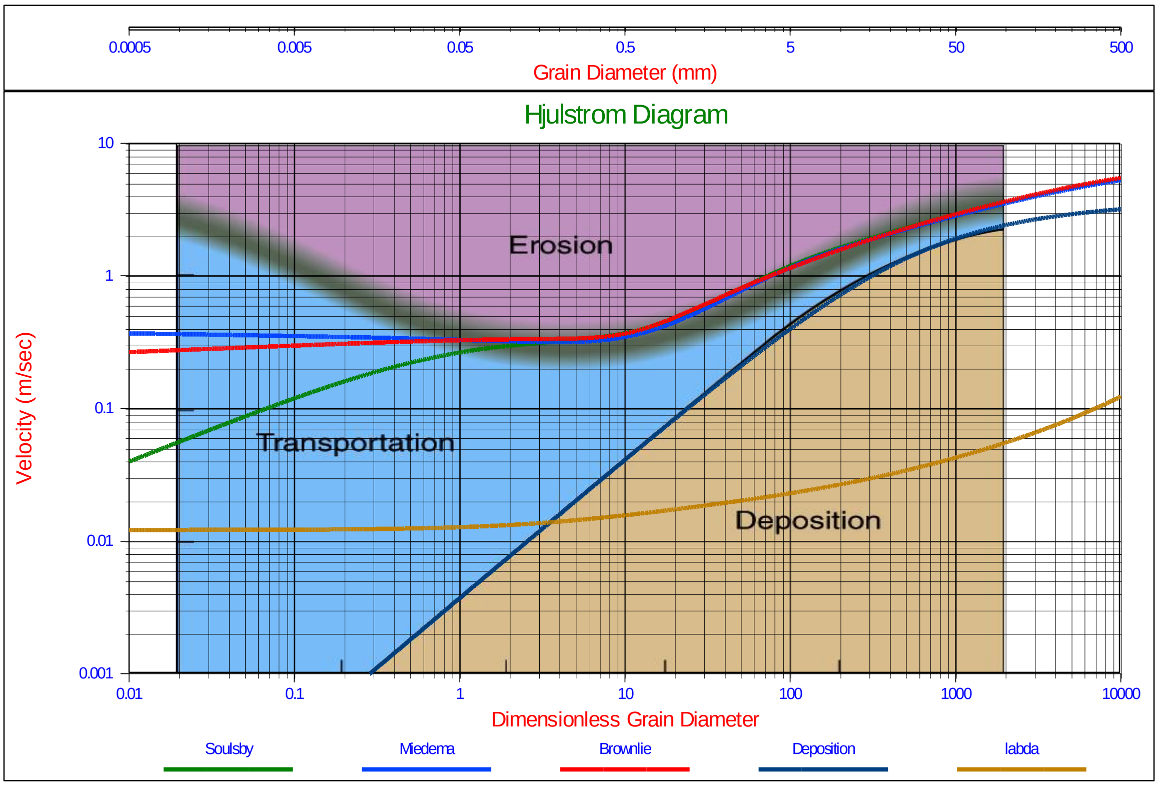

Figure 12-19: A comparison between the Hjulstrom curve and the Shields curve.

12.5 Friction Coefficient and Pressure Losses with Homogeneous Water Flow

In order to use the above derived theory, a value for the friction coefficient of water flowing above a bed of grains has to be determined. From literature the following relations can be applied. When clear water flows through the pipeline, the pressure loss can be determined with the well-known Darcy-Weisbach equation:

$$\Delta \mathbf{p_w} = \lambda \cdot \frac{\mathbf{L}}{\mathbf{D}} \cdot \frac{1}{2} \cdot \rho_w \cdot \mathbf{v}^2 \tag{12-44}$$

The value of the friction factor λ depends on the Reynolds number:

$$\mathbf{Re} = \frac{\mathbf{v} \cdot \mathbf{D}}{\nu} \tag{12-45}$$

For laminar flow (**Re<2320**) the value of λ can be determined according to Poiseuille:

$$\lambda = \frac{\mathbf{64}}{\mathbf{Re}} \tag{12-46}$$

For turbulent flow (**Re>2320**) the value of λ depends not only on the Reynolds number but also on the relative roughness of the pipe **ε/D**. A general implicit equation for λ is the Colebrook-White equation:

$$\lambda = \frac{1}{\left(2 \cdot \log\left(\frac{2.51}{\mathbf{Re} \cdot \sqrt{\lambda}} + \frac{0.27 \cdot \varepsilon}{\mathbf{D}}\right)\right)^2} \tag{12-47}$$

For very smooth pipes the value of the relative roughness **ε/D** is almost zero, resulting in the Prandl & von Karman equation:

$$\lambda = \frac{1}{\left(2 \cdot \log\left(\frac{2.51}{\mathbf{Re} \cdot \sqrt{\lambda}}\right)\right)^2} \tag{12-48}$$

This can be approximated by:

$$\lambda = \frac{0.309}{\left(\log\left(\frac{\mathbf{Re}}{7}\right)\right)^2} \tag{12-49}$$

At very high Reynolds numbers the value of **2.51/(Re·√λ)** is almost zero, resulting in the Nikuradse equation:

$$\lambda = \frac{1}{\left(2 \cdot \log\left(\frac{0.27 \cdot \varepsilon}{\mathbf{D}}\right)\right)^2} \tag{12-50}$$

Because equations 21 and 22 are implicit, for smooth pipes approximation equations can be used. For a Reynolds number between 2320 and 10^5 the Blasius equation gives a good approximation:

$$\lambda = 0.3164 \cdot \left(\frac{1}{\mathbf{Re}}\right)^{0.25} \tag{12-51}$$

For a Reynolds number in the range of 10^5 to 10^8 the Nikuradse equation gives a good approximation:

$$\lambda = 0.0032 + 0.221 \cdot \left(\frac{1}{Re}\right)^{0.237} \tag{12-52}$$

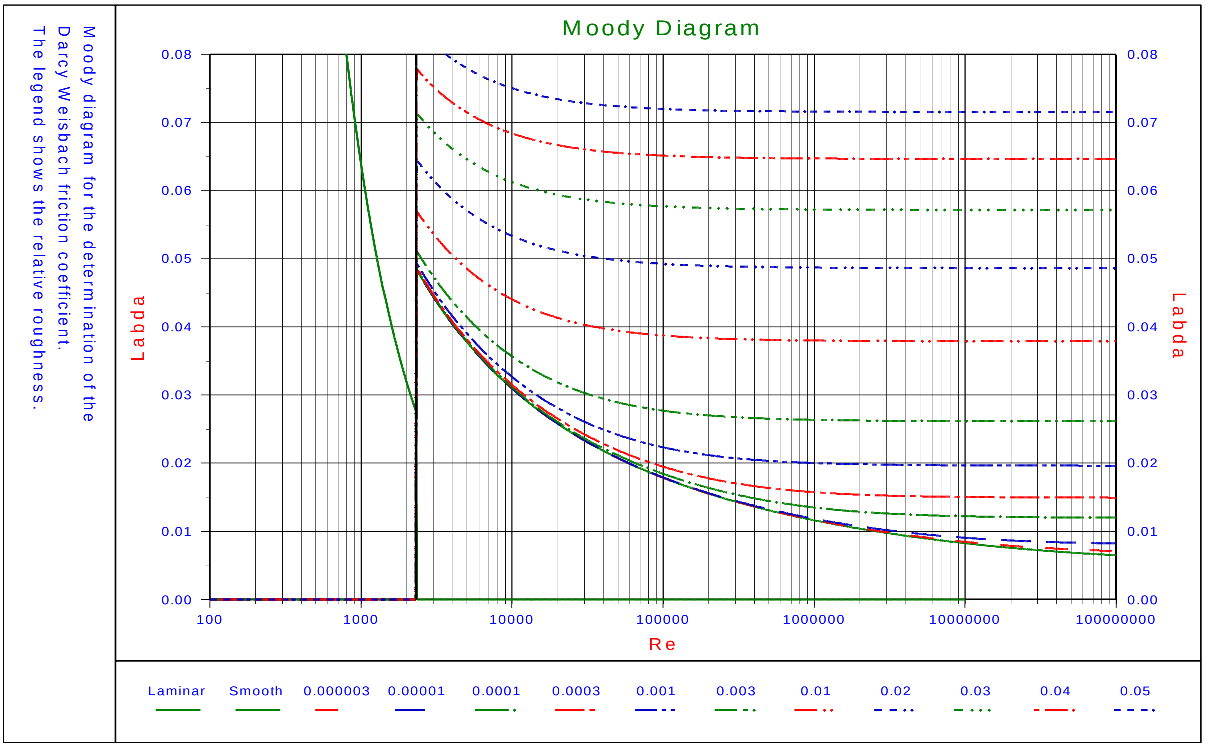

Figure 12-20: The Moody diagram determined with the Swamee Jain equation.

Over the whole range of Reynolds numbers above 2320 the Swamee Jain equation gives a good approximation:

$$\lambda = \frac{1.325}{\left(\ln\left(\frac{d}{3.7 \cdot D} + \frac{5.75}{Re^{0.9}}\right)\right)^2} = \frac{0.25}{\left(\log\left(\frac{d}{3.7 \cdot D} + \frac{5.75}{Re^{0.9}}\right)\right)^2} \quad \text{Swamee Jain}$$

$$\lambda = 0.163 \cdot \left(\frac{d}{H}\right)^{0.286} \quad \text{Burt} \tag{12-53}$$

$$\lambda = 0.128 \cdot \left(\frac{k}{R}\right)^{0.333} \quad \text{Strickler}$$

Figure 12-20 gives the so called Moody diagram, in this case based on the Swamee Jain equation, while Figure 12-19 also gives a the value of this coefficient based on the relative roughness of the bed for a 100cm deep channel.

12.6 Determination of Scour related to the TSHD

After discussing the erosion phenomena extensively in the previous chapters, it is the question how to apply this in the model for determining the loading process of a TSHD. The first step is to find which particles will not settle due to scour at which average velocity above the sediment in the hopper. The relation between the shear velocity $\mathbf{u_*}$ and the average velocity above the bed is $\mathbf{U_{cr}}$:

$$u_*^2 = \frac{\lambda}{8} \cdot U_{cr}^2 \tag{12-54}$$

Substituting this in equation (12-12) for the Shields parameter gives:

$$\theta_{cr}=\frac{u_*^2}{R_d\cdot g\cdot d}=\frac{\lambda}{8}\cdot\frac{U_{cr}^2}{R_d\cdot g\cdot d} \tag{12-55}$$

Re-arranging this gives an equation for the critical average velocity above the bed $\mathbf{U_{cr}}$ that will erode a grain, with diameter ds:

$$U_{cr}=\sqrt{\frac{8\cdot\theta_{cr}\cdot R_d\cdot g\cdot d_s}{\lambda}} \tag{12-56}$$

Equation (12-56) is almost identical to equation (12-3) as derived according to the simple Camp (1946) and Huisman (1995) approach. In the same way as equation (12-5) this can be written as:

$$d_s=\frac{u_*^2}{R_d\cdot g\cdot d}=\frac{\lambda}{8}\cdot\frac{U_{cr}^2}{R_d\cdot g\cdot\theta_{cr}} \tag{12-57}$$

With a value of $\boldsymbol{\lambda}$**=0.03** and $\boldsymbol{\theta_{cr}}$**=0.05** equation (12-57) would be equal to equation (12-5).

Since the final phase of the hopper loading process is dominated by scour, the above assumption is too simple. Figure 12-8 shows that the grain sizes we are interested in, from 0.05mm up to 0.5mm, give Shields values $\boldsymbol{\theta_{cr}}$ of 0.2 to 0.03 if we use the original Shields curve or one of the approximation curves. The friction coefficient $\boldsymbol{\lambda}$, may vary from about 0.01 for fine grains and a smooth bed to 0.03 or higher for a hydraulic rough bed. Figure 12-19 shows how the value of $\boldsymbol{\lambda}$ varies as a function of the grain diameter. In the grain size range of interest this $\boldsymbol{\lambda}$ varies from about 0.01 to 0.02. This results in a range for the ratio between the Shields parameter and the friction coefficient of $\boldsymbol{\theta_{cr}/\lambda}$ of 0.2/0.01 to 0.03/0.02, giving a range of 20 to 1.5. Equation (12-3) gives a ratio of 1.66 which is in the range and matches with grains of about 0.5 mm, giving an upper limit to the scour velocity.

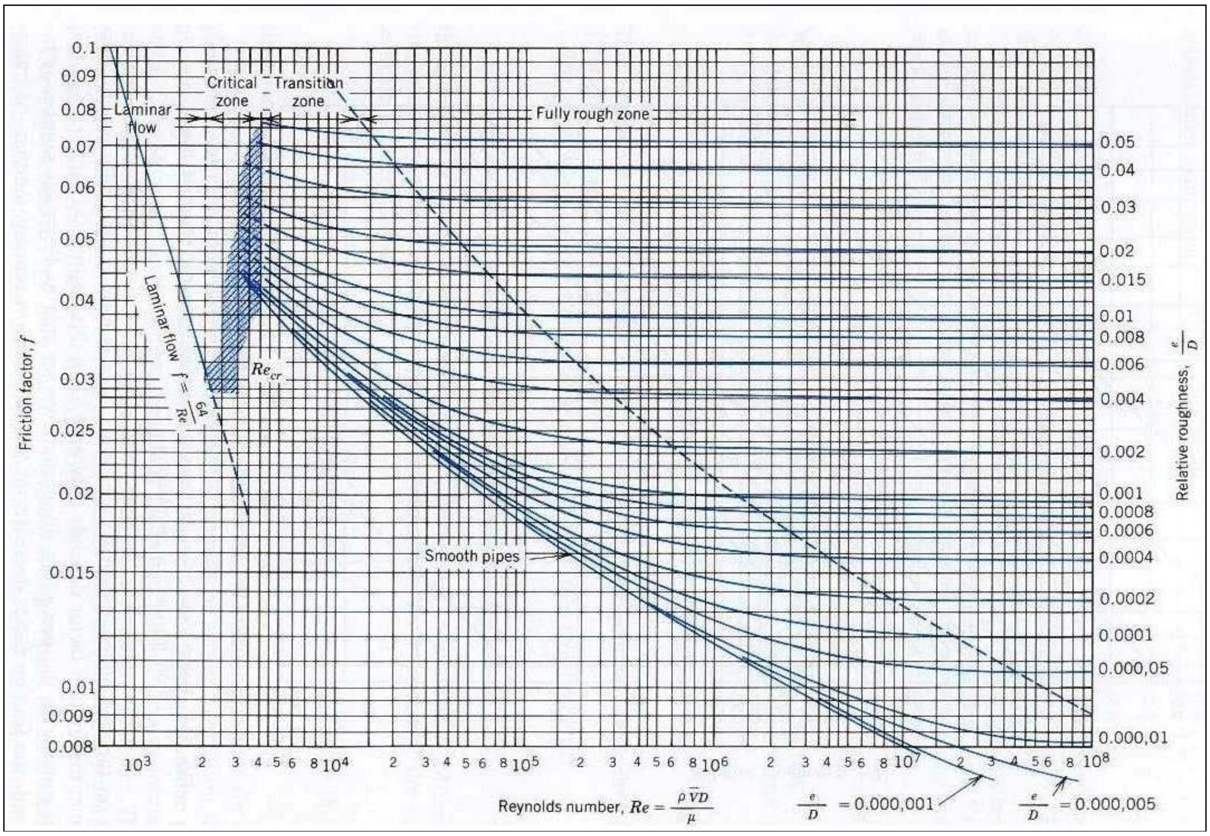

Figure 12-21: The original Moody diagram.

12.7 Conclusions & Discussion

The Camp approach matches the Shields approach for one specific case. The Camp approach as used by Huisman (1995) is more a design approach for designing sedimentation tanks. This approach in fact contains some safety in order to be sure there will never be erosion in the sedimentation tank. This approach should not be used for determining erosion in the final stage of the loading of a TSHD.

The Hjulstrøm approach matches the Shields approach for grains from 0.05 mm up to 100 mm (see Figure 12-19). However a proper scientific and mathematical background of the Hjulstrøm curves was not found. The author had the impression that Hjulstrøm graphs are often copied and redrawn without having a proper background. The Shields approach is based on a fundamental force and moment equilibrium on grains and has been proven by many scientists in literature. So the Shields approach is the most promising.

Now the question is, which Shields curve to use. Figure 12-7 shows 7 levels of erosion as defined by Delft Hydraulics (1972). To decide which of these 7 levels is appropriate for the physics of the final stage of hopper loading, these physics should be examined. During this final stage, a high density mixture is flowing over the sediment. Part of the particles in this mixture flow will settle, part will not settle because the settling velocity is to low and part will not settle because of erosion and suspension. This process differs from the erosion process in the fact that there is not water flowing over the sediment, but a high density mixture. In fact the mixture is already saturated with particles and it is much more difficult for a particle to get eroded that in a clean water flow. One could call this hindered erosion. From the experience until now with the erosion model described in this paper (Miedema & van Rhee (2007)) and comparing it with other models, level 7 from Figure 12-7 should be chosen, this level is achieved by using **β=0.475**.

Chapter 13: **Conclusions & Discussion**

The Camp and Dobbins model can be used to estimate loading time and overflow losses; however, the model should be tuned with measurements of the overflow rate in tons/sec as well as the particle size distribution in the overflow, as a function of time. The model can then also be used for the calculation of the decaying of the overflow plume in the dredging area.
If the model is used for the calculation of the production rate of the dredge a distinction has to be made whether the production is expressed in T.D.S./sec or in m^3/sec. In the first case the theory can be applied directly, while in the second case it has to be realized, that the overflow losses in T.D.S./sec do not always result in the same overflow loss in m^3/sec, since fine particles may situate in the voids of the bigger ones. The loss of fines does not reduce the total volume, but increases the void ratio. Although the fines leave the hopper in this case, they do not result in a reduction of the volume of the settled grains.
Those fractions which can be considered to apply to the overflow losses and those which do not, can be estimated from the difference between the real particle size distribution and the optimal particle size distribution, giving a maximum dry density, the so called Fuller distribution. If the gradient of the distribution curve for the fines is less steep then the corresponding gradient of the Fuller distribution, than that fraction of fines will not effectively contribute to the overflow losses if they are expressed in m^3/sec. In such a case, in-situ, the fines were situated in the voids of the courser grains. If the gradient is however steeper, the fines also form the grain matrix and the volume of settled grains will decrease if the fines leave the hopper through the overflow.
In the model a number of assumptions are made. Except from numerical values for the parameters involved, the Camp and Dobbins approach is used for the influence of turbulence, while separately the influence of scour is used instead of using it as a boundary condition.

The models of Miedema & Vlasblom (1996) and van Rhee (2002C) give the same magnitude for the overflow losses, but the shapes of the curves are different due to the differences in the physical modeling of the processes. Due to the lower losses the computed optimal loading time will be shorter for the Vlasblom /Miedema approach. The strong point of the van Rhee model is the accurate physical modeling, giving the possibility to model the geometry of the hopper in great detail, but also describing the physical processes in more detail. The van Rhee model is verified and validated with model and prototype tests and can be considered a reference model for other models. The strong point of the Miedema/Vlasblom model is the simplicity, giving a transparent model where result and cause are easily related.

One question before this research started, was how do the cumulative overflow losses behave when TSHD's are scaled from small to very big. The second question was, are that scale laws that should be applied when scaling TSHD's in order to create similar or maybe even identical processes.

First the answer on the second question, there are scale laws that should be applied and the main law is, to keep the hopper load parameter constant and from there derive the scale laws for the flow and other dimensions, but don't scale the sand. If the scale laws are applied correctly, the simulations show that scaling the TSHD has hardly any influence on the cumulative overflow losses and the loading processes are similar.
The overflow losses however depend strongly on the position of the grain diameter with respect to the hopper load parameter in the particle size distribution diagram. The fraction of the sand with diameters smaller than this diameter has a very strong relation with the cumulative overflow losses. A large silt fraction will increase these overflow losses.

Finally we have noted that the modified Hopper Load Parameter will reduce in magnitude compared with the unmodified Hopper Load Parameter. For particles with a settling efficiency greater than 1, this will not influence the settling efficiency, but for particles with a settling efficiency near 1 or smaller than 1, this may increase the settling efficiency slightly. So the sedimentation velocity in this respect has a positive effect on the cumulative settling efficiency. The current model seems to give rather accurate predictions. This conclusion is based on the comparison with the van Rhee model on one hand and the comparison with real data on the other hand.

Four effects are considered that were not part of the original Miedema & Vlasblom (1996) model, based on the Camp model. Those effects have been added later to the model by Miedema (2008A), (2008B), (2009A), (2009B), (2010) and Miedema & van Rhee (2007).

- Equations (1-25) and (1-29) give a good estimate of the thickness of the layer of water above the overflow level and Figure 1-15 proves that this estimate is accurate.
- The Shields approach is based on a fundamental force and moment equilibrium on grains and has been proven by many scientists in literature. Now the question is, which Shields curve to use. Figure 12-7 shows

7 levels of erosion as defined by Delft Hydraulics (1972). To decide which of these 7 levels is appropriate for the physics of the final stage of hopper loading, these physics should be examined. During this final stage, a high density mixture is flowing over the sediment. Part of the particles in this mixture flow will settle, part will not settle because the settling velocity is to low and part will not settle because of erosion and suspension. This process differs from the erosion process in the fact that there is not water flowing over the sediment, but a high density mixture. In fact the mixture is already saturated with particles and it is much more difficult for a particle to get eroded that in a clean water flow. One could call this hindered erosion. From the experience until now with the erosion model described (Miedema & van Rhee (2007)) and comparing it with other models, level 7 from Figure 12-7 should be chosen, this level is achieved by using $\boldsymbol{\beta=0.475}$.

- The concentration of the mixture above the bed, often called the near bed concentration $\mathbf{c_b}$, can be estimated with equation (7-20), and based on a black box approach. This concentration is used to determine the hindered settling effect on the settling velocity. Although equation (7-20) will not give the near bed concentration at a certain place at a certain time, it is derived for the entire hopper and loading cycle, it's a good estimate for determining the cumulative overflow losses.
- The storage, time delay or buffer effect can be implemented by using equation (1-30). Miedema & van Rhee (2007) compared both the Miedema & Vlasblom (1996) model, including the features as discussed here, and the sophisticated 2DV model, van Rhee (2002C). The result is shown in Figure 1-18. It is clear from this figure that there is a difference between the two methods if the storage effect is omitted in the Miedema & Vlasblom model, but including this storage effect gives almost the same results.
- It looks like the modified model gives results that match the van Rhee (2002C) model closely; of course the models are compared for just a few cases, specifically regarding the grain distributions used. This is remarkable because the physics of the two models are different. The van Rhee (2002C) model is based on the density flow as shown in Figure 1-6 and Figure 1-7, where there is an upward flow in the hopper. The modified model as presented here is based on the old Camp theory and assumes a uniform inflow of particles over the height of the hopper, as shown in Figure 2-2, a horizontal flow of the mixture and vertical downward transport of particles. So it seems that the dominating parameter in both models is the so called hopper load parameter, since this is the upward flow velocity in the van Rhee model and it is the settling velocity of a particle entering the hopper at the top and just reaching the sediment at the other end of the hopper in the Miedema & Vlasblom model.

Using the equations to determine the near bed concentration as derived here are based on known cumulative overflow losses and should thus not be used to predict overflow losses because that is a self-fulfilling prophecy. The modeling should be used to verify experiments where the near bed concentration is measured.

The use of the sedimentation or bed rise velocity to determine the sedimentation process when loading a TSHD with sand can only give good predictions if the correct near bed concentration is used and measured. Using the assumption that the near bed concentration equals the inflowing mixture concentration may lead to results that do not obey the conservation of mass principle.

Using the empirical equation (7-23) of van Rhee (2002C) to predict the overflow losses with the assumption that $\mathbf{c_b=c_{in}}$ is a good first approximation, but with some restrictions. It should be noted that van Rhee used the assumption of $\mathbf{c_b=c_{in}}$ to find this equation by curve fitting. The dimensionless overflow rate $\mathbf{S^*}$ in this equation has to be considered to be the reciprocal of the settling efficiency, that is the correct physical meaning.

The analytical model derived in this paper matches this empirical equation, but has the advantage that sands with different grading can be taken into account.

The model derived for the sedimentation velocity, the near bed concentration and the overflow losses matches both the experiments as carried out by van Rhee (2002C) and Ooijens et al. (2001).

The model however is very sensitive for the values of the parameters **a** and **b** describing the PSD in equation (8-2), but with correct values, the model gives a very good prediction of the cumulative overflow losses.

Chapter 14: Nomenclature

a	Steepness of the PSD	mm
b	Offset of the PSD	mm
b	Width of the weir	m
c_b	Near bed concentration	-
c_{bed}	Bed/sediment concentration	-
c_{in}	Volume concentration	-
c_v , c_i	Volumetric concentration	-
C_e	Dimensionless discharge (contraction) coefficient with a value near 0.6.	-
C_d	Coefficient	-
C_D	Drag coefficient	-
C_L	Lift coefficient	-
d	Grain diameter	mm
d_o	Grain diameter matching the hopper load parameter	mm
d_{50}	Grain diameter at 50% of PSD	mm
d_s	Grain diameter (scour)	m
F_D	Drag force	kN
F_L	Lift force	kN
F_w	Submerged weight	kN
g	Gravitational constant (9.81)	m/sec^2
h	Height	m
h	is the overfall height (measured about a distance of 5·h upstream from the crest)	m
h_{max}	Maximum water layer thickness	m
H	Height of hopper	m
H_w	Height of the water above the sediment	m
H*	Dimensionless hopper load parameter	-
L	Length of basin	m
M	Height of the weir crest above the headwater bottom	m
n	Porosity	-
ov	Overflow losses	-
ov_{cum}	Cumulative overflow losses	-
p	Fraction of grains	-
p_o	Fraction of grains that settle partially (excluding turbulence)	-
p_{fs} , p_s	Fraction of grains that do no settle due to scour or fines	-
p_0	Atmospheric pressure	kPa
Q	Mixture flow	m^3/sec
$Q_{in, out}$	Mixture flow (in or out)	m^3/sec
Q_m	Mixture flow (mass)	ton/sec
R_d	Relative density	-
R	Reduction factor	-
s_o	Flow velocity in basin	m/sec
s_s	Scour velocity	m/sec
S*	Dimensionless overflow rate	-
S	Sedimentation flux	
t, T	Time	sec
TDS	Tonnes dry solid	ton
u_*	Shear velocity	m/sec
U_{cr}	Critical velocity above bed	m/sec
v	Mean velocity in the headwater this is equal to **Q/b (M + h)**	m/sec
v_c	Settling velocity including hindered settling	m/sec
v_o	Hopper load parameter	m/sec
v_s	Settling velocity of individual particle	m/sec
v_{sed}	Sedimentation/bed rise velocity	m
W	Width of basin	m
α	Fraction of hopper to be filled with mixture at start of loading process	-
α	Velocity factor	-
β	Power for hindered settling	-
β	Height factor	-
ε	Fraction of hopper filled with sediment when reaching the overflow	-

ρ_f	Density of fluid	ton/m^3
ρ_q	Density of particles (quarts=2.65)	ton/m^3
ρ_w	Density of water (1.025)	ton/m^3
ρ_m	Density of a sand/water mixture	ton/m^3
ρ_q	Density of quarts	ton/m^3
ρ_s	Density of sediment	ton/m^3
η	Settling efficiency	-
η_{cum}	Cumulative settling efficiency	-
η_g	Settling efficiency individual grain	-
η_b	Settling efficiency for basin	-
η_t	Turbulence settling efficiency for individual grain	-
η_p	Settling efficiency individual particle	-
λ	Concentration ratio c_b/c_{in}	-
λ	Viscous friction coefficient	-
κ	Concentration ratio c_{in}/c_{bed}	-
κ	Ratio mixture concentration versus bed concentration	-
μ	Settling velocity factor	-
μ	Friction coefficient	-
τ	Time constant	sec
ν	Kinematic viscosity	St
θ	Shields parameter	-

Chapter 15: **References**

Braaksma, J., Klaassens, J., Babuska, R., & Keizer, C. d. (2007). A computationally efficient model for predicting overflow mixture density in a hopper dredger. *Terra et Aqua, 106(16)* , pp. 16-25.

Bree, S. d. (1977). The loading of hopper dredgers. *Ports & Dredging & Oil Report No. 92.*

Brownlie, W. (1981). *Compilation of alluvial channel data: laboratory and field, Technical Report KH-R-43B.* Pasadena, California, USA: California Institute of Technology.

Camp, T. (1936). Study of rational design of settling tanks. *Sewage Works Journal 8-5.* , pp. 742-758.

Camp, T. (1946). Sedimentation and the design of settling tanks. *ASCE Transactions* , pp. 895-936.

Camp, T. (1953). Studies of sedimentation design. *Sewage & Industrial Wastes 25* , pp. 1-14.

Chabert, J., & Chauvin, J. (1963). Formation de dunes et de rides dans les modeles fluviaux. *Bulletin du Centre de Researche et D'essais de Chatou, no.4.* , pp. 345-376.

Clift, R., Grace, J., & Weber, M. (1978). *Bubbles, drops and particles.* Academic Press.

Coulson, J., Richardson, J., Backhurst, J., & Harker, J. (1996). *Chemical Engineering, Vol. 1, Fluid flow, heat transfer & mass transfer.* Butterworth Heineman.

DHL. (1972). *Systematic Investigation of Two Dimensional and Three Dimensional Scour, Report M648/M863.* Delft, Netherlands: Delft Hydraulics Laboratory.

Di Filice, R. (1999). The sedimentation velocity of dilute suspensions of nearly monosized spheres. *International Journal of Multiphase Flows 25* , pp. 559-574.

Dobbins, W. (1944). Effect of Turbulence on Sedimentation. *ASCE Transactions Vol. 109, No. 2218* , pp. 629-656.

Garside, J., & Al-Dibouni, M. (1977). Velocity-Voidage Relationships for Fluidization and Sedimentation in Solid-Liquid Systems. *2nd Eng. Chem. Process Des. Dev., 16, 206* .

Grace, J. (1986). Contacting modes and behaviour classification of gas-solid and other two-phase suspensions. *Canadian Journal of Chemical Engineering, vol. 64.* , pp. 353-363.

Groot, J. (1981). *Rapport Beunbezinking (in Dutch).* Papendrecht: Royal Boskalis Westminster.

Huisman, L. (1973-1995). *Sedimentation & Flotation 1973-1995.* Delft, Netherlands: Delft University of Technology.

Huisman, L. (1980). *Theory of settling tanks.* Delft, Netherlands: Delft University of Technology.

Huisman, L. (1995). *Sedimentation & Flotation 1973-1995.* Delft, Netherlands: Delft University of Technology.

Julien, P. (1995). Erosion and sedimentation. *Cambridge University Press* .

Koning, J. d. (1977). Constant Tonnage Loading System of Trailing Suction Hopper Dredges. *International Course on Modern Dredging* (p. D6). The Hague, The Netherlands: Delft University of Technology & KIVI.

Liu, Z. (2001). *Sediment Transport.* Aalborg, Denmark: Aalborg University.

Madsen, O. (1991). Mechanics of cohesion less sediment transport in coastal waters. *Coastal Sediments 91,* (pp. 15-27). Seattle, Washington, USA: ASCE.

Madsen, O., & Grant, W. (1976). *Sediment transport in the coastal environment.* Cambridge, Massachusetts, USA: Technical report 209, M.I.T.

Miedema, S. (1981). *The flow of dredged slurry in and out hoppers and the settlement process in hoppers.* Delft, The Netherlands: Delft University of Technology, ScO/81/105, 147 pages.

Miedema, S. (2008A). An Analytical Approach to the Sedimentation Process in Trailing Suction Hopper Dredges. *Terra et Aqua 112* , pp. 15-25.

Miedema, S. (2008B). An analytical method to determine scour. *WEDA XXVIII & Texas A&M 39.* St. Louis, USA: Western Dredging Association (WEDA).

Miedema, S. (2009A). The effect of the bed rise velocity on the sedimentation process in hopper dredges. *Journal of Dredging Engineering, Vol. 10, No. 1* , pp. 10-31.

Miedema, S. (2009B). A sensitivity analysis of the scaling of TSHD's. *WEDA 29 & TAMU 40 Conference.* Phoenix, Arizona, USA: WEDA.

Miedema, S. (2010). Constructing the Shields curve, a new theoretical approach and its applications. *WODCON XIX* (p. 22 pages). Beijing, September 2010: WODA.

Miedema, S., & Rhee, C. v. (2007). A sensitivity analysis on the effects of dimensions and geometry of Trailing Suction Hopper Dredges. *WODCON.* Orlando, Florida, USA: WODA.

Miedema, S., & Vlasblom, W. (1996). Theory of Hopper Sedimentation. *29th Annual Texas A&M Dredging Seminar.* New Orleans: WEDA/TAMU.

Ooijens, S. (1999). Adding Dynamics to the Camp Model for the Calculation of Overflow Losses. *Terra et Aqua 76* , pp. 12-21.

Ooijens, S., Gruijter, A. d., Nieuwenhuizen, A., & Vandycke, S. (2001). Research on Hopper Settlement Using Large Scale Modeling. *CEDA Dredging Days 2001* (pp. 1-11). Rotterdam: CEDA.

Patankar, S. (1980). *Numerical heat transfer and fluid flow.* New York, USA: McGraw-Hill.

Rhee, C. v. (2002A). The influence of the bottom shear stress on the sedimentation of sand. *11th International Symposium on Transport and Sedimentation of Solid Particles.* Ghent, Belgium.

Rhee, C. v. (2002B). Numerical modeling of the flow and settling in a Trailing Suction Hopper Dredge. *15th International Conference on Hydrotransport.* Banff, Canada.

Rhee, C. v. (2002C). *On the sedimentation process in a Trailing Suction Hopper Dredger.* Delft, Netherlands: Delft University of Technology, PhD Thesis.

Richardson, J., & Zaki, W. (1954). Sedimentation & Fluidization: Part I. *Transactions of the Institution of Chemical Engineering 32* , pp. 35-53.

Rijn, L. (1984). Sediment pick up functions. *Journal of Hydraulic Engineering, vol. 110, no. 10.*

Rijn, L. (1987). *Mathematical modelling of morphological processes in case of suspended sediment transport, PhD Thesis.* Delft, Netherlands: Delft University of Technology.

Rijn, L. v. (1993). *Principles of sediment transport in rivers, estuaries and coastal seas, Part I.* Utrecht & Delft: Aqua Publications, The Netherlands.

Rijn, L. v. (2006). *Principles of sediment transport in rivers, estuaries and coastal areas, Part II: Supplement 2006.* Utrecht & Delft: Aqua Publications, The Netherlands.

Rodi, W. (1993). *Turbulence models and their application in hydraulics, a state of the art review.* IAHR, Third Edition.

Rowe, P. (1987). A convinient empirical equation for estimation of the Richardson-Zaki exponent. *Chemical Engineering Science Vol. 42, no. 11* , pp. 2795-2796.

Shields, A. (1936). Anwendung der Aehnlichkeitsmechanik und der Turbulenzforschung auf die Geschiebebewegung. *Mitteilung der Preussischen Versuchsanstalt fur Wasserbau und Schiffbau, Heft 26, Berlin.* Belin.

Soulsby, R. (1987). Calculating bottom orbital velocity beneath waves. *Coastal Engineering 11.*, (pp. 371-380).

Soulsby, R. (1997). *Dynamics of marine sands.* London, United Kingdom: Thomas Telford Publications.

Soulsby, R., & Whitehouse, R. (1997). Threshold of sediment motion in coastal environment. *Proceedings Pacific Coasts and Ports 1997 Conference*, (pp. 149–154). University of Canterbury, Christchurch, New Zealand.

Stansby, P. (1997). Semi-implicit finite shallow-water flow and solute transport solver with k-epsilon turbulence model. *International Journal for Numerical Methods in Fluids, vol. 25.* , pp. 285-313.

Stelling, G., & Kester, J. (1994). On the approximation of horizontal gradients in sigma coordinates for bathymetry with steep bottom slopes. *International Journal for Numerical Methods in Fluids, vol. 18* , pp. 915-935.

Sundborg, A. (1956). The River Klarålven: Chapter 2. The morphological activity of flowing water erosion of the stream bed. *Geografiska Annaler , 38*, pp. 165-221.

Turton, R., & Levenspiel, O. (1986). A short note on the drag correlation for spheres. *Powder technology Vol. 47* , pp. 83-85.

Vlasblom, W., & Miedema, S. (1995). A Theory for Determining Sedimentation and Overflow Losses in Hoppers. *WODCON IV.* Amsterdam, Netherlands: WODA.

Wallis, G. (1969). *One Dimensional Two Phase Flow.* McGraw Hill.

Wilson, K., Addie, G., Clift, R., & Sellgren, A. (1997). *Slurry Transport using Centrifugal Pumps.* Glasgow, UK.: Chapman & Hall, Blackie Academic & Professional.

Yagi, T. (1970). Sedimentation effects of soil in hopper. *WODCON III* (pp. 1-22). Singapore: WODA.

Zanke, U. C. (1977). *Berechnung der Sinkgeschwindigkeiten von Sedimenten.* Hannover, Germany: Mitteilungen Des Francius Instituts for Wasserbau, Heft 46, seite 243, Technical University Hannover.

Zanke, U. C. (2003). On the influence of turbulence on the initiation of sediment motion. *International Journal of Sediment Research , 18* (1), pp. 17–31.

Chapter 16: List of Figures

Chapter 17: List of Tables

Dredging Processes
The Loading of Trailing Suction Hopper Dredges

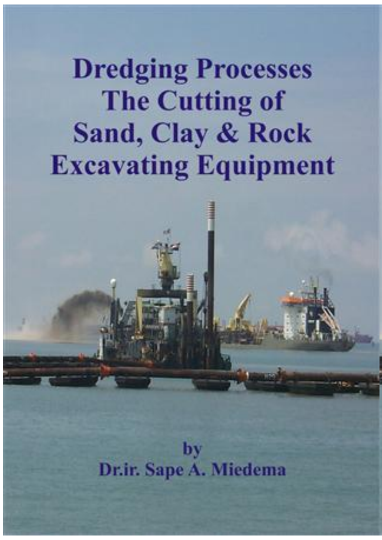
Dredging Processes
The Cutting of
Sand, Clay & Rock
Excavating Equipment
by
Dr.ir. Sape A. Miedema

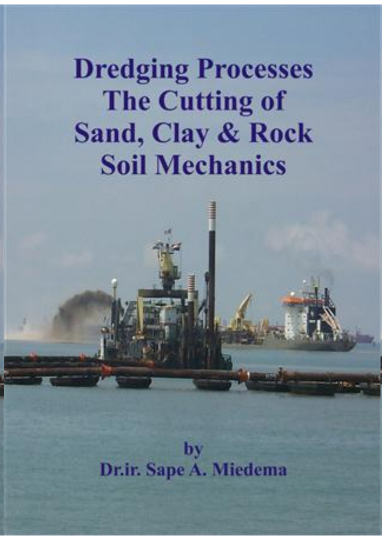
Dredging Processes
The Cutting of
Sand, Clay & Rock
Soil Mechanics
by
Dr.ir. Sape A. Miedema

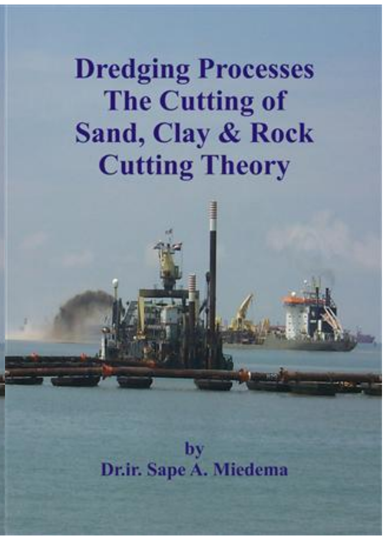
Dredging Processes
The Cutting of
Sand, Clay & Rock
Cutting Theory
by
Dr.ir. Sape A. Miedema

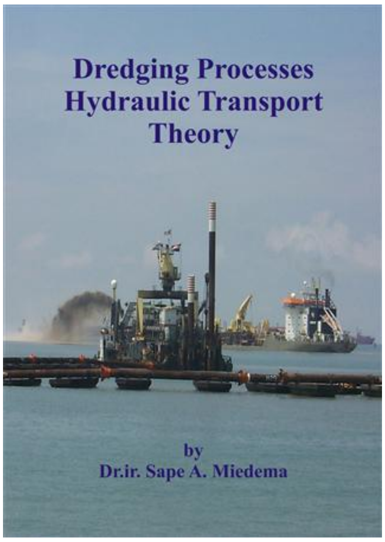
Dredging Processes
Hydraulic Transport
Theory
by
Dr.ir. Sape A. Miedema

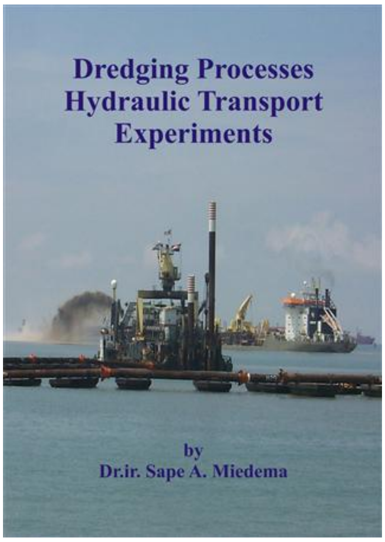
Dredging Processes
Hydraulic Transport
Experiments
by
Dr.ir. Sape A. Miedema

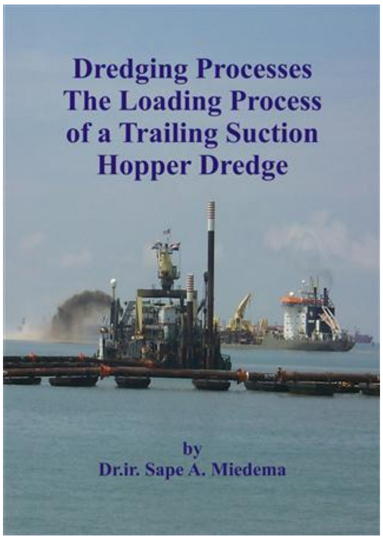
Dredging Processes
The Loading Process
of a Trailing Suction
Hopper Dredge
by
Dr.ir. Sape A. Miedema

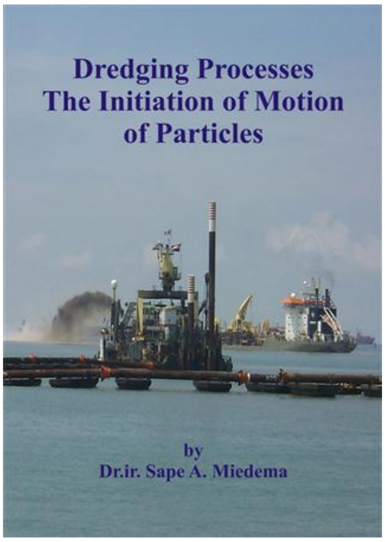
Dredging Processes
The Initiation of Motion
of Particles
by
Dr.ir. Sape A. Miedema

Chapter 18: **About the Author.**

Dr.ir. Sape A. Miedema (November 8th 1955) obtained his M.Sc. degree in Mechanical Engineering with honors at the Delft University of Technology (DUT) in 1983. He obtained his Ph.D. degree on research into the basics of soil cutting in relation with ship motions, in 1987. From 1987 to 1992 he was assistant professor at the chair of Dredging Technology. In 1992 and 1993 he was a member of the management board of Mechanical Engineering & Marine Technology of the DUT. In 1992 he became associate professor at the DUT with the chair of Dredging Technology. From 1996 to 2001 he was appointed educational director of Mechanical Engineering and Marine Technology at the DUT, but still remaining associate professor of Dredging Engineering. In 2005 he was appointed educational director of the MSc program of Offshore Engineering and he is also still associate professor of Dredging Engineering. In 2011 he was also appointed as director of the MSc program Offshore Engineering of the Petrovietnam University.

Dr.ir. S.A. Miedema teaches (or has taught) courses on soil mechanics and soil cutting, hopper sedimentation, mechatronics, applied thermodynamics, drive system design principles, mooring systems and mathematics. His research focuses on the mathematical modeling of dredging systems like, cutter suction dredges, hopper dredges, clamshell dredges, backhoe dredges and trenchers. The fundamental part of the research focuses on the cutting processes of sand, clay and rock, sedimentation processes in Trailing Suction Hopper Dredges and the associated erosion processes. Lately the research focuses on hyperbaric rock cutting in relation with deep sea mining and on hydraulic transport of sand/water slurries.

Dredging Processes
The Loading of Trailing Suction Hopper Dredges

By

Dr.ir. Sape A. Miedema

In dredging, trenching, (deep sea) mining, drilling, tunnel boring and many other applications, sand, clay or rock has to be excavated. The productions (and thus the dimensions) of the excavating equipment range from mm^3/sec - cm^3/sec to m^3/sec. In oil drilling layers with a thickness of a magnitude of 0.2 mm are cut, while in dredging this can be of a magnitude of 0.1 m with cutter suction dredges and meters for clamshells and backhoe's. Some equipment is designed for dry soil, while others operate under water saturated conditions. Installed cutting powers may range up to 10 MW. For both the design, the operation and production estimation of the excavating equipment it is important to be able to predict the cutting forces and powers. After the soil has been excavated it is usually transported hydraulically as a slurry over a short (TSHD's) or a long distance (CSD's). Estimating the pressure losses and determining whether or not a bed will occur in the pipeline is of great importance. Fundamental processes of sedimentation, initiation of motion and ersosion of the soil particles determine the transport process and the flow regimes. In TSHD's the soil has to settle during the loading process, where also sedimentation and erosion will be in equilibrium. In all cases we have to deal with soil and high density soil water mixtures and its fundamental behavior.

This book gives an overview of the sedimentation process in TSHD's.

This book will enable engineers to determine the loading process of Trailing Suction Hopper Dredges and is the **4th** of **7** books.

Part 1: The Cutting of Sand, Clay & Rock – Excavating Equipment.
Part 2: The Cutting of Sand, Clay & Rock – Soil Mechanics.
Part 3: The Cutting of Sand, Clay & Rock – Cutting Theory.
Part 4: The Loading Process of a Trailing Suction Hopper Dredge.
Part 5: The Initiation of Motion of Particles.
Part 6: Hydraulic Transport – Theory.
Part 7: Hydraulic Transport – Experiments.